Intelligent Scheduling and Charging Optimization for CAEVs and UAVs in Urban Transportation Networks

By

Palwasha Waheed Shaikh

A thesis submitted to the University of Ottawa
in partial fulfillment of the requirements for the degree of
Doctor in Philosophy (PhD.) in Electrical and Computer Engineering

School of Electrical Engineering and Computer Science
Faculty of Engineering
University of Ottawa
Ottawa, ON, CA

Abstract

Urban transportation systems are increasingly strained by congestion, air pollution, and greenhouse gas emissions, motivating the need for scalable and sustainable mobility solutions. Connected Autonomous Electric Vehicles (CAEVs) and Uncrewed Aerial Vehicles (UAVs) are key enablers of next generation intelligent transportation systems (ITS), yet their adoption remains constrained by limited battery capacity, fragmented charging infrastructure, and the absence of reliable coordination mechanisms under dynamic and heterogeneous conditions. Existing research often addresses individual charging technologies or isolated vehicle classes, leaving a gap in system-level coordination across ground and aerial platforms.

This thesis addresses this gap by demonstrating that charging coordination, rather than charging technology alone, is a critical barrier to sustainable deployment of autonomous electric mobility. A scalable and interoperable three-layer charging network architecture is proposed to support static charging, dynamic wireless charging, and vehicle-to-vehicle (V2V) charging across heterogeneous charging node types. A hybrid coordination topology and unified handshake protocol enable interoperable charging discovery, reservation based scheduling, and execution while remaining compatible with existing communication infrastructure.

Building on this architectural foundation, coordinated charging scheduling and trip planning mechanisms that consider both vehicle routing and charging resource allocation are developed using heuristic and learning-based approaches. Two heuristic strategies, Static Heuristic Charging Scheduling Policy (SH-CSP) and Dynamic Heuristic Charging Scheduling Policy (DH-CSP), provide interpretable baselines and handle early and late arrivals. To address scalability and non-stationary demand, Safety, Sustainability, and Scheduling-Aware Feasibility-Enhanced Deep Deterministic Policy Gradient (SAFE-DDPG) is introduced to enable adaptive, real-time scheduling under heterogeneous charging conditions.

Reliability and fairness are embedded as system-level properties within the architecture and scheduling framework. Simulation-based evaluation demonstrates charging reservation fulfillment rates approaching 98%, waiting time reductions of up to approximately 80% relative to heuristic baselines, and consistently high fairness across heterogeneous charging networks. Comparative evaluation against baseline deep reinforcement learning methods, including DDPG and TD3, and explainable artificial intelligence (XAI) techniques further validate effectiveness and interpretability. Overall, this thesis presents a unified, reliable, and scalable framework for intelligent scheduling and charging optimization through learning-based decision-making in next-generation urban transportation systems.

Dedication

This thesis is dedicated to the memory of my supervisor, Dr. Hussein T. Mouftah, whose guidance, encouragement, and passion for research have left an indelible mark on my life. His mentorship inspired me to pursue excellence and fostered a deep love for learning. May Allah grant him Jannah and elevate his rank in the hereafter. I will always carry his lessons and dedication with me in my academic and personal journey.

Acknowledgement

Firstly, praises and thanks to Almighty Allah for bestowing me with the understanding and strength needed to complete this thesis successfully.

I would like to express my deepest gratitude to my thesis supervisor, Dr. Hussein T. Mouftah, who gave me the opportunity to do research. The completion of this thesis would not have been possible without his persistent support and guidance. I thank him for his timely advice and confidence in me and my abilities. His words have always convincingly conveyed a spirit of adventure and fostered inspiration and excitement in research. His dedication to supporting students has been deeply inspiring, strengthening my desire to contribute to the field and pursue a doctorate. It was a great privilege to work under his guidance, and I look forward to applying these lessons with dedication and passion.

I would also like to sincerely thank Dr. Burak Kantarci for stepping in as my co-supervisor during a challenging time. His patience, understanding, and encouragement have been deeply appreciated. I am truly grateful for his guidance and constructive feedback, which have helped me navigate challenges and strengthen my work. It has been a privilege to learn from his expertise, and I deeply value his support and insights, which have meaningfully contributed to the completion of this thesis.

I would like to sincerely express my appreciation towards the entire University of Ottawa's School of Electrical Engineering and Computer Science for cultivating an environment where researchers and life-long learners like me can freely explore, learn, and grow. I am deeply indebted to all the professors who have taught me during my graduate studies and have passed on their invaluable teachings that helped develop my skills and personality.

I revere the strength, moral support, and endless prayers and blessings extended with love by my supportive and loving parents, Eng. Abdul Waheed Shaikh and Dr. Farah Waheed, my sweet brother, Eng. Shahroz Waheed Shaikh, and my kind grandma/nanoo, Sitara Latif. Their unwavering support has guided me through the most challenging of situations, and their cheers have always been the loudest for even my smallest of achievements. Their reassuring smiles and silent prayers have always been the loudest to motivate and renew my confidence. Their unfaltering belief in me and my skills is overwhelming, and without them I would not have been able to reach this far. They have always let me spread my wings, and their unconditional love has always helped me fearlessly soar higher into the unknown. A mere thank you may not be able to express the deep gratitude, yet I try. Thank you!

Palwasha W. Shaikh

Table of Contents

List of Acronyms

1G	First Generation
2G	Second Generation
3G	Third-Generation
3GPP	3rd Generation Partnership Project
4G	Fourth-Generation
5G	Fifth Generation
6G	Sixth-Generation
6G-ITS	6G-enabled Intelligent Transportation Systems
AHuber	Average Huber Loss
AI	Artificial Intelligence
AIoT	Artificial Intelligence of Things
AMAE	Average Mean Absolute Error
AMSE	Average Mean Squared Error
AR	Augmented Reality
ARMSE	Average Root-Mean-Square Error
ATIS	Alliance For Telecommunications Industry Solutions
AVCNM	Aerial Vehicle Charging Network Manager
BSS	Battery Storage Systems
CAD	Canadian Dollars
CAEV	Connected And Autonomous Electric Vehicle
CCN	Cabled Charging Network
CCNM	Cabled Charging Network Manager
CDC	Coded Distributed Computing
CDMA	Code-Division Multiple Access
CEM	Centralized Energy Management
CNM	Charging Network Manager
CN	Charging Network
CPs	Credit Points
CPT	Capacitive Power Transfer
CRN	Common Random Numbers
CUPS	Control Plane And User Plane Separation
DAB	Dual Active Bridge
DBN	Deep Belief Network
DDPG	Deep Deterministic Policy Gradient
DH-CSP	Dynamic Heuristic Charging Scheduling And Planning
DQN	Deep Q-Network
DRL	Deep Reinforcement Learning
DSO	Distribution System Operator
DSRC	Dedicated Short Range Communication
DVC	Dynamic Var Controller
DWC	Dynamic Wireless Charging

DWCN	Dynamic Wireless Charging Network
DWCNM	Dynamic Wireless Charging Network Manager
EC	Edge Computing
EDC	Energy Distribution Center
EDGE	Enhanced Data Gsm Evolution
EHC	Enhanced Human Communication
EI	Edge Intelligence
EIUAV	Edge Intelligent Uncrewed Aerial Vehicle
ELM	Extreme Learning Machine
ELU	Exponential Linear Unit
eMBB	Enhanced Mobile Broadband
EMC	Enhanced Machine Communication
EMC	Electromagnetic Compatibility
EMF	Electromagnetic Field
ES	Enabling Services
ESP	Energy Service Provider
ETSI	European Telecommunications Standards Institute
EVCRP	Electric Vehicle Charging Routing Problem
EVEC	Electric Vehicle Edge Computing
EVF	Expected-Value Formulation
EVSE	Electric Vehicle Supply Equipment
FEL	Future Event List
FL	Federated Learning
GPRS	General Packet Radio Service
GPS	Global Positioning System
GSM	Global System For Mobile Communications
GVCNM	Ground Vehicle Charging Network Manager
HD	High-Definition
HFL	Hierarchical Federated Learning
IEC	Intelligent Edge Computing
IMU	Inertial Measurement Unit
IoE	Internet of Everything
IoT	Internet of Things
IoV	Internet of Vehicles
IPT	Inductive Power Transfer
ISAC	Integrated Sensing And Communication
ITS	Intelligent Transportation System
ITU	International Telecommunication Union
IWPT	Inductive Wireless Power Transfer
j-PPO+ConvNTM	Joint Proximal Policy Optimization Combined With Convolutional Neural Turing Machines
KAIST	Korea Advanced Institute of Science & Technology
KDC	Key Distribution Center
LB-WPT	Laser Beaming Wireless Power Transfer

LBCNM	Laser-Beaming Charging Network Manager
LBCN	Laser Beaming Charging Network
LBET	Laser Beam Energy Transmitter
LBUAV	Laser-Beaming Uncrewed Aerial Vehicle
Li-Fi	Light-Fidelity
LiDAR	Light Detection And Ranging
LOS	Line-of-Sight
LSTM	Long Short-Term Memory
MADDQN	Multi-Agent Double Deep Q Learning
MAE	Mean Absolute Error
MCS	Mobile Charging Station
MDP	Markov Decision Process
MEC	Mobile Edge Computing
MIMO	Massive Multiple-Input Multiple-Output
ML	Machine Learning
MMS	Multimedia Messaging Service
mMTC	Massive Machine-Type Communication
MR-WPT	Magnetic Resonance Wireless Power Transfer
mULC	Massive Ultrareliable Low Latency Communication
NE	Network Evolution
NGMN	Next Generation Mobile Networks Alliance
NOMA	Non-Orthogonal Multiple Access
O-RAN	Open RAN
OBU	Onboard Computing Unit
OFDMA	Orthogonal Frequency Division Multiple Access
OOK	On–Off Keying
ORA	Online Resource Allocation
OU	Ornstein–Uhlenbeck
OWPT	Optical Wireless Power Transfer
P2P	Peer-To-Peer
PAER	Peak-To-Average Energy Ratio
PDC	Personal Digital Cellular
POMDP	Partially Observable Markov Decision Process
PPO	Proximal Policy Optimization
QoS	Quality of Service
ReLU	Rectified Linear Unit
RL	Reinforcement Learning
RMSE	Root-Mean-Square Error
RSU	Roadside Unit
SAC	Soft Actor-Critic
SAE	Stacked Autoencoder
SAFE-DDPG	Safety, Sustainability, And Scheduling-Aware Feasibility-Enhanced DDPG
SCOS	Stochastic Coded Offloading Scheme

SDN	Software Defined Networks
SFTA	Shortest Flight-Time Allocation
SH-CSP	Static Heuristic Charging Scheduling and Planning
SIP	Stochastic Integer Programming
SMS	Short Message Service
SoC	State of Charge
SP-A2C	Shortest-Path-Based Advantage Actor-Critic
SPA	Second Price Auction
SWC	Static Wireless Charging
SWCN	Static Wireless Charging Network
SWCNM	Static Wireless Charging Network Manager
Tbps	Terabit-Per-Second
TD	Temporal-Difference
TD3	Twin Delayed Deep Deterministic Policy Gradient
TDFT	Time Division Flight Trajectory
THz	Terahertz
TOU	Time of Use
U2U	UAV-to-UAV
U2V	UAV-to-Vehicle
UAV	Uncrewed Aerial Vehicle
ULBC	Ultra-Reliable Low Latency Broadband Communications
uMBB	Ultra-Mobile Broadband
URLLC	Ultra-Reliable Low-Latency Communication
V2I	Vehicle-to-Infrastructure
V2U	Vehicle-to-UAV
V2U	Vehicle-to-UAV
V2V	Vehicle-to-Vehicle
V2X	Vehicle-to-Everything
VAR	Virtual Augmented Reality
VAr	Reactive Power
VLC	Visible Light Communication
VoLTE	Voice over LTE
VoWiFi	Voice over Wi-Fi
VR	Virtual Reality
WCP	Wireless Charging Pad
WER	Wireless Energy Receiver
WET	Wireless Energy Transmitter
WPT	Wireless Power Transfer
XAI	Explainable Artificial Intelligence
XR	Extended Reality
ZB	Zettabytes
μ PMUs	Micro-Phasor Measurement Units

List of Symbols

Symbol	Description
P_{mhov}	Total hovering power of UAV (W)
W	UAV weight (N)
n	Number of rotors (dimensionless)
r	Rotor radius (m)
A	Rotor disk area (m²)
C_T	Thrust coefficient (dimensionless)
ρ	Air density (kg/m³)
δ_s	Profile drag coefficient of rotor blades (dimensionless)
k	Induced power correction factor (dimensionless)
V_h	Horizontal flight velocity (m/s)
v_0	Induced velocity in hover (m/s)
$SFP_{\parallel}$	Equivalent flat plate area for horizontal drag (m²)
$P_{mf}(V_h)$	Total power consumption during horizontal flight (W)
V_v	Vertical velocity (m/s)
$sgn(V_v)$	Sign of vertical velocity (+1 ascent, -1 descent)
$SFP_{\perp}$	Equivalent flat plate area for vertical drag (m²)
$P_{mv}(V_v)$	Total power consumption during vertical motion (W)
$\Delta P_h(V_h)$	Horizontal-motion power component excluding hover (W)
$\Delta P_v(V_v)$	Vertical-motion power component excluding hover (W)
$P_{total}(V_h, V_v)$	Total UAV power during 3D flight (W)
F_W	Total wheel force acting on CAEV (N)
m	Vehicle mass (kg)
g	Gravitational acceleration (m/s²)
α	Road slope angle (radians or degrees)
f_r	Rolling resistance coefficient (dimensionless)
c_w	Aerodynamic drag coefficient (dimensionless)
A_f	Vehicle frontal area (m²)
v	Vehicle velocity (m/s)
a	Vehicle acceleration (m/s²)
e_i	Equivalent inertia factor (dimensionless)
T_W	Wheel torque (Nm)
r_W	Wheel radius (m)
T_{EM}	Motor shaft torque (Nm)
i_T	Gear ratio (dimensionless)
η_T	Transmission efficiency (dimensionless)
$P_{EM,loss}$	Motor power loss (W)
n_{EM}	Motor speed (rpm or rad/s)
$P_{Bat,chem}$	Battery chemical power consumption (W)
U_0	Battery voltage (V)
R_i	Battery internal resistance (Ω)
$P_{EM,el}$	Electrical motor power (W)
$P_{aux,el}$	Auxiliary electrical power (W)
P_{LRec}	Received optical charging power (W)
η_{LRec}	Optical-to-electrical conversion efficiency (dimensionless)
P_{LTrans}	Laser transmitter power (W)
A_{LRec}	Receiver effective aperture area (m²)
d_L	Transmitter–receiver separation distance (m)
LOS	Line-of-sight factor (dimensionless)
Env_λ	Atmospheric attenuation (dimensionless)

η_{CTrans}	Optical communication transmission efficiency (dimensionless)
E_b	Energy per bit (J)
T_b	Bit duration (s)
A_{CRec}	Communication receiver aperture area (m²)
d_C	Communication link distance (m)
P_{min}	Minimum power required for charging (W)
d_{crit}	Critical charging distance (m)
P_{req}	Minimum received power for decoding (W)
d_{comm}	Critical communication distance (m)
P_{comm}	Average optical communication power (W)
P_{LMax}	Maximum allowable received optical power (W)
θ	Optimal alignment angle (rad)
$\hat{r}(t)$	Actual battery charging rate (kW)
$r(t)$	Pilot signal charging rate (kW)
$\bar{r}$	Max charging rate of onboard charger (kW)
$\hat{e}(t)$	Difference between battery capacity and stored energy (kWh)
SoC	State-of-charge between (%)
th	Transition threshold between charging stages (%)
c_i	Charging cost at node (monetary units)
t_i	Estimated travel time to node (s)
w_i	Waiting time at node (s)
b_i	Battery energy consumption to reach node (Wh)
d_i	Travel distance to node (m)
$\lambda_1, \ldots, \lambda_5$	Adaptive weight coefficients (dimensionless)
$ChargeReq_i$	Charging request trigger
SoC_{req}	Mission-required SoC at node
SoC_{th}	Emergency threshold SoC in transit
t_{arr_i}	Predicted arrival time at node (s)
t_{res_i}	Reservation start time (s)
t_{dep_i}	Predicted departure time (s)
$d(i,j)$	Travel distance between nodes i and j (m)
D_{max}	Maximum allowable travel distance (m)
E_{rem}	Remaining stored energy after last charging (Wh)
E_{cons_i}	Energy consumed over segment i (Wh)
N	Set of segments before next charging event
E_{min}	Minimum operational reserve energy (Wh)
η_i	Measured charging efficiency at node (dimensionless)
η_{min}	Minimum acceptable charging efficiency (dimensionless)
$f(n)$	Total estimated path cost through node n (cost units)
$g(n)$	Accumulated path cost from start to node n (cost units)
$h(n)$	Heuristic cost estimate from node n to goal (cost units)
$c_{alt(n)}$	Altitude-related energy cost at node n (cost units)
$c_{obs(n)}$	Obstacle-avoidance cost at node n (cost units)
$D(v)$	Minimal cumulative travel cost to node v (cost units)
$Pred(v)$	Set of predecessor nodes to v
$c(u,v)$	Travel cost between nodes u and v (cost units)
E_{deliv}	Total electrical energy delivered to the vehicle (kWh)
C_{CAD}	Cost of delivered energy (CAD)
r_{energy}	Time-of-use electricity pricing rate (CAD/kWh)
r_{CP}	Conversion rate from CAD to CPs (CAD/CP)
C_{CP}	Charging cost (CP)
$v_{a,SWC}$	Actual vehicle speed during SWC (m/s)
Δx_{SWC}	Longitudinal offset between pad center and receiver coil in SWC (m)
Δy_{SWC}	Lateral offset between pad center and receiver coil in SWC (m)
$X_{c,SWC}$	Longitudinal coordinate of charging pad center in SWC (m)

$Y_{c,SWC}$	Lateral coordinate of charging pad center in SWC (m)
$x_{a,SWC}$	Longitudinal coordinate of receiver coil center in SWC (m)
$y_{a,SWC}$	Lateral coordinate of receiver coil center in SWC (m)
$\varepsilon_{x,SWC}$	Allowable longitudinal misalignment tolerance in SWC (m)
$\varepsilon_{y,SWC}$	Allowable lateral misalignment tolerance in SWC (m)
$v_{t,DWC}$	Target vehicle speed during DWC (m/s)
$\delta_{v,DWC}$	Allowable speed deviation during DWC (m/s)
Δy_{DWC}	Lateral misalignment during DWC (m)
$\varepsilon_{y,DWC}$	Allowable lateral misalignment tolerance in DWC (m)
$v_{a,LB}$	Actual relative velocity during LB-WPT (m/s)
Δx_{LB}	Longitudinal offset between laser transmitter and receiver (m)
Δy_{LB}	Lateral offset between laser transmitter and receiver (m)
$\varepsilon_{x,LB}$	Allowable longitudinal offset in LB-WPT (m)
$\varepsilon_{y,LB}$	Allowable lateral offset in LB-WPT (m)
d_{LB}	Distance between laser transmitter and receiver apertures (m)
$d_{min,LB}$	Minimum safe operating distance for LB-WPT (m)
$d_{max,LB}$	Maximum safe operating distance for LB-WPT (m)
$d_{a,MR}$	Measured coil separation distance in MR-WPT (m)
$d_{t,MR}$	Optimal resonant coil separation distance in MR-WPT (m)
$\delta_{d,MR}$	Allowable deviation from optimal coil distance in MR-WPT (m)
$\delta_{v,MR}$	Allowable speed deviation in MR-WPT (m/s)
$r_{v,k}$	Mode-specific acceleration or deceleration rate (m/s²), , where $k \in$ {DWC,MR}
$X_{s,k}$	Start longitudinal coordinate of charging segment for mode k (m)
$X_{e,k}$	End longitudinal coordinate of charging segment for mode k (m)
$Y_{s,k}$	Start lateral coordinate of charging segment for mode k (m)
$Y_{e,k}$	End lateral coordinate of charging segment for mode k (m)
$X_{c,k}$	Center longitudinal coordinate of charging segment for mode k (m)
$Y_{c,k}$	Center lateral coordinate of charging segment for mode k (m)
Δx_k	Longitudinal misalignment for charging mode k (m)
Δy_k	Lateral misalignment for charging mode k (m)
$\varepsilon_{x,k}$	Allowable longitudinal misalignment tolerance for mode k (m)
$\varepsilon_{y,k}$	Allowable lateral misalignment tolerance for mode k (m)
$\mathbf{u}_k$	Unit direction vector between coupled vehicles in mode k (dimensionless)
$\mathbf{p}_{1,k}$	Position vector of first vehicle or platform in mode k (m)
$\mathbf{p}_{2,k}$	Position vector of second vehicle or platform in mode k (m)
$P_{r,LB}$	Received power in laser-based wireless power transfer (W)
$P_{t,LB}$	Transmitted laser power in LB-WPT (W)
$\eta_{sys,LB}$	Overall system efficiency of LB-WPT (dimensionless)
$D_{r,LB}$	Receiver aperture diameter in LB-WPT (m)
$D_{b0,LB}$	Initial laser beam waist diameter (m)
θ_{LB}	Laser beam divergence angle (rad)
$P_{req,LB}$	Minimum required received power for LB-WPT (W)
$\alpha_{opt,LB}$	Optimal laser beam elevation or steering angle (rad)
$\mathcal{A}_{LB}$	Feasible set of laser steering angles (dimensionless)
$\eta_{jitter,LB}$	Power attenuation factor due to beam jitter (dimensionless)
$\sigma_{jitter,LB}$	Standard deviation of beam pointing jitter (m)
$\sigma_{beam,LB}$	Laser beam spot radius at the receiver (m)
$t_{arr,CAEV}$	Predicted arrival time of a CAEV at the charging node (s)
$t_{arr,UAV}$	Predicted arrival time of a UAV at the charging node (s)
$t_{current}$	Current system clock time (s)
d_{CAEV}	Road distance from CAEV to charging node entry point (m)
v_{CAEV}	Predicted CAEV travel speed based on traffic and routing data (m/s)
$\Delta t_{traffic}$	Estimated delay due to traffic conditions (s)
Δt_{queue}	Expected waiting time before entering the charging node or EVSE (s)
d_{UAV}	Straight-line distance from UAV to charging node (m)

v_{UAV}	Cruise velocity of the UAV (m/s)
Δt_{wind}	Time delay or gain due to wind speed and direction affecting UAV travel (s)
$n_{track(t)}$	Number of vehicles charging on the dynamic wireless charging track at time t (dimensionless)
n_{max}	Maximum allowable number of vehicles on the charging track (dimensionless)
Δt_{update}	Time window for updating reservations for early-arriving vehicles (s)
t_{free}	Estimated departure time of the next vehicle vacating the charging lane (s)
q_{len}	Current length of the UAV charging queue (dimensionless)
q_{max}	Maximum allowable UAV queue length (dimensionless)
$status_i$	Charging status decision of UAV i (Wait or Rebook) (dimensionless)
$t_{arr,CDV}$	Predicted arrival time of the charge delivery vehicle (s)
$t_{arr,CRV}$	Predicted arrival time of the charge receiving vehicle (s)
Δt_{sync}	Allowable synchronization time offset between CDV and CRV (s)
$t_{dep,CAEV}$	Scheduled departure time of a CAEV after charging (s)
$t_{\mathrm{dep,CAEV}'}$	Updated departure time of a CAEV after late-arrival adjustment (s)
$t_{dep,UAV}$	Scheduled departure time of a UAV after charging (s)
$t_{\mathrm{dep,UAV}'}$	Updated departure time of a UAV after late-arrival adjustment (s)
Δt_{late}	Additional charging time required due to late arrival (s)
s_t	State at time step t
s_{t+1}	Next state at time step t+1
a_t	Action at time step t
r_t	Immediate reward
γ	Discount factor
$Q(s_t, a_t; \theta^Q)$	Critic value function
θ^Q	Critic network parameters
$L(\theta^Q)$	Critic loss function
y_t	TD target
Q'	Target critic network
$\mu(s_t; \theta^\mu)$	Actor policy
θ^μ	Actor network parameters
μ'	Target actor network
$\theta^{Q'}$	Target critic parameters
$\theta^{\mu'}$	Target actor parameters
θ'	Target network parameters
τ	Soft update coefficient
J	Expected return
$\nabla_a Q(s_t, a; \theta^Q)$	Critic gradient w.r.t. action
$\nabla_{\theta^\mu} \mu(s_t; \theta^\mu)$	Actor gradient w.r.t. parameters
SoC_{curr}	Current state of charge (normalized)
SoC_{req}	Requested state of charge (normalized)
D_{dest}	Distance to destination (normalized)
$D_{static_{min}}$	Min. distance to static CN (normalized)
$D_{dynamic_{min}}$	Min. distance to dynamic CN (normalized)
N_{CAEV}	Number of nearby CAEVs
N_{UAV}	Number of nearby UAVs
ρ_{CAEV}	CAEV density measure
ρ_{UAV}	UAV density measure
f_{CAEV}	CAEV presence flag
f_{UAV}	UAV presence flag
L	Vector of CN load levels (normalized)
U	Vector of CN historical usage (normalized)
n_{sched}	Scheduled vehicles (normalized)
n_{wait}	Waiting vehicles (normalized)
τ_{dec}	Decision time index (normalized)
τ_{int}	Decision interval (normalized)

η_{last}	Previous static charging energy share
a_t	Continuous action vector
$\mathcal{F}(\mathbf{s}_t, \mathbf{a}_t)$	Action feasibility indicator
$\mathbf{a}_t^{\mathbf{DRL}}$	Actor-generated action
$\mathbf{a}_t^{\mathbf{heuristic}}$	Heuristic fallback action
$\mathbf{a}_t^{\mathbf{final}}$	Executed action
R_t	Immediate (local) reward
$\hat{\mathrm{S}}oC$	Predicted post-charge SoC
L_{dyn}	Dynamic CN load imbalance
L_{stat}	Static CN load imbalance
d_{dyn}	Distance to dynamic CN
d_{stat}	Distance to static CN
d_{max}	Maximum considered distance
$B_{lowLoad}$	Reward for low-load CN usage
$P_{fallback}$	Penalty for heuristic use
$P_{feasibility}$	Penalty for infeasible action
R_{global}	Episode-level global reward
U_{CN}	Mean CN utilization
W_{avg}	Average wait time (normalized)
I_{avg}	Average idle time (normalized)
C_{travel}	Travel cost (normalized)
C_{batt}	Battery consumption cost (normalized)
w_{util}	Utilization weight
w_{wait}	Waiting-time weight
w_{idle}	Idle-capacity weight
w_{travel}	Travel-cost weight
w_{batt}	Battery-cost weight
$P(i)$	Sampling probability of transition i
δ_i	Temporal-difference error of transition i
ϵ	Small constant for numerical stability
α	Priority exponent
w_i	Importance-sampling weight
N	Replay buffer size
β	Importance-sampling exponent
σ_t	Exploration noise variance at time t
σ_0	Initial noise variance
σ_{min}	Minimum noise variance
$decay$	Noise decay factor
T_Q	Average queue wait time per EV
Q_i	Queue waiting time of i^{th} EV
N_D	Number of departed EVs
λ	Throughput (departures per unit time)
T	Total simulation time
c	Number of parallel servers (EVSEs)
T_s	Average service time per EV
B	Total server busy time
T_i	Service time of i^{th} EV
ρ	Server utilization
A_L	Offered load
λ_A	Arrival rate
β_T	Proportion of server idle time
w	Average system wait time
W_i	System time of i^{th} EV
N_A	Number of arriving EVs
L	Average number of EVs in system

$\boldsymbol{P_a}$	Road accident probability
$\boldsymbol{P_s}$	Probability of skipping charging
$\boldsymbol{ts_{dur}^{CN}}$	Time slot duration per CN
$\boldsymbol{N_{days}}$	Number of simulated days
$\boldsymbol{N_{ts}}$	Number of time slots per EVSE
$\boldsymbol{J}$	Jain's fairness index
$\boldsymbol{x_i}$	CAEVs served by i^{th} CN
$\boldsymbol{N}$	Total number of CNs
% $\boldsymbol{Improvement}$	Relative performance improvement

List of Figures

List of Tables

Chapter 1 Introduction

1.1 Short Background

We are living in an era of continuous and rapid technological advancements that are reshaping various sectors, with transportation and telecommunications at the forefront. Rapid urbanization has increased traffic demand in urban areas, leading to congestion and significant air pollution. For instance, Toronto, ON, Canada, is reported as the 3rd most traffic-congested city globally for 10-kilometre travel times, with an average person losing 89 hours stuck in traffic annually [1]. Additionally, the Canadian transportation sector is the 10th largest greenhouse gas emitter, with 156 megatons of CO_2 emissions in 2024 [2]. The current transportation model predominantly relies on internal combustion engine vehicles, contributing to noise and air pollution, parking issues in densely populated cities, and low utilization rates [3]. Given the projected increase of 2.5 billion people in the global urban population by 2050, this model is deemed environmentally unsustainable [4][5]. However, the rapid evolution of telecommunication and networking technologies has ushered in the era of 6G networks, promising unparalleled connectivity, ultra-low latency, and ubiquitous computing [4]. Concurrently, the transportation sector is witnessing significant advancements with the rise of connected and autonomous electric vehicles (CAEVs) [5], [6] and uncrewed aerial vehicles (UAVs) [7]. These innovations herald a promising future for intelligent transportation systems (ITS), offering a sustainable solution to current urban transportation challenges.

CAEVs embody the integration of internet of things (IoT) and ITS, leveraging sophisticated sensors and computing systems to enable autonomous driving and efficient electric propulsion [6], [8], [9]. CAEVs rely on LiDAR, radar, cameras, and ultrasonic sensors to perceive and navigate their surroundings with high precision and accuracy [9]. Further, CAEVs offer numerous applications and advantages [6], [9]. They can promote autonomous driving to assist individuals who cannot drive, facilitate ride-sharing services, and streamline parcel delivery operations. Moreover, the widespread adoption of CAEVs presents a significant benefit for the environment, as they can help mitigate air pollution and reduce dependence on fossil fuels, paving the way for a more sustainable ITS ecosystem. However, despite these benefits, CAEVs still face challenges that must be addressed to fully realize their potential.

In a typical scenario, consider a commuter relying on a CAEV for daily transportation. As they embark on their journey, they confront the persistent issue of range anxiety, exacerbated by the scarcity of charging infrastructure along their route. The fear of running out of battery power before reaching a charging station significantly impacts their confidence in

the vehicle's reliability for long-distance travel. Upon reaching a designated charging station, frustration ensues due to prolonged wait times caused by limited availability or congestion at fixed charging infrastructure. This scenario underscores the practical challenges faced by consumers or users of CAEVs, emphasizing the urgent need to address issues of range anxiety and prolonged waiting times at charging stations to overcome obstacles to widespread CAEV adoption.

Transitioning to above-ground vehicles, we have UAVs. UAVs [7], [10] are a versatile aircraft that operate autonomously. They leverage a variety of sensors, often integrated with IoT and ITS, to gather data and navigate through airspace safely and efficiently. UAVs typically incorporate sensors such as GPS, gyroscopes, accelerometers, and cameras to precisely determine their position, orientation, and surroundings [7], [10]. Further, the onboard sensors enable UAVs to perform a wide range of tasks, from aerial surveillance and mapping, extending cellular coverage [11] to disaster response and infrastructure inspection. Moreover, UAVs' flexibility and accessibility make them indispensable for accessing remote or hazardous areas, thus aiding in precision farming, disaster management, and environmental conservation efforts.

However, UAV operations are constrained by battery life, presenting a significant obstacle to continuous operation. Imagine a case where a UAV is deployed to extend cellular coverage to a remote area affected by a natural disaster. Despite its capabilities, the UAV's limited battery life forces an early return for recharging, hampering vital communication efforts and potentially delaying crucial assistance to affected individuals. This scenario highlights the urgent need to address battery limitations in UAVs to optimize their operational efficiency in essential missions.

Wireless power transfer (WPT) is promising for alleviating concerns related to wired EV and AEV charging, offering benefits such as reduced battery cost, recharge time, and weight [12]. Three types of WPT exist: static wireless charging (SWC) for parked EVs, quasi-dynamic charging systems for dynamic environments like bus stations, and dynamic wireless charging (DWC) installed on roads to charge EVs in motion [13]. Now, we identify DWC [5], [10], [14] as a transformative solution to further enhance the capabilities of CAEVs and UAVs in smart cities. The two most promising WPT technologies with high power transmission over longer charging distances is magnetic resonance coupling due to its efficiency of 96 % at resonant frequency [15], and laser beaming with reported end-to-end power transfer efficiencies approaching 90% under controlled conditions [10], [16], [17]. The latter is an active area of research, and ways to deploy this technology in a cost-effective manner on a wider scale are

being explored. By embedding mobile wireless charging infrastructure along roadways and airspace, DWC has the potential to reduce reliance on traditional fixed charging stations and support opportunistic and in-motion charging under coordinated control. This technology can not only help address range anxiety for CAEVs by providing seamless charging on the go but also extend the mission time of UAVs by enabling mid-flight charging.

The intersection of advanced transportation technologies, the growing demand for efficient charging solutions, and the convergence of CAEVs and UAVs is gaining significant attention. Within this context, 6G networks provide an ideal foundation for transforming charging infrastructure from static stations into dynamic, distributed networks. Intelligent edge computing (IEC) further enhances this ecosystem by bringing computation closer to data sources and leveraging machine learning to optimize charging, reduce latency, and maintain grid stability [18], [19]. IEC also enables seamless integration of renewable energy, supporting faster and more reliable charging for CAEVs and UAVs in 6G networks. As cities evolve into smarter, interconnected environments, the fusion of DWC with 6G-IoT has the potential to revolutionize mobility, offering sustainable, efficient, and future-ready intelligent transportation systems.

Despite these advances, existing solutions remain fragmented across vehicle types, charging technologies, and infrastructure systems. Current approaches do not provide a unified mechanism to coordinate charging decisions, routing, and resource allocation across heterogeneous CAEV and UAV networks under dynamic operating conditions. Moreover, existing methods typically address scheduling or optimization in isolation, without jointly considering mobility, energy constraints, and time-coupled resource availability.

This gap highlights the need for coordinated, intelligent scheduling frameworks capable of operating under uncertainty, supporting heterogeneous charging modalities, and enabling scalable real-time decision-making in 6G-enabled urban transportation networks.

The problem considered in this thesis is therefore a coordinated and sequential decision-making problem that integrates both vehicle-side routing and energy constraints with infrastructure-side charging resource allocation under dynamic operating conditions, rather than treating them independently.

1.2 Motivation

This research investigation is fueled by the urgent need to tackle escalating greenhouse gas emissions and the mounting challenges within urban transportation systems. The prevalent dependence on fossil fuel vehicles exacerbates environmental degradation and traffic congestion, necessitating immediate solutions. While the transition towards EVs offers a

promising alternative, it faces formidable obstacles such as range anxiety, heavy batteries, and prolonged charging and wait times. In response, we identify the convergence of 6G networks, IEC, and ITS with wireless charging technologies as a potential solution. Powered by 6G for future ITS, DWC systems in particular hold the key to mitigating these challenges for both CAEVs and UAVs. These systems can reduce battery costs and weight for vehicles as they receive charging on the move and extend their operation time. Moreover, DWC opens the possibility for vehicles to support one another through controlled bidirectional and infrastructure-assisted charging mechanisms, further enhancing their efficiency and autonomy. The challenge, however, becomes significantly more intricate within heterogeneous vehicular networks, where vehicles differ not only in type but also in communication standards, charging interfaces, and battery characteristics. Variations in how CAEVs and UAVs exchange information, draw power, and deplete energy create highly uneven operational conditions, making joint scheduling and energy management a complex, dynamic, and sequential optimization task under uncertainty, where effective decision policies are learned through interaction with the environment. At the same time, the vulnerability of both CAEVs and UAVs to traffic congestion and long waiting times at charging stations underscores the critical need for a smart charging infrastructure equipped with a charging reservation and trip planning system. At present, charging remains fragmented across wired, wireless, and aerial platforms, limiting scalable coordination, interoperability, and cross-modal energy management. A unified, intelligent system that is interoperable across diverse charging methods holds the potential to revolutionize transportation, unlocking the full capabilities of CAEVs and UAVs while ushering in a new era of sustainable mobility. This necessitates the development of coordinated scheduling mechanisms capable of operating under dynamic and uncertain conditions.

1.3 Objectives

This thesis aims to introduce an intelligent charging network infrastructure tailored for 6G ITS applications, capable of accommodating both static and dynamic wireless charging systems for UAVs and CAEVs. The research seeks to explore the intricate interactions between CAEVs and UAVs, leveraging UAVs as mobile, edge-aware participants in 6G-enabled coordination and service extension, and CAEVs for autonomous mobility on demand. The objectives are to propose a system design and handshake protocol that ensures seamless integration with existing wired infrastructure and ITS standards in smart cities, while enabling IoT-based applications such as reservation-based charging scheduling and trip planning. The work further seeks to support diverse charging methods, including bidirectional vehicle-to-

vehicle (V2V) charging between same and different vehicle types, alongside conventional infrastructure-based systems. Both heuristic-based and deep reinforcement learning (DRL)-enhanced coordinated charging scheduling algorithms are developed to improve wait times, travel costs, energy consumption, vehicle operation time, and fairness in the use and allocation of charging resources under dynamic operating conditions, thereby improving system reliability. The performance of the proposed architecture and scheduling algorithms is validated through architectural design verification, simulation-based evaluation, and comparative analysis to highlight efficiency, scalability, and real-world applicability. Additional objectives include handling early and late arrival reservations through adaptive re-scheduling, addressing misalignment and speed-related errors in DWC systems, mitigating charge stealing and unfair billing, and maintaining reliable operation under disruptions such as traffic incidents and adverse weather.

1.4 Thesis Contributions

The following are the main contributions of this thesis:

1. **Scalable and Interoperable Charging Network Architecture:** This thesis develops a unified three-layer charging network architecture for coordinated CAEV and UAV operations, supporting static, dynamic, and V2V charging modes. The architecture integrates magnetic-resonance and laser-based wireless charging models with realistic power representations and a lightweight, interoperable communication framework compatible with existing wired/wireless infrastructure and ITS standards. By abstracting communication and charging coordination within a common framework, the proposed architecture enables scalable deployment, interoperability across heterogeneous nodes, and support for IoT-enabled services such as charging reservation and trip planning, without relying on tightly coupled communication assumptions.
2. **Coordinated Scheduling with SAFE-DDPG:** This thesis designs a coordinated scheduling framework combining heuristic-based approaches (SH-CSP and DH-CSP) with a domain-optimized deep reinforcement learning algorithm (SAFE-DDPG) for scalable, real-time charging decisions. The proposed SAFE-DDPG formulation incorporates feasibility-aware action selection, adaptive exploration through noise modulation, heuristic fallback strategies, and explainable AI (XAI) components to enhance transparency and provide design insights into learned scheduling policies under dynamic traffic and infrastructure conditions.

3. **Reliable and Fair Resource Allocation Mechanisms:** This thesis introduces safety- and fairness-aware resource allocation mechanisms for heterogeneous charging networks, including alignment correction strategies for dynamic wireless charging and coordination policies that discourage charge stealing and unfair resource usage. These mechanisms are embedded directly within the scheduling and control framework to ensure safe operation, equitable access to charging resources, and balanced utilization across charging nodes in large-scale autonomous charging environments.

1.5 Thesis Outline

This thesis is organized around the design, validation, and evaluation of coordinated charging and scheduling solutions for heterogeneous CAEV and UAV systems in 6G-enabled urban transportation networks. **Chapter 2** presents background and related work on 6G-enabled intelligent transportation systems, wireless charging technologies, coordinated scheduling, and reliability and fairness mechanisms, and identifies key research gaps motivating this work. **Chapter 3** introduces a scalable and interoperable charging network architecture, including the system model, communication topology, and unified handshake protocol, together with architectural validation and design verification. **Chapter 4** develops coordinated charging scheduling and trip planning approaches using heuristic methods and the proposed SAFE-DDPG learning-based framework, supported by detailed modeling and experimental evaluation. **Chapter 5** focuses on reliability, fairness, and scalability through comprehensive performance analysis, ablation studies, and interpretability assessment. **Chapter 6** concludes the thesis by summarizing the main contributions and outlining future research directions.

1.6 List of Publications

The following are the list of publications produced from this thesis:

1. P. W. Shaikh and H. T. Mouftah, “A Review of Dynamic Wireless Charging and Reservations for CAEV and UAV in 5G/6G ITS,” in *Proc. IEEE ICC 2024*, Denver, CO, USA, 2024, pp. 5371–5376. [Online]. Available: https://doi.org/10.1109/ICC51166.2024.10622598
2. P. W. Shaikh and H. T. Mouftah, “Intelligent DWC Reservation and Trip Planning of CAEV and UAV for 6G ITS,” in *Proc. IEEE IWCMC 2024 Vehicular Communications Conf.*, Ayia Napa, Cyprus, May 2024, pp. 238–243. [Online]. Available: https://doi.org/10.1109/IWCMC61514.2024.10592358

3. P. W. Shaikh and H. T. Mouftah, “Dynamic Wireless Charging of UAVs in 6G-enabled ITS,” in *Proc. 2024 IEEE 10th WF-IoT Conf.*, Ottawa, ON, Canada, Nov. 2024, pp. ADTW1.1.1–ADTW1.1.6
4. P. W. Shaikh and H. T. Mouftah, “An Overview on Intelligent Edge Computing for Enhancing CAEV and UAV Charging in 6G ITS,” in *Proc. IEEE Int. Conf. Smart Mobility (SM 2024)*, Niagara Falls, ON, Canada, 2024, pp. 248–253. [Online]. Available: https://doi.org/10.1109/SM63044.2024.10733427
5. P. W. Shaikh and H. T. Mouftah, “Edge Computing-aided Dynamic Wireless Charging and Trip Planning of UAVs,” *J. Sensor Actuator Netw.*, vol. 14, p. 8, 2025. [Online]. Available: https://doi.org/10.3390/jsan14010008
6. P. W. Shaikh and H. T. Mouftah, “Deep Reinforcement Learning for UAV Wireless Charging and Trajectory Planning: A Review,” in *Proc. 2025 IEEE 102nd Vehicular Technology Conference (VTC2025-Fall)*, Chengdu, China, 19–22 Oct. 2025.
7. P. W. Shaikh and H. T. Mouftah, “Deep reinforcement learning for wireless charging of UAVs and CAEVs,” *IEEE Communications Magazine*, Series on Internet of Things, accepted for publication, May 2025. https://doi.org/10.1109/MCOM.001.2500209
8. P. W. Shaikh, H. T. Mouftah, and B. Kantarci, “Intelligent Charging Reservation and Trip Planning of CAEVs and UAVs,” submitted for publication in *Electronics*, 4 Dec. 2025.

The following are the list of other relevant publications:

1. P. W. Shaikh and H. T. Mouftah, “Connected and Autonomous Electric Vehicles Charging Reservation and Trip Planning System”, Proceedings IEEE IWCMC’2021 Vehicular Communications Conference, Harbin, China, June-July 2021, pp. WM-4.6.1- WM-4.6.6 2.
2. P. W. Shaikh and H. T. Mouftah, “Intelligent Charging Infrastructure Design for Connected and Autonomous Electric Vehicles in Smart Cities”, Proceedings IEEE IM 4th International workshop on Intelligent Transportation and Autonomous Vehicles Technologies (ITAVT2021), Bordeaux, France, May 2021, pp. 992-997.
3. P. W. Shaikh, M. El-Abd, M. Khanafer, and K. Gao, “A Review on Swarm Intelligence and Evolutionary Algorithms for Solving the Traffic Signal Control Problem,” IEEE Transactions on Intelligent Transportation Systems, vol. 23, no. 1, pp. 48–63, Jan. 2022.
4. I. W. Damaj, P. W. Shaikh, and H. T. Mouftah, “Distinctive Landmarks in the History of Computing and Engineering: The Past, the Present, and the Future,” The International Journal for the History of Engineering & Technology, vol. 94, no. 2, pp. 89–107, 2024.

Chapter 2 Background and Literature Review

In this chapter, the literature review is presented to establish the background and context for intelligent charging scheduling and optimization in 6G-enabled ITS. Rather than treating scheduling in isolation, the chapter adopts a layered perspective in which scheduling decisions emerge from the interaction between communication capabilities, charging infrastructure characteristics, vehicle energy dynamics, and system-level performance objectives.

The discussion begins by tracing the evolution of cellular communication toward 6G, which provides the enabling substrate for real-time, large-scale coordination in ITS. This is followed by a review of scalable and interoperable charging network architectures, where the heterogeneity of charging technologies, vehicle types, and infrastructure capabilities defines the feasible decision space for scheduling.

Building on this foundation, the chapter then examines coordinated charging scheduling and routing mechanisms, including reservation-based systems, dynamic arrival handling, and learning-based decision-making approaches. These works collectively address intelligent scheduling under mobility uncertainty, where decisions must be made sequentially and under partial system information.

In parallel, the chapter reviews reliability and fairness considerations, which introduce additional system-level objectives and constraints that directly shape the formulation of scheduling and optimization problems. These aspects are essential for ensuring that scheduling policies are not only efficient but also robust, scalable, and equitable across heterogeneous users and charging resources.

Accordingly, the chapter is organized to progressively connect enabling technologies, system architectures, and decision-making frameworks to the formulation of intelligent scheduling and optimization in 6G-ITS. It begins with communication and system foundations, then advances to charging network design, scheduling and routing strategies, and reliability-aware resource allocation, before concluding with a comparative analysis that positions this work within the existing literature.

2.1 Introduction

The realization of ITS capable of supporting autonomous ground and aerial vehicles is tightly coupled with advances in wireless communication technologies. As mobility services become increasingly data-driven, time-sensitive, and distributed, communication networks must provide not only high data rates but also ultra-reliable, low-latency, and intelligent

connectivity. Understanding the evolution of cellular communication and the vision of 6G is therefore essential to contextualize emerging ITS applications and the charging and coordination challenges addressed in this thesis.

2.1.1 History and Evolution of Cellular Communication

The evolution of cellular communication technologies provides essential context for understanding the increasing system complexity, performance demands, and architectural requirements that motivate next-generation networks.

In the late 19th century, Guglielmo Marconi demonstrated the feasibility of wireless long-distance communication through experiments with electromagnetic waves [20]. In 1898, Marconi's transceiver successfully transmitted a wireless message across 18 miles, marking an important milestone in the development of wireless communication systems. Early advancements in radio transmission, followed by innovations such as television broadcasting and satellite communication, significantly contributed to the evolution of wireless technologies and their impact on modern society. Over the past five decades, mobile communication systems have progressed from the first generation (1G) to the current fifth generation (5G), each providing substantial improvements in service quality, capacity, and application support.

The 1G of mobile networks, introduced in the 1980s, relied on analog techniques to enable basic voice communication through mobile devices equipped with bulky antennas and large batteries [1], [2]. Each voice call was assigned a dedicated narrow frequency channel, allowing wireless communication between two supported devices over a cellular network. While 1G represented a breakthrough in mobile communication, it suffered from significant limitations, including susceptibility to interference, frequent call drops during handoffs, short battery lifetimes, and limited security [3], [4]. Furthermore, the absence of standardized protocols restricted roaming and interoperability across different service providers. Despite these shortcomings, 1G established the foundation for the mobile communication revolution and provided the push for the development of the second generation (2G), which sought to address its deficiencies and expand wireless communication capabilities.

The 2G, introduced in the early 1990s, brought about two major modifications. First, it shifted wireless mobile communication from analog to digital technology, exemplified by the Global System for Mobile Communications (GSM) [1], [2]. GSM addressed the issue of standardization in Europe and was later adopted in other regions over competing technologies such as code-division multiple access (CDMA) and personal digital cellular (PDC) [5]. Second, 2G expanded the market from niche users to a broader population. The global proportion of

users increased from approximately 10% to 20% within two decades [6], supported by a reduction in call costs from $0.10 to $0.01 per minute. This was enabled by improved voice quality, as well as data services such as short message service (SMS) and multimedia messaging service (MMS), coupled with roaming capabilities [3], [4], [5].

By the end of the 1990s, with several mobile service providers competing for the market, 2G had become widely accessible. Anticipating the growing demand for internet-based multimedia services, the focus shifted to incorporating data support, giving rise to 2.5G through General Packet Radio Service (GPRS) and later Enhanced Data GSM Evolution (EDGE), serving as a migration path toward third-generation (3G) networks [3], [4]. These technologies allowed operators to provide basic data services at low bit rates, which would later be expanded in 3G.

Introduced in 2000 as IMT-2000 by the International Telecommunication Union (ITU), 3G aimed to enhance telecommunications through improved voice services, higher data throughput, quality of service (QoS), and information security [2], [4]. Supporting data rates from 144 Kbps to 2 Mbps, 3G utilized packet switching for voice and data communication, except for the air interface [2], [3]. Key features included digital broadband, high-speed internet, and enhanced QoS. Alongside technologies such as WCDMA and CDMA2000 [2], 3G enabled the emergence of smartphones and a broad application ecosystem. Despite challenges including increased power consumption and higher network costs, 3G facilitated innovations such as video calls, mobile television, online radio, email, and mobile applications, paving the way for the introduction of 4G technology.

Fourth-generation (4G) mobile technology evolved from 3G [1], [2], [4], adopting systems such as WiMAX and LTE, and replacing circuit switching with an all-IP system that improved broadband speed and reliability globally. By 2010, 4G introduced higher network capacity and peak speeds of up to 100 Mbps during handoffs [2]. It also implemented LTE for simultaneous voice and data transmission, incorporating technologies such as carrier aggregation and massive multiple-input multiple-output (MIMO) to enhance network capacity. Through orthogonal frequency division multiple access (OFDMA), 4G improved spectrum efficiency, reduced latency, and increased bandwidth, supporting enhanced mobile services and fixed internet capabilities. The introduction of services such as Voice over LTE (VoLTE) and Voice over Wi-Fi (VoWiFi) enabled internet-based calling and improved voice connectivity in areas with limited cellular coverage [7]. With its focus on high-speed data and real-time streaming, 4G supported features including high-speed handoff, MIMO technology, and global mobility, enabling a wide range of services such as high-definition (HD) voice,

SMS, MMS, mobile television, wearable device integration, HD video streaming, global roaming, and online gaming [21], [23], [24]. Overall, 4G substantially increased data capacity and enhanced the user experience. While these advances enabled high-speed mobile broadband, they also marked the beginning of increasingly dense, heterogeneous, and data-driven network environments.

From 1G to 4G, the primary focus of cellular networks was on connecting people. Fifth-generation (5G) networks expanded this focus to connect all types of devices, enhancing the Internet of Things (IoT) and various industries by enabling three major usage scenarios [28], [29]: enhanced mobile broadband (eMBB) with data rates in Gbps, massive machine-type communication (mMTC) to connect millions of devices per square kilometer, and ultra-reliable low-latency communication (URLLC) with air-interface latency measured in milliseconds. These capabilities improved latency, throughput, and data speeds, facilitating applications such as remote surgery and intelligent transportation systems.

5G operates in the millimeter-wave spectrum using OFDMA for data rates up to 20 Mbps and frequency bands of 2-8 GHz, with MIMO technology increasing network capacity without additional transmission power [30]. Introducing mid-band and high-band frequencies to increase coverage distance and resilience against interference, 5G enables high-speed data transmission for video streaming, accurate location tracking, low-latency communication, and real-time analytics [30]. Its architecture supports cloud-native, software-defined networks (SDN), and virtualization technologies, enabling flexible, programmable networks with simplified management through control plane and user plane separation (CUPS) [29], [31], [32]. Network slicing optimizes resource allocation by dividing the physical network into virtual networks tailored for specific use cases [30], [33]. Multi-connectivity support across 5G, LTE, Wi-Fi, and fixed access resolves previous limitations in handling large numbers of devices, extends cloud service capabilities as distributed data centers, improves battery efficiency and performance for mobile users, and drives innovation in IoT applications [30], [33]. However, the stringent requirements of emerging applications increasingly challenge the ability of existing network paradigms to scale efficiently and operate reliably.

Despite the rapid deployment of 5G, which is expected to reach 85% of the world's population by end of 2029 [34], its limitations have become apparent, paving the way for 6G. While 5G connects diverse devices and supports the IoT, its complexity and limited capacity hinder the full realization of the Internet of Everything (IoE). Many areas still lack network access, and traditional management struggles with increasing network density and complexity [34], [35]. Critical applications like virtual augmented reality (VAR), extended reality (XR),

and telemedicine require terabit-per-second (Tbps) data support, beyond 5G's capabilities [35], [36]. Although 5G employs advanced technologies such as SDN, network slicing, and virtualization to improve analytics, video streaming, and location tracking, its frequency bands limit information capacity and resource allocation. In contrast, sixth-generation (6G) networks aim to establish a ubiquitous communication infrastructure integrating air, sea, and satellite systems, transforming the physical world into a digital domain [35], [36], [37]. By utilizing advanced technologies such as terahertz (THz) bands, artificial intelligence (AI), and massive MIMO, 6G will enable precise sensing, context-aware networks, and efficient data management [4], [28]. With a focus on sustainability, reliability, and universal accessibility, 6G is expected to support innovative applications and lay the foundation for Industry 5.0 and beyond.

This historical perspective highlights the continuous evolution of mobile networks and the increasing demands on capacity, reliability, and intelligence. Building on this context, the next section examines the envisioned capabilities, key technologies, and potential use cases of 6G networks, establishing a foundation for understanding their role in future applications.

2.2 Path Towards 6G

2.2.1 Envisioning 6G

The vision of 6G extends beyond terrestrial mobile networks to integrate air, sea, and satellite communications, creating a ubiquitous mobile network with humans at its center [28]. This transformation is expected to digitize the physical world, enabling immersive communication and connected intelligence through domain-to-domain twinning [21], [36], [38]. To manage the vast amounts of data generated and facilitate efficient inter-communication among IoT and IoE devices including CAEVs and UAVs, 6G will employ machine learning (ML) and distributed computing [39]. Intelligent edge computing solutions and SDNs will leverage data insights for context-aware networks, supported by THz-band, AI, and Massive-MIMO technologies [39], [40], [41]. These advancements aim to minimize energy consumption, resource usage, and operational costs, aligning with the need for a sustainable network design [41], [42]. Ensuring reliability, security, trustworthiness, fairness, and accessibility, 6G will adhere to global standards and policies while prioritizing equitable access for all users [43], [44].

By providing controllable interfaces for diverse applications such as holographic telepresence, remote surgery, and real-time coordination of autonomous vehicles, 6G will define requirements and key performance indicators relevant to ITS. These envisioned

capabilities will also inform standardization efforts by organizations such as the ITU, shaping the evolution of future connectivity and enabling scalable, interoperable ITS infrastructures.

2.2.2 6G Use Cases

The shift from 5G to 6G networks is driven by the recognition that current 5G usage scenarios eMBB, URLLC, and mMTC, may soon be insufficient for emerging applications [28]. To address these limitations, three novel usage scenarios have been proposed, building on and extending the 5G framework [28]. The first scenario, ultra-mobile broadband (uMBB), aims to realize ubiquitous, high-quality communications for a connected world. This scenario, formed at the intersection of eMBB and mMTC, facilitates applications such as digital twins, universal connectivity, and enhanced on-board communications for CAEVs, UAVs and ITS [28], [45]. The ultra-reliable low latency broadband communications (ULBC) scenario, on the other hand, caters to applications that demand both extremely low latency and high throughput, including holographic telepresence, tactile internet, and real-time coordination of CAEVs and UAVs. Lastly, the massive ultrareliable low latency communication (mULC) scenario combines low latency with ultra-dense connectivity to support the deployment of actuators and sensors in vertical industries and smart mobility networks [28], [45].

Moreover, the Next Generation Mobile Networks Alliance (NGMN) [46] further identifies four key usage scenarios expected to guide 6G deployment and investment from 2030 onward: Enhanced Human Communication (EHC), Enhanced Machine Communication (EMC), Enabling Services (ES), and Network Evolution (NE). EHC applications focus on immersive human interaction, holographic telepresence, and teleoperation, relevant to both mobility and remote operations. EMC emphasizes collaboration between autonomous machines, UAVs, and robotics, enabling intelligent sensing, vehicle-to-everything (V2X) communication, and coordination across ITS infrastructures. ES use cases highlight location-aware services, environmental sensing, and secure data exchange for applications including digital healthcare and ITS. NE addresses technological evolution in AI-driven networks, energy efficiency, and ubiquitous coverage, all critical for managing complex, multi-modal ITS networks [21].

Finally, 6G usage scenarios are expected to evolve continually until 2030 and can be grouped into three overarching categories: production, life, and society. Smart production leverages UAVs, drones, and CAEVs with digital twins, Virtual Reality (VR), and Augmented Reality (AR) to enhance manufacturing, logistics, and mobility efficiency. Smart life applications aim to improve daily living through advanced body-area networks, tactile internet, and context-aware ITS services. Smart society applications utilize 6G's ubiquitous

connectivity to enable rapid information dissemination, multi-modal communication, and real-time coordination across transportation networks, ensuring that ITS infrastructure can scale to meet future mobility demands [21].

Building on these envisioned applications and usage scenarios, understanding the key performance indicators and underlying architecture of 6G is essential for evaluating its suitability to support emerging ITS applications, including CAEVs and UAVs.

2.2.3 6G Key Performance Indicators

Mobile data traffic is expected to quadruple in the coming years, driven by the proliferation of connected devices and demanding applications. With the advent of 6G, which aims to create a truly connected world, the volume of digital data generated by billions of IoT devices including connected vehicles, aerial platforms, and human users is anticipated to reach unprecedented levels, measured in Zettabytes (ZB) [36]. To meet the heightened demands of emerging applications such as immersive VR/AR, real-time traffic management, and digital twin-enabled transportation systems, 6G networks must surpass the capabilities of existing 5G networks, necessitating a 100-fold improvement in spectrum efficiency [36], [46], [47].

In pursuit of enhanced performance and QoS, 6G targets peak data rates of around 1 Tbps and ultra-low latency ranging from 10 to 100 microseconds [21]. These specifications are vital for supporting bandwidth-intensive tasks such as remote surgery and immersive VR experiences, demanding high-definition video resolutions like 8K. To achieve these ambitious goals, 6G networks plan to leverage THz frequencies and spatial multiplexing to increase capacity by up to 1000 times, while prioritizing sustainability and energy efficiency through the integration of AI and other enabling technologies [47], [48]. Moreover, 6G aims for ubiquitous connectivity by integrating air, sea, and space communication, ensuring seamless coverage in three-dimensional space [28], [47], [48]. By deploying mobile base stations and increasing the density of connected devices to 107 per square kilometer, along with achieving traffic capacities of 1 Gb/s per square meter [48], 6G networks aim to enable highly responsive, context-aware ITS and IoE systems.

In addition to the impressive advancements in connectivity, 6G technology promises enhanced reliability, positioning accuracy, and receiver sensitivity. The perceived availability of nearly 100% uptime and support for high mobility exceeding speeds of 1000 km/h are indicative of the robustness of 6G networks [28], [48]. Moreover, the coverage percentage is expected to increase from 99% to an astonishing 99.9999% reliability, significantly reducing

the likelihood of service disruptions [28], [48]. Additionally, positioning error is slated to decrease from the meter to centimeter level, ensuring greater accuracy in location-based services. Furthermore, receiver sensitivity is anticipated to surpass 130 dBm [28], enabling more reliable and efficient data transmission.

These improvements in reliability, positioning accuracy, and receiver sensitivity underscore the transformative potential of 6G technology in revolutionizing communication and connectivity. Moreover, the heightened emphasis on cybersecurity and encryption reflects a proactive approach to safeguarding data transmission against potential threats from eavesdroppers [28], [43], [44]. By prioritizing the confidentiality and integrity of data, 6G networks aim to provide users with a secure and seamless communication experience, paving the way for a future of unprecedented connectivity and innovation.

Achieving these ambitious performance targets requires a carefully designed 6G architecture that integrates terrestrial, aerial, and satellite networks with intelligent control and edge computing, forming the foundation for context-aware and highly reliable transportation systems.

2.2.4 6G Architecture

Authors in [28], [35] have proposed a 6G architecture that builds on 5G advancements and is characterized by its three-dimensional nature, encompassing infrastructure for ubiquitous 3D coverage, a network for enhanced stratification, and control for intelligent connections as seen in Figure 2.1 [28]. A four-tiered infrastructure integrates non-terrestrial networks (space, air, and sea) with terrestrial networks to create a large-scale, cell-free network supporting diverse applications such as space internet services, undersea sensing and ITS. The terrestrial tier, utilizing THz frequency bands, will be more crowded and denser, necessitating additional base stations to mitigate path loss. UAVs and satellites in other tiers will extend coverage, and real-time control and intelligence will support tactile internet and coordination of connected autonomous and aerial vehicles. Visible Light Communication (VLC) is identified as key for THz applications due to its propagation performance, bandwidth, and energy efficiency, particularly in air and sea networks.

Table 2.1: Comparing features of 4G, 5G and 6G technologies.

Features	**4G**	**5G**	**6G**
Usage Scenarios	Mobile Broadband (MBB)	eMBB, uRLLC, mMTC,	UMBB, ULBC, mULC,
Applications	• High-Definition Videos • Voice • Mobile TV • Mobile Internet • Mobile Pay	• VR/AR/360 Videos • UHD Videos • V2X, early connected vehicle support • IoT • Smart City/Factory/Home • Telemedicine • Wearable Devices	• Holographic Verticals and Society • Tactile/Haptic Internet • Full-Sensory Digital Sensing and Reality • Fully Automated Driving • Industrial Internet • Space and Sea-travel • IoE and ITS Management Systems, Connected UAV/CAEV fleets
Network	Flat and All-IP	• Cloudization • Softwarization • Virtualization • Slicing	• Intelligentization • Cloudization • Softwarization • Virtualization • Slicing
Connecting	People	People and Things	People, Machines, and World
Peak Data rate	1 Gbps	10 Gbps	1 Tbps
Latency	10-50 ms	1 ms	10-100 microseconds
Connection Density (devices/ km^2)	100,000	1,000,000	10,000,000
Reliability	99.99%	99.999%	99.9999%
Spectrum and Energy Efficiency	Moderate	High	100 times more efficient than 5G
Coverage	95%	99%	99.9999%
Positioning Accuracy	10 m	1 m	1 cm
Frequency Bands	< 3GHz	3-100 GHz	THz bands
AI Integration	Minimal	Emerging	Advanced, integrated for autonomous mobility and ITS management
Technologies	• OFDM • MIMO • Turbo Code • Carrier Aggregation • HetNet • ICIC • D2D Communications Unlicensed Spectrum	• mm-wave Communications • Massive MIMO • Low-Density Parity-Check (LDPC) and polar codes • Flexible Frame Structure • Ultra-dense Networks • NOMA • Cloud/Fog/Edge Computing	• THz Communications • Sub multi-meter wave MIMO • Intelligent surfaces and beam forming • Orbital angular momentum (OAM) Multiplexing • Laser and visible light communication (VLC) • Blockchain-Based Spectrum Sharing • Quantum Communications and Computing AI and ML

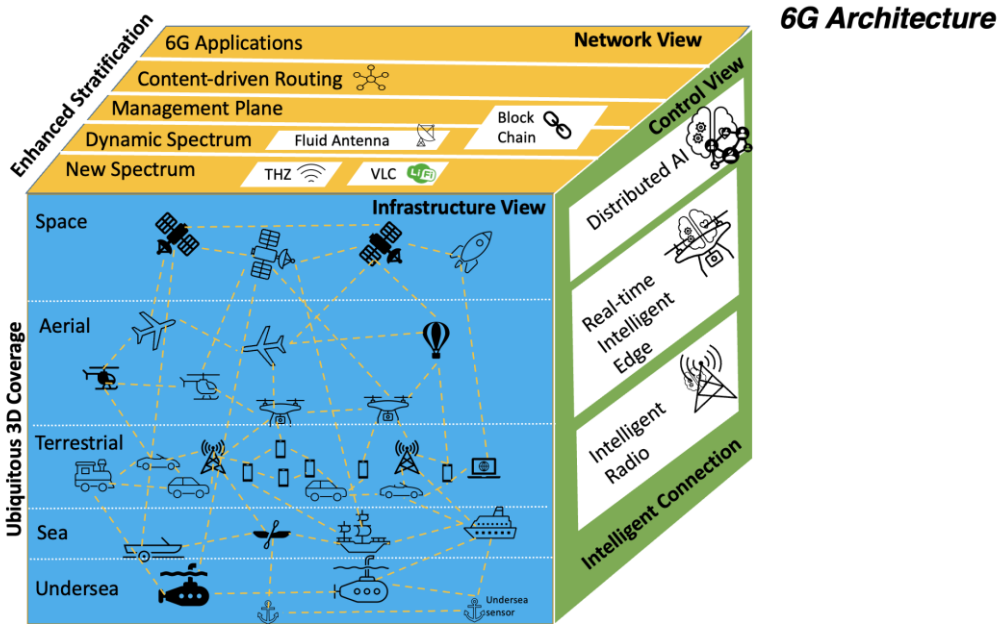

Figure 2.1: 6G Architecture.

Alternatively, the 6G architecture can be seen from different perspectives as proposed in [49]. 6G will include mobile cellular, satellite communications, airplane communications, underwater communications, and VLC from the network access perspective. The goal of 6G services extends from people, machines, and objects in the physical world to the virtual world when considering network service boundaries. 6G integrates air, sea, ground, and space networks to achieve global seamless connectivity. Compared to 5G, 6G improves transmission rates, spectrum efficiency, network efficiency, energy efficiency, end-to-end latency, reliability, and connection density. Unique to 6G is the network-intelligent perspective, in which the network and its users form a unified system. AI and ML learn from individual and system-level behaviors to enhance QoE and QoS, supporting applications such as ITS, digital twins, and UAV coordination.

China Mobile Research Institute's SOLIDS architecture proposed in [38], [50] for 6G exemplifies six features: soft, on-demand fulfillment, lite, native intelligence, digital twin, and native security. This architecture emphasizes ultimate QoS and QoE, easy and on-demand network deployment, scalability, expandability, independence, and automation. SOLIDS addresses intelligent management and sharing of multi-party data, computation resources, storage, and radio frequency resources, while also tackling inherent Internet security issues. The logical architecture comprises three layers including resource, network function, and application, and four planes: data collection, AI, security, and sharing and cooperation. These planes enable AI capabilities, security services, and resource sharing, supporting applications like digital twins, VR and ITS management.

2.2.5 6G Research and Standardization Efforts

To achieve 6G's objective of ubiquitous connectivity and support emerging applications such as ITS management, UAV coordination, and CAEV integration, global standardization efforts and policies must be accepted worldwide. Previous generations have shown that adherence to global standards is effective for wider acceptance and adoption of mobile communication technology, particularly in supporting advanced vehicular and aerial systems. Various local initiatives and research projects, guided by existing global standards, are in development and testing phases. International standardization organizations like 3rd Generation Partnership Project (3GPP), European Telecommunications Standards Institute (ETSI), ITU, and Open RAN (O-RAN) will drive the principal design of 6G and help define network interactions [51]. The goal of these efforts is to enable commercial application with proposed controllable interfaces [51]. The first 6G networks are expected around 2030, with research efforts currently underway and expected to continue until 2026, followed by standardization work [36]. Beyond 5G research projects are scheduled to end in 2023.

Several notable European research projects are contributing to 6G development. The 6G Flagship [52], funded by the Finnish Academy and operated under the University of Oulu, aims to build sustainable 6G technology and develop vertical applications on a 6G test network. European 6G projects [53] [54], under the 5G Infrastructure Public Private Partnership (5G PPP) [55] and funded by Horizon Europe, include initiatives like TeraFlow [56], [57], Hexa-X [58], [59], 6G BRAINS [60], [61], DAEMON [62], [63], AI@EDGE [64], [65], and MARSAL [66], [67], focusing on various aspects such as SDN controllers, AI integration, and resource management, which are critical for applications including autonomous vehicles, UAV operations, and ITS coordination. Other projects, such as DEDICAT 6G [68], [69] and REINDEER [70], [71], aim to develop intelligent applications and smart connectivity platforms. Additional projects like RISE-6G [72], [73] and B5G-OPEN [74], [75] are designing innovative communication technologies and prototypes. As earlier projects ended around 2023, new initiatives worth €250 million have been announced in Europe under the Smart Networks and Services Joint Undertaking (SNS JU) [76], targeting sustainable, reliable, and climate-friendly network infrastructure and services through four streams of research projects. The Next Generation Mobile Networks (NGMN) Alliance [77], based in Germany, also plays a crucial role in ensuring future networks meet user demands and expectations.

In Asia, particularly in China, Japan, and South Korea, significant 6G research efforts are underway. China's Purple Mountain Laboratories, in collaboration with China Mobile and Fudan University, achieved a world record 6G level wireless transmission speed of 206.25

gigabits per second [78]. China has formed a consortium involving government departments, universities, research institutes, and enterprises to work on 6G, with a focus on contributing to standardization efforts [79]. Companies like Huawei, ZTE, and China Unicom are actively engaged in 6G research and development, with China holding the most 6G application patents globally, many of which cover high-speed communication, aerial platforms, and vehicular networks relevant to ITS. [80]. In Japan, a $450 million investment has been allocated for 6G research, with companies like NTT DOCOMO, NEC, and Fujitsu collaborating with NOKIA to conduct experiments on commercial 6G communication technologies [81], [82]. Additionally, Japan's B5G Promotion Consortium and the ATIS's Next G Alliance have entered into agreements to cooperate in the development of 6G networks [83], [84], [85]. South Korea's Ministry of Science and ICT is overseeing significant funding KRW 220 billion until 2025 to drive research in areas like low earth orbit satellites and ultra-precision networks, with investments in the establishment of 6G research centers in universities including Korea Advanced Institute of Science & Technology (KAIST) and Sungkyunkwan University and Korea University [86].

In North America, the NEXT G Alliance [87], [88], established within the Alliance for Telecommunications Industry Solutions (ATIS) [88], leads wireless communication technology development, including 6G, through collaboration with private sector entities. Founding members include major companies [89] like AMD, Apple, AT&T, NOKIA [90], Ericsson [91], [92], Bell [90], and Verizon, among others, while contributing members comprise research institutions and industry players [89], [93]. The Next G Alliance has identified various 6G use case groups in [94], including multi-sensory extended reality, distributed sensing and communication, personalized user experiences, and network-enabled robotics and autonomous systems, which directly align with research in UAV and CAEV coordination within ITS. Projects like 6G@UT [95] at the University of Texas at Austin and the NSF's RINGS [96], [97] program are actively contributing to 6G research and development in the United States, with a focus on areas like machine learning, pervasive sensing, and resilient network architectures. Internationally, organizations like the ETSI [98] and the ITU [99] are laying the groundwork for 6G standards, with efforts to bridge research, standards, and industry [99], [100], [101], [102], [103].

The journey from 1G to 6G represents a transformative evolution in mobile communication, marked by ground-breaking innovations and technological advancements. Each generation has brought forth new capabilities and features, shaping the way we connect and interact with the world. As we anticipate the arrival of 6G, with its promises of unparalleled

connectivity and ubiquitous computing, we stand at the brink of yet another revolution in wireless communication. Table 2.1 provides a succinct overview of the key technologies, KPIs, and features of 4G, 5G, and 6G, highlighting progress that enables emerging applications such as ITS, UAV coordination, and CAEV management.

2.3 Scalable and Interoperable Charging Network Architecture

The transition toward zero-carbon transportation systems, with global targets aiming for net-zero emissions by 2050 [104], places increasing emphasis on electrified and autonomous mobility across both ground and aerial domains. In this context, CAEVs and UAVs are expected to operate as integral components of future ITS, supported by scalable charging infrastructures capable of sustaining continuous, large-scale operation. Meeting these sustainability and operational objectives requires charging network architectures that move beyond isolated deployments and enable interoperable and coordinated energy delivery across heterogeneous vehicles and charging technologies.

Future ITS are expected to operate over heterogeneous environments that combine ground and aerial vehicles, diverse charging technologies, and distributed communication infrastructures. Existing studies address these components largely in isolation, focusing on specific vehicle types, individual charging methods, or narrowly defined network topologies. This section reviews the fundamental building blocks relevant to large-scale charging networks, including vehicle classifications, wireless charging technologies, charging modes, communication topologies, and edge-enabled management paradigms. By examining how these elements are treated across the literature, this section establishes a consolidated view of the architectural design space and highlights the fragmentation that persists across current approaches.

2.3.1 Types of Vehicles

The considered 6G-enabled smart city environment consists of CAEVs and UAVs. These vehicle classes are widely studied as key components of future intelligent transportation systems, yet are often treated independently in existing literature, particularly with respect to charging and coordination mechanisms.

2.3.1.1 Connected and Autonomous Electric Vehicles (CAEVs)

CAEVs, or self-driving vehicles, operate on the ground and can form platoons to enhance traffic flow and energy efficiency [6], [8], [9]. Each CAEV is generally equipped with an onboard computing unit (OBU), GPS, and V2X communication devices. Environmental

perception typically relies on LiDAR, radar, and 2D/3D cameras, while odometry and ultrasonic sensors provide localization and collision detection [9].

CAEVs are powered by batteries charged either via cables or wireless technologies. Current studies often focus on single-mode or fixed-location wireless charging, but emerging research considers bidirectional wireless energy exchange using Wireless Energy Transmitters (WETs) and Receivers (WERs) [5], [6]. Near-field wireless technologies, such as magnetic resonance, typically integrate WERs beneath the chassis, while WETs/ WERs can be mounted on bumpers, headlights, or rooftops to support vehicle-to-vehicle (V2V) and vehicle-to-UAV (V2U) energy transfer [5], [6]. Optical and laser-based transmitters are additionally proposed for long-range communication and energy transfer [105], though current production CAEVs rarely combine all these features simultaneously.

Overall, while these technologies highlight the potential of CAEVs in 6G-enabled intelligent transportation systems, practical deployments currently integrate only a subset of sensors and energy transfer mechanisms, leaving gaps in fully autonomous and connected operations.

2.3.1.2 Uncrewed Aerial Vehicles (UAVs)

UAVs operate in the aerial domain and are increasingly considered complementary to ground vehicles. Existing literature categorizes UAVs by energy capacity and operational roles, ranging from long-endurance vehicles capable of extended missions to energy-constrained platforms reliant on frequent recharging [7].

UAVs are generally equipped with computation units, GPS, communication modules, batteries, and perception sensors, including LiDAR, radar, cameras, accelerometers, IMUs, and collision-detection sensors [7], [10]. Most studies assume UAVs can receive energy from fixed ground stations or other UAVs. However, only a few works explore bidirectional energy transfer or cooperative charging between UAVs and ground vehicles [7], [10]. Both near-field wireless pads [7], [10] and long-range laser transmitters [16] are proposed in the literature for flexible energy delivery, though integration is limited in current systems.

These configurations demonstrate the design space and potential roles of UAVs in future 6G-enabled ITS (6G-ITS), including autonomous flight, energy delivery, and cooperative task execution. However, current implementations typically focus on a subset of capabilities, leaving room for fully integrated and flexible UAV-ground vehicle energy networks.

Taken together, these vehicle capabilities motivate reviewing how charging technologies and charging modes are currently supported, and where interoperability breaks

down when both domains must be served by a single network. While CAEVs and UAVs are widely studied, most work treats charging and coordination within a single domain and under fixed infrastructure assumptions. This leaves open questions on how heterogeneous vehicles, charging technologies, and charging modes can be coordinated within one scalable and interoperable network.

2.3.2 Wireless Charging Technologies and Charging Modes

Wireless charging technologies provide flexible, contactless energy transfer for both CAEVs and UAVs, forming the foundation for scalable and interoperable charging networks.

Wired charging remains the most widely adopted method for powering electric vehicles including CAEVs and UAVs. Conductive wired systems provide high efficiency and reliable performance across charging networks. However, they require physical connectors, are subject to mechanical wear, and often involve significant waiting times at charging stations or landing pads. To address some of these limitations, SWC systems have been introduced, where CAEVs and UAVs can recharge without connectors while parked over a charging pad or landed at a designated station. SWC improves convenience and reduces connector degradation, but like wired charging, it requires vehicles to remain stationary, leading to operational downtime. These challenges motivate research into more advanced DWC solutions.

From an operational perspective, charging approaches for CAEVs are commonly categorized into three infrastructure-based modes: cabled charging networks (CCN), static wireless charging networks (SWCN), and dynamic wireless charging networks (DWCN). CCNs rely on direct physical connections between electric vehicle supply equipment (EVSE) and parked CAEVs, while SWCNs use near-field wireless technologies such as magnetic resonance through wireless charging pads (WCPs) embedded in parking areas or road surfaces. DWCNs extend wireless charging to in-motion scenarios by embedding WCPs along roadways, enabling CAEVs to receive energy while driving. While CCN and SWCN approaches typically involve queuing and waiting times, DWCNs reduce stationary charging delays but often provide partial charging intended to extend driving range rather than fully replenish batteries. As a result, these charging modes are generally viewed as complementary rather than standalone solutions.

Wireless charging technologies offer convenient solutions for powering devices without the need for physical cables. Traditional wireless charging methods for CAEVs typically involve inductive and capacitive charging technologies [106]. Inductive charging [8], [106] utilizes electromagnetic fields to transfer energy between a charging pad on the ground

and a receiver coil installed in the vehicle. While this method offers convenience and eliminates the need for physical connectors, it suffers from limited efficiency due to alignment issues. Capacitive charging [106], on the other hand, relies on electrical fields for energy transfer, but it also faces similar limitations in efficiency and coverage. Reference [106] provides a comparative analysis of Inductive Power Transfer (IPT) and Capacitive Power Transfer (CPT) systems for vehicle charging, highlighting their respective strengths and weaknesses. Simulation studies reveal that IPT exhibits decreasing efficiency above 500 Hz, whereas CPT demonstrates the opposite trend. CPT shows higher efficiency with low air gaps and high frequencies, making it suitable for certain low-powered applications. Conversely, IPT performs better with high air gaps and medium frequencies, making it ideal for high-power applications such as DWC of CAEVs. Our prior work [5], [6], [8] provides optimized track layouts and alignment strategies to improve efficiency and safety.

For UAVs, traditional wireless charging methods often include ground-based stations and high-voltage power lines [7], [10]. Ground-based stations typically require UAVs to land for charging, which can be time-consuming and limit mission durations. Static wireless charging for UAVs is commonly discussed in the context of pad-based or station-based systems, including two-dimensional and three-dimensional wireless charging pad configurations [10]. These approaches aim to improve alignment tolerance and charging reliability during landing or low-altitude hovering but still require UAVs to interrupt missions and remain within proximity of the charging infrastructure. Consequently, static wireless charging for UAVs is often treated as a complementary option rather than a complete solution for persistent or large-scale aerial operations. High-voltage power lines leverage the electromagnetic fields generated by the lines to charge hovering UAVs, but this method presents challenges related to alignment, environmental conditions, and safety. Moreover, laser-powered UAVs exhibit a remarkable 95% efficiency in data collection compared to conventional methods [16].

In contrast, [14] advocates for laser beaming charging as a superior alternative for both CAEVs and UAVs, backed by numerical analysis. Numerical simulations comparing the proposed dynamic optical wireless power transfer (OWPT) system with traditional methods such as resonant Inductive Wireless Power Transfer (IWPT) reveal the significant advantages of laser beaming charging. The proposed laser based dynamic OWPT system demonstrates superior charging energy for ground EVs, providing approximately 16.2919 kWh compared to 15.048 kWh from IWPT over 3.52 km. This evidence positions laser-beaming charging as a

leading solution for DWC, combining high efficiency with operational flexibility, and highlights its role as a key enabler for scalable and interoperable charging networks.

2.3.3 Dynamic Wireless Charging (DWC) System

This section provides an overview of existing DWC solutions for CAEVs and UAVs. DWC system architectures can be broadly categorized as: 1) infrastructure-based DWC and 2) ad-hoc DWC. Designing effective DWC systems for CAEVs and UAVs requires careful consideration of infrastructure layout, energy efficiency, and operational reliability, highlighting challenges that motivate the improvements proposed in later sections.

2.3.3.1 DWC for CAEV

One important aspect in DWC of CAEVs is the charging track layout. Two different DWC track designs popularly used in wirelessly transfer of energy to CAEVs in motion along a road or highway are: 1) long tracks and 2) array of wireless charging pads (WCPs).

The long track design [107] utilizes a single coil that encompasses the length of the road or highway. In comparison, the receiving side, installed underneath a CAEV, is significantly smaller. This simplistic design maintains its mutual inductance around a constant value and is easy to control. A DWC system with this design is comprised of an inverter, regulator, rectifier, power lines and receiving coils. Since maximizing WPT is the main goal of an optimal DWC system, authors in [108], [109] proved delivery of 100 kW power with 80% efficiency over an air gap of 26 cm. More recently, in [109] improved the efficiency to 95% by utilizing T-type tuned topology for WPT. However, long tracks are not very energy efficient as they remain active for the entire duration of charging. Further, they may raise both safety and environmental concerns with the generation of electromagnetic pollution [107], [110]. These limitations highlight opportunities for optimized track layouts and dynamic activation strategies, which are addressed in our proposed scalable and interoperable network design.

On the other hand, the array of WCPs design [5], [6], [107] also known as segmented track design is made up of segmented-coils or WCPs that are as large as the receiving coil installed underneath the CAEVs. These WCPs are laid in series with little to no gap between them. This layout offers higher efficiency and practicality, but the choice of the WCP's length can impact the efficiency due to the magnetic flux leakage. However, our DWC track builder proposed in [5] can suggest an optimal track layout to balance both efficiency and safety. Further, the alignment challenges for higher efficiency are addressed in [8] with an algorithm. This track design remains favored in both industry and academia. It significantly reduces electrical inefficiency and concerns regarding electromagnetic compatibility (EMC) and

electromagnetic field (EMF) safety [111] by activating and deactivating each WCP individually [107].

Besides this for even shorter bursts of charge, methods like V2V charging [112] are available. In this DWC technique, both vehicles come equipped with a transceiver and can transfer typically a small amount of charging wirelessly from one vehicle to the other while maintain an optimal gap for higher charging efficiency. Now, the technologies used for V2V DWC architecture are not limited to magnetic resonance but may include optical laser beaming charging supported by VLC [105]. However, this technique is primarily suitable for emergency use and is not ideal for longer charging sessions, highlighting the need for integrated, scalable network approaches. Further, there are alignment challenge, safety concerns, range limitations, and lack of vehicles with V2V support. Such ad-hoc charging modes are typically considered for short-duration or emergency support and are rarely integrated with fixed infrastructure-based charging networks.

2.3.3.2 DWC for UAV

DWC for UAVs while they hover and perform their operations introduces innovative designs and architectures. One interesting solution is the use of high-voltage power lines [113] that leverages the electromagnetic fields surrounding the lines to charge the UAVs. To transfer the energy from the power lines to the UAVs, methods like navigating the UAV based on the power line's electromagnetic field and using specially designed connectors that resemble the power line's magnetic core have been proposed. This architecture capitalizes on existing infrastructure to extend UAV mission times to save installation and maintenance costs, but alignment challenges, environmental conditions and potential electromagnetic interference may reduce DWC efficiency. These constraints illustrate the need for optimized network architectures for UAV charging. Also, this solution cannot be implemented in urban areas and limits operational range.

A popular DWC solution for UAVs especially for urban applications is DWC from ground-based stations or towers. This involves installing DWC systems in tall structures such as telecommunication towers, high-rise buildings, or roadside units (RSUs) [16]. UAVs can then fly to these towers for a DWC session. This method eliminates the need for UAVs to land on static charging stations, and minimizes the risk of collision, damage or interference with other ground operations while extending mission time. Two primary technologies implement this relatively safe and efficient charging architecture: 1) electromagnetic induction and 2) laser

beaming, with laser-beaming offering a promising path for high-efficiency, scalable DWC networks.

In electromagnetic induction, resonant coils are used on both the towers and the UAVs [114]. When a UAV approaches the charging station, the coils are aligned, and power is wirelessly transferred from the tower to the UAV through electromagnetic induction . This technology is safe, efficient and minimizes the risk of physical damage. However, precise alignment and control is required for efficient transfer. On the other hand, laser beaming charging [16] is a relatively new option to charge UAVs from towers. Laser emitters are installed on the tower to generate directed laser beams towards the UAV which is equipped with laser beam receiver like photovoltaic cells to convert the laser energy to electrical energy for charging. This technology is also practical, energy-efficient, reduces electromagnetic interference, provides longer range than its electromagnetic counterpart and is safer with the elimination of physical connectors. However, it also faces alignment issues and is susceptible to poor weather conditions. Line-of-sight (LOS) obstacles can impact its reliability and efficiency over longer distances, and high-voltage laser can cause safety concerns. Nevertheless, these can be mitigated with new technologies and operational protocols.

UAVs without charging capabilities maintained around 40% efficiency regardless of mission duration. In contrast, laser-powered drones achieved the highest efficiency at 95% outperforming UAVs with other charging methods including charged drones (using induction charging). UAVs with ground charging stations performed better than tethered or cabled UAVs. The efficiency improved as number of ground charging station increased. With laser powered UAVs requiring fewer due to their wider coverage radius. Therefore, laser-beaming charging is a pivotal technology for enabling high-efficiency and scalable UAV DWC solutions.

Like CAEVs, for emergency DWC options, V2V charging option is available. More specifically, UAV to UAV (U2U) charging option is also popular [115]. This involves two UAVs flying near one another, and once aligned, the power is wirelessly transferred from one drone to the other. Both UAVs are equipped with compatible transceiver, and like ground-based charging either electromagnetic induction or laser beaming technologies can be used. Of course, laser-beaming charging option would enable the UAVs to wireless transfer energy at greater distances and higher efficiency. Moreover, other ad-hoc DWC configurations such as CAEV-to-UAV and UAV-to-CAEV provide additional flexibility, scalability, and emergency charging options, which inform the integrated network design discussed later. Similar to V2V

charging for CAEVs, U2U charging is generally explored as a localized or emergency solution, rather than as part of a coordinated, large-scale charging framework.

Unlike existing wired charging systems, DWC frees the CAEVs from the confines of stationary charging stations such as cabled charging and SWC system [116] by eliminating waiting times.

To provide a unified perspective across both CAEVs and UAVs, Table 2.2 compares the main charging methods, highlighting their mobility characteristics, advantages, and limitations.

Table 2.2: Comparison of Charging Methods for CAEVs and UAVs.

Method	Technology	Mobility	Main Benefit	Key Limitation
Wired Charging	Physical connectors	Stationary	High efficiency	Requires vehicle to stop
SWC	IPT / CPT	Stationary	Contactless automation	Requires precise alignment
DWC	Embedded IPT / Laser Beaming	In-motion	Charging while moving	Alignment sensitivity
V2VCharging	Wireless / Optical/ Direct Link	Mobile	No fixed infrastructure needed	Coordination and safety challenges

While the charging technologies and modes summarized in Table 2.2 enable diverse mechanisms for energy transfer across CAEVs and UAVs, they do not, by themselves, define how charging decisions are coordinated at scale. Static, dynamic, and ad-hoc charging approaches such as DWC, V2V, and U2U improve operational flexibility but introduce new challenges related to scheduling, mobility coupling, fairness, and coordination across heterogeneous nodes and charging modalities. As charging networks evolve toward city-scale deployments involving multiple vehicle classes, infrastructure operators, and wireless charging technologies, scalable and interoperable operation increasingly depends on architectural support for computation and coordination rather than on charging hardware alone. This motivates the use of Intelligent Edge Computing as a key architectural enabler for scalable and interoperable charging network designs in 6G-ITS.

2.3.4 IEC-Enabled Coordination for Scalable Charging Networks in 6G-ITS

Since charging infrastructures are no longer limited to large static stations, they are evolving into dynamic and distributed networks that increasingly rely on Intelligent Edge Computing (IEC) for optimization. IEC enhances 6G-ITS by processing data closer to vehicles, charging assets, and grid interfaces, enabling faster decision making and improved reliability in transportation systems. More specifically, IEC moves computation closer to the data source and leverages AI and ML techniques to reduce end-to-end latency and enable responsive control loops for CAEV and UAV charging processes [18], [19]. In addition to improving

operational responsiveness, IEC can support grid stability, facilitate the integration of renewable energy sources, and strengthen security through localized monitoring and control. Figure 2.2 illustrates an IEC-aided view of CAEV and UAV charging within 6G-enabled ITS [117].

Although the literature demonstrates substantial progress in IEC for CAEV and UAV charging, most existing works address these domains separately and assume specific charging infrastructures, communication conditions, or local decision scopes. This creates challenges for city-scale deployment where heterogeneous charging modes, multiple vehicle classes, and multi-operator infrastructures must interoperate under mobility and safety constraints. These gaps motivate the need for scalable and interoperable network architectures in which IEC components can coordinate charging, scheduling, and resource allocation across both ground and aerial domains.

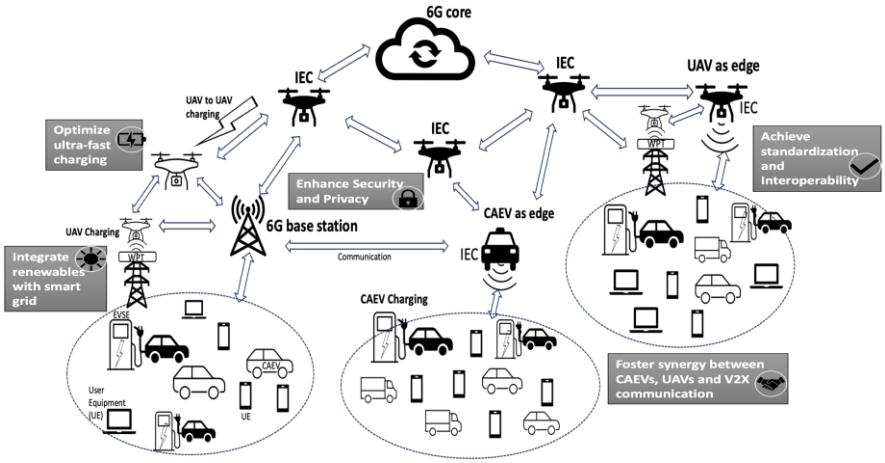

Figure 2.2: IEC-aided CAEV and UAV charging in 6G- ITS.

Next, the pivotal role of IEC in optimizing CAEV and UAV charging within 6G networks for ITS is explored. Various IEC techniques and architectures in the literature are surveyed, highlighting their contributions to charging efficiency, security, and reliability, while identifying open challenges that limit scalability, interoperability, and cross-domain coordination. This discussion provides the background needed to motivate integrated charging network designs in 6G-enabled ITS.

2.3.4.1 IEC for CAEV Charging

In the domain of CAEV charging, IEC signifies a shift from centralized control toward distributed intelligence at charging stations, roadside infrastructure, and vehicles. IEC enables real-time data processing and cooperative computing allocation, which can improve charging station operation, forecasting, and grid-aware control under dynamic traffic and demand. This subsection surveys IEC architectures and techniques for CAEV charging, focusing on practical

applications and highlighting limitations that remain when scaling beyond isolated stations or single-operator settings.

Reference [118] presents a stacked autoencoder neural network (SAE) approach for enhancing load forecasting at CAEV charging stations. The unpredictable CAEV charging behavior is accurately predicted by deploying SAEs at the edge platform. Influential factors like historical load, temperature, and weather conditions are recorded and fed into the IEC device for improved short-term load predictions. This model showcased an impressive 2.54% prediction error, surpassing the traditional approaches of Deep Belief Network (DBN) (2.87%) and Extreme Learning Machine (ELM) (3.71%). This technique lays the foundation for future applications of SAE, promising stable power grid operation and efficient charging station management through the prevention of distribution transformer overload during peak demand periods.

In [119], the concept of electric vehicle edge computing (EVEC) is introduced to leverage parked CAEVs as both energy prosumers and computing nodes. To realize the EVEC architecture for edge computing (EC), the authors employ the bilevel optimization technique where the upper level will optimize the matching of EVs and parking lots for computational offloading while the lower level will optimize the EV power management for power networks. Through innovative linearization techniques, the bilevel problem is transformed into a single-level, nonconvex mixed-integer nonlinear programming problem. Numerical results validated the efficiency and effectiveness of the model. Both the architecture and the optimization technique used for EC hold promise for enhancing CAEV charging and CAEV utility. This model strengthens the leader's role in EV parking and power management, resulting in increased leader utility. Both the architecture and the optimization technique used for EC indicate the potential of integrating CAEV charging decisions with edge-based computation, but practical deployment at scale remains challenged by heterogeneous infrastructure ownership, interoperability across charging assets, and coordination across distributed nodes.

Authors in [18] consider predicting energy demands of prosumer buildings that can be electric vehicle supply equipment (EVSE) to minimize average forecasting loss. The authors emphasize the need for a distributive solution due to the time-dependent nature of energy demand coupled with the unpredictability of CAEV numbers and randomness of energy demand patterns. Hence, the paper proposes an edge assisted attention-based federated learning (FL) algorithm for a multi-step energy demand prediction in prosumer buildings. The system architecture includes prosumer buildings with solar panels, EVSEs, BSS, and edge servers. These components are connected to a remote cloud data center, facilitating efficient energy

management and EV charging in a smart city setting. The methodology employs LSTM-based sequence-to-sequence models, collaboratively trained on local edge servers. The results show significant improvements over the FL approach without attention, achieving smaller values for Average Mean Absolute Error (AMAE), Average Mean Squared Error (AMSE), Average Root-Mean-Square Error (ARMSE), and Average Huber Loss (AHuber) by 8.875%, 14.80%, 7.664%, and 14.525%, respectively. Numerical results demonstrate its effectiveness in reducing forecasting errors compared to non-attention-based FL methods. Additionally, a time-based learning rate decay technique was introduced that further enhanced the model's performance.

Recently, authors in [120] addressed the increasing computational demands associated with CAEV and emerging technologies like AR and autonomous driving by introducing EC into the Internet of Vehicles (IoV). The architecture includes sinking vehicle computing tasks to nearby charging pile servers that are strategically placed on the edge. Thus, minimizing task delays to enhance overall computing capacity, and lowering computation costs. The proposed unloading technique did significantly better than other vehicle-based computing techniques with a 31.7% improvement in task computing efficiency. The paper in [120] showcased the optimization of computational resource allocation by leveraging EC for CAEV charging infrastructure.

Researchers in [121] propose a novel IEC system tailored for the future charging infrastructure in smart cities. The system aimed to address challenges related to CAEV charging and grid management. The modular architecture employs Docker containers for various software modules, thus enabling interoperability with various hardware systems and applications. LoRa-based communication enhances data security and decentralization, allowing for local data handling. Further, the system achieves precise control of CAEV charging stations using Micro-phasor Measurement Units (μ PMUs) to monitor grid conditions and an artificial neural network for state estimation. Grid stability is also enhanced through a reinforcement learning (RL) algorithm that addresses the overloading situation. It is suitable for real-world applications, as it can handle tasks of 13-22ms. However, communication issues, including up to 24% message loss, suggest the necessity of increasing message frequency for longer-distance transmission.

Like [121], researchers in [122] address the challenges of integrating CAEV charging infrastructure into existing distribution networks, particularly focusing on under-voltage issues. A dynamic EC architecture is introduced that uses Dynamic VAr Controllers (DVCs) strategically positioned at low-voltage nodes, which are part of the edge of the grid. These

autonomous DVCs inject reactive power (VAr) to provide voltage support precisely where it's needed, all while communicating and coordinating within the distributed network. Simulations across various scenarios, encompassing residential, commercial, and fleet CAEV charging facilities, reveal that DVCs effectively mitigate voltage issues and reduce imbalance. For instance, when adding 100 residential EV chargers and a 2.7 MW commercial station, which caused a 34% peak demand increase and lowered the minimum voltage to 112.6V, deploying 25 DVCs raised it to 113.7V, demonstrating their effectiveness in addressing network impedance and their cost-effectiveness for voltage control.

Table 2.3:Comparison of papers that focus on CAEV charging aided by IEC.

Ref.	**Architecture**	**Approach**	**Communication Topology**	**Benefits**	**Applications**
[118]	SAE at the edge	Load prediction with SAE	Centralized	Grid stability, 2.54% prediction error	Power grid management
[119]	EVEC for EVs as edge nodes and energy prosumers	Bilevel optimization	Hierarchical	Efficient EV management and increased leader utility	Dual role of EVs for computing and energy
[18]	Prosumer buildings, EVSEs, BSS, IEC, data center	Energy prediction with edge FL	Hierarchical	Enhanced forecasting with error reductions: AMAE (-8.875%), AMSE (-14.80%), ARMSE (-7.664%), AHuber (-14.525%).	Energy prediction tasks
[120]	Servers within EV charging piles	Edge-based offloading of EV tasks	Centralized	31.7% task delay reduction for cost-efficient computing	IoV computing
[121]	Modular design with Docker containers for versatility	LoRa for communication, precise CAEV control (μ PMUs, RL)	Distributed	Real-world ready (13-22 ms), needs better long-distance communication, efficient at 0.2 Hz, up to 24% loss.	CAEV charging and grid management
[122]	Dynamic EC with DVCs	Mitigating under-voltage with DVCs	Distributed	Cost-effective voltage control; 34% peak increase, 113.7V with 25 DVCs	Grid voltage stability for charging
This work	Three-layer IEC-enabled charging network	Charging scheduling and trip planning	Hybrid (Centralized and Distributed)	Reduced travel and waiting time; fairness-aware coordination	**CAEV and UAV** charging in 6G-ITS

Across these IEC-based charging studies, coordination typically follows centralized, hierarchical, or distributed control patterns, which can affect scalability when moving from isolated deployments to city-scale systems. However, most studies optimize charging decisions independently of trip planning and typically consider a single vehicle domain, which limits fairness, scalability, and interoperability under city-scale 6G-ITS conditions.

The rapid growth of CAEV charging demand calls for solutions that are not only accurate and efficient at a local scale, but also deployable across heterogeneous infrastructure.

The surveyed studies show that IEC can improve prediction accuracy, reduce task delay, and enhance grid management through distributed architectures and learning-based methods. However, most works focus on specific station-level functions such as forecasting, offloading, or voltage support, and often assume consistent communication quality and unified control over infrastructure. These assumptions limit interoperability across different EVSE vendors, charging network operators, and mixed charging modes. As summarized in Table 2.3, a key open challenge is developing IEC-enabled charging frameworks that remain scalable under city-scale demand and interoperable across distributed charging assets.

2.3.4.2 IEC for UAV Charging

Within the landscape of IEC, UAV charging introduces additional complexity due to mobility in three-dimensional space, stricter energy constraints, and greater sensitivity to environmental uncertainty. IEC can support UAV charging by enabling near-real-time scheduling, trajectory-aware planning, and distributed learning under privacy and resource constraints. This subsection surveys representative IEC architectures and techniques for UAV charging and highlights limitations that affect scalability, reliability, and interoperability when multiple charging nodes and UAV fleets must coordinate in shared 6G-ITS environments.

Reference [123] tackles the UAV charging challenge with a novel two-stage solution for next-day energy scheduling at urban prosumer operated drone charging stations. The first stage uses HFL with LSTM architecture to predict energy requirements while maintaining data privacy. The second stage deploys stochastic game-based MADDQN with a community agent-independent approach to optimize energy scheduling aiming to find Nash equilibrium. Experimental findings proved the prediction accuracy of this approach with a minimal mean squared error of 0.015. Further, it achieved the highest energy satisfaction and quality of experience compared to other existing methods. This approach leveraged IEC to enhance UAV charging efficiency and reliability.

An EC based approach for optimizing UAV swarm path planning and energy management in UAV charging scenarios is presented in [124]. Authors in [124] tackle the challenge of efficiently servicing multiple spatial locations with dynamic user demands using a large UAV swarm. The single UAV algorithm proposed offers low computational complexity. In a large-scale assessment with 100 locations and up to 400 demand releases, their algorithm consistently outperforms traditional partitioning as the number of UAVs increases, converging to a high percentage of serviced demands. Energy efficiency is enhanced by allowing UAVs to visit charging stations with planned paths, which is facilitated by an integer linear program and an iterative algorithm. Further integration of IEC could enhance real-time

decision-making, and exploring online algorithms for unknown user demands could make UAV charging systems even more robust.

Both papers, [19] and [125], delve into the realm of UAV charging within the context of Mobile Edge Computing (MEC) and aerial edge networks, with a shared emphasis on enhancing energy efficiency.

In [19], UAVs serve as a flying edge server and collect tasks from user devices. The challenge is to strike a balance between maximizing data collection and minimizing energy consumption. Hence, the authors in [19] introduce a Priority-based DRL approach that integrates trajectory planning, communication scheduling, charging scheduling, and task offloading. This approach outperformed baselines, thus making it a promising solution for energy-efficient UAV operations. The integration of charging stations ensured sustained performance, while the application of IEC enhanced real-time decision-making.

On the other hand, in [125], the focus on rechargeable UAVs within aerial edge networks is a prominent paradigm in the anticipated 6G era. These aerial networks rely on UAVs to provide task processing and data caching in areas lacking traditional infrastructure. The limited onboard capacity of UAVs is a primary concern affecting UAV endurance. Therefore, [125] proposes an aerial edge network aided by distributed charging services, optimizing energy consumption while considering UAV trajectory planning, battery charging scheduling, and edge resource allocation. This approach also uses DRL to design an intelligent iterative algorithm for obtaining energy-efficient aerial edge strategies. Further, significant reductions in UAV energy costs compared to benchmark approaches were achieved.

Benefits from the techniques of [19], [123], [124], [125] include improved energy management, energy-efficient charging strategies, and enhanced UAV performance, which can extend UAV flight times and sustain mission-critical operations. In the future, these innovations could revolutionize UAV charging by making it more sustainable and responsive. They might find applications in various domains such as surveillance, disaster response, and remote sensing, ensuring that UAVs can operate effectively in resource-constrained environments while supporting data-intensive tasks. Additionally, continued research and refinement of these algorithms will likely lead to even more energy-efficient and responsive UAV operations in edge computing environments, marking a promising direction for the future of UAV technology for ITS applications.

Like [124], authors in [126] advocate for a multi-UAV approach assisted by IEC for an Artificial Intelligence of Things (AIoT) application. The authors propose an optimized multi-UAV assisted FL framework to address the challenge of limited onboard resources and battery

capacity in each UAV node. Regular IoT devices are used to handle training tasks while multiple UAVs perform local and global aggregation tasks. An online resource allocation (ORA) algorithm minimizes training latency by jointly deciding client selection and global aggregation server decisions. Moreover, Lyapunov optimization and DRL schemes are harnessed to improve training performance, resulting in a 17.01% reduction in training latency and an 18.87% decrease in energy costs.

On the other hand, reference [127] addresses computation offloading to edge servers, overcoming UAV energy and computation constraints, particularly with straggling edge servers and weather uncertainty. As a result, a novel approach known as coded distributed computing (CDC) for computation offloading is presented. The framework includes UAVs that retrieve computation results when the number of returned copies meets a recovery threshold. To minimize network costs, UAV energy consumption, and resource allocation issues, the authors devise a two-phase stochastic coded offloading scheme (SCOS). In the first phase, appropriate UAVs are allocated to charging stations considering weather uncertainty. In the second phase, a z-stage stochastic integer programming (SIP) optimizes computation subtask offloading and local processing while considering uncertainty and demand variations. Simulation results demonstrated the effectiveness of this approach in minimizing the network costs and UAV energy consumption amid stochastic uncertainties. Simulation results also highlighted SIP's consistent superiority over Expected-Value Formulation (EVF) and random schemes in adapting to cost changes by reducing shortfall costs.

The benefits of approaches in [126] and [127] include improved scalability and precision for AIoT applications, particularly in resource-constrained and unpredictable UAV environments. These studies pave the way for more efficient and resilient AIoT deployments with UAV and IEC integration, promising advancements in the future.

Both papers, [128] and [115], explore innovative approaches to UAV charging with a focus on extending flight time and reducing human interventions with potential applications in IEC scenarios of ITS.

In [128], a capacitive power transfer system is introduced, emphasizing lightweight receivers and robust misalignment tolerance. The system’s architecture features a reconfigurable capacitive coupler with adaptable copper plates on the transmitter side, ensuring compatibility with various landing positions and directions. The receiver incorporates hollow cylindrical copper-foil sleeves, enhancing structural flexibility and misalignment tolerance. This technology offers efficient power delivery, capable of delivering 212.1W with an 82.5% dc-to-dc efficiency. It allows UAVs to be powered with significant stability and efficiency

across different landing positions and directions, making it suitable for UAV autonomous charging scenarios in ITS applications.

Table 2.4: Comparison of papers with focus on UAV charging aided by IEC.

Ref.	Architecture	Approach	Communication Topology	Benefits	Applications
[123]	HFL-LSTM, MADDQN	Stochastic Game	Hierarchical	Efficient energy scheduling, Data Privacy, MSE=0.015	Improved UAV charging, Enhancing QoE
[124]	Cooperative UAV swarms	Integer Linear Programming, Cooperative iterative algorithm	Distributed	Optimal routing and efficient energy use	Multi-UAV systems, Edge tasks
[19]	Priority-based DRL, UAV as edge servers	Integrating multiple aspects for energy efficiency with DRL	Centralized	Improved energy efficiency by 6.36%-54.42% over DDPG, DQN, GREEDY, and RANDOM.	Energy-efficient UAV operations and real-time decisions
[125]	Rechargeable UAVs in 6G-era Aerial edge network	DRL-based intelligent iterative algorithm	Distributed	UAV energy cost reduction	Sustainable edge aerial networks with enhanced endurance
[126]	Multi-UAV-assisted FL	Online Resource Allocation, Lyapunov optimization, DRL	Distributed	Reduced training latency (17.01%) and lower energy costs (18.87%)	Optimized UAV charging to enhance AIoT applications
[127]	CDC	Two-phase SCOS and Stochastic SIP	Centralized	Minimize energy use, lower network costs	Mitigating UAV constraints in dynamic environments
[128]	Capacitive power transfer	Reconfigurable coupler	Centralized	Lightweight, robust alignment, 212.1 W, 82.5% efficiency	Flexible UAV charging, Enhanced adaptability
[115]	Wireless bidirectional DAB converter	MATLAB/Simulink simulation of wireless power transfer between UAVs	Distributed	Extend flight time, reduce human intervention	Multi-agent systems, packet deliveries, inspections, surveillance
This work	Three-layer IEC-enabled charging network	Charging scheduling and trip planning	Hybrid (Centralized and Distributed)	Reduced travel and waiting time; fairness-aware coordination	**CAEV and UAV** charging in 6G-ITS

Reference [115], on the other hand, introduces wireless power transfer technology for autonomous drone charging, aiming to extend UAV flight time and reduce human interventions. The concept of drone-to-drone opportunity charging is explored. This is particularly relevant in the context of multi-agent systems where drones are used for various applications such as packet deliveries, inspections, and surveillance. The key technology discussed is the design and simulation of a wireless bidirectional dual active bridge (DAB) converter using MATLAB/SIMULINK. This technology has the potential to significantly enhance UAV performance by increasing flight duration through mid-air opportunity charging between drones. While addressing alignment challenges and alignment tolerance, [115] opens possibilities for more autonomous and extended UAV operations.

As UAV charging integrates with IEC through the surveyed techniques and architectures summarized in Table 2.4, new capabilities emerge in scheduling, privacy-preserving learning, and robust offloading under uncertainty. These studies demonstrate strong performance gains in specific settings, but they commonly assume a particular aerial edge architecture, a fixed charging service model, or a narrow operational objective. In city-scale ITS, UAV charging must often interoperate with heterogeneous ground infrastructures, mixed charging modes, and multi-operator deployments, while maintaining safety and reliability under mobility and weather variability. These requirements remain only partially addressed in existing works, indicating a need for scalable and interoperable architectures that can coordinate charging and computation across both CAEV and UAV domains.

2.3.5 Architectural Gaps and Motivation

The surveyed literature demonstrates meaningful advances in vehicle technologies, wireless charging mechanisms, and edge-enabled coordination for intelligent transportation systems. CAEVs and UAVs are widely recognized as complementary mobility agents, and multiple charging approaches including wired, static wireless, dynamic wireless, and ad hoc energy transfer have been proposed. However, these efforts are commonly developed in isolation, with most studies addressing a single vehicle class, charging mode, or energy transfer technology, rather than treating charging as a unified network-level problem.

Several gaps limit scalability and interoperability in city-scale deployments. CAEV and UAV charging are often considered independently, charging modes are analyzed in isolation, and magnetic-resonance and laser-based charging technologies are rarely unified within a common architectural framework. In addition, coordination and communication assumptions are frequently tied to a single control style, which constrains deployment across heterogeneous infrastructure ownership, diverse communication conditions, and multi-operator environments. These limitations complicate fair access to charging resources and coordinated decision making under dynamic mobility conditions.

Table 2.5 consolidates these gaps and positions the proposed architecture within the broader design space. By unifying CAEV and UAV charging, supporting multiple charging modes and technologies, and enabling hybrid coordination across centralized and distributed components, the proposed scalable and interoperable charging network architecture aligns with the 6G vision of flexible, service-oriented ITS. This architectural abstraction supports scalable deployment and provides a consistent foundation for coordinated charging operation in future 6G-enabled smart cities.

Table 2.5: Comparison of Identified Architectural Gaps and the Proposed Scalable and Interoperable Charging Network Design.

Gap observed in literature	***Why it matters at city scale?***	***How this work addresses it ?***
CAEV and UAV charging often treated separately	Prevents coordinated planning and interoperability across ground and aerial services	Unified three-layer architecture enabling coordinated CAEV and UAV charging
Charging modes studied in isolation (CCN, SWCN, DWCN, V2V/U2U)	Mixed deployments require coordination across modes and infrastructure operators	Single framework supporting static, dynamic, and ad hoc charging modes
Technology-specific solutions without unifying abstraction	Heterogeneous hardware and vendors limit deployability and scalability	Common abstraction for magnetic-resonance and laser-based charging with realistic power models
Coordination assumptions tied to a single control paradigm	Restricts scalability under multi-operator and heterogeneous ownership	Lightweight interoperable communication framework supporting hybrid coordination
Limited architectural support for system-level services	Lack of coordination leads to congestion, unfair access, and increased delay	Architecture designed to support charging reservation and trip-aware scheduling

2.4 Coordinated Charging Scheduling and Routing in 6G-ITS

Coordinated charging scheduling and routing are central to realizing the benefits of dynamic and wireless charging in 6G-enabled ITS. Unlike static charging environments, 6G-ITS must operate under continuous mobility, heterogeneous vehicle classes, and time-sensitive energy demands, where charging decisions are tightly coupled with routing, traffic dynamics, and infrastructure availability. In this context, charging coordination must account not only for where and how vehicles charge, but also for when they arrive, how they move, and how uncertainties such as congestion, delays, and alignment deviations affect charging opportunities. This section surveys existing scheduling, reservation, and learning-based routing approaches for CAEVs and UAVs, highlighting their capabilities and limitations under mobility uncertainty, and motivates the need for coordinated, adaptive charging and routing frameworks suitable for large-scale 6G-ITS deployments.

In addition to surveying existing approaches, this section also shows how the reviewed literature relates to the notions of intelligent scheduling and optimization. In particular, the works surveyed in this section primarily address intelligent scheduling through reservation mechanisms, time-slot allocation, routing-aware charging decisions, and adaptive coordination under mobility uncertainty. These approaches rely on heuristic rules, game-theoretic formulations, or learning-based policies to manage competing demands, dynamic arrivals, and time-coupled resource constraints.

At the same time, the notion of optimization in the body of literature is typically expressed through objective-driven formulations, rather than strict global optimality. Existing works define optimization in terms of performance objectives such as minimizing travel time, waiting delay, energy consumption, or operational cost, and pursue these objectives using mathematical programming, stochastic games, or reinforcement learning techniques. Due to the dynamic and uncertain nature of transportation systems, these approaches operate under partial and evolving system information, and therefore realize optimization through adaptive decision policies rather than closed-form globally optimal solutions.

From this perspective, the literature collectively addresses intelligent scheduling through coordinated decision-making mechanisms, while optimization is achieved through the continual improvement of system-level performance under operational constraints. However, most existing approaches rely on simplified assumptions, such as static environments, single vehicle domains, or decoupled charging and routing decisions, which limits their applicability in large-scale 6G-enabled ITS. These limitations motivate the need for integrated, adaptive scheduling frameworks that jointly consider charging and routing decisions, support heterogeneous vehicle and charging modalities, and operate effectively under uncertainty. This naturally leads to formulations based on online, sequential decision-making, where optimization is achieved over time through policy-driven actions rather than one-shot global solutions.

2.4.1 DWC Scheduling and Reservation

The mere existence of DWC infrastructure is not sufficient to harness its full potential. Scheduling of DWC is a fundamental requirement to ensure efficient and reliable charging of CAEVs and UAVs in 6G-ITS. This will unlock the true potential of DWC systems by optimizing available resources, reducing congestion at, and around charging stations, minimizing wait times, and optimizing battery health. The latter is important in case of CAEVs driving on highways and UAVs performing critical missions where inactivity can affect operational efficiency. Moreover, DWC reservations play a pivotal role in planning and securing charging sessions, ensuring that CAEVs and UAVs have guaranteed access to the charging infrastructure when they need it. Reservations offer users the convenience of booking charging time slots in advance which is important for UAVs and CAEVs operating on tight schedules. While these mechanisms improve utilization of DWC infrastructure, most existing solutions implicitly assume predictable vehicle arrivals and stable mobility patterns, which limits their effectiveness under real-world traffic and mission uncertainty.

In [129], the proposed system promotes efficient energy use and seamless integration of DWC in the city. The system optimized the usage of DWC with an online EV allocation algorithm within a DWC coordination strategy to reduce peak-to-average energy ratio (PAER) and balance load grid while ensuring customer satisfaction. The system model featured an EV aggregator coordinating EV allocation and a centralized energy management (CEM) system for overall system management with communication supported by dedicated short range communication (DSRC) and 5G communication. The focus was on EVs requesting charging from DWC lanes. The case study in U.A.E. demonstrated the effectiveness of the algorithm in reducing PAER by 44% even with doubled trip length. However, it sacrifices some energy allocation per EV, achieving 64.1% demand coverage, while the shortest distance method leads to uneven lane utilization without addressing energy limitations or recommended velocities.

Reference [130] introduces a double-layer game-based charging scheduling algorithm to address the conflict of interests between DWC lanes and EVs. In the lower layer, a potential game model is used for vehicle charging planning, and a three-way greedy strategy is used to solve dynamic charging sequences. The upper layer uses a reverse Stackelberg game model where DWC lanes regulate electricity prices to encourage EVs to make reasonable charging decisions. An iteration algorithm ensures Nash equilibrium convergence. Simulation results demonstrate the effectiveness of this model in enhancing DWC lane operations and improving EV endurance and travel experience. Results demonstrated higher initial state of charge (SoC) reduces EV charging demand, while low traffic flow attracts EVs to lower-priced DWC lane charging, and higher traffic flow raises electricity prices to discourage less needy EVs.

System in [5], [6], [8] proposes an intelligent charging scheduling and reservation system with trip planning for CAEVs to minimize waiting times, charging times, travel cost, energy consumption, and traffic congestion. This three-layer system proposes an algorithm to schedule charging over three different types of charging systems including DWC. It plans the shortest route for the CAEV to reach its destination, stopping along the way for the necessary charging with 90.25% charging efficiency.

These approaches demonstrate the benefits of coordinated scheduling and reservation for CAEVs, particularly in reducing congestion and improving energy utilization. However, they are largely designed for ground vehicles operating under relatively structured traffic assumptions and centralized or hierarchical coordination models. Extensions to scenarios involving mixed vehicle classes, tighter coupling between routing and charging decisions, or unpredictable arrival behavior remain limited.

References [131] and [123] both address issues associated with charging scheduling of UAVs. In [131], authors introduce an auction-based mechanism for controlling charging scheduling in multi-drone scenarios with the charging station serving as the auctioneer. It uses deep learning to adapt and optimize revenue with a second price auction (SPA) that allocates slots to the highest bidder, accommodating UAVs with diverse battery characteristics in a short-range communication system. More participating drones lead to higher bids and increased revenue for the charging station. In SPA-0, revenue rises from 4.7532 to 5.8493 as drone numbers grow from 5 to 10.

On the other hand, in [123], the focus is on day-ahead scheduling for UAV charging enabled urban prosumers aiming to maximize energy satisfaction while ensuring UAV's QoS. In this urban setting, prosumer communities have solar energy generation and helipads for UAV charging, and they employ Battery Storage Systems (BSS) for energy storage. Additionally, a Distribution System Operator (DSO) is available to provide grid energy if required. It presents a joint method based on hierarchical federated learning (HFL) with long short-term memory (LSTM) and stochastic game- based multi-agent double deep Q learning (MADDQN) to achieve this goal. HFL-LSTM predicts energy requirements, safeguarding data privacy, and a stochastic game model seeks a Nash equilibrium strategy. MADDQN, with a community agent-independent approach, handles optimal energy scheduling per prosumer. Results show the method's superior performance with the lowest average mean absolute error (MAE) of 0.002, lowest average root-mean-square error (RMSE) of 0.0152 and high energy satisfaction of 36388 compared to benchmarks, indicating better energy prediction and QoS maintenance.

Moreover, UAV-oriented scheduling frameworks are typically designed independently of ground traffic dynamics and do not consider joint coordination with CAEV charging or routing decisions, which restricts their applicability in integrated 6G-ITS environments.

Table 2.6 summarizes representative scheduling and reservation approaches and contrasts their underlying assumptions regarding coordination scope and mobility uncertainty. While these systems demonstrate performance gains within their targeted domains, they largely treat charging, routing, and vehicle classes independently, offering limited support for arrival variability, mobility uncertainty, and coordinated decision-making across CAEVs and UAVs. These limitations motivate integrated scheduling frameworks that account for interactions between charging and routing decisions under dynamic 6G-enabled ITS conditions.

These scheduling mechanisms are typically coupled with objective-driven formulations, where performance metrics such as delay, energy efficiency, or infrastructure

utilization are optimized under system constraints, consistent with the optimization perspective outlined in this section.

Table 2.6: Summary of recent DWC scheduling and reservation systems for CAEVs and UAVs.

Ref.	Objectives	Approach	Design and Architecture	Handling of Mobility Uncertainty	Results
[129]	Efficient energy use and seamless DWC integration	Optimize DWC with an online EV allocation algorithm	EV aggregator, CEM system, DSRC and 5G communication	Assumes predictable arrivals and predefined EV allocation	44% PAER reduction, 64.1% demand coverage, and enhanced energy allocation
[130]	Resolve DWC lane and EV conflict of interest	Two-layer algorithm: potential game for charging planning in the lower layer, reverse Stackelberg model in the upper layer for rational EV charging decisions and Nash equilibrium convergence	DWC lanes and EVs	Implicitly handled through pricing; no explicit arrival modeling	SOC affects demand, traffic influences pricing
[5], [6], [8]	Minimize waiting times, charging times, travel cost, energy consumption, and traffic congestion	A novel algorithm to schedule charging over three different types of charging systems along with trip planning	Three-layer design, reservation and trip planning system for CAEVs, cellular and RFID communication	Limited handling through trip planning	90.25% DWC efficiency
[131]	Optimize multi-drone charging scheduling for revenue	Deep learning with SPA for diverse UAV battery sizes	Charging system as auctioneer, UAVs, short-range communication based on IEEE 802.11-based wireless local area network (WLAN)	Not considered; auction assumes synchronized UAV participation	More drones, higher revenue; SPA-0: 4.7532 to 5.8493 with 5 to 10 drones
[123]	Day-ahead UAV charging scheduling for urban prosumers: maximizing energy satisfaction and UAV QoS	Combines HFL-LSTM for energy prediction, a stochastic game model for strategy, and MADDQN for community-based energy scheduling	Prosumer communities with solar generation, UAVs, charging helipads, BSS, and DSO grid backup	Day-ahead scheduling; does not address real-time arrival deviations	Outperformed benchmarks with lowest MAE (0.002), RMSE (0.0152), and high energy satisfaction (36388)
This work	Reduce waiting time and travel cost in DWC environments under mobility uncertainty	Reservation-based scheduling coordinated with route progression	Three-layer architecture supporting coordinated CAEV–UAV charging reservations	Explicitly considers arrival variability and mobility uncertainty through coordinated decision-making	Reduced waiting and travel times through coordinated decisions

2.4.2 Addressing Arrival Challenges

A critical source of mobility uncertainty in coordinated charging systems arises from deviations between planned and actual arrival times at charging locations. DWC scheduling and reservation systems for CAEVs and UAVs are bound to face several critical challenges

and issues. One of the most significant concerns is early and late arrivals, which impacts the following identified aspects:

1) *Operational Efficiency*: DWC scheduling, and reservation mechanisms aim to optimize resource utilization. However, early, and late arrivals can easily disrupt the scheduling and affect efficient use of the infrastructure. This will ultimately increase operational costs.
2) *Cost Management:* Early and late arrivals can lead to unnecessary expenses for both the users and operators. Late arrivals can incur additional charging costs, while early arrivals may require vehicles to wait and suffer additional financial burdens. Achieving cost-efficient operations is essential.
3) *Resource Balancing:* Balancing the allocation of charging time slots and resources between early, late arrivals and on-time vehicles is a fundamental challenge. This requires consideration of factors like number of charging stations, charging rates and demand of charging services.
4) *DWC Speed and Productivity:* The attractiveness of DWC lies in its fast, automatic, and efficient charging process. Failure to arrive on time can lead to disruption of the charging speed, thus affecting the productivity of CAEVs and UAVs. Further, inconsistent charging times can lead to operational delays and impact overall efficiency and productivity of the CAEVs and UAVS, which rely on timely charging.
5) *Optimization and Fairness:* Achieving a balance between optimization and fairness in DWC scheduling and reservation is a complex problem. Both late and early arrivals may demand preferential treatment causing conflicts and inefficiencies in resource allocation. The system needs to allocate resources optimally while trying to meet the energy demands while ensuring fairness among CAEV and UAV operators.
6) *Environmental Sustainability*: DWC systems are typically designed to prioritize the minimization of environmental impact. However, early arrivals can be forced to wait at or around charging stations, thus contributing to unnecessary congestion. This can also lead to increased energy consumption and emissions due to remaining idle for long periods. On the other hand, late arrivals will result in vehicles extending their charging sessions to compensate for the delay, and this can lead to additional energy consumption and raise concerns about sustainability of energy resources.

Early and late arrivals [132], [133] summarized Figure 2.3 introduce unpredictability into the system, leading to inefficient resource allocation. This inefficiency has a ripple effect, that impacts the overall efficiency, cost, and environmental sustainability of DWC systems. It necessitates adaptive scheduling to accommodate these variations while ensuring optimal

charging infrastructure usage. Hence, the effort to address this challenge is crucial in developing an efficient and sustainable DWC reservation and scheduling system for CAEVs and UAVs in future ITS.

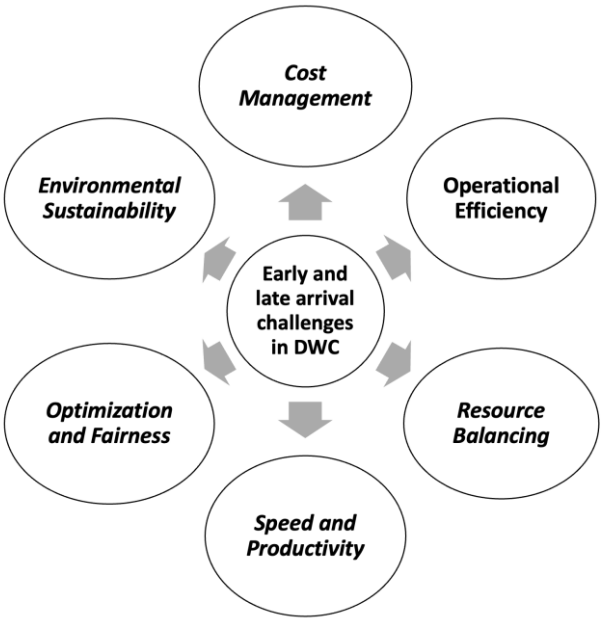

Figure 2.3: Early and late arrival challenges in DWC.

These arrival-related uncertainties highlight the limitations of static or rule-based scheduling mechanisms and motivate adaptive coordination strategies that jointly consider routing, charging, and real-time system state updates.

2.4.3 DRL Based Charging and Routing of EVs

To cope with the dynamic, stochastic, and high-dimensional nature of coordinated charging and routing under mobility uncertainty, recent research has increasingly explored DRL. DRL enables agents to learn adaptive decision policies from interaction with the environment, making it particularly suitable for scenarios involving time-varying traffic, uncertain arrivals, and heterogeneous charging infrastructure. This section surveys representative DRL-based approaches for CAEVs and UAVs, focusing on how they integrate routing, charging decisions, and system constraints.

2.4.3.1 DRL-Based Charging and Routing for CAEVs

DRL has gained traction as a promising solution for dynamic charging and route planning of CAEVs. The work in [134] presents a Shortest-Path (SP)-based Advantage Actor-Critic (A2C) algorithm to optimize the Electric Vehicle Charging Routing Problem (EVCRP). It reformulates the problem as a graph, using DRL to choose efficient routes based on location, energy, and available charging nodes. Though the approach demonstrates a 11%–27% reduction in routing costs over classical A2C and outperforms SP+Proximal Policy

Optimization (PPO) and SP+Deep Q-Network (DQN), it assumes relatively static environments and lacks real-time adaptability.

Reference [135] proposes a constraint-based route planning model using DRL that decouples from specific road network topologies, enhancing scalability. The agent observes parameters such as location, SoC, and nearby charging stations and receives rewards based on strategic charging decisions. Evaluations on real-world datasets like Beijing and synthetic networks like Sioux Falls show 20–30% travel time reductions and 15–25% charging efficiency gains over rule-based and classical optimization approaches. However, both [134] and [135] assume pre-trained, static deployments and lack mechanisms for real-time fallback or online adaptability during uncertain or congested operations.

In [136], a Mobile Charging Station (MCS) is modeled using PPO to dynamically respond to CAEV charging requests in urban environments. The agent learns to minimize total travel and service delay by adapting to real-time requests and traffic changes. Although it effectively demonstrates a learning-based approach for mobile energy dispatch, the system does not integrate with other vehicle types or consider different charging methods, such as DWC.

Further advancing the domain, [137] investigates DRL for ride-hailing scenarios with AEVs, optimizing both dispatch and charging under variable pricing and order volume. Using PPO on real-world datasets from Manhattan, the system reduces operational costs by up to 16.73%. Yet, it assumes a single charging model and overlooks issues like charging alignment, miscoordination with other agents (e.g., UAVs), and free-riding behavior. None of these studies consider shared infrastructure models supporting CAEV-UAV interoperability or secure payment and reservation systems.

Despite these advances, most CAEV-focused DRL frameworks assume static charging models and do not explicitly incorporate DWC constraints, arrival uncertainty, or coordination with aerial charging systems.

2.4.3.2 DRL-Based Charging and Energy Management for UAVs

The literature on UAVs similarly explores DRL for efficient energy and trajectory management. The work in [138] uses DRL to jointly optimize UAV flight height, speed, and radius to enhance energy and spectral efficiency in remote zones. Over 70 episodes, the agent maximizes user connectivity and minimizes power losses. However, the model is built around a static service area and does not account for alignment issues in optical charging or interoperability with ground vehicles.

Reference [139] proposes the Fair Charging-Trajectory Design Time Allocation (FC-TDTA) algorithm for UAVs to optimize 3D trajectory and energy harvesting time in hybrid-powered Non-Orthogonal Multiple Access (NOMA) IoT networks. The system achieves notable gains in throughput and fairness over Shortest Flight-Time Allocation (SFTA) and Time Division Flight Trajectory (TDFT) baselines, especially with ten terminals. Nonetheless, the DRL setup is pre-trained offline and lacks integration with any ground vehicle coordination or cross-mode charging, which hinders its deployment across unified ITS environments.

In [140], a DQN-based agent is introduced to manage UAV data collection and energy replenishment. The model includes variable energy charging efficiencies and data queue lengths, with rewards linked to long-term utility. While the system outperforms Q-learning and baseline heuristics in terms of stability and utility, it does not factor in free-rider avoidance, fairness enforcement, or alignment challenges inherent in laser-based charging.

Finally, [141] employs a Partially Observable Markov Decision Process (POMDP) framework with Joint Proximal Policy Optimization combined with Convolutional Neural Turing Machines (j-PPO+ConvNTM) for UAV crowdsensing involving multiple charging stations. The method achieves up to 40.68% improvement in energy efficiency. However, it focuses solely on UAVs within fixed infrastructure and does not address scalability to heterogeneous vehicle types or integration of diverse charging methods. This limitation highlights the need for frameworks that support joint management of both aerial and ground vehicle charging in dynamic environments.

Similarly, UAV-oriented DRL solutions typically optimize energy and trajectory decisions in isolation, without accounting for shared infrastructure, cross-domain coordination, or interaction with ground vehicle charging demand.

2.4.4 Open Challenges

Although various DRL-based methods have been proposed for electric vehicle charging coordination, several open challenges persist, particularly when considering real-time applicability and integration of heterogeneous vehicle types.

- *Lack of Integrated Ground-Aerial Charging Coordination:* Most existing approaches are designed either for CAEVs or UAVs, without considering how their charging demands might be jointly managed. This separation prevents cooperative energy sharing or efficient load distribution across aerial and ground-based platforms.
- *Incomplete Support for Different Charging Types*: Most studies rely on conventional static charging stations and do not include other forms such as DWC embedded in roads or in-flight charging through airborne systems. In practical deployments, these

charging methods face significant challenges, particularly due to misalignment issues. In both magnetic resonance-based inductive systems and OWPT, even slight positional deviations between the vehicle and charging field can lead to substantial losses in energy transfer efficiency. These issues are not explicitly addressed in most existing scheduling frameworks.

- *Misalignment Sensitivity in Charging Infrastructure*: DWC systems depend heavily on spatial alignment between transmitters and receivers. In real-world conditions, vehicles may deviate from optimal paths due to road curvature, wind disturbances, or traffic conditions. Without continuous correction or alignment-aware scheduling, charging efficiency drops sharply. This becomes particularly problematic for UAVs operating under environmental uncertainties or CAEVs traversing urban layouts with inconsistent infrastructure availability.
- *Early and Late Arrival Complications*: Most current frameworks assume ideal arrival timings for vehicles at their scheduled charging points. However, in practice, both CAEVs and UAVs may arrive earlier or later than expected due to traffic congestion, rerouting, or delays in preceding missions. These deviations can lead to idle charging infrastructure, unfair queuing, or scheduling conflicts. In DWC systems, where charging is location and time-sensitive, early or delayed arrivals can disrupt entire charging sequences and waste available energy transfer opportunities.
- *Lack of Real-Time Operation and Response*: Existing DRL solutions are often trained offline in fixed environments and are not designed to adapt in real time to changing network loads, fluctuating energy demand, or unforeseen operational conditions. This limits their applicability in real-world deployment, where decisions need to be made based on immediate context and updated system states.
- *Absence of Integrated Payment and Access Control*: Many proposed systems do not include mechanisms for secure payment handling, billing, or authorization. In dynamic systems, especially those involving DWC, vehicles may consume energy without proper scheduling or transaction logging, leading to unauthorized usage or "free-rider" issues. The lack of reservation validation and payment enforcement mechanisms poses both economic and operational risks.

Collectively, these challenges [133] illustrated in Figure 2.4 underscore the need for coordinated charging and routing frameworks that can operate across vehicle domains, support

diverse charging modalities such as DWC and in-motion wireless transfer, and adapt in real time to mobility uncertainty. In 6G-enabled ITS, such coordination must balance efficiency, fairness, and reliability while responding to unpredictable arrivals, alignment sensitivity, and dynamic traffic conditions. Addressing these gaps is essential for scalable deployment of intelligent charging services and motivates the coordinated learning-based approach developed in this work.

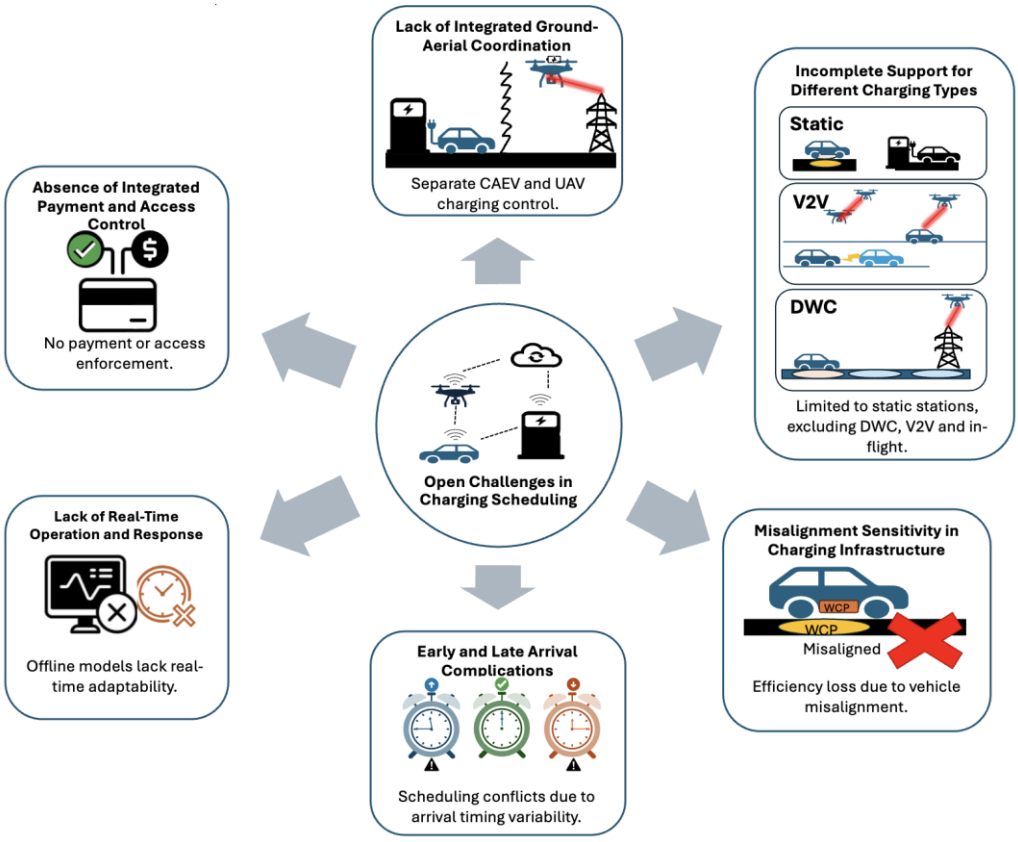

Figure 2.4: Open challenges in charging scheduling for CAEVs and UAVs .

Overall, the literature on coordinated charging scheduling and routing demonstrates the potential of optimization- and learning-based approaches to improve efficiency under dynamic conditions. However, existing works largely treat charging, routing, and vehicle domains in isolation, rely on static or single-mode charging assumptions, and exhibit limited robustness to mobility uncertainty such as early or late arrivals, misalignment-sensitive wireless charging, and fluctuating demand. While DRL-based solutions introduce adaptability, they often lack mechanisms for cross-domain coordination, real-time fallback under constraint violations, and integration with reservation, access control, or heterogeneous charging infrastructures. These limitations motivate the need for coordinated scheduling frameworks that jointly address charging and routing decisions across CAEVs and UAVs, support diverse charging modalities

including DWC, and remain responsive to uncertainty in 6G-enabled ITS environments. This gap directly motivates the coordinated scheduling approach developed in this thesis.

2.5 Reliable and Fair Resource Allocation Mechanisms

As charging networks evolve toward large-scale, multi-vehicle deployments in 6G-ITS, reliability and fairness emerge as essential design requirements alongside efficiency. In heterogeneous environments that integrate CAEVs, UAVs, static and dynamic wireless charging, and multiple infrastructure operators, charging resources must be allocated in a manner that ensures predictable operation, equitable access, and safe utilization under mobility uncertainty. These requirements are particularly critical for DWC, where charging opportunities are tightly coupled to vehicle motion, arrival timing, and spatial alignment.

2.5.1 Reliability in Edge-Enabled Charging Systems

Several studies address reliability in charging infrastructures through grid-aware control, edge-assisted monitoring, and predictive energy management. IEC-based architectures for CAEV charging emphasize stabilizing grid operation and preventing overload via localized forecasting and distributed control mechanisms [118], [121], [122] .These approaches demonstrate that edge intelligence can improve robustness and fault tolerance at the charging-station or feeder level.

However, as discussed earlier, such solutions are largely developed for static or semi-static charging scenarios and typically assume predictable arrivals and coordinated user behavior. In contrast, DWC-enabled systems introduce additional reliability challenges due to sensitivity to trajectory deviations, timing errors, and transmitter–receiver misalignment, where even small spatial deviations can result in disproportionate charging losses or service interruption. While some scheduling frameworks implicitly absorb these effects through centralized coordination or conservative planning assumptions [129], explicit mechanisms to maintain reliable charging service under mobility-induced uncertainty remain limited, particularly when multiple vehicle classes share charging resources.

2.5.2 Fairness in Charging and Scheduling Decisions

Fairness has received comparatively less attention than efficiency and throughput in charging network design. When considered, it is often enforced indirectly through pricing, auction mechanisms, or priority rules. Auction-based charging schemes for UAVs, such as the second-price auction framework in [131], improve revenue efficiency and slot utilization but do not guarantee equitable access for energy-critical or delayed vehicles. Similarly, pricing-based control strategies for DWC lanes [130] influence charging behavior through

economic incentives, yet fairness emerges only as a byproduct of pricing dynamics rather than as an explicit system objective.

In mixed CAEV–UAV environments, fairness challenges become more pronounced due to differences in energy constraints, mission urgency, and mobility patterns. Most existing approaches treat CAEVs and UAVs independently, resulting in fairness guarantees that apply within a single vehicle domain rather than across shared charging infrastructure. As a result, delayed or energy-critical vehicles may be disadvantaged when competing for limited DWC opportunities, especially under congested or time-sensitive conditions.

2.5.3 Resource Allocation Under Mobility Uncertainty

Mobility uncertainty directly impacts both reliability and fairness in charging systems. Deviations from planned arrival times can disrupt reservation schedules, lead to idle charging assets, or unfairly pre-empt other vehicles. In DWC systems, where charging is location- and time-sensitive, such deviations are particularly costly. Despite this, many existing allocation frameworks assume synchronized arrivals or day-ahead planning horizons [123], limiting their applicability under real-time traffic fluctuations and mission variability. In such settings, the absence of explicit reservation validation or access enforcement mechanisms further undermines reliability, as delayed or unscheduled vehicles may pre-empt charging opportunities intended for others.

Learning-based approaches improve adaptability in both CAEV and UAV charging contexts [136], [137], [140], [141], but they typically prioritize long-term performance metrics such as throughput, energy efficiency, or data collection utility. Fairness enforcement, reservation validation, and arrival variability are rarely modeled explicitly, and alignment-sensitive charging losses are often abstracted away. Consequently, reliability and fairness remain secondary considerations rather than integral components of the allocation process.

2.5.4 Architectural Implications for Reliable and Fair Allocation

The surveyed literature indicates that reliable and fair resource allocation cannot be achieved solely through local optimization or isolated scheduling decisions. Architectural support is required to coordinate access to charging resources across vehicles, charging assets, and edge controllers. Mechanisms such as reservation validation, access control, and lightweight accounting or authorization policies can improve predictability and discourage opportunistic or unfair charging behavior, while maintaining distributed operation and interoperability.

Within this architectural context, reliable and fair allocation mechanisms complement coordinated scheduling by ensuring that reserved charging opportunities are honored safely

and equitably, even under uncertain arrivals and mobility deviations. This perspective aligns with the broader 6G vision of resilient, service-oriented, and trustworthy ITS, where performance gains must be balanced with reliability, fairness, and operational robustness.

Table 2.7 summarizes representative approaches related to reliability and fairness in charging and resource allocation. While existing works address individual aspects such as grid stability [118], pricing-based fairness [130], auction efficiency [131], or adaptive learning [136], [137], [140], [141], they rarely integrate reliability and fairness explicitly within coordinated charging frameworks spanning both CAEVs and UAVs. In particular, limited attention is given to allocation mechanisms that jointly consider mobility uncertainty, arrival variability, and shared use of DWC infrastructure.

This work is positioned to address these gaps by embedding reliability- and fairness-oriented mechanisms within a coordinated charging and reservation framework, enabling predictable operation and equitable access across heterogeneous vehicles and charging modes under dynamic 6G-ITS conditions.

Table 2.7:Reliability and Fairness Considerations in Charging and Resource Allocation.

Ref.	Focus Area	Reliability Considerations	Fairness Considerations	Implications for Coordinated Charging Design
[121]	Edge-based CAEV charging control	Relies on stable communication; message loss observed over longer distances	Not explicitly addressed	Highlights the impact of communication reliability on charging coordination
[122]	Grid voltage support via DVCs	Improves electrical stability at charging nodes	Fairness across vehicles not considered	Motivates system-level mechanisms beyond grid-side reliability
[129]	DWC allocation for CAEVs	Assumes predictable arrivals and predefined allocation	Implicit fairness via energy balancing	Shows limitations of reliability under mobility uncertainty
[130]	Game-theoretic DWC pricing	Stability achieved through pricing equilibrium	Fairness indirectly influenced by pricing	Illustrates fairness without explicit reservation enforcement
[123]	UAV charging for urban prosumers	Reliable day-ahead scheduling under forecasted demand	Fairness considered at community level	Highlights lack of real-time robustness and cross-domain coordination
This work	Coordinated CAEV–UAV charging	Addresses alignment sensitivity, arrival variability, and access validation	Explicit fairness through reservation-aware coordination	Treats reliability and fairness as system-level design objectives

Together, the reliability and fairness challenges discussed in this section indicate that effective charging coordination in 6G-ITS cannot rely solely on isolated scheduling or optimization techniques. Charging decisions must remain robust to mobility uncertainty, alignment sensitivity, and access contention, while ensuring equitable use of shared infrastructure across heterogeneous vehicle classes. These requirements naturally intersect with learning-based decision frameworks capable of adapting to dynamic system states. This motivates a closer examination of existing DRL-based charging and routing approaches and

their ability to support coordinated, reliable, and fair operation, which is explored next through comparative analysis and research positioning.

2.6 Comparative Analysis and Research Positioning

Across both CAEV and UAV domains, existing learning-based charging and routing approaches demonstrate promising performance improvements, particularly in localized optimization of energy use, travel cost, or service efficiency. However, when viewed through the lens of large-scale 6G-ITS deployment, several structural limitations emerge. Most studies focus on either ground or aerial vehicles in isolation, assume static or homogeneous charging infrastructure, and decouple charging decisions from broader mobility dynamics. As a result, coordination across heterogeneous vehicle classes, charging modalities, and infrastructure operators remains largely unexplored.

Across both CAEV and UAV domains, existing learning-based charging and routing approaches demonstrate promising performance improvements, particularly for localized optimization of energy consumption, travel cost, or service efficiency. However, when considered in the context of large-scale 6G-ITS, several structural limitations become evident. Most studies focus exclusively on either ground or aerial vehicles and assume homogeneous charging environments, where vehicles interact with a single charging technology, a fixed infrastructure type, or a single operator-controlled network. In contrast, future ITS deployments are expected to involve heterogeneous charging environments, characterized by the coexistence of static wired stations, static wireless pads, dynamic wireless charging lanes, and ad hoc V2V or V2U charging, often managed by different operators and subject to varying access constraints.

From an architectural standpoint, the surveyed DRL-based approaches typically operate within narrowly defined system boundaries, often assuming predictable arrival behavior, uniform charging capabilities, or centralized control. This contrasts with the requirements of future 6G-ITS, where dense connectivity, ultra-low latency, and distributed intelligence must support dynamic interactions across heterogeneous charging modes and vehicle classes. While some methods adapt to traffic or demand fluctuations, few explicitly address mobility-induced uncertainties such as early or late arrivals, alignment sensitivity in DWC scenarios, contention for shared charging resources, or the need for integrated payment and reservation validation mechanisms.

Table 2.8 presents a comparative overview of representative DRL-based charging and routing approaches, highlighting their primary focus, adaptability, supported charging

technologies, and coordination scope. The comparison shows that most existing solutions are tailored to homogeneous charging assumptions and static infrastructure models, with limited support for DWC or coordinated operation across ground and aerial domains. Even adaptive or context-aware methods typically optimize decisions within a single vehicle domain, leaving cross-domain coordination and reservation-based charging decisions insufficiently addressed. Table 2.9 further summarizes these gaps, indicating that alignment handling, arrival variability, and secure access control are largely absent from existing designs.

Table 2.8:Comparison of DRL Approaches for Ground and Aerial Vehicle Charging and Scheduling.

Study	**Primary Focus**	**Adaptability**	**Charging Support**	**Coordination Scope**	**Key Outcomes**	**Main Contribution**
[134] ***A2C EVCRP***	EV routing and charging	Static	Plug-in	Ground	Minimize travel cost through optimized routing	Efficient route selection using SoC and charging availability
[135] ***Constraint-DRL***	Path planning under constraints	Limited	Plug-in	Ground	Reduce travel time and improve charging efficiency	Constraint-based planning decoupled from road topology
[136] ***PPO-MCS***	Mobile charging station dispatch	Adaptive	Plug-in	Ground	Improve utilization and reduce delays	Dynamic dispatch of mobile chargers
[137] ***Autonomous fleet dispatch***	Fleet dispatch and charging	Adaptive	Plug-in	Ground	Optimize fleet operations under variable demand	Fleet-level routing and charging optimization
[138] ***UAV mission optimization***	UAV energy and trajectory	Predefined	Wireless	Aerial	Optimize UAV energy use and flight paths	Flight path and energy optimization for individual UAVs
[139] ***FC-TDTA***	UAV path and energy optimization	Adaptive	Wireless	Aerial	Improve fairness and throughput in UAV scheduling	Fairness-aware trajectory and energy scheduling
[140] ***DQN UAV***	UAV energy management	Adaptive	Wireless	Aerial	Efficient energy usage for UAV data collection	Energy-aware UAV routing with queue management
[141] ***j-PPO+ConvNTM***	Multi-UAV coordination	Context-aware	Wireless	Aerial	Coordinate multiple UAVs efficiently	Multi-UAV scheduling for improved resource allocation
SAFE-DDPG (This work)	**Integrated aerial and ground charging**	**Adaptive**	**Plug-in, Wireless, DWC, V2V**	**Aerial and Ground**	**Reduce waiting and travel times, improve charging efficiency**	**Unified scheduling across platforms and charging technologies**

Beyond adaptability, issues of reliability and fairness further distinguish the proposed approach from prior work. As discussed in Section 2.6, existing learning-based frameworks rarely incorporate explicit mechanisms for reservation validation, access control, or fairness enforcement. These capabilities are critical in heterogeneous charging environments where multiple vehicles compete for shared charging resources under mobility uncertainty. Without such mechanisms, scalable deployment across mixed charging modes and operators becomes difficult, particularly at city scale.

Table 2.9: Gaps Addressed by Existing DRL Approaches and SAFE-DDPG.

Key Focus	[134]	[135]	[136]	[137]	[138]	[139]	[140]	[141]	**Ours (SAFE-DDPG)**
Ground + aerial coordination	–	–	–	–	–	–	–	–	**Full**
Diverse charging types	Plug-in	Plug-in	Plug-in	Plug-in	Wireless	Wireless	Wireless	Wireless	**Multi-type**
Alignment handling	–	–	–	–	Limited	Limited	Limited	Limited	**Adaptive**
Early/late arrivals	–	–	–	–	–	–	–	–	**Included**
Real-time adaptability	–	–	Partial	Partial	–	Limited	Partial	Context-aware	**Full**
Secure payment and access	–	–	–	–	–	–	–	–	**Included**

In this context, the proposed SAFE-DDPG framework is positioned as a coordination oriented scheduling approach aligned with the 6G vision for ITS. SAFE-DDPG brings together three core dimensions identified throughout this chapter. First, it supports a scalable and interoperable charging network architecture that accommodates heterogeneous charging modes, including static charging, dynamic wireless charging, and V2V charging. Second, it enables coordinated charging and routing decisions under mobility uncertainty by aligning charging reservations with route progression rather than treating them as isolated decisions. Third, it incorporates reliable and fair resource allocation through reservation based control and access validation. Rather than treating charging, routing, and vehicle classes as independent problems, SAFE-DDPG supports coordinated decision making across CAEVs and UAVs while operating across diverse charging technologies and infrastructure conditions. By accounting for arrival variability, alignment sensitivity, and shared infrastructure contention, and by incorporating real time adaptability, fairness, and secure access, the proposed framework addresses key architectural, operational, and scalability challenges that are only partially addressed in existing learning-based approaches. This positioning distinguishes SAFE DDPG from prior work and provides a coherent foundation for the system design and evaluation presented in the subsequent chapters.

Chapter 3 Charging Network Architecture

3.1 Introduction

As discussed in the previous chapters, charging solutions for CAEVs and UAVs are typically designed around isolated infrastructures and technology-specific assumptions, which limits their ability to support coordinated operation in emerging 6G-ITS. In practice, future ITS deployments must accommodate heterogeneous charging technologies, dynamic mobility patterns, and interactions between ground and aerial platforms, while consistently enforcing safety, authorization, and billing constraints. The lack of a unified architectural framework to manage these interactions remains a key barrier to scalable and interoperable charging coordination.

Motivated by this need, this chapter proposes a scalable and interoperable charging network architecture for coordinated charging reservation and trip planning in 6G-ITS environments. The chapter focuses on the design of a three-tier architectural framework and an associated lightweight handshake protocol that together enable consistent coordination across static, dynamic, and mobile wireless charging modalities. By abstracting charging coordination from physical power transfer mechanisms and vehicle-specific characteristics, the proposed design provides a common operational foundation for heterogeneous charging networks involving both CAEVs and UAVs.

This abstraction is applied at the coordination level and does not imply that charging infrastructures are interchangeable. The proposed architecture explicitly preserves compatibility constraints between vehicle classes, charging modes, and charging network types, ensuring that only physically feasible charging assignments are considered during reservation and session establishment. As a result, the problem addressed is not confined to fleet management or infrastructure management in isolation, but instead requires their joint coordination. Vehicle-side charging destination selection and infrastructure-side reservation, authorization, and session management are therefore integrated within a unified framework. To support this at scale, the architecture adopts a three-layer design that separates physical charging execution, edge-level coordination, and back-end service functions, rather than merging them into a single control plane.

This separation is both structural and operational. It enables coordinated reservation handling and scheduling decisions to be executed consistently across heterogeneous charging networks, while maintaining clear functional boundaries between system layers. In this context, 6G serves as the enabling communication substrate that supports low-latency, reliable, and scalable interaction among vehicles, infrastructure, and coordination entities, ensuring that

reservation decisions and physical charging execution remain synchronized under dynamic operating conditions.

The chapter begins by introducing the system context, modeling assumptions, and communication structure required for coordinated operation. It then presents the proposed architecture and handshake protocol, followed by design-level validation and verification based on protocol execution, implementation-level testing, and examination of representative operating and edge conditions. The chapter concludes with a discussion of architectural implications and a summary that consolidates the design, establishing a validated architectural foundation upon which coordinated system behavior is examined in later chapters.

3.2 System Overview

In this proposed UAV and CAEV charging reservation and trip planning system, the smart city is considered a typical 6G application scenario where multiple UAVs are employed as MEC devices. These MECs function as edge intelligence (EI) devices, or edge intelligent UAVs (EIUAVs). The EIUAVs assist CAEVs by collecting relevant data and executing tasks such as charge scheduling and trip planning in a coordinated manner. In this capacity, EIUAVs effectively act as airborne RSUs, extending the reach and functionality of 6G services. It is assumed that the energy capacity of EIUAVs is insufficient to complete their mission plans, which include servicing CAEV requests. Hence, one or multiple laser-beaming UAVs (LBUAVs) are deployed to dynamically and intelligently charge EIUAVs, thereby extending their operation time. LBUAVs differ from EIUAVs in having a larger size, battery capacity, and weight, and are capable of bi-directional charging, whereas EIUAVs can only receive charging.

LBUAVs are fully charged by fixed ground charging stations, which can be laser-beaming stations for far-field charging or magnetic resonance stations for near-field charging. Far-field charging is adopted in the proposed system due to its higher degree of automation, ease of use, and efficiency compared to near-field charging. However, LBUAVs must maintain a LOS with the EIUAVs for efficient and safe wireless power transfer. In the proposed system, CAEVs are assumed to operate in platoon formations to effectively reduce energy consumption, traffic congestion, and improve safety. In a platoon, CAEVs can share information using V2X communication with other CAEVs and surrounding infrastructure, including UAVs and charging stations.

CAEVs can be charged using wired and SWC stations installed at homes or parking lots and can be partially charged using DWC stations typically installed on highway routes to extend their driving range. Further, CAEVs are capable of bi-directional charging, such as V2V

charging, for emergency situations like driving in remote regions or when they do not have sufficient charge to reach a static charging station. Since this is a 6G smart city application, UAVs and CAEVs can also aid each other in charging using heterogeneous charging methods such as vehicle-to-UAV (V2U) and UAV-to-vehicle (U2V) charging. In V2U, a CAEV can partially charge either an LBUAV or EIUAV to aid their flight towards a ground charging station for full charging. Similarly, an LBUAV can provide charging to a CAEV using U2V charging in situations where no dynamic charging stations are available or when a CAEV is stuck in a remote location.

With near-field heterogeneous charging, CAEVs can be parked or in motion as UAVs need to be mounted onto the static wireless charging device. However, in far-field charging such as laser-beaming, the CAEV needs to be parked, and the LBUAV should be hovering at a fixed altitude for safe WPT.

There are two types of vehicles interacting in the smart city environment supported by 6G-enabled communication services such as laser beaming for data exchange and coordination. First, UAVs, which include: 1) LBUAVs that receive charging from ground charging stations and provide dynamic charging to EIUAVs and CAEVs, and 2) EIUAVs that receive charging and perform EI operations like servicing requests for charge scheduling and trip planning from CAEVs. Second, CAEVs, typically part of a platoon, can both receive and give charging to both CAEVs and UAVs. CAEVs also request EIUAVs for optimal trip routes with charging.

3.3 System Description

Emerging 6G-enabled smart city environments, as mentioned earlier, are assumed to provide advanced capabilities such as URLLC, mMTC, integrated sensing and communication (ISAC), and native AI support [142], [143], [144], [145]. In the proposed system, these capabilities are treated as operating assumptions that enable data-intensive and time-critical mobility services, including coordinated charging, predictive route planning, and real-time energy orchestration for CAEVs and UAVs. Furthermore, 6G architectures are assumed to support semantic communication for context-aware data exchange, pervasive edge intelligence for distributed decision-making, and advanced network slicing to meet diverse QoS demands across heterogeneous applications. A key enabler within this context is peer-to-peer (P2P) connectivity among intelligent infrastructure elements, forming a connected backbone that supports low-latency coordination, scalable resource allocation, and seamless service delivery. In this work, these capabilities are invoked not as a claim about a specific future radio implementation, but as enabling conditions for dense, low-latency, and heterogeneous coordination across ground and aerial charging domains.

The challenge becomes even more complex in heterogeneous vehicular networks, which encompass diverse communication standards, power transfer methods, hardware capabilities, and battery characteristics. Variations in how vehicles deplete energy, interact with infrastructure, or receive power through static plug-in systems, wireless transfer, or optical beams create irregular operating conditions that complicate coordinated scheduling and resource allocation. These conditions make real-time optimization increasingly difficult, necessitating coordination mechanisms that can operate reliably under dynamic and diverse operating conditions. These considerations motivate the system design adopted in this work, which enables real-time coordination, interoperable charging operations, and autonomous decision-making within dense, dynamic ITS ecosystems.

The role of 6G in the proposed system arises from the need to support large-scale coordination across heterogeneous ground and aerial charging domains rather than simple point-to-point connectivity. In dense smart-city deployments, numerous CAEVs, UAVs, edge intelligence devices, charging nodes, and charging network managers may simultaneously exchange reservation, availability, routing, monitoring, and safety-related information within the same service area. This coordination requires multiple communication modes operating concurrently.

V2I communication supports charging reservation requests and infrastructure availability updates with charging network managers and EI devices. V2V communication supports cooperative charging interactions and platoon coordination among CAEVs. UAV-to-UAV (U2U) communication enables coordination between aerial vehicles involved in in-air energy transfer and replenishment operations. In addition, cross-platform vehicle-to-UAV (V2U) and UAV-to-vehicle (U2V) communication supports heterogeneous charging assistance between ground and aerial platforms.

These interactions create a coordination environment in which communication reliability, scalability, and responsiveness directly affect the correctness of reservation enforcement, charging synchronization, and safe session management. Within this context, the architecture assumes a 6G-enabled ITS environment capable of sustaining dense multi-entity coordination and supporting tightly coupled communication among vehicles, aerial platforms, and edge intelligence nodes operating across heterogeneous charging networks. This enables consistent reservation handling and safe coordination of charging operations across the system.

Without such communication support, inconsistencies may arise between reservation decisions and actual infrastructure availability, leading to infeasible assignments or unsafe charging conditions. Therefore, 6G capabilities are invoked here as a functional requirement

for maintaining consistent and scalable coordination across heterogeneous charging networks rather than as a nominal system assumption.

To support this coordination framework, communication in the proposed architecture is modeled at the system and coordination levels rather than at the detailed physical-layer level. Accordingly, link-level quantities such as bit error rate (BER), packet error probability, modulation-specific decoding behavior, and channel fading are not explicitly parameterized. Instead, their aggregate impact is represented through communication-level uncertainty, including message loss, delayed responses, timeout-triggered re-synchronization, and temporary node unavailability. This abstraction reflects the objective of this chapter, which is to establish a scalable and interoperable coordination architecture across heterogeneous charging networks rather than to optimize a specific wireless interface.

From a system perspective, link-level impairments manifest through their effect on control-plane message delivery. For example, non-zero BER and channel variability in practical V2X systems translate into packet loss, retransmissions, and variable latency at higher layers. The proposed architecture captures these effects through acknowledgment-based message exchange, timeout mechanisms, and safe re-initiation of protocol states. Consequently, the architectural validity and protocol correctness are evaluated based on their ability to maintain safe and consistent operation under communication disruptions, rather than through direct numerical characterization of BER.

This modeling choice does not ignore link-level effects, but incorporates their impact at the control and coordination levels, which are the primary concern of the architectural design. As a result, the proposed framework remains applicable across different communication technologies, including current V2X systems and future 6G-enabled deployments. From an analytical standpoint, link-level reliability directly influences the probability of successful control-message delivery and the expected delay due to retransmissions. These effects are reflected at the protocol level as message loss events, delayed acknowledgments, and timeout-triggered recovery, which are explicitly incorporated into the coordination logic and handshake protocol design. Accordingly, explicit numerical analysis of BER or link failure rates is outside the scope of this chapter, as the focus is on architectural correctness and robustness at the coordination level.

Building on prior work on coordinated charging for CAEVs [6], [8], [146], the proposed system supports both far-field and near-field wireless charging for UAVs and platoons of CAEVs operating within 6G-enabled ITS environments. The system integrates heterogeneous charging networks through seamless communication, enabling scalable and interoperable

operations for both CAEVs and UAVs. This section introduces the charging network types, communication topologies, and architectural components adopted in the proposed system. These requirements directly motivate the three-layer architectural design introduced in the following section, which structures coordination, communication, and service functions to operate efficiently under the dense, low-latency, and heterogeneous conditions enabled by 6G-ITS.

3.3.1 Vehicle Model and Capabilities Assumed in the Proposed System

The considered smart city environment consists of CAEVs and UAVs:

3.3.1.1 CAEV Onboard Capabilities Assumed in the System

In the proposed system, each vehicle is assumed to be a connected and autonomous ground vehicle equipped with the sensing, communication, computation, and energy transfer capabilities required for 6G-enabled ITS operation. As illustrated in Figure 3.1, each proposed CAEV includes an OBU, GPS, and V2X communication interfaces to support low-latency coordination with infrastructure, neighboring vehicles, and aerial platforms. Autonomous driving and precise positioning are enabled through LiDAR, radar, and 2D/3D cameras, together with odometry and ultrasonic sensors, which also support safe platoon formation and charging alignment. From an energy perspective, CAEVs are battery-powered and support both wired and wireless charging. Near-field wireless charging based on magnetic resonance is enabled through a wireless energy receiver installed beneath the chassis, while bidirectional energy exchange is supported via wireless energy transmitters and receivers positioned at the bumpers, headlights, and roof. Far-field laser transmitters and receivers located at the front, rear, and roof enable V2V and V2U communication and charging interactions. These assumed capabilities allow CAEVs to participate in static, dynamic, and cooperative charging operations, align charging reservations with route progression, and support coordinated, energy-aware mobility under the latency, reliability, and scalability requirements of 6G-enabled ITS.

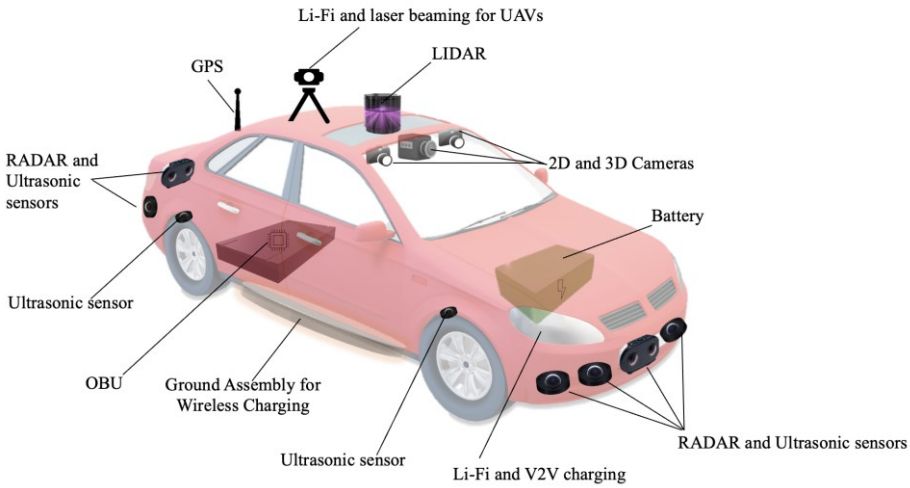

Figure 3.1: Connected and Autonomous Electric Vehicle.

3.3.1.2 UAV Operational Capabilities Assumed in the System

In the proposed system, UAVs operate in the aerial domain and are categorized into LBUAVs and EIUAVs. LBUAVs are assumed to have higher onboard energy capacity and bidirectional wireless charging capability through integrated wireless energy transmitters (WETs) and receivers (WERs), enabling them to receive energy from ground infrastructure and recharge EIUAVs during operation. EIUAVs have limited energy capacity and are assumed to receive charging only from LBUAVs or fixed charging stations. As illustrated in Figure 3.2, all UAVs are equipped with onboard computing units, GPS, communication modules, batteries, and essential perception sensors, including cameras, LiDAR or radar, inertial measurement units (IMUs), accelerometers, and collision detection sensors, supporting autonomous flight and charging alignment. Far-field laser transmitters and receivers enable in-air communication and charging, while near-field wireless charging pads (WCPs) support stationary or low-altitude charging when required.

Within this architecture, CAEVs and UAVs equipped with WETs and WERs can support limited cross-platform energy transfer during emergency or infrastructure-limited scenarios. EIUAVs function as mobile edge nodes that assist with charge scheduling and trip planning, while LBUAV trajectories are coordinated to replenish EIUAV energy without interrupting mission execution. These assumed capabilities enable coordinated charging, route-aware scheduling, and edge-assisted services under the latency, reliability, and adaptability requirements of 6G-ITS.

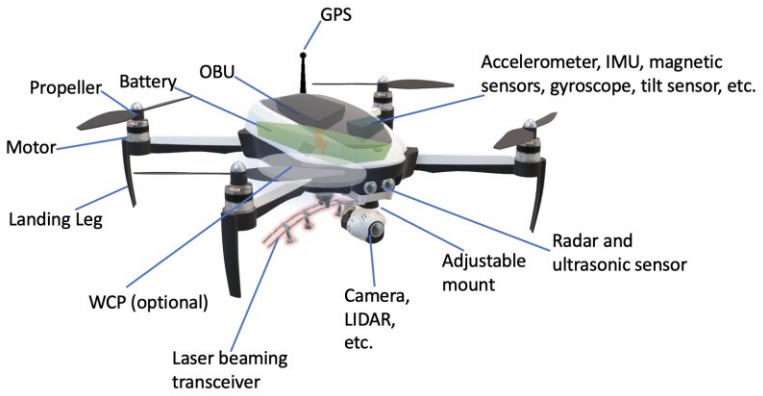

Figure 3.2: Uncrewed Aerial Vehicle.

3.3.2 Charging Modes Supported by the Proposed System

The proposed system is designed to support multiple charging modes for CAEVs and UAVs within a 6G-enabled ITS, reflecting the heterogeneous operating conditions assumed in the system model. The architecture accommodates both conventional and wireless charging infrastructures and enables coordinated energy transfer under defined safety, alignment, and scheduling constraints. Charging interactions are supported among homogeneous vehicles, such as CAEV-to-CAEV (V2V) and UAV-to-UAV (U2U), as well as heterogeneous vehicles, including CAEV-to-UAV (V2U) and UAV-to-CAEV (U2V), particularly in scenarios where static infrastructure is unavailable or operational continuity is required.

For CAEVs, the system supports three infrastructure-based charging networks: the cabled charging network (CCN), the static wireless charging network (SWCN), and the dynamic wireless charging network (DWCN). CCNs consist of conventional EVSE connected to parked CAEVs. SWCNs employ near-field wireless power transfer, such as magnetic resonance, through wireless charging pads (WCPs) installed beneath parking areas or road surfaces. DWCNs extend wireless charging to in-motion scenarios by connecting EVSEs to an array of WCPs embedded along roadways, enabling CAEVs to receive energy while driving. While CCN and SWCN require vehicles to remain stationary and may incur waiting times, DWCN is used in the proposed system to provide partial charging that extends driving range and reduces dependence on stationary charging. The proposed system is designed to support charging coordination strategies that reduce waiting times associated with CCN and SWCN while leveraging DWCN for range extension.

Because the supported charging networks rely on different physical energy transfer mechanisms, alignment requirements, and operational constraints, they are not treated as interchangeable within the proposed architecture. Hardware compatibility between vehicle types and charging infrastructures is therefore explicitly modeled and enforced within the architecture. CCN, SWCN, and DWCN infrastructures are designed to serve CAEV charging

operations, whereas LBCN infrastructures are designed for UAV charging through laser-based energy transfer. AVCN primarily supports UAV charging but may assist CAEVs in exceptional situations where a CAEV is unable to access a compatible ground charging network or when emergency charging support is required from nearby aerial infrastructure. Conversely, GVCN primarily supports CAEV charging but may assist UAVs only in emergency situations when dedicated aerial charging infrastructure is unavailable. These compatibility constraints are incorporated into the charging candidate selection process and enforced during reservation validation so that only physically feasible and safe charging assignments supported by the underlying infrastructure are considered by the coordination framework.

In addition to fixed infrastructure, the proposed system supports mobile charging for CAEVs through V2V interactions. CAEVs equipped with bidirectional charging capability can exchange energy using either near-field wireless technologies, such as magnetic resonance, or far-field technologies, such as laser beaming. V2V charging is coordinated through V2V communication to ensure synchronization and safety, with laser beaming preferred due to its higher efficiency and reduced alignment constraints in mobile scenarios.

For UAVs, the system supports both fixed and mobile charging options. U2U charging is enabled under the assumption that only LBUAVs provide energy to EIUAVs, while EIUAVs are limited to receiving charging. U2U charging may employ near-field wireless transfer in close-proximity scenarios, but laser beaming is adopted as the primary mechanism due to its efficiency, operational range, and suitability for in-air charging.

UAVs can also receive energy from fixed infrastructure. The proposed system adopts laser beaming charging networks (LBCNs) as the primary fixed charging option for UAVs. An LBCN consists of laser beam energy transmitters (LBETs) mounted on towers that dynamically adjust beam direction to maintain line-of-sight with UAVs. Laser-based charging is adopted in the proposed system as the primary wireless charging mechanism for UAVs, as it enables long-range, line-of-sight energy transfer during flight or hovering.

This design choice is grounded in established analyses of wireless charging technologies, which indicate that laser-based transfer can sustain substantially higher energy delivery over extended distances than near-field methods, with reported energy delivery on the order of 16.29 kWh over multi-kilometer ranges under continuous operation [14]. Building on these findings, the proposed system assumes laser beaming as a practical charging option for aerial vehicles operating under controlled conditions. Environmental factors such as weather effects and laser safety constraints are treated as system-level considerations and are addressed through operational protocols and reservation-based coordination.

To enhance robustness under near-field charging conditions, the proposed system also supports three-dimensional static wireless charging networks (3D-SWCNs) for UAVs. In a 3D-SWCN, orthogonally arranged wireless charging pad configurations improve tolerance to alignment deviations during landing or low-altitude hovering, as established in prior review [10]. Within the proposed architecture, 3D-SWCNs serve as a complementary charging mode when far-field laser beaming is unavailable, while preserving the same scheduling, reservation, and coordination mechanisms.

Heterogeneous charging between CAEVs and UAVs is supported as part of the system design. Both near-field magnetic resonance and far-field laser beaming can be used for V2U and U2V charging. Near-field charging requires close proximity and typically involves UAVs descending onto a charging interface, while far-field laser charging requires controlled relative positioning. For safety reasons, the system assumes that CAEVs remain stationary during U2V and V2U laser beaming operations.

CCNs are included in the system to preserve backward compatibility with existing charging infrastructure. Similarly, 3D-SWCNs are supported to ensure interoperability with near-field wireless charging technologies. However, laser beaming is adopted as the primary charging method for UAVs due to its higher efficiency, operational flexibility, and suitability for dynamic and mobile charging scenarios. By combining laser beaming, DWCN principles, and heterogeneous charging interactions, the proposed system enables scalable, flexible, and energy-efficient operation in 6G-ITS environments.

Figure 3.3 provides a system-level overview of the charging modes supported for CAEVs and UAVs. Yellow-colored UAVs represent EIUAVs, while gray-colored UAVs represent LBUAVs. Figures 3.3 (1) and (3) illustrate UAV charging from ground-based laser charging stations that are part of an LBCN. Figures 3.3 (2) and (4) demonstrate homogeneous charging between UAVs and CAEVs, respectively. Figures 3.3 (5), (7), and (8) illustrate heterogeneous charging between CAEVs and UAVs, with Figure 3.3 (5) showing near-field magnetic resonance-based mobile charging. For safety considerations, Figures 3.3 (6) and (7) show that CAEVs are stationary during U2V and V2U laser beaming operations. Finally, Figures 3.3 (6), (9), and (10) highlight DWCN, CCN, and SWCN charging of CAEVs.

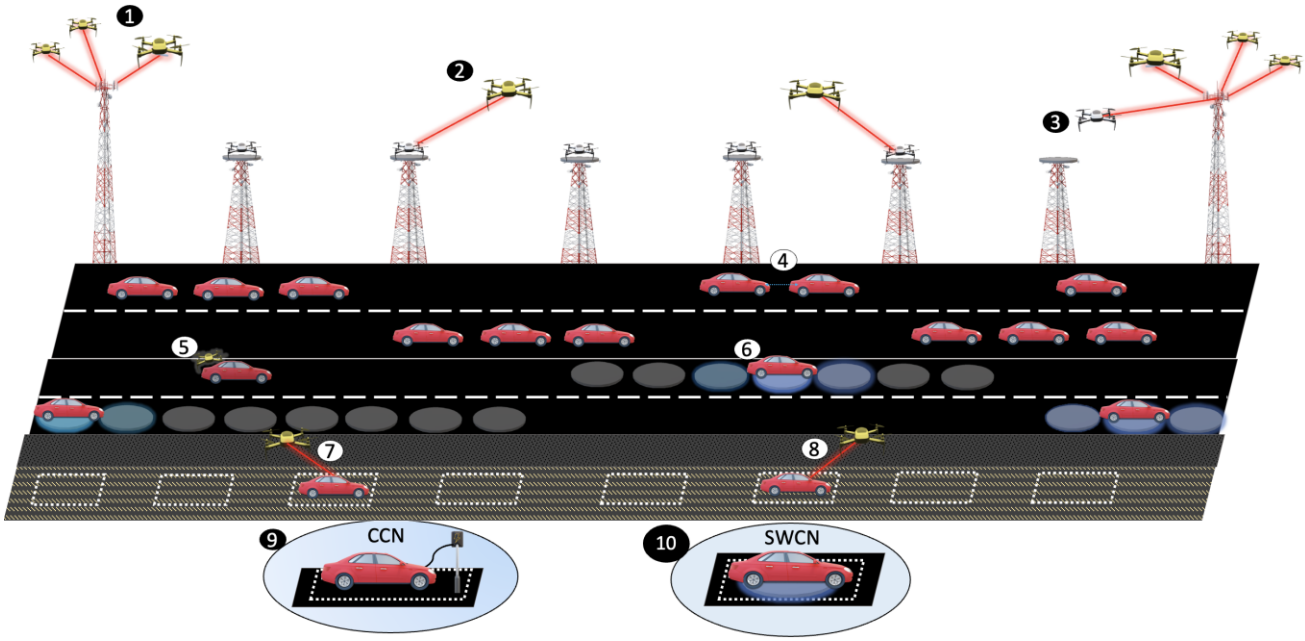

Figure 3.3: System overview of CAEV and UAV charging methods.

Considering the presence of multiple charging networks (CNs) and heterogeneous charging interactions, the coordination problem addressed by the proposed architecture extends beyond either fleet management or charging infrastructure management in isolation. Instead, the system must support coordination between vehicle-side charging destination selection and infrastructure-side charging reservation and session enforcement within a unified framework. Vehicles are directed toward compatible charging networks based on their current energy state, travel trajectory, proximity to available infrastructure, and the spatial availability of specific charging modes. At the same time, charging networks must manage limited charging capacity and allocate charging sessions among competing vehicles through reservation and session management mechanisms.

Consequently, the coordination problem combines elements of both mobility management and infrastructure resource management. On the vehicle side, charging destination selection determines where a CAEV or UAV should travel in order to obtain charging while maintaining mission continuity and energy feasibility. On the infrastructure side, charging network managers must enforce reservations, authenticate vehicles, and manage charging session scheduling to ensure safe and efficient utilization of available charging resources. By integrating these aspects within a unified coordination framework, the proposed architecture enables energy-aware vehicle mobility while ensuring efficient utilization and safe operation of heterogeneous charging infrastructures. To support this coordination, the communication topology is introduced next.

Importantly, these coordinated decisions are not independent one-shot allocations, even though they are triggered at the level of individual requests. Each confirmed reservation occupies charging resources over a time interval and directly affects future availability and feasible assignment options for subsequent vehicles. As a result, decisions are inherently time-coupled, and the coordination process must account for an evolving system state under dynamic arrivals. This transforms the problem from a static allocation view into a sequential, time-coupled scheduling problem with coordinated resource management across heterogeneous charging networks.

3.3.3 Communication Topology

This section describes the communication topology adopted by the proposed system to coordinate charging, scheduling, and energy exchange across heterogeneous CNs.

The system adopts a hybrid mesh–star communication topology [133], [146] illustrated in Figure 3.4 to balance coordination efficiency, scalability, and fault tolerance. While a fully centralized star topology offers simplicity and low coordination overhead, it introduces a single point of failure through reliance on a central Charging Network Manager (CNM). Conversely, a fully decentralized approach improves robustness but incurs higher communication, computation, and maintenance overhead due to the need for direct peer-level coordination among all charging entities. To avoid these limitations, the proposed architecture combines the strengths of both models.

In the adopted hybrid topology, each CN type is managed by a dedicated CNM. Specifically, the Cabled Charging Network (CCN) is managed by the Cabled Charging Network Manager (CCNM), the Static Wireless Charging Network (SWCN) by the Static Wireless Charging Network Manager (SWCNM), and the Dynamic Wireless Charging Network (DWCN) by the Dynamic Wireless Charging Network Manager (DWCNM). Laser-beaming infrastructure for UAV replenishment is coordinated by the Laser-Beaming Charging Network Manager (LBCNM). Aerial charging operations involving LBUAVs are managed by the Aerial Vehicle Charging Network Manager (AVCNM), while CAEV fleets are coordinated through the Ground Vehicle Charging Network Manager (GVCNM).

Each CNM maintains a star connection with its associated charging nodes, enabling efficient local coordination. At the same time, P2P connectivity is established among CNMs, forming a mesh backbone that enables cross-network coordination. This structure supports same-type and cross-type charging sessions, including V2V, U2U, and V2U/U2V interactions, while allowing charging requests to be dynamically distributed across networks to balance load

and maintain service continuity. The mesh layer ensures that localized failures do not disrupt system-wide coordination.

The hybrid topology also enables seamless interaction between ground and aerial charging domains, supporting coordinated UAV-to-CAEV and CAEV-to-UAV energy exchange. The communication topology is designed to support scheduling, routing, and resource allocation mechanisms, including heuristic- or learning-based approaches, operating at higher layers. In particular, the topology enables distributed scheduling and reservation enforcement by allowing charging decisions to be coordinated across multiple charging networks while preserving local autonomy at the CNM level. A lightweight handshake protocol with semantic communication support enables efficient exchange of mission-critical information, while network slicing provisions communication resources according to service requirements, such as low-latency support for DWC operations and high-throughput links for laser-based charging.

By integrating these design choices with emerging 6G capabilities, the proposed communication topology provides a scalable and interoperable foundation for coordinated energy management across heterogeneous charging networks in future ITS.

The hybrid topology establishes P2P connectivity among CNMs, forming a fully connected backbone that supports coordinated interaction between ground and aerial charging domains, including UAV-to-CAEV and CAEV-to-UAV energy exchange, dynamic load distribution, and cross-network scheduling. Over this backbone, coordination signaling enables higher-level decision-making modules, including AI-based approaches, to operate consistently across heterogeneous CNs. A lightweight handshake protocol is proposed to support efficient exchange of mission-critical information required for charging coordination and reservation validation. The communication architecture is designed to operate over 6G-enabled networks and is therefore compatible with emerging capabilities such as semantic communication and network slicing, which can be leveraged at the network level to meet heterogeneous service requirements, including low-latency support for dynamic wireless charging and high-throughput links for laser-based charging. Together, these design choices provide a scalable and interoperable foundation for intelligent energy management in next-generation ITS.

Communication reliability in the proposed architecture is ensured through protocol-level mechanisms embedded in the coordination and handshake design, together with distributed coordination, rather than relying on ideal communication links. Critical control messages, including reservation confirmation, charging authorization, session continuation, and termination, are protected through explicit acknowledgment exchange, timeout-based

monitoring, and controlled re-initiation of protocol states when communication is interrupted but safely recoverable, reflecting link-level variability at the coordination level.

In addition, coordination responsibilities are distributed across EI devices and CNMs, ensuring that temporary communication failures remain localized and do not propagate across the entire system. Safety-critical operations, such as charging initiation and continuation, depend on verified control states rather than continuous connectivity, allowing the system to maintain correct and safe operation under intermittent communication conditions. This approach reflects realistic V2X and future 6G-ITS environments, where link variability is expected but must not compromise system-level coordination.

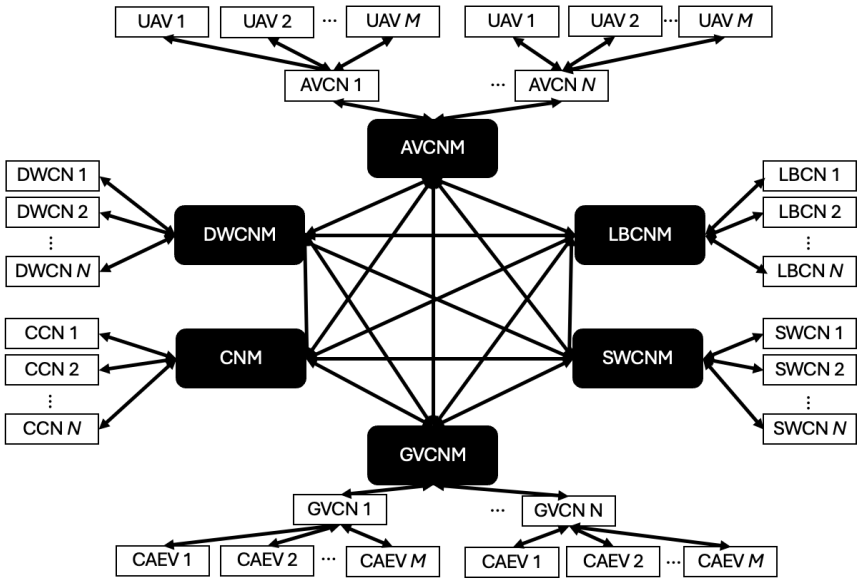

Figure 3.4: Communication Topology of Charging Networks.

3.4 System Architecture

The proposed system leverages a three-layer edge computing architecture to support efficient charging reservation and trip planning across heterogeneous networks. Computation and communication tasks are distributed among End Devices, Edge Intelligence Devices, and Core Cloud components to reduce latency, optimize processing, and enable real-time decision-making in line with 6G smart city requirements. This three-layer design [133], [146] is illustrated in Figures 3.5 through 3.8, with each figure depicting the architecture applied to different types of CNs and corresponding charging technologies.

1) End Devices: These include CAEVs, UAVs, and electric vehicle supply equipment (EVSE) in our system. The vehicles can communicate with the grid using vehicle-to-grid (V2G) communication and with each other using V2V communication. These devices are highly responsive but must forward their requests to other servers due to

limited capacity and resources. Furthermore, the vehicles can both buy and sell charging.

2) EI Devices: Located along roadways and in remote areas, this layer includes roadside units (RSUs), communication towers, and EIUAVs. These devices oversee network traffic flow and support resource functions such as data collection, computation offloading, caching, and real-time processing. EIUAVs provide flexibility by extending coverage to remote locations and compensating for failing or unavailable edge servers. Using V2I communication, they enhance network responsiveness and efficiency, and although they may have higher latency than end devices, they substantially reduce the load on cloud servers.
3) Core Cloud: This layer contains the cloud entities, providing faster computation resources and larger data storage with increased latency compared to lower levels. The cloud entities in the system include the Key Distribution Center (KDC), Bank, Energy Service Provider (ESP), and Energy Distribution Center (EDC). The KDC enables symmetric encryption for secured communication. The Bank acts as the middleman between the EDC and the vehicle to complete Credit Points (CPs) purchase and sales transactions. CPs, an encrypted virtual currency, help avoid forgeries, maintain vehicle anonymity, and enable secure payments of charging sessions. The ESP manages both billing and energy distribution. The EDC communicates with the ESPs and charging network managers to make charging reservations and support coordinated route planning. It is also responsible for energy distribution and setting energy pricing rates.

The introduction of a coordination layer is necessary because charging infrastructure operation and system-level service management operate at different spatial scopes and decision timescales. Charging infrastructures must respond to local operational conditions such as alignment constraints, safety enforcement, and charging availability, whereas reservation handling, charging network selection, and route planning require awareness of system-level information across multiple charging networks. If vehicles were required to directly interact with all charging infrastructures or back-end services, they would need to independently discover, query, and negotiate with heterogeneous charging entities, resulting in excessive signaling overhead and inconsistent policy enforcement. The coordination layer therefore aggregates charging requests, maintains localized awareness of charging infrastructure state, and enforces reservation decisions without requiring end devices to directly interact with all charging infrastructures or centralized services. In this role, it serves as the operational interface

through which scheduling and allocation decisions are enforced in real time. By maintaining consistent reservation state and infrastructure awareness, it enables sequential decision-making where each confirmed charging session influences subsequent system behavior and resource availability.

Alternative architectural organizations were considered during the design of the proposed system. A single-layer architecture, in which vehicles, charging infrastructures, coordination logic, and service functions operate within a unified control plane, would tightly couple infrastructure execution with higher-level coordination and service management. Such coupling limits scalability as system size increases and complicates integration of heterogeneous charging technologies. A two-layer architecture that merges infrastructure execution with coordination logic reduces one communication boundary but still introduces strong coupling between infrastructure-specific operations and system-level decision making. This structure limits architectural flexibility when new vehicle classes or charging networks are introduced.

The three-layer architecture adopted in this work provides the minimum architectural separation required to support scalable coordination in heterogeneous ITS environments. In this structure, End Devices perform infrastructure-facing charging operations, EI Devices provide edge-level coordination and monitoring, and Core Cloud entities manage system-level services and persistent data. Physical charging operations must remain close to the infrastructure where alignment conditions, safety constraints, and energy transfer control are enforced. Physical energy transfer and communication coordination cannot be merged into a single layer, because charging hardware control operates under infrastructure-specific timing and safety constraints, whereas coordination functions must manage reservation signaling and network-wide decision making. These coordination functions must operate near the network edge to support low-latency reservation handling, charging availability monitoring, and route-aware charging decisions. Service-level functions such as billing, pricing, authentication, and key management operate at longer timescales and require persistent system-wide resources. Separating these responsibilities into end devices, edge intelligence, and core cloud layers enables modular system design, reduces coupling between infrastructure control and service management, and preserves interoperability across heterogeneous charging networks.

This architectural separation also reflects the practical mismatch between charging infrastructure deployment and communication infrastructure coverage. Charging resources are spatially constrained by roadway layout, embedded charging segments, parking facilities, and aerial service regions, whereas communication coverage may be broader, overlapping,

intermittent, or technology-dependent. As a result, communication availability does not necessarily imply immediate access to compatible charging infrastructure, and charging access does not require one-to-one co-location with communication assets.

The proposed three-layer architecture addresses this mismatch by explicitly decoupling charging execution from communication support while coordinating them through EI devices and CNMs. Vehicles use available communication paths to discover, reserve, and authenticate charging sessions, while the actual charging execution remains bound to physically compatible infrastructure. This design enables coordinated operation even when communication and charging assets are not co-located, ensuring that heterogeneity in infrastructure deployment does not degrade system-level coordination.

In addition to architectural separation, the proposed three-layer design supports low-latency coordination and distributed computation closer to end devices. Rather than relying exclusively on centralized cloud computing, which can introduce end-to-end delays on the order of tens of milliseconds, such as approximately 80 ms for cloud access in representative scenarios [147], [148], the proposed system integrates EI to localize delay-sensitive processing. Prior analyses indicate that edge computing can reduce packet delivery latency to below 10 ms under suitable deployment conditions [149], motivating its inclusion as a core architectural component for time-sensitive charging coordination.

Within this design, EIUAVs are assumed to operate as mobile edge servers to support delay-sensitive and computationally intensive tasks related to charging coordination and monitoring. Selected applications operating at the mobile edge may still communicate with the core cloud to access shared services, applications, or long-term data storage for synchronization purposes. These interactions are treated as not delay-sensitive within the proposed architecture. By preprocessing data at the edge, the system reduces both the distance data must travel and the volume of data transmitted to the cloud, which in turn limits communication overhead and the energy consumption associated with large-scale data transfer. This consideration is particularly important for EIUAVs with constrained battery capacity and aligns with the system's objective of energy-aware operation. The resulting design is scalable and flexible, allowing future charging systems and services to be incorporated without modifying the underlying architectural framework.

The three-layer architecture is designed to support communication and interaction across heterogeneous wireless technologies, including Wi-Fi and 6G, enabling real-time data exchange, low-latency coordination, and massive device connectivity. Within this architectural framework, charging requests are distributed across heterogeneous charging networks to

support coordinated reservation and session management for both CAEVs and UAVs, while maintaining a unified control structure and consistent protocol execution. In conjunction with the adopted communication topology for CN management, the proposed architecture supports the coordinated handling of large charging demands by enabling charging sessions to be allocated across available networks of different types in alignment with vehicle routes and operational constraints. All CN types considered in this work are instantiated using the proposed three-layer edge architecture, as illustrated in Figures 3.5 to 3.8.

Figure 3.5 shows the three-layer architecture for the CCN. This configuration emphasizes reliable wired connections for charging and distributed coordination of charging requests among end devices, edge intelligence nodes, and the core cloud. It ensures stable operation for stationary CAEVs.

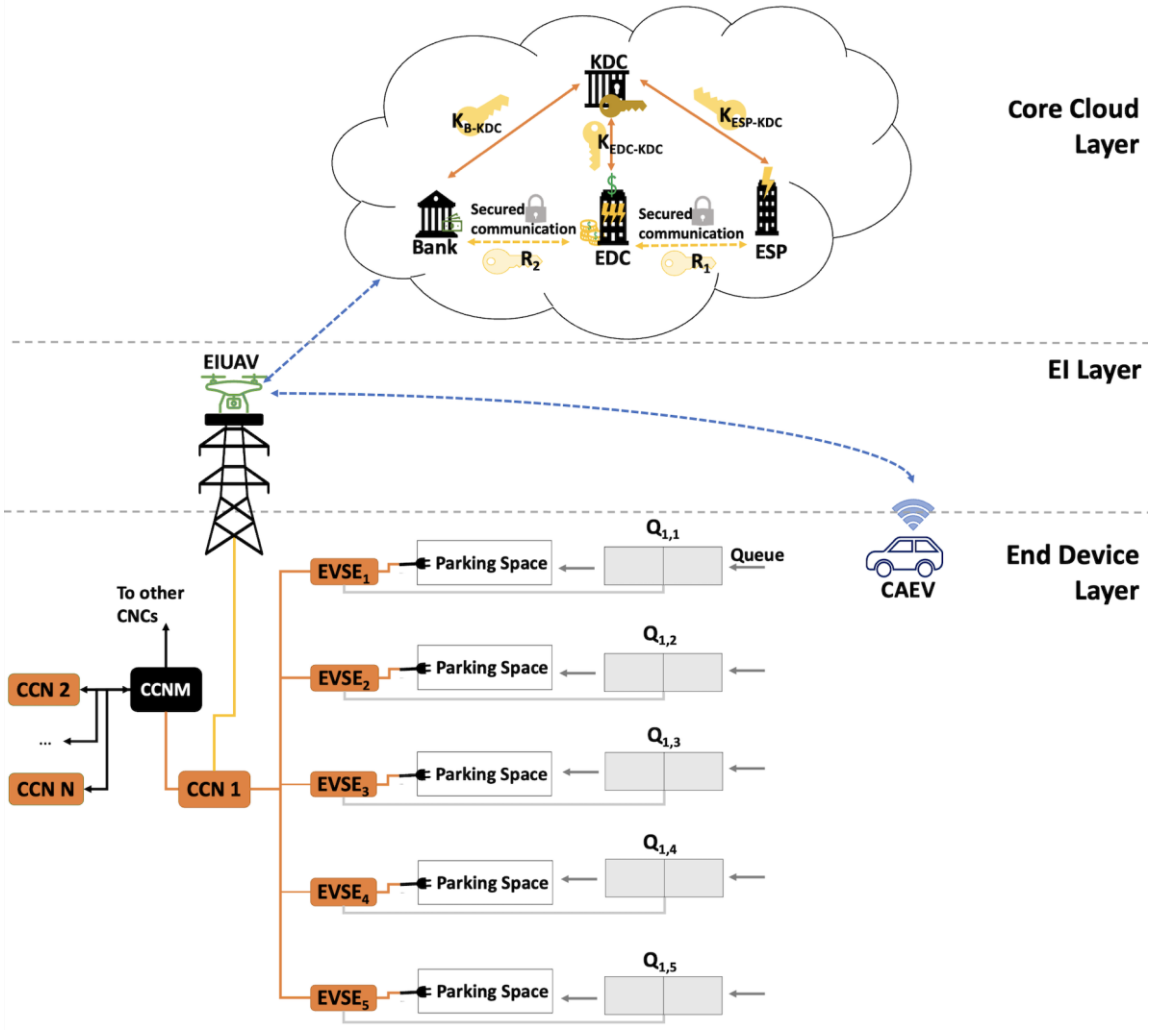

Figure 3.5: CCN following the proposed three-layer architecture.

Figure 3.6 illustrates the SWCN, highlighting inductive charging for stationary vehicles. The three-layer design facilitates precise alignment for energy transfer, local computation at edge intelligence devices, and cloud-level coordination for billing and reservation management.

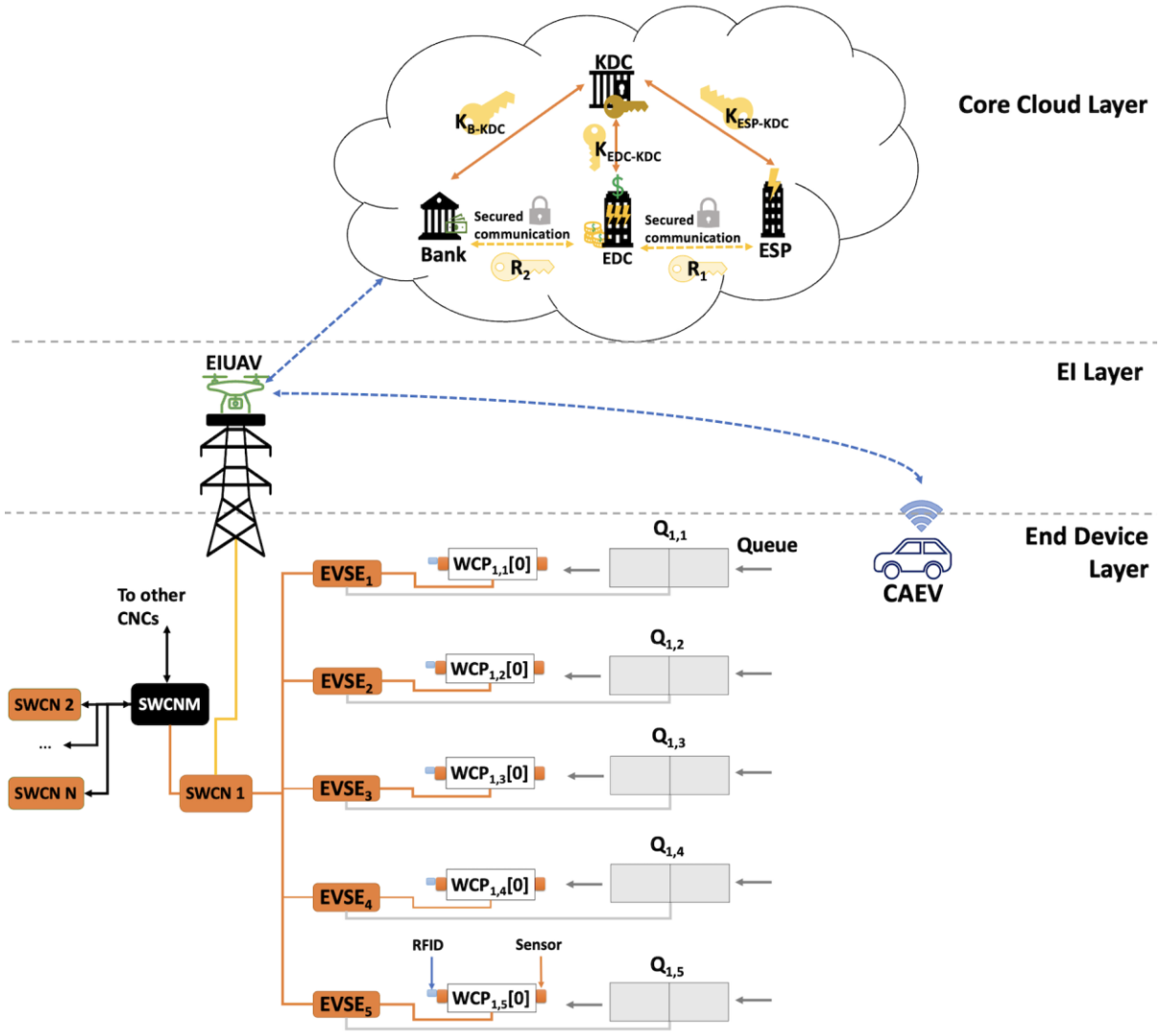

Figure 3.6: SWCN following the proposed three-layer architecture.

Figure 3.7 depicts the DWCN, which supports in-motion charging via embedded roadway coils. Edge devices and UAVs interact with the core cloud to manage real-time scheduling, route planning, and dynamic load distribution. This reduces latency and improves responsiveness.

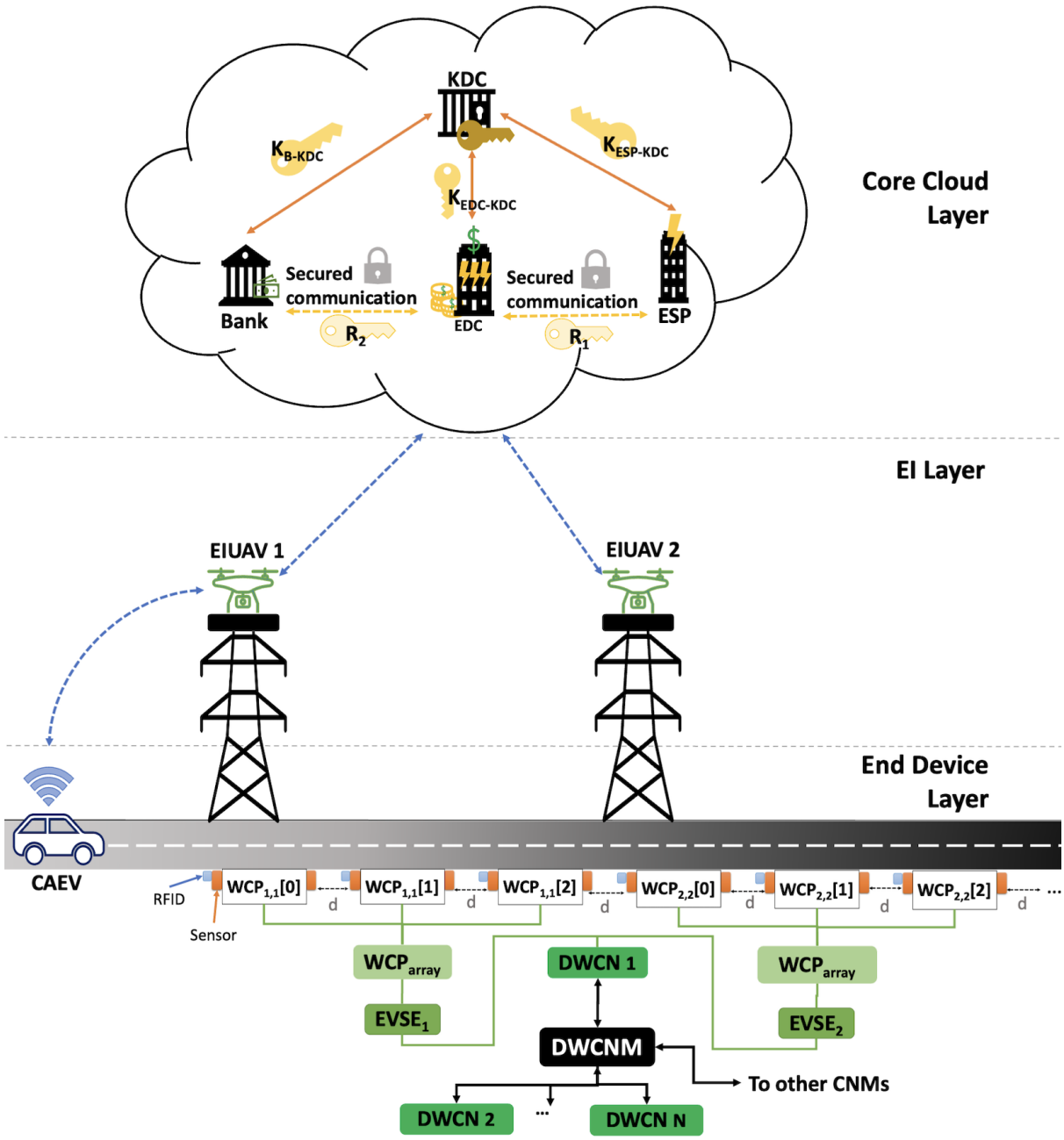

Figure 3.7: DWCN following the proposed three-layer architecture.

Figure 3.8 combines the LBCN, AVCN, and GVCN. This configuration demonstrates advanced charging methods, including laser beaming, UAV-to-CAEV coordination, and cross-network energy sharing. It is supported by distributed EI and core cloud orchestration.

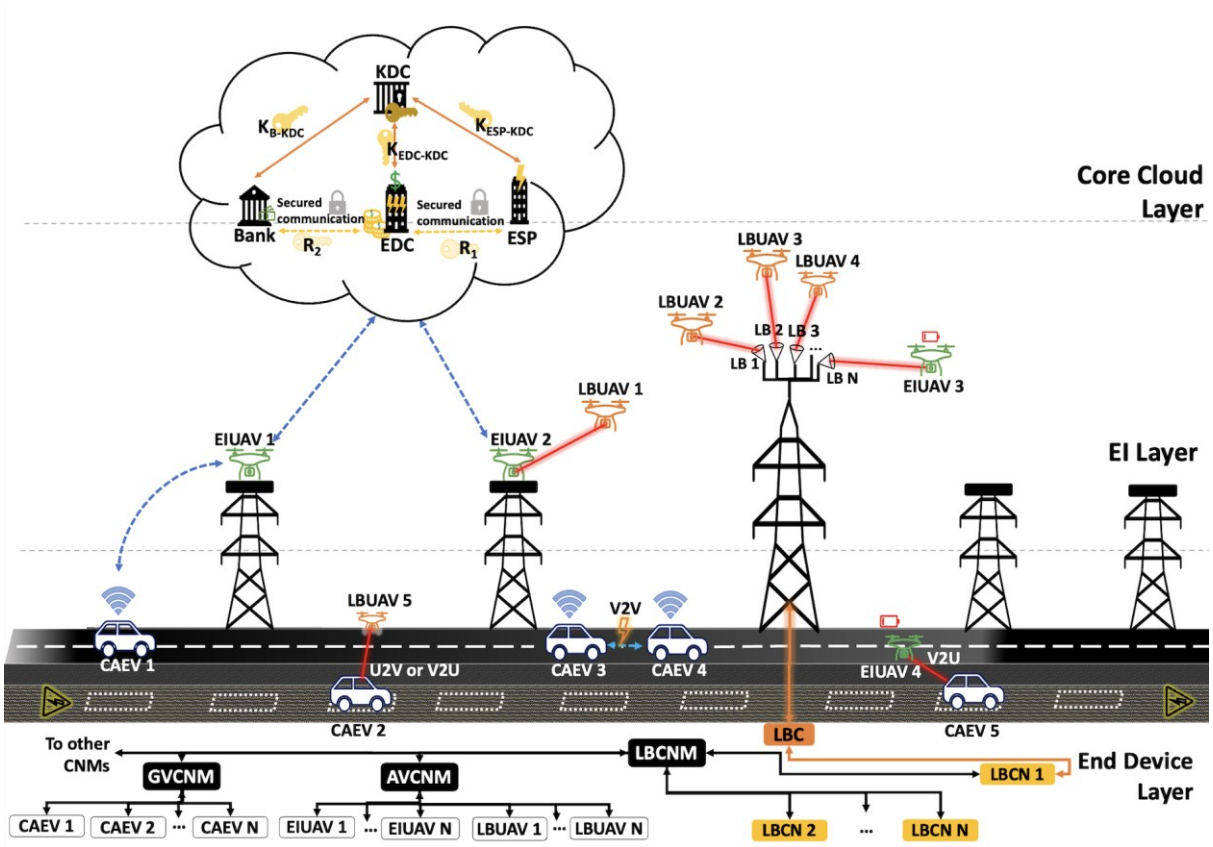

Figure 3.8: LBCN, AVCN and GVCN following the proposed three-layer architecture.

Next, to maintain compatibility with both existing and future wireless charging standards, a handshake protocol is presented.

3.5 Handshake Protocol

To support interoperable charging across heterogeneous charging networks and maintain compatibility with both existing and emerging wireless charging standards, the proposed architecture incorporates a unified handshake protocol. The protocol governs charging session initiation, authorization, monitoring, and billing, ensuring that charging reservations are securely authenticated and accurately billed using one of the supported payment schemes. By defining a common, technology-agnostic control flow, the handshake protocol enables consistent reservation handling and session management across vehicle types and charging modalities, while incorporating protocol-level monitoring to detect and mitigate

unsafe charging conditions such as misalignment, loss of line-of-sight, and speed-related violations.

The proposed handshake protocol is designed as a coordination-layer procedure that operates above the underlying communication stack and is therefore aligned with, rather than a replacement for, existing vehicular and charging standards. In particular, the message exchanges defined for request submission, reservation confirmation, authentication, session monitoring, and termination can operate over established V2X communication frameworks such as IEEE 802.11p/ITS-G5, Cellular Vehicle-to-Everything (C-V2X), and New Radio Vehicle-to-Everything (NR-V2X) [33], [35], [45]. From the charging perspective, the protocol is conceptually consistent with session-oriented interaction models used in established EV charging standards, such as ISO 15118 [150] and IEC 61851 [151], where authentication, controlled energy transfer, and billing-related operations are performed through structured message exchange [33], [35], [45], [116].

The contribution of the proposed handshake protocol lies in unifying reservation-based coordination and charging session management across heterogeneous charging networks and vehicle types, including both CAEVs and UAVs, rather than redefining lower-layer communication procedures. Existing standards primarily focus on point-to-point charging interactions between a single vehicle and a single charging infrastructure under a fixed communication context, and do not address coordinated reservation handling, cross-network charging selection, or interoperability across diverse charging modalities such as stationary, dynamic, and aerial charging. In contrast, the proposed protocol extends the standard session model by introducing a coordination-driven control flow that enables multi-network interaction, route-aware reservation, and consistent session management across heterogeneous infrastructures. In this sense, the proposed protocol maps its control stages to standard-compliant session procedures, where reservation corresponds to pre-session negotiation, authentication aligns with existing authorization exchanges, and session monitoring and termination follow established control and billing interactions. As such, it can be implemented on top of existing and emerging ITS communication infrastructures, including those envisioned for 6G, while preserving compatibility with current standard-compliant systems [33], [35], [45].

The handshake protocol [133], [146] is organized into three main stages corresponding to charging request initiation, session establishment and monitoring, and session termination with billing settlement.

3.5.1 Requesting a Charging Session

Initially, a vehicle requests a charging session. A CAEV (Figure 3.9) or UAV (Figure 3.10) seeking charging communicates with the nearest EI device. A CAEV communicates with the nearest EIUAV, while an LBUAV forwards its request to an EIUAV. If the UAV itself is an EIUAV, it handles the request directly. A lightweight request message is proposed, carrying the requested SoC, the vehicle's current location, and intended destination. Upon receiving the message, the EIUAV appends a random ID to the request message frame for tracking while preserving the requester's anonymity. For optimized charging and trip planning, the EIUAV contacts the relevant CNMs to evaluate the availability of charging stations, vehicle chargers, and DWC options along the planned route for both CAEVs and UAVs. Using the information reported by the CNMs, the EIUAV, together with the EDC and ESP, calculates a coordinated and performance-driven route and charging schedule based on the vehicle's remaining energy, infrastructure availability, traffic or aerial congestion, and operational constraints. A lightweight reservation message frame is designed to convey the optimal route and reservation details, including charging network location and scheduled time. The same random ID from the charging request is used for traceability. Once the charging reservation message frame reaches the vehicle, it follows the route and stops at the charging networks for scheduled charging.

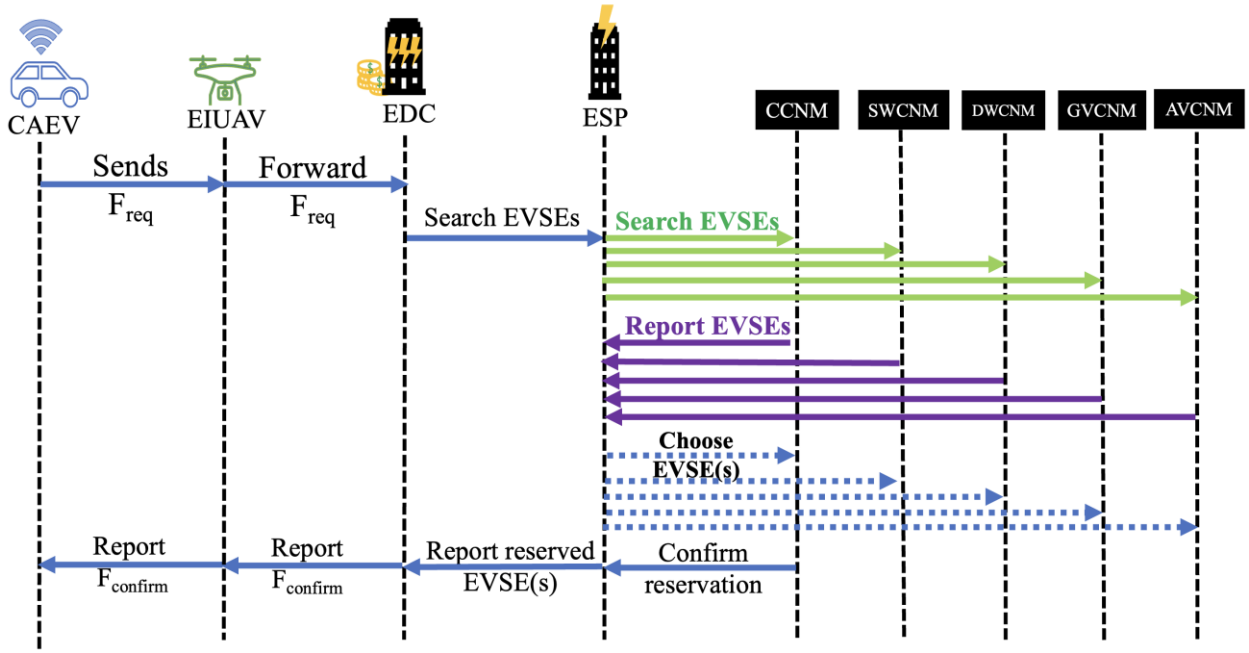

Figure 3.9: CAEV sends charging reservation request and receives confirmation message.

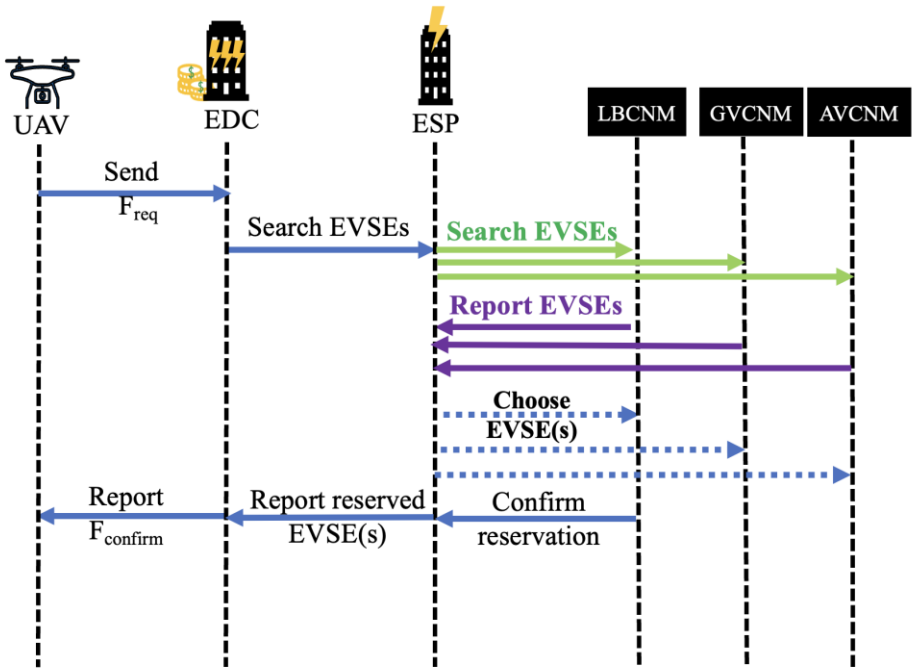

Figure 3.10: UAV sends charging reservation request and receives confirmation message.

3.5.2 Establishing a Charging Session

Next, a vehicle with a reservation confirmation frame ($F_{confirm}$) establishes a charging session with its scheduled fixed or mobile charging networks. In fixed networks like CCN, SWCN, DWCN, and LBCN, the vehicle proceeds to the scheduled charging network and authenticates with its EVSE by exchanging the ID from the confirmation frame. This process is depicted for CAEVs in Figure 3.11 and for UAVs in Figure 3.12. Once successfully authenticated, the EVSE provides high power for charging after initial communication in low power mode. This staged transition from low-power control exchange to high-power transfer is consistent with safety-oriented charging session establishment practices in existing standards, where authorization and readiness verification precede sustained energy delivery [33], [35], [45]. In near-field wireless networks, the vehicle communicates with the WCPs for authentication and proper alignment, crucial for maximum WPT efficiency. While synchronization occurs once in SWCN, it is done for every WCP in DWCNs, allowing vehicles to exit and re-enter the lane before a timeout to prevent free riders. Additionally, individual authentication of WCPs enables the system to shut down damaged or obstructed units.

Similarly, in far-field networks like LBCNs, the vehicle approaches the laser beaming tower and exchanges the reservation confirmation ID with its EVSE. After authentication, the EVSE adjusts the LBET to maintain direct LOS with the vehicle for efficient WPT, with continuous communication ensuring alignment using VLC or low power mode. WPT occurs when the vehicle is properly aligned and at a safe distance.

In mobile charging like charging between vehicles of the same or different types, as shown in Figure 3.13, vehicles communicate directly for charging. In homogeneous vehicle charging, a vehicle approaches the energy transmitting vehicle of the same type, exchanging the reservation confirmation ID for authentication. Continuous communication maintains alignment between their energy transmitter and receivers, thus enabling WPT when properly aligned. It is important to note that in U2U charging, only the LBUAV can deliver charging to EIUAVs.

For heterogeneous vehicle charging like V2U and U2V charging, near-field or far-field technology can be employed. With magnetic resonance, the CAEV can move while receiving or delivering charging to the UAV mounted on the WCP. However, in laser beaming WPT, both vehicles must be stationary and maintain LOS to comply with safety regulations. Authentication and synchronization of WET and WER follow the same steps as in homogeneous vehicle charging.

3.5.3 Payment and End of a Charging Session

A vehicle's onboard unit monitors the energy received by the battery over time. Two proposed payment schemes for billing vehicles are: 1) Pay-per-charging session, where the vehicle is billed at the end of the session. 2) Pay-per-energy-unit (kW), where the vehicle is metered and billed in real-time for each energy unit (kW) received. This is depicted in Figures 3.11 to 3.13. Both schemes use real-time metering. Following the Time of Use (TOU) electricity billing model, the EDC fairly bills the vehicle at the end of the session. Encrypted virtual currency called CPs ensures vehicle owner anonymity in payments. The EDC records all paid anonymous charging sessions with randomly assigned reservation IDs for tracing. To ensure fair billing, the vehicle verifies the bill issued by the EDC. Any discrepancies can be addressed by sending a negative acknowledgment to the EDC for recalculation.

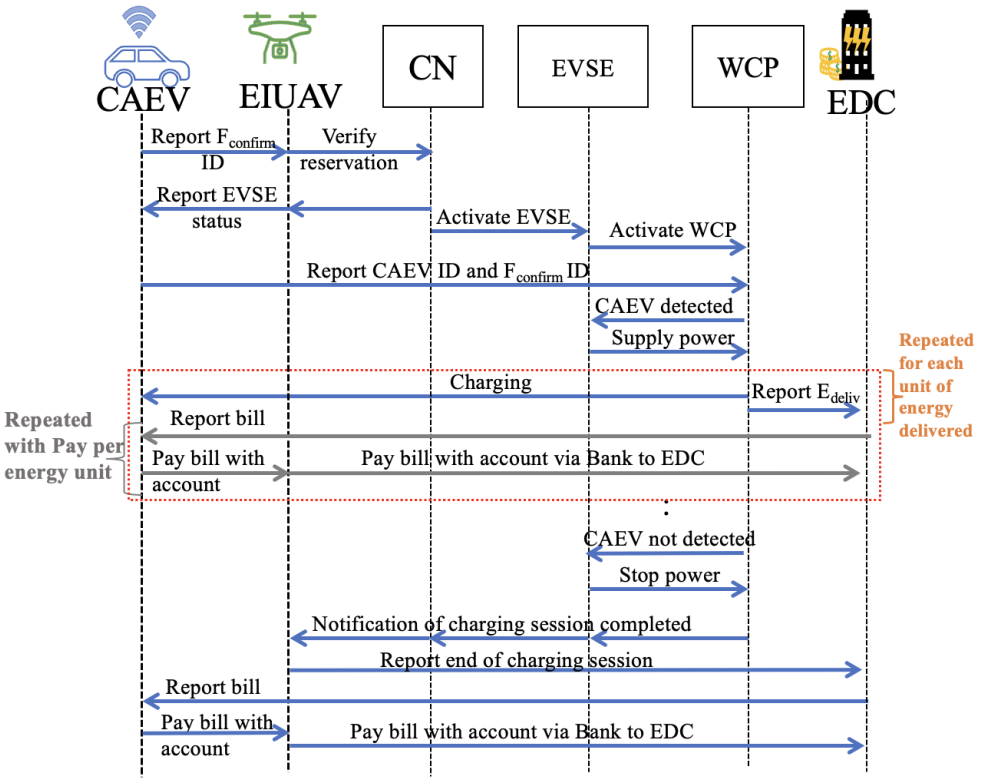

Figure 3.11: Process of CAEV Establishing, Completing, and Paying for a Charging Session.

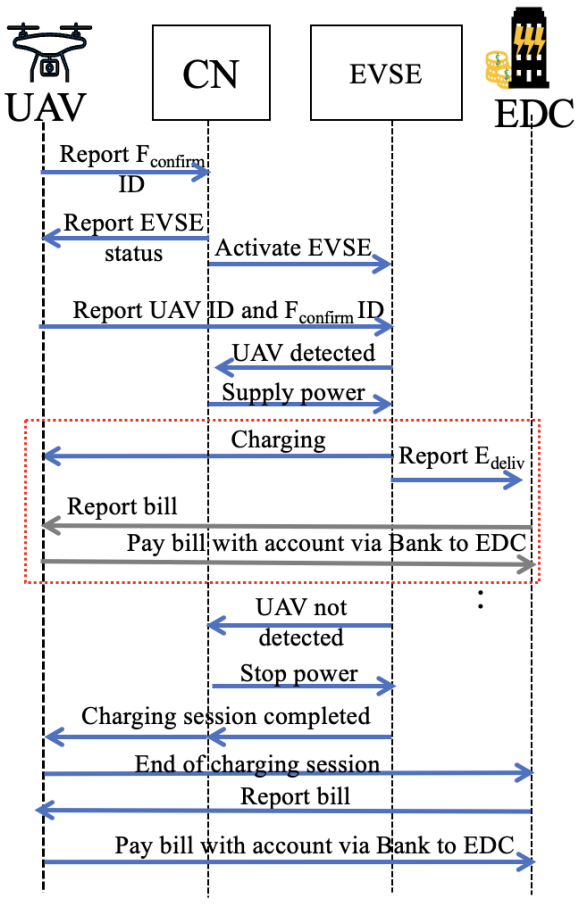

Figure 3.12: Process of UAV Establishing, Completing, and Paying for a Charging Session.

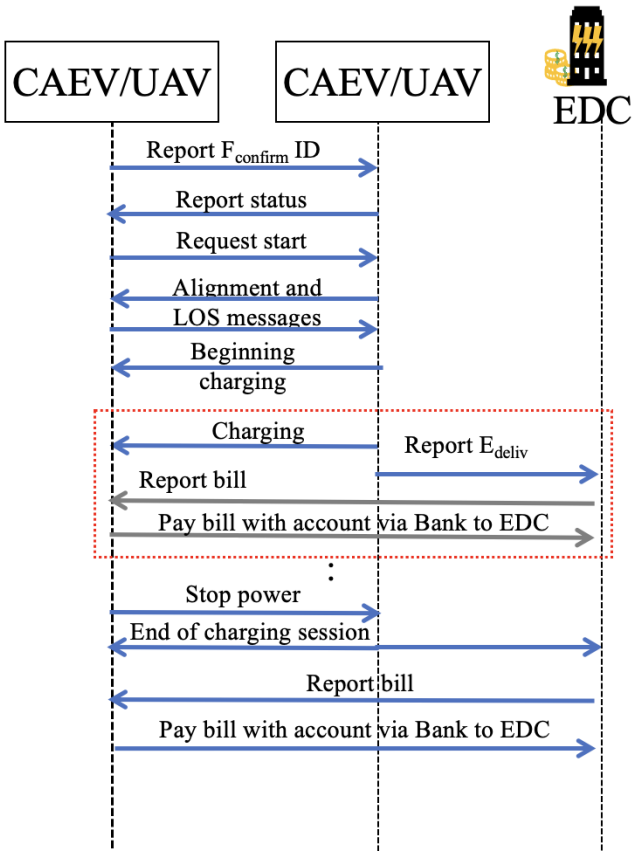

Figure 3.13: Inter-vehicle charging session establishment, completion and payment.

The end of a charging session can be determined by exchanging end session messages between the WPT transmitting and receiving entities. Alternatively, sensors and a timer can detect the session's end. If the sensor detects misalignment between the WET and WER, a probing message is sent to the vehicle, and a timer starts. If the timer expires, as shown in Figures 3.14 and 3.16 for fixed and mobile charging respectively, and the vehicle does not respond in time or signals an end, the charging session ends. However, if the vehicle responds with an acknowledgment in time, as illustrated in Figures 3.15 and 3.17 for fixed and mobile charging, respectively, then the charging session will re-initiate the charging establishment process and resume charging.

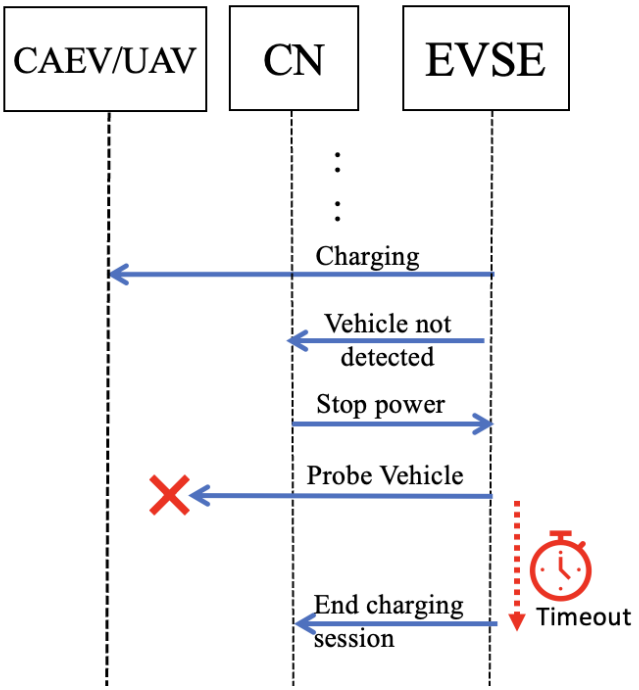

Figure 3.14: Ending a charging session for unresponsive vehicle.

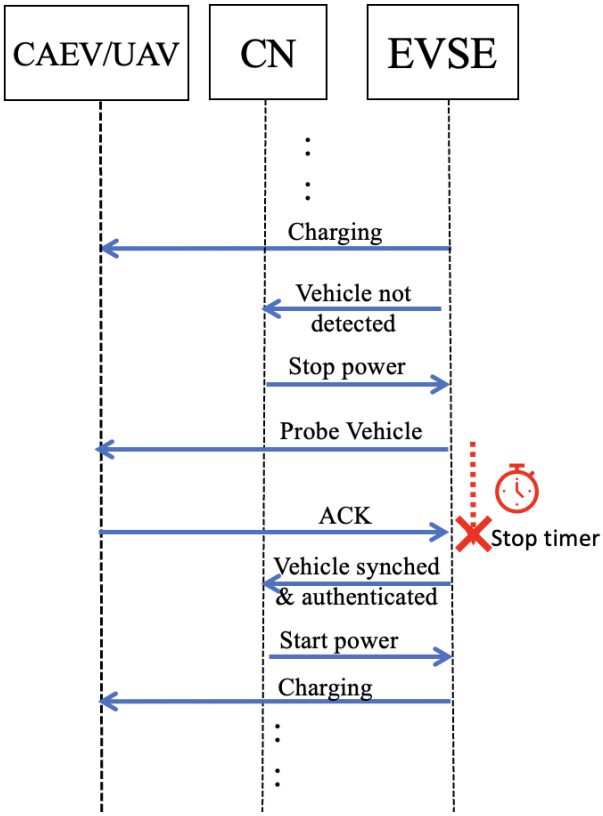

Figure 3.15: Initiating a session cancellation but resuming it after vehicle acknowledgement.

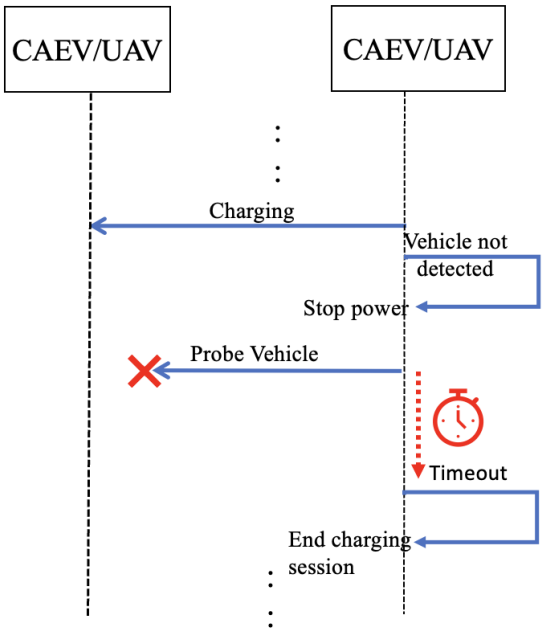

Figure 3.16: Ending a charging session for unresponsive vehicle in inter-vehicle charging.

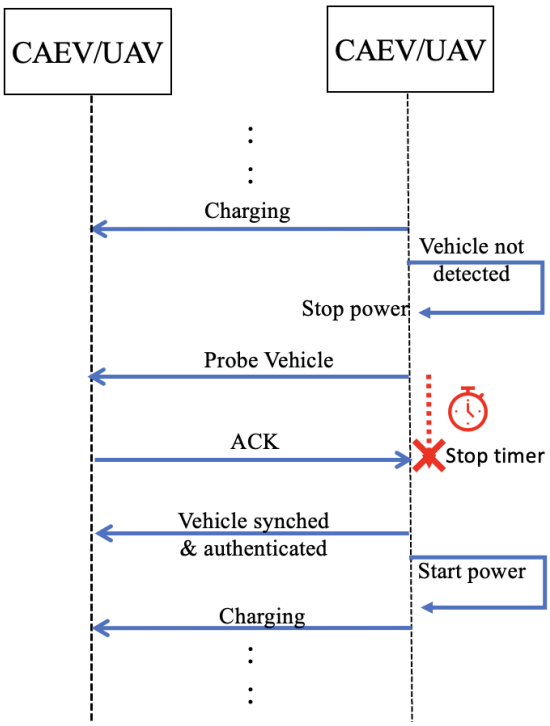

Figure 3.17: Initiating a session cancellation but resuming it after vehicle acknowledgement in inter-vehicle charging.

3.6 Architectural Validation and Design Verification

This section validates the proposed CN architecture from a design and protocol perspective. The objective is to demonstrate that the architectural components, communication topology, and handshake protocol operate correctly and cohesively when coordinating charging across heterogeneous CNs and vehicle types. While subsequent chapters investigate

algorithmic behavior and system-level performance, the focus here is on verifying architectural correctness and architectural consistency, protocol execution, and feasibility of coordinated operation under 6G-enabled ITS assumptions.

3.6.1 Validation Objectives and Scope

Architectural validation focuses on three primary aspects. First, correctness, ensuring that charging sessions follow a well-defined sequence of request submission, reservation confirmation, authentication, charging execution, and termination, with safety and authorization constraints enforced throughout. Second, interoperability, ensuring that heterogeneous charging technologies and vehicle types can be coordinated using a unified architectural framework. Third, scalability by design, ensuring that additional vehicles and CNs can be incorporated without structural modification or global reconfiguration.

These objectives are addressed through a combination of design consistency analysis, protocol execution verification, and implementation-level testing. Together, these validation steps confirm that the proposed architecture behaves as intended and provides a stable foundation for the coordinated scheduling and system-level evaluations presented in later chapters.

3.6.2 Architectural Consistency and Interoperability Verification

Architectural consistency was verified by exercising a common control flow across all supported charging interactions, including fixed infrastructure charging, mobile homogeneous charging, and heterogeneous CAEV to UAV charging. In all cases, charging coordination follows the same sequence of control states, independent of the underlying power transfer technology. This confirms that charging coordination is abstracted from physical energy delivery mechanisms and enforced at the architectural level.

Interoperability was further verified through the hybrid mesh star communication topology. Localized control within individual CNs is maintained by dedicated CNMs, while peer coordination among managers enables cross-network charging sessions. This structure allows charging interactions to span multiple charging networks without centralized orchestration or protocol specialization. As a result, new CNs and vehicle classes can be integrated through standard interfaces while preserving existing coordination logic.

3.6.3 Handshake Protocol Execution and Safety Verification

The handshake protocol was validated by analyzing its execution across all supported charging modes. Protocol execution confirms that WPT is initiated only after successful reservation validation and authentication. Continuous alignment monitoring and timeout-based probing ensure that charging sessions are suspended or terminated under unsafe or

unauthorized conditions, including misalignment, loss of line-of-sight, or unresponsive behavior.

These behaviors were verified through implemented protocol execution paths rather than assumed analytically. They explicitly demonstrate robustness of the protocol under control-level communication interruptions, including delayed responses, message loss, and temporary disconnections, without requiring continuous or error-free connectivity. Safety and authorization constraints are therefore enforced by the protocol logic itself, independent of the specific charging technology or vehicle type involved. This validates the technology-agnostic nature of the handshake protocol and its suitability for dynamic and heterogeneous ITS environments.

3.6.4 Scalability and Distributed Coordination Verification

Scalability was verified by examining how coordination responsibilities are distributed across EI devices that are EIUAVs and CNMs. Reservation handling, authentication, and session monitoring are confined to local control domains, avoiding centralized coordination bottlenecks. Lightweight message frames carrying anonymized identifiers and minimal state information further reduce signaling overhead.

From an architectural standpoint, this distributed coordination model ensures that increases in the number of vehicles or charging nodes do not require changes to the global architecture. The same architectural design is subsequently employed without modification in algorithmic simulations and system-level evaluations in subsequent chapters, thus confirming its suitability for larger-scale operation.

3.6.5 Design-Level Implementation Verification

Design-level verification was carried out through an object-oriented software implementation developed in Python. The architecture was instantiated using modular classes representing vehicles, CNMs, EI devices, and protocol entities. This implementation enabled controlled execution of charging requests, reservation enforcement, session establishment, alignment monitoring, and session termination across representative CAEV and UAV scenarios.

The use of object-oriented design allowed architectural components to interact exclusively through defined interfaces, closely reflecting the intended deployment structure. This approach facilitated systematic testing of protocol execution paths and edge conditions while ensuring that the architecture remains extensible and reusable. Summary results of these proof-of-concept tests are provided in Appendix C for completeness and serve to confirm that

the proposed architecture and handshake protocol can be realized and executed in practice. These results are intended as design verification rather than final performance evaluation.

3.6.6 Verification Cases and Edge Condition Coverage

To further substantiate architectural correctness, the proposed design was verified against a set of representative operational cases and edge conditions that exercise the full control flow of the architecture and handshake protocol. These cases validate correct session establishment, enforcement of safety and authorization constraints, interoperability across CNs, and robustness under mobility-related uncertainties. The verified cases are summarized in Table 3.1.

Table 3.1: Architectural Verification Cases and Coverage.

Verification Case	Scenario Description	Architectural Component Exercised	Verified Behavior
Nominal charging session	Vehicle requests charging and completes session	End devices, CNM, handshake protocol	Correct request handling, authentication, and termination
Heterogeneous charging	CAEV to UAV and UAV to CAEV charging	Unified control flow, protocol abstraction	Interoperable coordination across vehicle types
Fixed infrastructure charging	CCN, SWCN, and LBCN sessions	CNMs, edge coordination	Consistent session establishment
DWC	In-motion charging with periodic checks	DWCN manager, alignment monitoring	Enforcement of authorization and alignment
Misalignment detection	Loss of alignment during charging	Handshake protocol, safety logic	Immediate session suspension or termination
Line-of-sight loss	Laser-based charging interruption	Timeout and probing mechanisms	Safe termination of charging
Unresponsive vehicle	No acknowledgment during session	Protocol timeout logic	Charging termination without energy leakage
Early arrival	Vehicle arrives before reserved time	Reservation enforcement	Controlled session initiation
Late arrival	Vehicle arrives after reserved time	Re-authentication logic	Safe resumption or reassignment
Cross-network coordination	Charging spans multiple networks	CNM peer coordination	Seamless handoff without central control
Edge intelligence involvement	EIUAV manages coordination	Three-layer architecture	Correct delegation to edge layer
Local failure containment	Temporary node unavailability	Distributed control	Continued operation in unaffected domains

These verification cases collectively exercise both nominal operation and edge conditions, providing concrete evidence that the proposed architecture and protocol enforce correctness, safety, and interoperability across heterogeneous charging scenarios.

3.6.7 Design Guarantees of the Proposed Architecture

The proposed CN architecture provides a set of explicit guarantees that are enforced by construction rather than through post hoc optimization or parameter tuning. These guarantees arise from the separation of responsibilities across the three-layer architecture, the hybrid communication topology, and the protocol-driven coordination of charging operations.

Together, these design choices ensure predictable behavior under heterogeneous operating conditions and support reliable coordination in 6G-ITS.

From a safety perspective, WPT is permitted only after successful authentication, reservation verification, and confirmation of proper alignment between energy transmitting and receiving entities. Alignment and session activity are continuously monitored during charging, enabling immediate suspension or termination under unsafe operating conditions such as misalignment, loss of line-of-sight, or unresponsive vehicles. While the specific algorithms used to compute and correct alignment are introduced in the subsequent chapter, the architecture and handshake protocol defined here ensure that alignment constraints are enforced consistently across all supported charging modes.

Interoperability is achieved by enforcing a unified control flow that is independent of vehicle type and underlying charging technology. Fixed infrastructure charging, mobile homogeneous charging, and heterogeneous CAEV–UAV charging are coordinated using the same handshake protocol and reservation framework. This design enables interoperable operation across CCN, SWCN, DWCN, LBCN, AVCN, and GVCN without protocol specialization, allowing heterogeneous CNs to coexist and cooperate within a single architectural framework.

Scalability is ensured by confining coordination and control decisions to local CNMs and EI devices. Charging requests, reservations, and session monitoring are handled within localized domains, enabling new CNs, vehicles, or infrastructure elements to be incorporated through registration with the appropriate manager. This approach avoids global reconfiguration and allows the architecture to scale naturally with system size and deployment density.

The architecture also provides failure containment by design. Localized failures, such as the temporary unavailability of a CNM or an EI node, do not compromise system-wide operation. Peer coordination among managers enables alternative routing of charging requests and preserves operational continuity within unaffected domains, ensuring resilience in dynamic and partially unreliable environments.

Finally, privacy and billing integrity are supported through the use of anonymized identifiers and encrypted CP transactions. Charging reservations and payment operations can therefore be completed without revealing sensitive identity information, while maintaining verifiable and auditable billing records. This design supports secure and fair charging interactions across heterogeneous networks and ownership domains.

The relationship between these design guarantees and the architectural mechanisms that enforce them is summarized in Table 3.2.

Table 3.2: Design Guarantees and Enforcing Architectural Components.

Design Guarantee	Enforcing Architectural Components	Enforcement Scope
Safety	Authentication logic, reservation validation, alignment enforcement, session termination	Protocol and edge coordination
Interoperability	Unified control flow and handshake protocol	System-wide coordination
Scalability	Localized coordination via CNMs and EI devices	CN domains
Failure containment	Peer coordination and localized control domains	CNM interactions
Privacy and billing integrity	Anonymized identifiers and encrypted CP transactions	Billing and authorization services

3.6.8 Summary of Architectural Validation

The validation presented in this section confirms that the proposed CN architecture operates correctly at the design and protocol levels. Unified control flow, distributed coordination, and technology-independent protocol execution aligned with 6G-ITS requirements enable safe and interoperable charging across heterogeneous networks. The architectural components verified here are used by the scheduling algorithms and system-level simulations examined in subsequent chapters, establishing a clear and consistent foundation for the overall framework.

3.7 Architectural Differentiation and Design Implications

Building on the validated properties and design guarantees established in the preceding section, the architectural significance of the proposed design lies in the coordinated integration of communication, computation, and energy management functions within a single, cohesive framework. Rather than optimizing a single subsystem in isolation, the architecture is designed to support coordinated charging decisions across heterogeneous vehicles, charging technologies, and network domains. The preceding sections established that the architecture operates correctly and enforces key design guarantees. This subsection elaborates on how the resulting architectural structure differs from conventional charging coordination approaches and why these differences matter from a system design perspective. This architectural structure therefore provides the necessary foundation for coordinated scheduling and policy-driven decision-making, which are developed and evaluated in subsequent chapters.

A fundamental point of differentiation is the adoption of a three-tier architectural structure that explicitly separates end devices, edge intelligence, and back-end service functions. This separation enables localized decision-making while preserving global consistency through standardized interfaces. In contrast to single-layer or partially centralized designs, this structure limits the propagation of local state changes and reduces the need for system-wide synchronization. As a result, the architecture preserves tractable coordination complexity as system scale increases, which is critical for dense and heterogeneous deployments.

Another distinguishing aspect is the unified treatment of ground and aerial vehicles within the same architectural framework. Conventional designs typically address CAEVs and UAVs independently due to their differing mobility characteristics and operational constraints. By abstracting charging coordination at the architectural and protocol levels, the proposed design enables coordinated CAEV–UAV interactions without embedding vehicle-specific logic into the control plane. This abstraction is essential for supporting mixed ground–aerial charging scenarios in future intelligent transportation systems.

The architecture also departs from conventional approaches by integrating multiple charging technologies under a single control flow. Fixed, dynamic, and mobile charging mechanisms are coordinated through a unified handshake protocol rather than through technology-specific controllers. This design choice avoids fragmentation of the control logic and ensures that safety, authorization, and billing policies are enforced consistently across all charging modes. Importantly, the architecture does not assume a dominant charging technology, making it suitable for heterogeneous and evolving 6G-ITS deployments.

From a coordination standpoint, the hybrid mesh star topology balances local autonomy with cross-network interaction. Fully centralized architectures suffer from scalability and latency limitations, while fully decentralized approaches incur high signaling overhead and inconsistent policy enforcement. The proposed topology confines most coordination decisions to local charging network managers while enabling peer interaction when cross-network charging is required. This structure supports scalable deployment while maintaining coherent system behavior.

Table 3.3 summarizes the structural characteristics of the proposed architecture in comparison with conventional charging coordination approaches. The comparison emphasizes architectural properties and design implications rather than performance metrics. These architectural choices directly enable the coordinated scheduling algorithms and system-level evaluations presented in subsequent chapters by providing a stable and extensible control foundation.

To make this relationship explicit, Table 3.4 maps the principal architectural design choices to their immediate effects and resulting system-level implications. The table highlights how specific structural decisions translate into coordination, scalability, and safety properties that hold independently of the scheduling and optimization mechanisms examined later. This mapping clarifies how the architecture constrains and enables system behavior by design, providing a clear link between architectural structure and subsequent algorithmic and system-level analyses.

Table 3.3: Architectural Characteristics and Design Implications.

Design Dimension	Conventional Charging Architectures	Proposed Architecture
Architectural structure	Single-layer or partially centralized	Three-layer structure with end devices, EI, and back-end services
Vehicle support	Ground vehicles only or UAVs only	Unified support for CAEVs and UAVs
Charging technologies	Single or homogeneous charging mode	Integrated support for CCN, SWCN, DWCN, LBCN, V2V, U2U, V2U, and U2V
Coordination model	Centralized or fully decentralized	Hybrid mesh star topology with local autonomy
Protocol design	Technology-specific or ad hoc	Unified, technology-independent handshake protocol
Safety enforcement	Implicit or externally managed	Embedded alignment and authorization enforcement
Scalability	Limited by central controller	Scalable by design through local control domains
Interoperability	Limited cross-network interaction	Native interoperability across heterogeneous networks
Extensibility	Requires redesign	Plug-in extension via CNMs

Table 3.4: Architectural Design Choices and Resulting System Implications.

Architectural Design Choice	Immediate Effect	System-Level Implication
Three-tier separation of end devices, EI, and back-end services	Localizes control decisions	Scalable coordination without global synchronization
Unified protocol for all charging technologies	Eliminates technology-specific controllers	Consistent enforcement of safety and billing policies
Abstraction of vehicle type at control plane	Decouples coordination from mobility model	Native support for CAEV–UAV interaction
Hybrid mesh star coordination topology	Limits signaling scope	Balanced scalability and policy consistency
CNM-based extensibility	Enables plug-in integration of new CNs	Incremental deployment without redesign
Protocol-level enforcement of alignment and authorization	Prevents unsafe charging by construction	Safety independent of scheduling algorithm

3.8 Conclusion

This chapter presented the design and validation of a scalable and interoperable charging network architecture for coordinated CAEV and UAV operations in 6G-enabled intelligent transportation systems. The architecture was defined through a three-tier structure that separates end devices, edge intelligence, and back-end service functions, supported by a hybrid mesh star coordination topology and a unified handshake protocol.

Architectural validation demonstrated that the proposed design operates correctly at the protocol and coordination levels, enforcing safety, authorization, and interoperability across heterogeneous charging technologies and vehicle types. Design-level implementation and verification confirmed that the architecture can be instantiated and exercised in practice, while explicit design guarantees formalized the properties enforced by construction, including safety, scalability, failure containment, and billing integrity.

The architectural differentiation and design implications discussed in this chapter highlighted how specific structural decisions enable coordinated operation without relying on centralized control or technology-specific assumptions. By abstracting charging coordination

from physical energy delivery and vehicle-specific logic, the proposed architecture provides a stable and extensible foundation upon which coordinated scheduling algorithms and system-level evaluations are built.

Building on this architectural foundation, the next chapter focuses on coordinated charging scheduling and decision-making, introducing algorithmic formulations and evaluating their behavior within the architectural framework established here.

Chapter 4 Coordinated Charging Scheduling Using Heuristic and Learning-Based Approaches

4.1 Introduction

The growing integration of connected autonomous electric vehicles and unmanned aerial vehicles places new demands on charging coordination within intelligent transportation systems. Heterogeneous charging technologies, dynamic vehicle arrivals, and strict operational constraints require coordinated charging scheduling and trip planning mechanisms that go beyond isolated or static decision making. Addressing these challenges is essential for enabling scalable and responsive energy management in next-generation, 6G-enabled intelligent transportation systems.

This chapter contributes coordinated charging scheduling solutions based on both heuristic and learning-based approaches. Building on the three-layer charging network architecture introduced in Chapter 3, the chapter focuses on the decision logic required to translate charging requests into feasible reservations, routing decisions, and executed charging actions under dynamic operating conditions. In this work, coordinated charging scheduling is formulated as a reservation-based scheduling problem, where each decision allocates both charging resources and time intervals, creating time-coupled dependencies that influence future system feasibility and performance. To support this objective, the chapter develops the system model, operational cycle, and supporting models for power consumption, charging feasibility, battery management, and alignment correction, establishing a practical foundation for coordinated scheduling.

On this foundation, heuristic charging scheduling and trip planning algorithms are first developed to provide interpretable baseline solutions with static and dynamic arrival handling. The chapter then introduces SAFE-DDPG as a learning-based coordinated charging scheduler designed for real-time operation in heterogeneous charging environments. The proposed approaches are evaluated through systematic experimental analysis under identical system conditions, highlighting their relative performance and trade-offs.

Through this progression, the chapter demonstrates how coordinated charging scheduling can be effectively realized using both heuristic and learning-based methods within ITS. Consistent with the terminology used throughout this thesis, intelligent scheduling refers to adaptive, state-aware coordination of charging and routing decisions under dynamic system conditions, including mobility, reservation coupling, and resource constraints. In this setting, optimization is interpreted in an objective-driven sense aligned with the literature, where

decision policies are designed to improve performance metrics such as waiting time, travel cost, and charging utilization under uncertainty. Rather than computing a static globally optimal solution with complete future information, optimization in this context refers to improving expected system-level performance through sequential decision policies, which is more consistent with dynamic and real-time charging environments. This formulation remains fully aligned with established definitions of stochastic and online optimization, where optimality is defined in terms of expected performance over time rather than a one-shot global optimum. It reflects the real nature of the problem, where future vehicle arrivals, system states, and charging demands are not known in advance, making sequential decision-making approaches more appropriate than global optimization formulations that assume complete future information.

4.2 System Overview and Methodology

The construction of the system model begins with defining the decision environment and interactions of the charging reservation and trip planning system required for coordinated charging scheduling. Key elements include a finite population of CAEVs and UAVs, arrival and service times defined by distributions, travel times to CN locations, and queuing discipline at static charging stations. Each CN is characterized by its service capacities, waiting areas, and dynamic behavior in response to vehicle arrivals and departures.

The system is organized into interconnected modules representing cloud entities, network components, vehicles, and charging stations, following the three-layer charging network architecture discussed earlier. These modules interact through structured message exchanges and reservation protocols, enabling coordinated charging scheduling decisions between aerial and ground vehicles. The modeling framework captures the essential features of each vehicle type, including energy consumption, battery dynamics, charging alignment requirements, and service requests, which together define the constraints and inputs for the scheduling algorithms proposed later in this chapter.

System events such as vehicle movement, arrival at a charging station, charging initiation, and departure are defined to represent the sequence of operations governing coordinated charging and trip planning. These events form the basis for algorithmic decision making, enabling both heuristic and learning-based approaches to optimize charging scheduling and associated trip planning decisions. The detailed sequence of these operations is presented in the next section, which outlines the complete system cycle for coordinated CAEV–UAV operation.

By conceptualizing the system in terms of modular entities and event-driven interactions, the framework supports the development, implementation, and evaluation of coordinated scheduling algorithms under a variety of operational conditions. This modeling approach emphasizes the structure, constraints, and decision making logic of the system and provides the foundation for the algorithm design, simulation setup, validation, and performance analysis presented later in this chapter.

The proposed coordinated charging scheduling framework explicitly incorporates mobility. Vehicle motion influences the scheduling state through route-dependent travel times, projected arrival times, dynamic charging feasibility, and event-triggered reservation updates. For CAEVs, mobility is governed by roadway routing, traffic conditions, and en-route charging opportunities, whereas for UAVs it is characterized by three-dimensional flight movement, energy-aware repositioning, and line-of-sight constraints for charging. Consequently, mobility is treated as an intrinsic component of the scheduling problem rather than as an external or secondary factor.

In addition, reliable coordination is ensured through protocol-level and architectural mechanisms, including acknowledgment-based reservation handling, timeout-triggered recovery, safe revalidation of charging states, and feasibility-aware execution. These mechanisms, defined in Chapter 3 and enforced within the scheduling process, ensure that coordination decisions remain valid and executable under intermittent communication conditions. As a result, the proposed framework enables coordinated charging scheduling under both mobility uncertainty and communication uncertainty, while maintaining safe, consistent, and system-level reliable operation across heterogeneous charging networks.

4.3 System Cycle of the Charging Reservation and Trip Planning

The overall operation of the proposed charging reservation and trip planning system can be described through six main phases that define the end-to-end process of coordinated CAEV-UAV interaction:

1. **Moving Phase:** The vehicle drives or flies toward its destination following the shortest feasible route. It makes scheduled stops at CNs to obtain energy from their EVSEs based on previously determined scheduling decisions.
2. **Charging Request Phase:** When a vehicle's SoC falls below a defined threshold enroute, it generates a charging reservation request containing its current state and destination. This request is forwarded to the system via the connected roadside or aerial infrastructure for validation and processing.

3. **Charging Scheduling and Trip Planning Phase:** The system processes the received reservation request to identify available EVSEs across CNs located near the vehicle's projected route. It selects charging options that minimize travel distance, cost, waiting time, and energy consumption, while maintaining balanced load distribution across the network. This phase constitutes the core coordinated scheduling problem addressed by the heuristic and SAFE-DDPG-based approaches proposed in this chapter.
4. **Reservation and Route Confirmation Phase:** Based on the scheduling decision outcome, the system confirms a set of EVSEs and corresponding time slots. A reservation confirmation, including route and schedule details, is then communicated back to the vehicle.
5. **Waiting Phase:** This phase occurs only if a vehicle arrives earlier than its reserved time and no immediate adjustment can be made to accommodate the early arrival. In such cases, the vehicle enters a short waiting period until the scheduled session begins.
6. **Charging Phase:** The vehicle establishes a secure charging session with the selected EVSE. Alignment and synchronization mechanisms ensure safe power transfer. Real-time metering records energy delivery and billing. Upon completion, the vehicle departs to continue its trip or proceeds to the next CN along the planned route.

The overall system cycle, illustrated in Figure 4.1, begins with a vehicle generating a charging request, followed by coordinated scheduling decisions, reservation confirmation, and energy transfer along the optimized route to its destination. This cycle encapsulates the logical flow of coordinated charging scheduling and trip planning in a 6G-ITS environment and defines the operational context for the heuristic and learning-based scheduling algorithms developed and evaluated in this chapter.

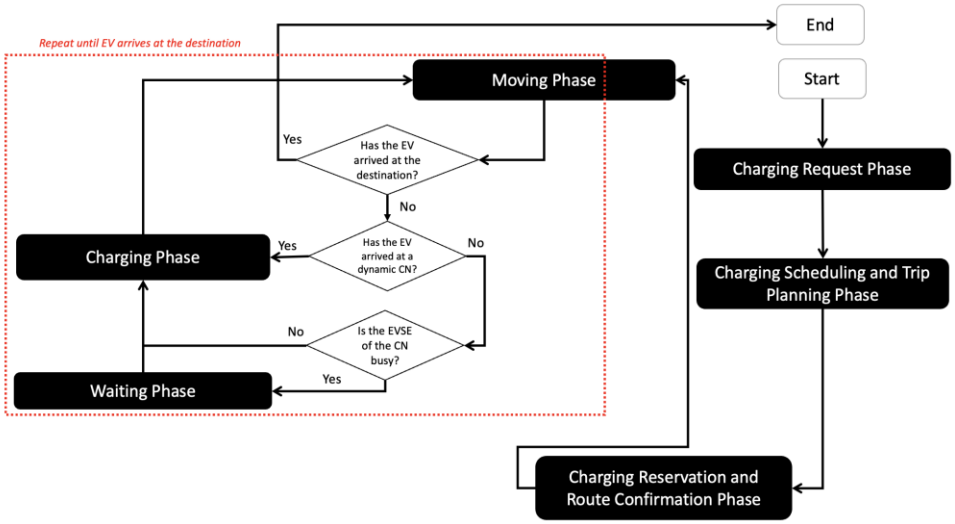

Figure 4.1: System phases from vehicle charging request to reaching the destination.

4.4 Coordinated Charging Scheduling Models and Heuristic Algorithms

This section presents the models adopted and the heuristic algorithms developed in this work to enable coordinated charging scheduling and trip planning for heterogeneous CAEV and UAV fleets under conditions representative of 6G-ITS. The modeling assumptions define the energy dynamics, communication processes, alignment constraints, and operational rules that govern coordinated scheduling decisions, while the associated heuristic algorithms regulate reservation handling, arrival management, and safe charge execution. Together, these components establish a deterministic coordination layer that supports the learning-based SAFE-DDPG scheduling framework introduced later in this chapter.

Within this framework, coordinated charging scheduling is formulated as an online, reservation-based, sequential decision-making problem under dynamic arrivals, reservation coupling, and mobility uncertainty. Although scheduling decisions are triggered per request, they are not independent one-shot allocations, since each confirmed reservation occupies charging resources over time and directly influences future feasibility, system load, and congestion conditions. Accordingly, the problem is treated as a sequential optimization problem, in which per-request allocation decisions act as control actions within a dynamic system. The objective is to improve system-level performance over time, including delay, charging utilization, and energy efficiency, under evolving and uncertain operating conditions. This formulation is consistent with stochastic and online optimization frameworks and reflects the practical nature of coordinated charging systems, where future arrivals, traffic conditions, and charging demand are not known in advance, making classical global optimization approaches with complete future information neither tractable nor representative of real-world deployment.

4.4.1 Power Consumption Models for CAEVs and UAVs

The rotary-wing UAV power consumption model adopted in this work captures the essential aerodynamic and mechanical characteristics of multirotor drones, grounded in well-established single-rotor physics [152], [153]. This foundation allows consistent extension to multi-rotor UAVs [154], [155], accommodating various designs while preserving physical realism and enabling accurate estimation of energy requirements for flight and charging operations.

The first component of the model is the total hovering power, P_{mhov}, which accounts for blade profile and induced power losses. It depends on the UAV weight W (N), number of rotors n (dimensionless), rotor radius r (m), rotor disk area $A = \pi r^2$ (m²), thrust coefficient C_T

(dimensionless), air density ρ (kg/m³), profile drag coefficient δ_s (dimensionless), and induced power correction factor k (dimensionless). The relationship is defined in (4.1).

$$P_{mhov} = \frac{\delta_s}{8}\sqrt{\frac{n}{\rho A}}\left(\frac{W}{C_T}\right)^{3/2} + (1+k)\frac{W^{3/2}}{\sqrt{2n\rho A}} \tag{4.1}$$

When the UAV moves horizontally at a constant velocity V_h (m/s), the total power $P_{mf}(V_h)$ increases due to parasitic drag and changes in induced velocity. In addition to the parameters above, this regime introduces v_0 (m/s), the induced velocity in hover, and $SFP_{\parallel}$ (m²), the equivalent flat plate area for horizontal drag. The horizontal flight model is defined in (4.2).

$$P_{mf}(V_h) = \frac{\delta_s}{8}\sqrt{\frac{n}{\rho A}}\left(\frac{W}{C_T}\right)^{3/2} + \frac{3\delta_s}{8}\sqrt{\frac{Wn\rho A}{C_T}}V_h^2 + (1+k)\frac{W^{3/2}}{\sqrt{2n\rho A}}\left(\sqrt{1+\frac{V_h^4}{4v_0^4}} - \frac{V_h^2}{2v_0^2}\right) + \frac{n}{2}SFP_{\parallel}\rho V_h^3 \tag{4.2}$$

Vertical motion, either ascent or descent, is modeled by $P_{mv}(V_v)$, where V_v (m/s) is the vertical velocity and $\mathrm{sgn}(V_v)$ is the sign function, returning $+1$ for ascent and -1 for descent. This regime also uses $SFP_{\perp}$ (m²), the equivalent flat plate area for vertical drag. Using $\mathrm{sgn}(V_v)$ allows a single unified expression for both cases as defined in (4.3).

$$\begin{aligned} P_{mv}(V_v) = {} & P_{mhov} + \frac{1}{2}W|V_v| + \mathrm{sgn}(V_v)\frac{n}{4}SFP_{\perp}\rho|V_v|^3 \\ & + \left(\frac{W}{2} + \mathrm{sgn}(V_v)\frac{n}{4}SFP_{\perp}\rho V_v^2\right)\sqrt{\left(1+\mathrm{sgn}(V_v)\frac{SFP_{\perp}}{A}\right)V_v^2 + \frac{2W}{n\rho A}} \end{aligned} \tag{4.3}$$

Finally, the total power consumption for steady three-dimensional flight with horizontal velocity V_h and vertical velocity V_v is given by (4.4), where $\Delta P_h(V_h)$ is obtained from (4.2) by removing the hover term P_{mhov}, leaving only the velocity-dependent parasitic and induced power components for horizontal motion, and $\Delta P_v(V_v)$ is obtained from (4.3) by removing the hover term P_{mhov}, leaving only the vertical velocity–dependent aerodynamic and induced power components for ascent and descent.

$$P_{total}(V_h, V_v) = P_{mhov} + \Delta P_h(V_h) + \Delta P_v(V_v) \tag{4.4}$$

This formulation captures hover, horizontal flight, vertical ascent and descent, and combined 3D maneuvers maintaining a compact and physically interpretable power representation. It incorporates essential physical and aerodynamic parameters to provide a realistic and computationally efficient estimation of UAV power consumption during critical maneuvers. This adaptability enables accurate energy estimation within the coordinated charging scheduling framework**,** supporting informed charging and routing decisions across diverse UAV platforms and operating conditions.

While UAV energy modeling is critical for aerial charging coordination, accurate modeling of ground vehicle energy consumption is equally important for end-to-end charging scheduling in heterogeneous networks. The power consumption of CAEVs is modeled using a component-level physics-based approach [156] to support coordinated charging scheduling and trip planning decisions, capturing drivetrain, battery, and vehicle dynamics. The total wheel force F_W acting on the vehicle is modeled as shown in (4.5), which accounts for gravitational force on a slope, rolling resistance, aerodynamic drag, and inertial effects of acceleration. Here, m is the vehicle mass, g the gravitational acceleration, α the road slope angle, f_r the rolling resistance coefficient, ρ the air density, c_w the aerodynamic drag coefficient, A_f the frontal area, v the velocity, a the acceleration, and e_i the equivalent inertia factor representing rotating components.

$$F_W = mg\sin\alpha + mgf_r\cos\alpha + \frac{1}{2}\rho c_w A_f v^2 + me_i a \tag{4.5}$$

The wheel torque T_W is derived by multiplying the total wheel force $\mathrm{F_W}$ by the wheel radius r_W, as expressed in (4.6).

$$\mathrm{T_W} = \mathrm{F_W} \cdot \mathrm{r_W} \tag{4.6}$$

This wheel torque is then converted to the motor shaft torque T_{EM} by accounting for the gear ratio i_T and transmission efficiency η_T, as described in the piecewise function in (4.7). The case distinction allows proper handling of driving and regenerative braking torques.

$$\mathrm{T_{EM}} = \begin{cases} \mathrm{T_W} \cdot \mathrm{i_T^{-1}} \cdot \eta_\mathrm{T}^{-1}, & \mathrm{T_W} \geq 0 \\ \max\left(\mathrm{T_W} \cdot \mathrm{i_T^{-1}} \cdot \eta_\mathrm{T}, \mathrm{T_{W,min}}\right), & \mathrm{T_W} < 0 \end{cases} \tag{4.7}$$

The motor power loss map $P_{EM,loss}$ is modeled as a nonlinear function of motor speed n_{EM} and torque T_{EM} in (4.8). This function captures the efficiency characteristics of the electric motor more accurately than constant-efficiency assumptions.

$$\mathrm{P_{EM,loss}} = \mathrm{f}(\mathrm{n_{EM}}, \mathrm{T_{EM}}) \tag{4.8}$$

Finally, battery power consumption $P_{Bat,chem}$ is computed using the nonlinear relationship given in (4.9), which models battery voltage U_0 and internal resistance R_i, and relates electrical motor power $P_{EM,el}$ and auxiliary power $P_{aux,el}$ to actual battery chemical power consumption.

$$\mathrm{P_{Bat,chem}} = \frac{\mathrm{U_0^2}}{2\mathrm{R_i}} - \frac{\mathrm{U_0}}{2\mathrm{R_i}}\sqrt{\mathrm{U_0^2} - 4\mathrm{R_i}\left(\mathrm{P_{EM,el}} + \mathrm{P_{aux,el}}\right)} \tag{4.9}$$

Compared to simplified energy representations that rely on constant coefficients or aggregated power estimates, the adopted component-level CAEV model provides more precise and physically realistic energy estimates. This level of detail is essential for capturing vehicle

behavior under varying traffic conditions and operational scenarios, and for evaluating wireless charging strategies effectively.

The CAEV power model is flexible and can be implemented in various computational frameworks or platforms, enabling large-scale analysis without being tied to a specific simulation tool. Its comprehensive modeling capability makes it well suited for accurate estimation of energy usage and operational planning across heterogeneous CAEV fleets.

Together with the UAV power consumption model, these CAEV models establish a realistic and tractable foundation for coordinated charging scheduling and trip planning under operating conditions representative of 6G-enabled intelligent transportation systems. By capturing vehicle energy dynamics across heterogeneous fleets, the adopted modeling assumptions support effective implementation and fair comparison of the heuristic and SAFE-DDPG-based scheduling strategies evaluated later in this chapter. When embedded within wireless charging optimization frameworks, these modeling assumptions enable informed scheduling decisions that improve charging efficiency and extend the operational endurance of both UAVs and CAEVs in practical deployment scenarios.

4.4.2 Charging Communication Model

Laser beaming is employed in this work as a high-efficiency mechanism for DWC of both CAEVs and UAVs. Within the proposed charging framework, high-power laser beams are used for energy transfer, while lower-power beams enable optical communication based on light-fidelity (Li-Fi) principles using on–off keying (OOK) modulation [45]. Laser beaming charging nodes can be fixed infrastructure such as LBCN towers or mobile platforms including CAEVs and UAVs and may serve as transmitters delivering optical energy to receivers mounted on UAVs or CAEVs. This enables CAEV–UAV, UAV–UAV, CAEV–CAEV, and LBCN–UAV charging in motion. The same optical links also support high-speed LOS communication, with laser power dynamically allocated between charging and communication according to scheduling and operational priorities.

The following models are used to estimate charging feasibility, communication reliability, and alignment constraints that directly inform coordinated scheduling and reservation decisions. The received optical charging power P_{LRec} is modeled in (4.10) where η_{LRec} is the optical-to-electrical conversion efficiency of the receiver, P_{LTrans} is the laser transmitter power (W), A_{LRec} is the effective aperture area of the receiver (m²), and d_L is the transmitter–receiver separation (m). The term $\mathrm{LOS} \in [0,1]$ captures geometric line-of-sight

availability relevant to charging and communication feasibility during coordinated scheduling, while $\mathrm{Env}_\lambda \in [0,1]$ represents wavelength-dependent atmospheric attenuation.

$$\mathrm{P_{LRec}} = \eta_{\mathrm{LRec}}\, \mathrm{P_{LTrans}}\, \frac{\mathrm{A_{LRec}}}{\mathrm{d_L^2}}\, \mathrm{LOS}\, \mathrm{Env}_\lambda \tag{4.10}$$

The average optical communication power for OOK modulation is expressed in (4.11), where η_{CTrans} is the optical communication transmission efficiency, E_b is the energy per bit (J), T_b is the bit duration (s), A_{CRec} is the communication receiver aperture area (m²), and d_C is the communication link distance (m). The term $\frac{E_b}{T_b}$ represents the average transmission power per bit, which determines communication feasibility during charging coordination.

$$P_{comm} = \eta_{CTrans}\, \frac{E_b}{T_b}\, \frac{A_{CRec}}{d_C^2}\, \mathrm{LOS}\, \mathrm{Env}_\lambda \tag{4.11}$$

The critical charging distance d_{crit} is obtained by inverting (4.10) for d_L when $P_{LRec} = P_{min}$, the minimum power required by the receiver for sustained charging, yielding (4.12), where P_{min} is in watts. This applies equally to CAEV–UAV, UAV–UAV, CAEV–CAEV, and LBCN–UAV charging links and defines the spatial feasibility constraints used during coordinated scheduling.

$$d_{\mathrm{crit}} = \sqrt{\frac{\eta_{LRec}\, P_{LTrans}\, A_{LRec}\, \mathrm{LOS}\, \mathrm{Env}_\lambda}{P_{min}}} \tag{4.12}$$

Similarly, the critical communication distance d_{comm} is obtained by inverting (4.11) for d_C when $P_{comm} = P_{req}$, the minimum received power required for reliable decoding and reservation confirmation, as shown in (4.13).

$$d_{\mathrm{comm}} = \sqrt{\frac{\eta_{CTrans}\, E_b\, A_{CRec}\, \mathrm{LOS}\, \mathrm{Env}_\lambda}{T_b\, P_{req}}} \tag{4.13}$$

Finally, the optimal alignment angle θ between transmitter and receiver for maximum charging efficiency is given in (4.14), where P_{LMax} is the maximum allowable received optical power (W). This factor accounts for geometric beam alignment and defines the alignment constraints enforced by the charging coordination and correction algorithms to ensure safe operation while maintaining high energy transfer efficiency, regardless of whether the source is an LBCN tower, a CAEV, or another UAV.

$$\theta = \arccos\left(\frac{P_{LRec}}{P_{LMax}}\right) \tag{4.14}$$

Equations (4.10)–(4.14) together provide a unified and dimensionally consistent framework for joint charging and communication modeling in coordinated CAEV–UAV

charging networks. By incorporating physical optical link parameters, atmospheric attenuation, and receiver conversion efficiency, the adopted modeling assumptions reflect operating conditions relevant to 6G-ITS. Their parametric structure enables adaptation to heterogeneous hardware capabilities, environmental conditions, and operational priorities, allowing the coordinated scheduling and alignment algorithms developed in this chapter to make informed feasibility, reservation, and power allocation decisions under realistic deployment conditions.

4.4.3 Battery Management System and Charge Delivery

After successful authentication and synchronization, the EVSE starts to deliver charging in the reserved duration compatible with the vehicle's charging acceptance rate. The system follows a linear two-stage battery model for charging that captures realistic battery acceptance behavior beyond the idealized charging rate defined in (4.15).

The linear two-stage battery model [157] approximates the piecewise linear charging behavior of lithium-ion batteries and defines the effective battery-accepted charging rate $\hat{r}(t)$ in (4.16), based on the idealized charging rate in (4.15). Here, $r(t)$ denotes the pilot charging rate requested by the EVSE, $\bar{r}$ is the maximum charging rate supported by the on-board charger, and $\hat{e}(t)$ represents the remaining energy-constrained charging capability over the scheduling interval. The state-of-charge (SoC) determines the transition between charging stages, with th marking the boundary between bulk and absorption charging. Charging rates are positive during energy intake and become negative only when discharging behavior is explicitly modeled.

The first stage, called bulk charging, lasts from 0% to between 70% to 90% SoC, where the current draw, neglecting changes in pilot, is nearly constant. The second stage, called absorption, is distinguished by the linear decrease in charging current while the battery voltage stays constant. In practice, the charging rate decreases as the battery approaches full capacity, and the actual charging profile depends on the pilot signal, the on-board charger characteristics, the current SoC, and environmental conditions. Thus, this piecewise linear model is a very good approximation of real-world charging behavior.

$$\mathrm{r}^{\mathrm{ideal}}(\mathrm{t}) = \min\{r(t), \bar{r}, \hat{e}(t)\} \tag{4.15}$$

$$\hat{r}(t) = \begin{cases} r^{ideal}(\mathrm{t}), & \text{if SoC} \le th \\ \min\left\{\left(1 - \dfrac{\mathrm{SoC} - th}{1 - th}\right)\mathrm{r}, r^{ideal}(\mathrm{t})\right\}, & \text{otherwise} \end{cases} \tag{4.16}$$

The linear two-stage battery model is applicable to wired, magnetic-resonance wireless, and laser-based charging technologies because it captures the intrinsic battery acceptance behavior governed by the battery management system rather than charger-specific

characteristics. By allowing the effective charging current and voltage to be adjusted to reflect environmental conditions such as temperature variations and weather-dependent efficiency losses, as well as alignment effects and charger limitations, the model provides a realistic yet tractable representation of charge delivery across heterogeneous platforms. Its computational efficiency and faithful approximation of lithium-ion charging dynamics make it well suited for integrated energy management of CAEV and UAV fleets, while supporting realistic operational assumptions relevant to 6G-ITS.

Both the battery and its battery management system are modeled to support coordinated charging scheduling and reservation enforcement. The charge delivery procedure processes the pilot signal, EVSE voltage, and scheduling time step to compute the effective charging rate and update the battery state. Charging is applied from the vehicle's arrival time, which may differ from the reserved start time, until the scheduled completion or vehicle departure, ensuring consistency with the coordinated scheduling framework.

4.4.4 Charging Scheduling and Trip Planning

The charging scheduling and trip planning algorithm developed in this work coordinates charging decisions for both CAEVs and UAVs across heterogeneous charging networks, building on the three-layer system architecture introduced earlier. Charging requests are generated based on the evolving residual battery state of each vehicle rather than from an idealized initial condition. Prior to issuing a request, CAEVs and UAVs consume energy through driving, flight, sensing, and communication activities, resulting in a potentially significant reduction in battery state before the scheduling decision is made. As a result, the scheduler observes the battery state after this depletion has already occurred, and all scheduling decisions are made based on the remaining available energy at request time.

This distinction is important because residual energy directly affects charging feasibility, routing options, and reachable charging networks. Therefore, candidate charging assignments must be evaluated not only in terms of availability and cost, but also in terms of whether the requesting vehicle can feasibly reach the selected charging resource under current energy constraints.

The process begins when a vehicle sends its current SoC, the requested SoC, vehicle type, trip start location, and trip destination to the nearest EIUAV or RSU. These parameters are encapsulated in a reservation request frame that is processed by the scheduling layer and forwarded for coordinated charging and trip planning decisions. If two vehicles request charging simultaneously, priority is given to the one with the lower current SoC.

At the ESP, candidate CNs are first filtered using heuristic criteria based on geographic proximity, availability within the predicted arrival–departure time window and charging cost. Candidate vehicles for V2V DWC are also identified according to distance, availability, and ability to supply energy to the requesting vehicle. The requested charging demand is then allocated across dynamic charging network types (DWCN, AVCN, GVCN) and, if required, static charging networks (SWCN, LBCN, CCN), subject to vehicle-type compatibility constraints. CAEVs exclude LBCN from consideration, whereas UAVs exclude CCN, SWCN, and DWCN. Operational thresholds for each CN type are configurable parameters. The remaining candidate CNs are evaluated using a weighted multi-criteria scoring function that balances economic, temporal, and energy-related considerations.

Each CN is evaluated using a dynamic weighted score, shown in (4.17), where c_i is the charging cost at CN i (monetary units), t_i is the estimated travel time to CN i (s), w_i is the waiting time at CN i (s), b_i is the battery energy consumption to reach CN i (Wh), d_i is the travel distance to CN i (m), and λ_1 through λ_5 are adaptive weight coefficients.

$$\text{score} = \lambda_1 c_i + \lambda_2 t_i + \lambda_3 w_i + \lambda_4 b_i + \lambda_5 d_i \tag{4.17}$$

To ensure feasibility, safety, and reliable reservation enforcement, the scheduling decision is subject to the following triggering, timing, distance, energy, and efficiency constraints. The trigger condition for initiating charging is improved in (4.18) to unify both at-CN and in-transit triggers. Here, $\text{ChargeReq}_i = 1$ indicates a charging request for vehicle i is triggered, SoC_{req} is the mission-required charge level at a CN, and SoC_{th} is the emergency threshold in transit.

$$\text{ChargeReq}_i = \begin{cases} 1, & SoC_i < SoC_{\text{req}} \text{ at CN} \\ 1, & SoC_i < SoC_{\text{th}} \text{ in transit} \\ 0, & \text{otherwise} \end{cases} \tag{4.18}$$

Reservation timing is ensured by (4.19), where t_{arr_i} is the predicted arrival time at CN i, t_{res_i} is the reservation start time, and t_{dep_i} is the predicted departure time.

$$t_{\text{arr}_i} \le t_{\text{res}_i} \le t_{\text{dep}_i} \tag{4.19}$$

Travel distance constraints between consecutive CNs are enforced in (4.20), where $d(i,j)$ is the travel distance between CN i and CN j, and $D_{\max}$ is the maximum allowable distance.

$$d(i,j) \le D_{\max} \tag{4.20}$$

Energy sufficiency is checked using (4.21), where E_{rem} is the remaining stored energy after the last charging event, E_{cons_i} is the energy consumed over segment i, $\mathcal{N}$ is the set of segments before the next charging event, and $E_{\min}$ is the minimum operational reserve.

$$E_{\text{rem}} - \sum_{i \in \mathcal{N}} E_{\text{cons}_i} \geq E_{\min} \tag{4.21}$$

Finally, charging efficiency is verified via equation (4.22), where η_i is the measured efficiency at CN i and $\eta_{\min}$ is the minimum acceptable efficiency.

$$\eta_i \geq \eta_{\min} \tag{4.22}$$

Following CN scoring and constraint verification, the CNM identifies available EVSEs that satisfy the scheduling requirements, and the ESP selects the optimal option according to vehicle-type priority rules. For CAEVs, the order from least to most priority is CCN, SWCN, GVCN, AVCN, DWCN, excluding LBCN. For UAVs, the order is LBCN, AVCN, GVCN, excluding CCN, SWCN, and DWCN. When scores tie, the CN with the shortest travel distance is selected. Once dynamic and, if needed, static CNs are reserved, the Reservation Confirmation Frame is issued with a unique anonymized identifier to enable secure verification while preserving privacy.

Routing is then performed online to follow the reserved CN locations. For UAVs, trip routing is performed online using a three-dimensional A* search, as expressed in (4.23), where $f(n)$ is the total estimated path cost through node n, $g(n)$ is the accumulated cost from the start node to n, $h(n)$ is the heuristic estimate from n to the goal, $c_{alt}(n)$ is the altitude-related energy cost, and $c_{obs}(n)$ is the obstacle-avoidance cost.

$$f(n) = g(n) + h(n) + c_{alt}(n) + c_{obs}(n) \tag{4.23}$$

CAEV routing is performed online using Dijkstra's shortest-path algorithm [158], reflecting road-network constraints. The minimal cumulative travel cost $D(v)$ to reach node v from source s is calculated according to (4.24), where $\text{Pred}(v)$ denotes the set of predecessor nodes to v and $c(u, v)$ is the travel cost between nodes u and v.

$$D(v) = \min_{u \in \text{Pred}(v)} \{D(u) + c(u, v)\} \tag{4.24}$$

Algorithm 1 and **Algorithm 2** together implement the heuristic charging scheduling and trip planning procedure developed in this work for coordinated CAEV and UAV operations [133]. The algorithms prioritize charging requests, filter candidate charging networks, enforce feasibility constraints, and select routes consistent with vehicle type and real-time operating conditions, enabling efficient reservation decisions and reliable trip planning in heterogeneous

charging environments. This deterministic coordination mechanism supports effective energy management and operational reliability within the proposed framework

Algorithm 1 Charging Scheduling for CAEVs and UAVs [133]

Input: SoC_i, SoC_{req}, SoC_{th}, veh_{type}, $start_{loc}$, $dest_{loc}$
Output: Reserved dynamic CN (optional static CN), Reservation Confirmation ID
BEGIN
1. Send reservation request frame from nearest EIUAV/RSU to EDC.
   1.1 Include SoC_i, SoC_{req}, veh_{type}, $start_{loc}$, and $dest_{loc}$.
2. Forward processed request from EDC to ESP.
3. **IF** multiple simultaneous requests **THEN**
   3.1 Assign priority to vehicle with lower SoC_i.
   END IF
4. Filter candidate CNs at ESP by:
   4.1 Geographic proximity to $start_{loc}$.
   4.2 Availability within predicted arrival and departure window.
   4.3 Charging cost.
5. Identify candidate vehicles for V2V DWC based on distance, availability, and compatibility.
6. Distribute requested charging amount among CN types:
   6.1 Dynamic CNs: DWCN, AVCN, GVCN.
   6.2 Static CNs: SWCN, LBCN, CCN.
   6.3 **IF** $veh_{type} =$ CAEV **THEN** exclude LBCN.
   6.4 **IF** $veh_{type} =$ UAV **THEN** exclude CCN, SWCN, DWCN.
   END IF
7. **FOR EACH** candidate CN **DO**
   7.1 Compute score (4.17)
   7.2 Verify constraints: (4.19)– (4.22)
   END FOR
8. Select optimal dynamic CN by veh_{type} priority.
9. **IF** scores tie **THEN** select CN with minimum d_i.
10. Reserve selected dynamic CN.
11. **IF** additional charging required **THEN**
   11.1 Reserve optimal static CN using same procedure.
   END IF
12. Generate reservation confirmation frame with anonymized ID.
13. Return reservation details to vehicle.

END

Algorithm 2 Online Trip Routing Following Charging Reservation [133]

Input: Reserved CN locations, veh_{type}, traffic/flight data
Output: Optimal route to CN(s) and final destination
BEGIN
1. Receive confirmed CN locations from ***Algorithm 1***.
2. **IF** veh_{type} = UAV **THEN**
   2.1 Use (4.23)
   END IF
3. **IF** veh_{type} = CAEV **THEN**
   3.1 Use (4.23)
   END IF
4. Generate initial route from current location to reserved CN.
5. **WHILE** en route **DO**
   5.1 Monitor traffic conditions (CAEV).
   5.2 Monitor flight obstacles and altitude costs (UAV).
   5.3 **IF** major delay or blockage detected **THEN**
      5.3.1 Recalculate route to CN using same algorithm.
      END IF
   END WHILE
6. Upon arrival at CN:
   6.1 **IF** additional CN reserved **THEN**
      6.1.1 Repeat Steps 4–6 for next CN.
      END IF
7. After final charging, route to destination.

END

4.4.5 Charging Billing and Accounting Model

Within the proposed charging framework introduced earlier, the system supports two billing schemes to complete the execution of coordinated charging scheduling decisions: pay per charging session and pay per energy unit delivered (kWh). Since delivered energy is continuously metered, real-time records of the total charging delivered during a scheduled session are available.

For the pay-per-energy scheme, the total amount of energy delivered, E_{deliv}, is converted to CAD, C_{CAD}, using the appropriate TOU pricing rate, r_{energy} as shown in (4.25). Based on the defined purchase rate of virtual charging credit points r_{CP}, introduced earlier within the proposed framework, the monetary cost is converted to charging credits C_{CP}, using (4.26) to compute the corresponding cost for the CAEV user.

If discrepancies are detected between scheduled and delivered energy, an error message or negative acknowledgement may be issued under either payment option, prompting recalculation. Charging credits are deducted from the vehicle's account only after validation, ensuring consistency between scheduled charging decisions and executed energy delivery, which supports the evaluation of charging cost and reservation fulfillment metrics presented later in this chapter.

$$C_{CAD} = E_{deliv} * r_{energy} \tag{4.25}$$

$$C_{CP} = \frac{C_{CAD}}{r_{CP}} \text{ , where } C_{CAD} \geq r_{CP} \tag{4.26}$$

4.4.6 Charging Alignment and Correction for CAEVs and UAVs

This section presents the alignment and correction mechanisms proposed in this work to support the execution of coordinated wireless charging scheduling decisions. These mechanisms translate scheduling outcomes into enforceable operational constraints across different charging technologies and vehicle types, ensuring that charging sessions proceed under valid physical conditions. By integrating continuous monitoring and local correction, the proposed approach maintains consistency between scheduled charging plans and real-time execution and contributes to reliable charging operation under dynamic conditions.

4.4.6.1 Pre-Charging Operational Constraints

After reservation, authentication, and verification between the CAEV or UAV and the EVSE, the charging mode identifier contained in the CN message determines the operational constraints for that session. The selected wireless charging type may be static or dynamic, as determined by the coordinated scheduling decision. Magnetic Resonance Wireless Power Transfer (MR-WPT), which can operate in SWC, DWC, or V2V configurations between vehicles of the same or different types, or Laser Beaming Wireless Power Transfer (LB-WPT), which may occur between a LBCN tower and a UAV, or between two vehicles in a V2V configuration.

Before wireless power is delivered, the EVSE verifies that the vehicle's speed, relative angle, separation distance, and orientation meet the requirements of the chosen charging mode. These requirements are defined in (4.27)–(4.38) and are specific to the selected technology. This continuous monitoring ensures that scheduled charging sessions are executed under valid physical conditions consistent with the coordination assumptions used during scheduling. If any parameter deviates from its permissible bounds such as lateral misalignment in SWC or DWC, excessive beam misalignment in LB-WPT, or coupling distance variation in MR-WPT, then charging is immediately halted for safety. Power transfer resumes automatically once all monitored parameters are restored to their acceptable ranges, thereby maintaining operational safety and sustained energy transfer efficiency.

4.4.6.2 Mode-Specific Geometric and Kinematic Requirements

In SWC, the CAEV must remain stationary with minimal misalignment between the receiver coil center and the wireless charging pad center. Let $v_{a,SWC}$ be the actual vehicle speed, $\Delta x_{SWC} = X_{c,SWC} - x_{a,SWC}$ and $\Delta y_{SWC} = Y_{c,SWC} - y_{a,SWC}$ be the longitudinal and lateral offsets

between the pad center $(X_{c,SWC}, Y_{c,SWC})$ and the actual receiver coil center $(x_{a,SWC}, y_{a,SWC})$. The tolerances $\epsilon_{x,SWC}$ and $\epsilon_{y,SWC}$ define the allowable misalignment. The SWC condition is expressed in (4.27). SAE J2954 recommends $\epsilon_{y,SWC}$ within ±75–100 mm laterally and negligible longitudinal motion for efficient coupling [159].

$$v_{a,SWC} = 0, \quad |\Delta x_{SWC}| \le \epsilon_{x,SWC}, \quad |\Delta y_{SWC}| \le \epsilon_{y,SWC} \tag{4.27}$$

For DWC, the CAEV is in motion. Let $v_{t,DWC}$ be the target speed, $\delta_{v,DWC}$ the speed tolerance, and $\epsilon_{y,DWC}$ the lateral misalignment tolerance. The vehicle must satisfy (4.28). Field experiments from narrow-width IPT and high-power dynamic WPT systems indicate $\delta_{v,DWC} \approx 0.3\ \mathrm{m/s}$ and $\epsilon_{y,DWC} \approx 0.10\ \mathrm{m}$ for high transfer efficiency [160], [161].

$$|v_{a,DWC} - v_{t,DWC}| \le \delta_{v,DWC}, \quad |\Delta y_{DWC}| \le \epsilon_{y,DWC} \tag{4.28}$$

In LB-WPT for V2V charging between same or different vehicle types, both platforms must be stationary relative to each other, and UAVs must hover. For LBCN tower delivery to a UAV, the UAV must hover. Let $\epsilon_{x,LB}$ and $\epsilon_{y,LB}$ be the allowable offsets, d_{LB} the separation between laser transmitter and receiver apertures, and $d_{min,LB}$, $d_{max,LB}$ the minimum and maximum safe distances. The constraints are given in (4.29). Recent LB-WPT UAV charging tests report $d_{min,LB} = 10\ \mathrm{m}$, $d_{max,LB} = 500\ \mathrm{m}$, and lateral offsets $\epsilon_{x,LB} = \epsilon_{y,LB} = 0.05\ \mathrm{m}$ in controlled safe zones [17]. These may be adjusted to comply with national laser safety regulations.

$$v_{a,LB} = 0, \quad |\Delta x_{LB}| \le \epsilon_{x,LB}, \quad |\Delta y_{LB}| \le \epsilon_{y,LB}, \quad d_{min,LB} \le d_{LB} \le d_{max,LB} \tag{4.29}$$

In MR-WPT V2V operation, vehicles may be stationary or moving, provided relative speed and coupling distance remain within limits. Let $d_{a,MR}$ be the measured coil distance, $d_{t,MR}$ the optimal resonant distance, $\delta_{d,MR}$ the allowable distance deviation, and $\delta_{v,MR}$ the speed tolerance. The requirement is given in (4.30). Strongly coupled MR-WPT results suggest $\delta_{d,MR}$ should be maintained within ±7% of coil diameter for optimal coupling efficiency [162].

$$|v_{a,MR} - v_{t,MR}| \le \delta_{v,MR}, \quad |d_{a,MR} - d_{t,MR}| \le \delta_{d,MR} \tag{4.30}$$

These correction rules are applied locally during charging execution to maintain feasibility of the scheduled session without triggering rescheduling unless violations persist. Speed correction in any moving mode k where $k \in \{DWC, MR\}$ is governed by (4.31)–(4.33). Let $r_{v,k}$ be the mode-specific acceleration or deceleration rate. A rate $r_{v,k} \approx 0.005\ \mathrm{m/s\ per\ ms}$ $(5.0\ \mathrm{m/s^2})$ matches measured acceleration profiles from high-power DWC/MR-WPT trials [161], balancing fast convergence and passenger comfort.

$$|v_{a,k} - v_{t,k}| \le \delta_{v,k} \tag{4.31}$$

$$v_{a,k} \leftarrow v_{a,k} + r_{v,k} \quad \text{if} \quad v_{a,k} < v_{t,k} - \delta_{v,k} \tag{4.32}$$

$$v_{a,k} \leftarrow v_{a,k} - r_{v,k} \quad \text{if} \quad v_{a,k} > v_{t,k} + \delta_{v,k} \tag{4.33}$$

The pad center coordinates $(X_{c,k}, Y_{c,k})$ are given in (4.34).

$$X_{c,k} = \frac{X_{s,k} + X_{e,k}}{2}, \quad Y_{c,k} = \frac{Y_{s,k} + Y_{e,k}}{2} \tag{4.34}$$

Misalignment correction proceeds until (4.35) is met.

$$|\Delta x_k| \le \epsilon_{x,k}, \quad |\Delta y_k| \le \epsilon_{y,k} \tag{4.35}$$

For MR-WPT or LB-WPT V2V, the gap constraint (4.36) applies, with positions updated by (4.37)–(4.38) along unit vector $\mathbf{u}_k$.

$$|d_{a,k} - d_{t,k}| \le \delta_{d,k} \tag{4.36}$$

$$\mathbf{p}_{1,k} \leftarrow \mathbf{p}_{1,k} + \frac{(d_{a,k} - d_{t,k})}{2}\mathbf{u}_k \tag{4.37}$$

$$\mathbf{p}_{2,k} \leftarrow \mathbf{p}_{2,k} - \frac{(d_{a,k} - d_{t,k})}{2}\mathbf{u}_k \tag{4.38}$$

4.4.6.3 Power Transfer Modeling for LB-WPT

In LB-WPT, the received power $P_{r,LB}$ is modeled in this work as shown in (4.39). Compared with the earlier charging–communication model, which used an inverse-square law for free-space propagation, these equations adopt a beam divergence formulation and add practical considerations such as steering optimization and jitter effects, making them more realistic for UAV and CAEV laser charging applications. Here $P_{t,LB}$ is the transmitted power, $\eta_{sys,LB}$ is the system efficiency, $D_{r,LB}$ is the receiver aperture diameter, $D_{b0,LB}$ is the initial beam waist, θ_{LB} is the beam divergence angle, and d_{LB} is the transmission distance. This equation models the way received power falls with distance as the beam spreads out.

$$P_{r,LB} = P_{t,LB} \cdot \eta_{sys,LB} \cdot \left(\frac{D_{r,LB}}{D_{b0,LB} + \theta_{LB} \cdot d_{LB}}\right)^2 \tag{4.39}$$

The maximum distance meeting required power $P_{req,LB}$ is computed from (4.40) subject to (4.41). Equation (4.40) inverts the received-power relation to solve for distance, giving the maximum feasible range for power transfer, while (4.41) constrains it within allowable system bounds $[d_{min,LB}, d_{max,LB}]$ and ensures the received power exceeds the threshold.

$$d_{LB} = \frac{\sqrt{\frac{P_{t,LB} \cdot \eta_{sys,LB} \cdot D_{r,LB}^2}{P_{req,LB}}} - D_{b0,LB}}{\theta_{LB}} \tag{4.40}$$

$$d_{min,LB} \le d_{LB} \le d_{max,LB}, \quad P_{r,LB} \ge P_{req,LB} \tag{4.41}$$

The optimal beam elevation angle $\alpha_{opt,LB}$ is defined in (4.42). Here $\alpha_{opt,LB}$ is the steering angle chosen from the feasible set $\mathcal{A}_{LB}$ to maximize received power, ensuring the beam is directed optimally. The restriction to a feasible set rather than all possible angles reflects hardware and operational constraints: UAV or CAEV transmitters cannot mechanically scan or point beams arbitrarily, safety considerations limit angular ranges to prevent stray high-power laser exposure, and restricting the search domain significantly reduces computation time for real-time optimization.

$$\alpha_{opt,LB} = \underset{\alpha \in \mathcal{A}_{LB}}{\operatorname{argmax}} P_{r,LB}(d_{LB}(\alpha)) \tag{4.42}$$

To account for UAV hovering and CAEV vibration, a jitter attenuation term $\eta_{jitter,LB}$ is applied as in (4.43), where $\sigma_{jitter,LB}$ is the standard deviation of pointing error and $\sigma_{beam,LB}$ is the beam spot size at the receiver. This has been validated in controlled laser charging trials [17].

$$\eta_{jitter,LB} = e^{-\frac{\sigma_{jitter,LB}^2}{2\sigma_{beam,LB}^2}} \tag{4.43}$$

These model the degradation of received power caused by mechanical instabilities, reducing theoretical values to practical ones consistent with real laser charging trials.

The following **Algorithm 3** formalizes the alignment and correction procedure proposed in this work for monitoring, detecting, and correcting positional, speed, and beam-alignment deviations during coordinated wireless charging [133]. This ensures that scheduled charging sessions are executed under valid operating conditions across all supported vehicles, charging modes, and technologies, while laying the groundwork for the reliability aspects examined in the next chapter.

Algorithm 3 Charging Alignment and Correction for CAEVs and UAVs [133]

Input: Vehicle type $T \in$ {CAEV,UAV}, charging mode $k \in$ {SWC,DWC,LB,MR}, target parameters $v_{t,k}$, $\epsilon_{x,k}$, $\epsilon_{y,k}$, $\delta_{v,k}$, $\delta_{d,k}$, $d_{t,k}$, $d_{\min,k}$, $d_{\max,k}$, $\alpha_{\text{opt},k}$
Output: Charging status (ON/OFF), updated position and speed
Begin
1: Receive reservation, authentication, and CN message from EVSE
2: Identify vehicle type T
3: Determine charging mode k based on T and CN
4: **while** session_active **do**
5: Measure $v_{a,k}$, Δx_k, Δy_k, $d_{a,k}$, orientation, and beam angle (if LB)
6: **if** any constraint from (4.27)–(4.30) is violated **then**
7: Charging ← OFF
8: **if** $k \in$ {DWC,MR} **then**
9: Correct speed using (4.31)–(4.33)
10: **end if**
11: **if** positional or distance misalignment present **then**
12: For SWC or DWC, correct lateral/longitudinal offset using (4.34)–(4.35)
13: For MR or LB V2V, correct gap using (4.36)–(4.38)
14: **end if**
15: **else**
16: **if** $k =$ LB **then**
17: Compute $P_{r,LB}$ using (4.39)
18: Verify range and power conditions in (4.41)
19: Adjust beam angle via (4.42)
20: Apply jitter attenuation from (4.43)
21: **end if**
22: Charging ← ON
23: **end if**
24: **end while**
End

4.4.7 Dynamic Arrival Handling

This section introduces the dynamic arrival handling mechanisms proposed in this work to complement coordinated charging scheduling for CAEVs and UAVs. By explicitly accounting for early and late arrivals under both infrastructure-based and ad-hoc dynamic wireless charging modes, the proposed approach enables adaptive execution of scheduling decisions under real-time operating conditions. These mechanisms extend the heuristic scheduling framework presented earlier by allowing reservations and charging actions to be adjusted without full rescheduling.

The proposed charging coordination framework addresses both early and late arrivals for CAEVs and UAVs operating in infrastructure-based and ad-hoc DWC modes. By leveraging real-time communication, predictive arrival time estimation, and adaptive scheduling, the framework adapts scheduled charging actions to real-time vehicle arrivals, supporting reduced waiting time and improved utilization of charging resources.

Accurate arrival time estimation is required to determine whether a scheduled charging session can be executed as planned or requires adjustment. Vehicle arrival times are estimated using real-time traffic and flight data, route calculations, and environmental conditions. For

CAEVs, the arrival time $t_{\text{arr,CAEV}}$ is predicted using (4.44), where t_{current} is the system clock time, d_{CAEV} is the road distance to the CN entry point, v_{CAEV} is the predicted travel speed based on real-time traffic and routing data, $\Delta t_{\text{traffic}}$ is the estimated traffic delay, and Δt_{queue} is the expected waiting time before entering the CN. Equation (4.44) ensures that both route-dependent and congestion-related delays are accounted for in scheduling decisions. This formulation enables accurate assessment of arrival deviations that directly influence waiting time and reservation fulfillment during coordinated scheduling.

$$t_{\text{arr,CAEV}} = t_{\text{current}} + \frac{d_{\text{CAEV}}}{v_{\text{CAEV}}} + \Delta t_{\text{traffic}} + \Delta t_{\text{queue}} \tag{4.44}$$

Similarly, UAV arrival time $t_{\text{arr,UAV}}$ is computed as in (4.45), where d_{UAV} is the straight-line distance to the CN, v_{UAV} is the cruise velocity, Δt_{wind} is the delay or gain due to wind speed and direction, and Δt_{queue} represents waiting time if the reserved EVSE is occupied. Equation (4.45) allows UAV scheduling to reflect real atmospheric conditions, improving arrival accuracy and supporting consistent execution of scheduled charging sessions.

$$t_{\text{arr,UAV}} = t_{\text{current}} + \frac{d_{\text{UAV}}}{v_{\text{UAV}}} + \Delta t_{\text{wind}} + \Delta t_{\text{queue}} \tag{4.45}$$

4.4.7.1 Early Arrival Handling

For infrastructure-based DWC, a CAEV arriving before its scheduled time may enter the track immediately if the number of vehicles currently charging $n_{\text{track}}(t)$ is below the allowable maximum $n_{\max}$, as expressed in (4.46), where $n_{\max}$ is set to maintain safe throughput and charging efficiency. If condition (4.46) is not satisfied, the CAEV is routed along a parallel road until entry is possible.

$$n_{\text{track}}(t) < n_{\max} \tag{4.46}$$

Reservation updates for early arrivals are triggered when a currently charging CAEV is expected to vacate the lane within a predictable time window Δt_{update}, as given in (4.47), where t_{free} is the estimated departure time of the next vehicle. When (4.47) holds, the arriving CAEV's booking is updated, and its previous slot is released for reallocation.

$$t_{\text{free}} - t_{\text{current}} \leq \Delta t_{\text{update}} \tag{4.47}$$

For UAVs, if an EVSE is available upon arrival, charging begins immediately; otherwise, the UAV joins the queue, where the queue length q_{len} is updated according to (4.48).

$$q_{\text{len}} \leftarrow q_{\text{len}} + 1 \tag{4.48}$$

If $q_{len} > q_{max}$, the UAV must choose between waiting in a nearby holding position or cancelling and rebooking at an alternative location. This choice is represented in (4.49).

$$status_i = \begin{cases} \text{Wait}, & \text{if space available} \\ \text{Rebook}, & \text{if space unavailable} \end{cases} \tag{4.49}$$

In ad-hoc DWC, synchronization between the charge delivery vehicle (CDV) and charge receiving vehicle (CRV) is crucial. Successful rendezvous requires satisfying (4.50), where Δt_{sync} is the allowable time offset for initiating charging. If (4.50) is violated, the system may reschedule or reassign pairings to maintain efficiency.

$$|t_{\text{arr,CDV}} - t_{\text{arr,CRV}}| \leq \Delta t_{\text{sync}} \tag{4.50}$$

This synchronization condition ensures that ad-hoc charging pairings remain consistent with the timing assumptions used during coordinated scheduling.

4.4.7.2 Late Arrival Handling

For infrastructure-based DWC, late-arriving CAEVs may still enter the track if traffic flow constraints allow. Otherwise, they are rescheduled for the next available slot. If partial missed charging time can be recovered, the departure time $t_{\text{dep,CAEV}}$ is extended to (4.51), where Δt_{late} is the additional time required to meet the original charging requirement. If no extension is available, the CAEV is routed to a secondary charging site.

$$t_{\text{dep,CAEV}'} = t_{\text{dep,CAEV}} + \Delta t_{\text{late}} \tag{4.51}$$

For UAVs, the same approach applies, with departure time updated using (4.52).

$$t_{\text{dep,UAV}'} = t_{\text{dep,UAV}} + \Delta t_{\text{late}} \tag{4.52}$$

In ad-hoc DWC, if the CDV is late, the CRV may be reassigned to a different delivery vehicle or given the option to wait or rebook. If the CRV is late, the CDV is reassigned when possible.

Henceforth, the heuristic scheduling approaches are referred to as the **Static Heuristic Charging Scheduling and Planning (SH-CSP)** approach, which employs fixed scheduling without dynamic arrival handling, and the **Dynamic Heuristic Charging Scheduling and Planning (DH-CSP)** approach, which incorporates the dynamic arrival handling mechanisms introduced in this section.

Algorithm 4 summarizes the proposed logic for handling early and late arrivals for CAEVs and UAVs under coordinated charging scheduling [133].

Algorithm 4 Dynamic Arrival Handling for CAEVs and UAVs [133]

Input: Vehicle type $T \in \{\text{CAEV}, \text{UAV}\}$, Mode $\in \{\text{Infrastructure-DWC}, \text{Ad-hoc-DWC}\}$, t_{arr}, Reservation info
Output: Charging action

IF EarlyArrival **THEN**
  IF Mode == Infrastructure-DWC **THEN**
    IF T == CAEV (DWCN) **THEN**
      IF (4.46) holds **OR** (4.47) holds **THEN**
        Start charging immediately
      ELSE
        Wait in parallel lane or rebook
    ELSE IF T == UAV (LBCN) **THEN**
      IF EVSE available **THEN**
        Start charging
      ELSE IF queue length $< q_{\max}$ **THEN**
        Join queue
      ELSE
        Wait or rebook (4.49)
  ELSE IF Mode == Ad-hoc-DWC **THEN**
    IF (4.50) holds **THEN**
      Rendezvous charging
    ELSE
      Wait, reassign, or rebook
IF LateArrival **THEN**
  IF Mode == Infrastructure-DWC **THEN**
    IF T == CAEV (DWCN) **THEN**
      Resume charging; extend if possible (4.51) **ELSE** rebook or secondary site
    ELSE IF T == UAV (LBCN) **THEN**
      Resume charging; extend if possible (4.52) **ELSE** rebook or secondary site
  ELSE IF Mode == Ad-hoc-DWC **THEN**
    Reassign pairing, wait, or rebook
END Algorithm

4.5 SAFE-DDPG: Learning-Based Coordinated Charging Scheduling

This section presents SAFE-DDPG, the learning-based coordinated charging scheduling algorithm proposed in this thesis for real-time charging reservation and trip planning in heterogeneous CAEV-UAV charging networks. The algorithm is designed to operate under dynamic traffic, demand, and infrastructure conditions, where scheduling decisions must be computed with low latency while respecting feasibility, reachability, and capacity constraints. SAFE-DDPG enables adaptive, data-driven scheduling to capture temporal and spatial variability that is difficult to address with fixed heuristic rules. This section first motivates the selection of DDPG as the base learning framework and then details the domain-specific modifications that support safe execution through feasibility enforcement and stable learning behavior under dynamic conditions.

4.5.1 Selecting DDPG for Coordinated Charging Scheduling

The selection of DDPG as the base learning framework is made deliberately in relation to the operational structure of the coordinated charging problem and in comparison with alternative DRL methods that were considered but not adopted.

The adoption of CAEVs is a key pathway toward reducing greenhouse gas emissions and promoting sustainable mobility. However, the sustainability benefits of electrification also depend on the efficiency of the computational systems responsible for large-scale coordination. Coordinated charging reservation and trip planning introduce additional computation at the edge and cloud, which must remain computationally efficient to support large-scale deployment. Therefore, the scheduling method must balance decision quality, real-time responsiveness, and computational efficiency.

To select a suitable learning framework for this problem, several widely used DRL algorithms were evaluated, including PPO, SAC, TD3, and DDPG. The evaluation focused on characteristics relevant to coordinated charging scheduling, namely: (i) the ability to handle hybrid continuous decision variables, (ii) sample efficiency under stochastic vehicle arrivals and dynamic system conditions, (iii) computational efficiency for real-time scheduling at large scale, and (iv) stability and predictability of the resulting scheduling decisions. These criteria reflect the operational requirements of coordinated charging systems, where scheduling decisions must be computed rapidly and consistently under uncertain and time-varying conditions.

In this work, Deep Deterministic Policy Gradient (DDPG) [163] is selected as the base reinforcement learning framework and subsequently modified to meet the stringent demands of real-time CAEV charging reservation and trip planning. DDPG's deterministic policy outputs are particularly suitable for the hybrid and continuous action spaces inherent in this problem, where the system must make precise decisions on charging levels, CN selection, and routing. Deterministic policies reduce action variability relative to stochastic approaches, enabling stable and predictable scheduling behavior under safety and feasibility constraints. In addition, the off-policy nature of DDPG allows efficient reuse of past experiences, improving sample efficiency and reducing computational overhead for large-scale deployment.

Although the charging environment is inherently stochastic due to uncertain vehicle arrivals, traffic dynamics, and time-varying charging availability, this stochasticity is fully captured in the state transitions and reward realizations of the underlying Markov Decision Process. In such settings, the objective is to maximize the expected cumulative return over stochastic trajectories, which does not require a stochastic policy, as the expectation is taken over stochastic state transitions and rewards.

In the coordinated charging scheduling problem considered in this work, the scheduling decision is a structured control action that must be computed precisely for each observed system state, rather than sampled from a distribution. Introducing stochasticity at the policy

level would lead to unnecessary variance in actions, potentially resulting in infeasible assignments, unstable reservations, and inconsistent coordination behavior. In contrast, a deterministic policy provides stable, reproducible, and low-variance decisions that are essential for reservation-based charging systems operating under strict feasibility and safety constraints.

Within the DDPG framework, uncertainty is handled through repeated interaction with randomized environment dynamics during training, while exploration is introduced via controlled noise processes. This enables the agent to learn a robust state–action mapping that generalizes across stochastic system realizations and maximizes expected performance under uncertainty, without requiring stochastic action sampling during deployment. Therefore, DDPG provides a principled and efficient learning framework for this problem by combining deterministic decision-making with stochastic environment modeling, aligning well with the operational requirements of coordinated charging scheduling.

This selection is further supported by two key considerations. First, the problem involves continuous and coupled decision variables, for which deterministic policy gradients provide efficient and stable control. Second, real-time deployment requires low-latency and reproducible decisions, which are more practical with deterministic policies than with stochastic action sampling. The SAFE-DDPG enhancements further improve robustness by incorporating feasibility-aware decision filtering and adaptive learning mechanisms to handle stochastic system behavior.

To further contextualize this selection, alternative DRL algorithms were examined with respect to the same operational requirements. Policy Optimization (PPO) [164] was evaluated as a candidate for this application but eliminated due to its on-policy update scheme, which requires large volumes of freshly collected data for each policy iteration, leading to lower sample efficiency and higher computational demand than off-policy methods. In addition, PPO's stochastic action selection introduces variability in the resulting scheduling actions. While stochastic policies can be advantageous in some uncertain control problems, coordinated charging scheduling requires consistent and reproducible decisions once a policy is learned, particularly when operating under strict feasibility and safety constraints. PPO may still produce a workable policy in such environments, but its on-policy nature and stochastic action generation make it less suitable for the present problem, where sample efficiency, low-latency inference, and consistent scheduling actions are central requirements rather than secondary preferences. However, PPO's robustness and stability advantages in other domains are acknowledged, and its exclusion here reflects a deliberate trade-off favoring deterministic

control, sample efficiency, and low-latency execution required for coordinated charging scheduling.

Soft Actor-Critic (SAC) [165] was also considered for this scheduling problem. While SAC offers improved robustness through entropy maximization, it is inherently stochastic and incurs higher computational complexity due to its dual-critic structure and entropy temperature tuning. Although these properties may be advantageous in highly uncertain control domains, the added computational overhead conflicts with the low-latency and energy-conscious requirements of large-scale CAEV scheduling, where coordinated decisions must be generated for potentially thousands of vehicles within sub-second time frames. In the context of coordinated charging scheduling, where uncertainty is already captured through stochastic arrivals and dynamic system states, the additional policy stochasticity introduced by entropy maximization provides limited practical benefit relative to its increased computational cost.

Twin Delayed Deep Deterministic Policy Gradient (TD3) [166] is widely regarded as an improvement over DDPG in generic continuous-control tasks and was considered due to its mitigation of overestimation bias using twin critics and delayed policy updates. However, in the present application, the structure of the charging scheduling problem significantly reduces the impact of overestimation bias. Charging decisions are bounded by strict operational and feasibility constraints, which inherently limit the magnitude of potential value estimation errors. Introducing twin critics would nearly double the critic evaluation workload, increasing computational demand and decision latency. For real-time CAEV scheduling, where scheduling decisions must be computed rapidly across large vehicle populations, this additional overhead becomes detrimental to operational efficiency. Moreover, the stability benefits offered by TD3 can be achieved through targeted DDPG enhancements, such as adaptive noise scaling, state augmentation incorporating congestion trends, and domain-specific reward shaping, without incurring the computational cost of maintaining and training multiple critics. Given the bounded and feasibility-constrained action space of the proposed scheduling framework, the additional critic network and delayed update mechanisms of TD3 provide limited practical benefit relative to the computational overhead introduced.

The modified DDPG framework developed in this work extends the baseline formulation [163] through a set of domain-specific enhancements tailored to coordinated charging scheduling for CAEVs and UAVs. These enhancements include sequential per-vehicle decision-making, feasibility-aware action filtering with heuristic fallback to maintain uninterrupted operation, and a dual-stage reward structure that captures both immediate scheduling objectives and longer-term system efficiency. Additional modifications such as

adaptive Ornstein–Uhlenbeck exploration noise and state augmentation are introduced to account for non-stationary traffic conditions and time-varying energy demand, enabling stable and responsive decision-making under dynamic operating environments. For clarity and consistency, the resulting algorithm is termed ***Safety-, Scheduling-, and Sustainability-Aware Feasibility-Enhanced DDPG (SAFE-DDPG),*** reflecting its emphasis on safe execution, effective scheduling coordination, and energy-aware operation.

While alternative algorithms such as PPO, SAC, and TD3 offer advantages in general reinforcement learning settings, their reliance on stochastic policies or additional critic structures introduces trade-offs in sample efficiency, computational overhead, and decision consistency that are not aligned with the real-time, safety-constrained requirements of coordinated charging scheduling. In contrast, the bounded and feasibility-constrained nature of the proposed problem, together with the enhancements introduced in SAFE-DDPG, enables DDPG to achieve stable and efficient learning without incurring these additional overheads.

Table 4.1 summarizes the comparative design considerations that motivated the selection of DDPG as the base learning framework for SAFE-DDPG. In the context of large-scale coordinated charging scheduling, DDPG offers a favorable balance between deterministic control, sample efficiency, and computational efficiency while ensuring consistent decision behavior under stochastic system dynamics. By integrating safety- and feasibility-aware decision mechanisms directly into the learning loop, SAFE-DDPG provides a practical learning-based extension to the heuristic coordination framework developed earlier in this chapter.

Table 4.1: Comparative Evaluation of DRL Algorithm Choices.

FEATURE / REQUIREMENT	**PPO** [164]	**SAC** [165]	**TD3** [166]	**DDPG** [163]	**SAFE-DDPG (PROPOSED)**
Action Type	Stochastic	Stochastic	Deterministic	Deterministic	Deterministic
Sample Efficiency	Low	Moderate	High	High	High
Computational Efficiency	Low	Low	Moderate	High	High
Latency Suitability	Moderate	Low	Moderate	High	High
Handles Continuous Actions	Yes	Yes	Yes	Yes	Yes
Safety Filtering	No	No	No	No	Yes
Sequential Per-Vehicle Control	No	No	No	No	Yes
Adaptive Exploration	Limited	Entropy-based	Limited	OU noise (fixed)	OU noise (adaptive)
Domain Suitability	Low	Low	Medium	Medium	High

Therefore, DDPG is selected as the base framework not only for its ability to efficiently handle continuous and coupled decision variables, but also because its deterministic policy

structure supports low-latency and reproducible scheduling decisions, while uncertainty is effectively captured through environment dynamics and training-time exploration.

4.5.2 SAFE-DDPG: Safety-, Scheduling-, and Sustainability-Aware Feasibility-Enhanced DDPG

4.5.2.1 Baseline DDPG Formulation

For completeness, the baseline DDPG formulation is briefly summarized to highlight the limitations addressed by the proposed SAFE-DDPG [133] extensions. The DDPG algorithm employs an actor–critic architecture for continuous action control. The algorithm assumes that the environment can be modeled as a Markov Decision Process (MDP), in which the next state $\mathbf{s}_{t+1}$ and reward r_t depend only on the current state $\boldsymbol{s_t}$ and action $\boldsymbol{a_t}$, ensuring that the Markov property holds for policy evaluation and learning. In this framework, the critic network $Q(\boldsymbol{s_t}, \boldsymbol{a_t}; \theta^Q)$, parameterized by θ^Q, estimates the expected cumulative reward of taking action $\boldsymbol{a_t}$ in state $\boldsymbol{s_t}$. The objective of SAFE-DDPG is to learn a policy that maximizes the expected cumulative discounted reward over decision epochs, where the reward function encodes charging delay, feasibility, and resource utilization, thereby defining the optimization objective of the scheduling problem. To achieve this objective, the critic is trained by minimizing the temporal-difference (TD) error, expressed in (4.53), where y_t is the TD target at time step t, computed as shown in (4.54).

$$\mathrm{L}(\theta^{\mathrm{Q}}) = \mathbb{E}[(\mathrm{y_t} - \mathrm{Q}(\mathbf{s_t}, \mathbf{a_t}; \theta^{\mathrm{Q}}))^2] \tag{4.53}$$

In (4.54), r_t represents the immediate reward obtained after taking action $\boldsymbol{a_t}$ in state $\boldsymbol{s_t}$, $\gamma \in [0,1]$ is the discount factor that weights future rewards, and the primed networks Q' and μ' are slowly updated target copies of the critic and actor networks, respectively.

$$y_t = r_t + \gamma Q'\left(\mathbf{s}_{t+1}, \mu'(\mathbf{s}_{t+1}; \theta^{\mu'}); \theta^{Q'}\right) \tag{4.54}$$

The parameters of these target networks, denoted as θ', are updated using a soft update rule given in (4.55), where τ is a small coefficient that ensures smooth parameter updates and stabilizes training.

$$\theta' \leftarrow \tau\theta + (1-\tau)\theta', \quad \tau \ll 1 \tag{4.55}$$

The actor network $\mu(\boldsymbol{s_t}; \theta^\mu)$, parameterized by θ^μ, outputs the action to be taken in state $\boldsymbol{s_t}$. It updates its policy by following the deterministic policy gradient, approximated in (4.56). Here, $\nabla_{\mathrm{a}} Q(\mathbf{s}_t, \mathbf{a}; \theta^Q)|_{\mathrm{a}=\mu(\mathbf{s}_t)}$ denotes the gradient of the critic's output with respect to the action, evaluated at the action suggested by the current policy, and $\nabla\theta^\mu \mu(\boldsymbol{s_t}; \theta^\mu)$ represents the gradient of the actor's output with respect to its parameters. While DDPG is effective in general continuous control domains, the vanilla formulation does not inherently incorporate safety

constraints, fairness objectives, or adaptive exploration mechanisms, which are critical for real-time scheduling of vehicles.

$$\nabla_{\theta^\mu} J \approx \mathbb{E}_{\mathbf{s}_t}\left[\nabla_{\mathbf{a}} Q(\mathbf{s}_t, \mathbf{a}; \theta^Q)|_{\mathbf{a}=\mu(\mathbf{s}_t)} \nabla_{\theta^\mu} \mu(\mathbf{s}_t; \theta^\mu)\right] \tag{4.56}$$

In the present application, although UAVs and CAEVs exhibit different physical mobility and energy consumption dynamics, the SAFE-DDPG agent does not operate at the low-level motion control timescale of either platform. Instead, it operates at the charging coordination timescale, where decisions involve handling charging requests, selecting appropriate charging networks, allocating reservations, and coordinating route-aware charging. The detailed motion dynamics of UAV flight and CAEV driving are handled by the underlying mobility and energy consumption models within the simulation environment, while the reinforcement learning agent observes an abstracted scheduling state. This separation of layers is consistent with prior DRL-based charging and routing studies, where the learning agent acts on a higher-level coordination or routing state rather than directly controlling continuous vehicle motion [134], [136], [137]. As a result, the different temporal properties of UAVs and CAEVs are captured within the environment dynamics and reflected in the state transitions observed by the agent, without affecting the validity of the learning formulation.

Building on this abstraction, SAFE-DDPG operates in an event-driven scheduling mode. A decision epoch is triggered whenever a charging request arrives or when a system event modifies the feasible coordination state, such as the completion of a charging session or a change in charging network availability. Under this formulation, the timestep index t in the DDPG update equations corresponds to a decision epoch rather than a fixed physical-time interval. This interpretation is consistent with standard reinforcement learning theory. In particular, [134] formulates EV charging routing as an event-triggered MDP, where decisions are made only when system events occur and the time between decision epochs is state dependent. Related DRL-based charging and navigation frameworks also operate under dynamic traffic conditions and stochastic demand while preserving the sequential decision process [136], [137]. Therefore, variations in vehicle arrival patterns affect only the timing and frequency of decision epochs, not the structure of the learning problem. Each decision epoch still produces a valid state, action, reward, and next-state transition, and the agent continues to operate based on the current system state, preserving the validity of the MDP and DDPG formulation.

4.5.2.2 State–Action Representation for Heterogeneous Charging Networks

The state vector in SAFE-DDPG combines vehicle-centric and environment-centric features required for real-time coordinated scheduling. At scheduling decision epoch t, the state vector is defined as in (4.57).

$$\mathbf{s}_t = [SoC_{\text{curr}}, SoC_{\text{req}}, D_{\text{dest}}, D_{\text{static\_min}}, D_{\text{dynamic\_min}}, N_{CAEV}, N_{UAV}, \rho_{\text{CAEV}}, \rho_{\text{UAV}}, f_{\text{CAEV}}, f_{\text{UAV}}, \mathbf{L}, \mathbf{U}, n_{\text{sched}}, n_{\text{wait}}, \tau_{dec}, \tau_{\text{int}}, \eta_{\text{last}}]^T \quad (4.57)$$

Here, SoC_{curr} and SoC_{req} represent the normalized current and requested states-of-charge of the CAEV. D_{dest} denotes the normalized route distance to the trip destination, while D_{static_min} and $D_{dynamic_min}$ are the normalized minimum distances to the nearest static CN (CCN or SWCN) and dynamic CN (DWCN, AVCN, or GVCN), respectively. N_{CAEV} and N_{UAV} are measures of number of CAEVs and UAVs, respectively. Including explicit vehicle counts provides a clearer view of congestion and competition for charging resources, complementing density and presence indicators by capturing the absolute scale of nearby traffic. ρ_{CAEV} and ρ_{UAV} are composite density measures capturing the proximity and concentration of CAEVs and UAVs around the CAEV. f_{CAEV} and f_{UAV} are binary presence flags indicating whether any nearby CAEVs or UAVs exist. $\mathbf{L}$ is the vector of normalized current load levels for each CN instance including $L_{\text{CCN}_1}, L_{\text{CCN}_2}, L_{\text{SWCN}_1}, L_{\text{SWCN}_2}, L_{\text{DWCN}_1}, L_{\text{DWCN}_2}, L_{\text{GVCN}_1}, L_{\text{AVCN}_1}$. Similarly, $\mathbf{U}$ represents the normalized historical usage of each CN including $U_{\text{CCN}_1}, U_{\text{CCN}_2}, U_{\text{SWCN}_1}, U_{\text{SWCN}_2}, U_{\text{DWCN}_1}, U_{\text{DWCN}_2}, U_{\text{GVCN}_1}, U_{\text{AVCN}_1}$. The variables n_{sched} and n_{wait} denote the normalized numbers of scheduled and currently waiting vehicles. τ_{dec} is the normalized decision time index, τ_{int} is the normalized decision interval, and η_{last} represents the proportion of static charging energy in the previous decision.

The continuous action vector a_t in this implementation consists of four components: a normalized index for selecting a dynamic CN, a normalized index for selecting a static CN, the target SoC at the selected dynamic CN, and the target SoC at the selected static CN. These continuous indices are post-processed into discrete CN selections and admissible SoC targets, enabling simultaneous optimization of location choice and charging level within the heterogeneous charging network.

4.5.2.3 Feasibility-Aware Action Filtering with DH-CSP Fallback

Every actor-generated action $\mathbf{a}_t^{\text{DRL}}$ is evaluated by the feasibility function $\mathcal{F}(\mathbf{s}_t, \mathbf{a}_t)$, which enforces SoC reachability, CN capacity and booking constraints, and route feasibility, ensuring the vehicle can physically reach the selected charging node under current operational

conditions. If $\mathcal{F} = 0$, indicating an infeasible action, it is replaced by the heuristic output $\mathbf{a}_t^{\text{heuristic}}$ generated by the DH-CSP module as seen in (4.58).

$$\mathbf{a}_t^{\text{final}} = \begin{cases} \mathbf{a}_t^{\text{heuristic}}, & \mathcal{F} = 0 \\ \mathbf{a}_t^{\text{DRL}}, & \text{otherwise} \end{cases} \tag{4.58}$$

This feasibility-aware filtering layer prevents unsafe, infeasible, or operationally costly actions from being executed, while ensuring the replay buffer is populated with constructive experiences. As a result, it improves training stability and convergence efficiency compared to baseline DRL methods such as vanilla DDPG, PPO, or SAC.

4.5.2.3.1 Dual-Stage Reward

The local reward in (4.59) encourages immediate operational efficiency while penalizing imbalance, excessive routing overhead, and infeasible decisions:

$$R_t = -\frac{(\text{SoC}_{\text{req}} - \widehat{\text{SoC}})^2}{\text{SoC}_{\text{req}} + \epsilon} - \beta_1 L_{\text{dyn}} - \beta_2 \frac{d_{\text{dyn}}}{d_{\max}} - \beta_3 L_{\text{stat}} - \beta_4 \frac{d_{\text{stat}}}{d_{\max}} + B_{\text{lowLoad}} - P_{\text{fallback}} - \text{P}_{\text{feasibility}} \tag{4.59}$$

where $\widehat{\text{SoC}}$ is the predicted post-charge SoC, L_{dyn} and L_{stat} are load imbalance metrics, d_{dyn} and d_{stat} are travel distances, B_{lowLoad} rewards use of underloaded CNs, P_{fallback} penalizes heuristic reliance, and $P_{\text{feasibility}}$ penalizes infeasible CN selections. This design ensures that selected CNs meet SoC requirements, avoid overloaded CNs, and remain reachable within operational constraints.

The global reward in (4.60), applied after each episode, enforces long-term fairness and sustainability, and is adaptively scaled to match the magnitude of immediate rewards. In (4.60), U_{CN} is the mean CN utilization across CNs, W_{avg} is the average normalized wait time, I_{avg} is the average normalized idle time, C_{travel} is the normalized travel cost, C_{batt} is the normalized battery consumption cost, and P_{fallback} is a nonlinear penalty that increases with the fallback usage frequency. The final reward is scaled by a factor proportional to the mean absolute value of immediate rewards in the episode.

$$R_{\text{global}} = w_{\text{util}} U_{\text{CN}} - w_{\text{wait}} W_{\text{avg}} - w_{\text{idle}} I_{\text{avg}} - w_{\text{travel}} C_{\text{travel}} - w_{\text{batt}} C_{\text{batt}} - P_{\text{fallback}} \tag{4.60}$$

By combining utilization maximization with penalties for waiting time, idle capacity, travel, battery consumption, and fallback reliance, this reward structure incentivizes policies that maintain high network efficiency while avoiding congestion, unnecessary travel, and over-reliance on heuristics. The adaptive scaling ensures that the global reward remains balanced

with immediate rewards, preventing one objective from dominating the learning process and encouraging stable, long-term improvements in system performance.

The coefficients used in (4.59) and (4.60) are not intended to represent optimal parameters in a formal multi-objective optimization sense. Instead, they provide a scalarized reward signal that allows the reinforcement learning agent to balance several operational objectives within a single learning framework, which is a common approach in reinforcement-learning-based scheduling and resource allocation problems. The values were selected through sensitivity analysis to ensure stable learning behavior and balanced performance across utilization, waiting time, travel cost, and energy efficiency. The resulting scheduling policy therefore emerges from the agent's interaction with the environment during training rather than being analytically determined by the reward weights themselves. In this context, the weights express the relative importance of the objectives that guide the learning process, while the SAFE-DDPG agent discovers the policy that maximizes the resulting cumulative reward. Different weight selections would therefore influence the trade-offs emphasized during learning rather than determining the optimality of the final policy itself.

4.5.2.4 Neural Architecture and Action Selection

The SAFE-DDPG agent employs deep actor–critic networks with fully connected layers and Exponential Linear Unit (ELU) activation to avoid the "dead neuron" problem common with Rectified Linear Unit (ReLU) and to ensure smooth learning in low-gradient regions. Careful initialization and batch normalization in hidden layers support stable gradient propagation under non-stationary charging demands. Regularization and dropout enhance robustness against sensor noise and unpredictable vehicle arrivals without excessively dampening learning capacity. In the critic, state and action vectors are concatenated at the input stage to enable early joint representation learning, while the actor produces actions via a sigmoid output layer, inherently bounding them to [0, 1] and providing stable gradients during policy updates for smoother convergence compared to vanilla DDPG.

To improve stability in dynamic charging scenarios, the agent applies online reward normalization [167] to both individual step rewards and distributed global rewards. Extreme outliers are clipped before normalization to maintain a consistent learning signal across varying operational conditions. Gradient norms are constrained to prevent instability from sudden policy shifts, and training is deferred until a sufficient number of transitions are available to ensure representative minibatches. Domain-specific post-processing maps the continuous actor outputs to discrete charging-station selections and target state-of-charge values, enabling direct integration with heterogeneous charging network constraints.

Relative to vanilla DDPG, these refinements are designed to improve stability, convergence behavior, and robustness under dynamic arrival patterns. Compared to stochastic approaches like PPO and SAC, SAFE-DDPG's deterministic, bounded-action policy avoids unnecessary exploration noise and converges more quickly under operational constraints. Unlike TD3, which mitigates overestimation bias through twin critics and delayed updates, SAFE-DDPG achieves stability through architectural regularization, careful initialization, and reward normalization, preserving sample efficiency while reducing computational overhead. These design choices enable the agent to operate with high precision and low latency, critical for real-time coordination in heterogeneous charging networks.

4.5.2.4.1 Stabilized Prioritized Experience Replay

In the proposed framework, the standard experience replay mechanism in vanilla DDPG is replaced with a stabilized prioritized experience replay (PER) strategy to improve convergence speed and training stability in dynamic charging network environments. The sampling probability of each stored transition is defined in (4.61), where δ_i denotes the TD error, ϵ avoids zero probabilities, and α controls the degree of prioritization.

$$P(i) = \frac{(|\delta_i| + \epsilon)^\alpha}{\sum_j (|\delta_j| + \epsilon)^\alpha} \tag{4.61}$$

The associated importance-sampling weights are computed as shown in (4.62) with β gradually annealed during training to correct sampling bias as learning progresses. For numerical stability, all w_i values are normalized by dividing them by the maximum weight before being applied in gradient updates.

To further enhance stability, newly observed transitions are optimistically assigned the current maximum priority, ensuring they are rapidly integrated into the learning process. TD-error updates are smoothed through a weighted blending of previous and current priorities to mitigate sudden fluctuations, and rewards are normalized before storage to prevent large magnitudes from dominating updates. These refinements collectively accelerate convergence and improve robustness under dynamic arrival patterns and heterogeneous charging network conditions compared to standard replay mechanisms.

$$w_i = \left(\frac{1}{N} \cdot \frac{1}{P(i)}\right)^\beta \tag{4.62}$$

4.5.2.5 Adaptive Ornstein–Uhlenbeck Exploration Noise

To further improve policy exploration, an adaptive Ornstein–Uhlenbeck (OU) process for action noise is introduced. In contrast to vanilla DDPG, which employs fixed-variance OU noise, the noise variance σ_t in SAFE-DDPG evolves according to (4.63). This gradual decay

ensures that large exploratory deviations dominate early in training, when policy uncertainty is high, while a moderate level of stochasticity is preserved in later stages to allow continual adaptation to changing system conditions.

$$\sigma_t = \max(\sigma_{\min}, \sigma_0 \cdot \text{decay}^t) \tag{4.63}$$

Through the combination of stabilized prioritized experience replay and adaptive OU noise, SAFE-DDPG is designed to improve learning stability, adaptability, and convergence behavior compared to vanilla DDPG, particularly in highly dynamic, safety-critical scheduling environments.

4.5.2.6 Training Algorithm

The training process for SAFE-DDPG summarized in **Algorithm 5** [133] is designed for online, sequential scheduling in heterogeneous charging networks. At each step, the actor network produces a deterministic continuous action (dynamic CN index, static CN index, target SoCs) perturbed by adaptive OU noise (4.63) for exploration. Actions are evaluated by a feasibility filter (4.58) that enforces SoC reachability and CN capacity constraints, with infeasible actions replaced by a DH-CSP heuristic fallback to ensure safety and operational continuity. Local rewards are computed immediately (4.59) and transitions are stored in a prioritized experience replay buffer (4.61–4.62). After each episode, a global reward is calculated (4.60) to reflect fairness, network utilization, wait times, and fallback usage, and distributed across the stored transitions. The actor and critic networks are updated from mini-batches sampled from the buffer using DDPG loss functions (4.53–4.56), with target networks softly updated for stability. This procedure enables the agent to balance short-term efficiency with long-term objectives while maintaining safety and robustness in dynamic, non-stationary charging networks.

Algorithm 5 *SAFE-DDPG Training with Feasibility Filtering and Dual-Stage Rewards [133]*

Begin
procedure TrainSAFE-DDPG()
  Initialize actor $\mu(\cdot\,|\theta^{\mu})$, critic $Q(\cdot\,|\theta^{Q})$, and target networks μ', Q'
  Initialize PER buffer $\mathcal{D}$, noise params σ_0, $\sigma_{\min}$, decay
  for each episode **do**
    Observe initial environment state
    for each decision epoch t **do**
      for each vehicle v in active set **do**
        $\mathbf{s}_t^v \leftarrow$ vehicle-specific state from (4.57)
        $\mathbf{a}_t^v \leftarrow \mu(\mathbf{s}_t^v|\theta^{\mu}) + \text{OU\_Noise}(\sigma_t)$ # per (4.63) for adaptive OU noise
        if $\mathcal{F}(\mathbf{s}_t^v, \mathbf{a}_t^v) = 0$ # per (4.58)
          $\mathbf{a}_t^v \leftarrow$ heuristic decision (DH-CSP fallback)
        end if
        Execute $\mathbf{a}_t^v$, observe R_t^v per (4.60), $\mathbf{s}_{t+1}^v$
        Store $(\mathbf{s}_t^v, \mathbf{a}_t^v, R_t^v, \mathbf{s}_{t+1}^v)$ in $\mathcal{D}$ with PER (4.61)–(4.62)
      end for
      Sample mini-batch from $\mathcal{D}$, update Q via (4.53)–(4.54), μ via (4.56)
      Soft-update targets μ', Q' via (4.55)
      $\sigma_t \leftarrow \max(\sigma_{\min}, \sigma_t \times \text{decay})$ # per (4.63)
    end for
    Compute R_{global} per (4.60)
    Distribute R_{global} to episode transitions
  end for
end procedure
End

4.5.2.7 Highlights of the SAFE-DDPG Algorithm

SAFE-DDPG extends vanilla DDPG into a domain-optimized, feasibility-aware, safety-aware, fairness-aware by design, and computationally efficient controller for large-scale online CAEV scheduling. Its feasibility-aware state–action representation integrates operational load, travel distance, time features, and direct feasibility indicators across heterogeneous charging network topologies. This encoding is topology-parameter-agnostic, meaning it supports deployment across different CN layouts, load distributions, and operational conditions without retraining, provided the number and type of CNs remain unchanged. Within this constraint, policies can be directly transferred to new infrastructures and traffic patterns, avoiding the environment-specific tuning often required by PPO and SAC. Sequential per-vehicle decision-making within each timestep ensures fine-grained updates that preserve responsiveness under strict latency requirements, making the framework suitable for real-time operational control.

Before detailing the internal components of SAFE-DDPG, it is useful to position it relative to the two heuristic scheduling approaches introduced earlier in this chapter. All three

methods operate within the same three-layer system architecture and employ the same handshake protocol, ensuring comparable scalability and deployment assumptions. The comparison therefore focuses on differences in decision logic, adaptability, and constraint handling, rather than architectural capabilities.

Table 4.2 summarizes the progression of coordinated charging scheduling approaches developed in this chapter, highlighting how SH-CSP and DH-CSP provide interpretable heuristic baselines, while SAFE-DDPG extends this logic with learning-based adaptability under the same architectural framework. These proposed approaches motivate the subsequent performance evaluation, where the trade-offs among simplicity, adaptability, and efficiency are quantified under identical operating conditions.

Table 4.2: Comparison of Proposed Coordinated Charging Scheduling Approaches.

Aspect	SH-CSP	DH-CSP	SAFE-DDPG
Scheduling paradigm	Static heuristic	Dynamic heuristic	Learning-based
Online decision-making	Yes	Yes	Yes
Dynamic arrival handling	No	Yes	Yes
Constraint handling	Rule-based	Rule-based	Learned awareness + rule-based screening
Responsiveness to evolving system load	Snapshot-based	Event-driven	Proactive / predictive
Adaptation to demand variability	Limited	Moderate	High
Online decision overhead	Low	Low	Low (single actor network inference pass)
Interpretability	High	High	Moderate–High (vs. learning-based methods)
Training requirement	None	None	Required (offline; online optional)

SAFE-DDPG's main advancement over vanilla DDPG lies in its integration of a mathematically defined dual-stage reward with embedded feasibility checks and stability mechanisms. The local reward penalizes deviations from target post-charge state-of-charge, load imbalance, and excessive travel, while rewarding use of underloaded charging networks and discouraging infeasible or fallback-based scheduling. The global reward, applied post-episode, encourages balanced utilization and fairness objectives while penalizing waiting time, idle capacity, travel cost, battery consumption, and excessive fallback reliance. A nonlinear penalty function increases with frequent fallback use while rare fallback actions incur minimal cost. This reward structure is adaptively scaled to balance short-term efficiency with long-term sustainability, preventing instability from reward magnitude shifts. These fairness-oriented and efficiency-driven reward components are incorporated at the design stage, with their quantitative impact examined in the evaluation results presented later in this chapter.

Feasibility is enforced in both training and inference through an action screening layer that rejects unreachable or capacity-violating actions and substitutes safe alternatives from a DH-CSP fallback module. Stability is further supported through online reward normalization using Welford's method, outlier clipping, gradient norm constraints, delayed training until the replay buffer contains a sufficiently diverse set of transitions, and domain-specific post-

processing that maps continuous outputs to discrete station assignments and target SoC values. These combined measures are designed to improve learning stability, convergence behavior, and robustness under non-stationary traffic and charging demand conditions, which pose challenges for vanilla DDPG.

The neural architecture is designed for stability and efficiency without the computational burden of TD3's twin critics. ELU activations, batch normalization, L2 regularization, and dropout collectively reduce overfitting and improve robustness under non-stationary operating conditions. Stabilized prioritized experience replay, with optimistic priority initialization, smoothed temporal-difference error updates, and reward normalization, focuses updates on high-impact transitions without destabilizing online learning. Adaptive OU noise modulation further enhances training by enabling controlled exploration early on and precise exploitation as the policy matures.

Compared to PPO, SAFE-DDPG achieves higher sample efficiency through off-policy training, enabling faster adaptation in online settings where data arrive incrementally. Compared to SAC, it avoids the complexity and sensitivity of entropy tuning while retaining adaptability. Compared to TD3, it achieves stability with reduced computational cost, making it more suitable for latency-sensitive operations. With inference latency on the order of sub-milliseconds per decision on standard GPUs, SAFE-DDPG is well suited for edge-based real-time CAEV scheduling in large-scale, heterogeneous smart transportation networks.

The coordinated charging scheduling models and algorithms developed in this chapter establish the decision logic for charging reservation, routing, and execution under dynamic operating conditions. The following section evaluates these methods through simulation to validate their correctness and to assess their performance across a range of traffic, demand, and infrastructure scenarios.

4.6 Experimental Methodology

This section presents the experimental methodology used to evaluate the coordinated charging scheduling and trip planning methods developed in this chapter. The methodology defines the simulation framework, verification steps, evaluation metrics, and scenario setup used to ensure a fair and reproducible assessment of scheduling performance.

4.6.1 Simulation Framework for Algorithm Evaluation

This section describes the simulation framework used to evaluate the coordinated charging scheduling and trip planning methods developed in this chapter. The framework provides a controlled, event-driven execution environment in which heterogeneous CAEVs, UAVs, charging networks, and cloud-level coordination services interact over time. Its purpose

is to enable systematic evaluation of scheduling, reservation, and charging decisions under dynamic traffic, demand, and infrastructure conditions. The execution of these decisions follows the coordinated system cycle introduced earlier in this chapter, allowing algorithm behavior to be evaluated within a consistent operational flow.

The simulation framework models the charging system as a collection of interacting entities with clearly defined roles and constraints. Vehicles represent mobile energy consumers with heterogeneous mobility patterns, energy consumption characteristics, and charging requirements. Charging networks represent static and dynamic charging infrastructures with limited capacity, technology-specific constraints, and availability profiles. Cloud-level coordination services manage authentication, reservation validation, energy metering, and accounting, ensuring consistency between scheduled decisions and executed charging sessions. This abstraction allows both heuristic and learning-based scheduling algorithms to be evaluated consistently across a wide range of operating scenarios. The simulation framework instantiates the charging network architecture and communication protocol introduced in Chapter 3 at an abstract level, ensuring consistency between the system design and the scheduling and execution logic evaluated in this chapter. In particular, the reliability mechanisms embedded in the Chapter 3 handshake design, including acknowledgment exchange, timeout-based recovery, and reservation revalidation, are reflected in the execution logic used here so that scheduling performance is evaluated under realistic coordination constraints rather than idealized communication assumptions.

The main entities, interactions, and their roles in the experimental evaluation are summarized in Table 4.3.

Table 4.3: Simulation Framework Entities, Interactions, and Evaluation Roles.

Entity / Component	Modeled Characteristics	Key Events / Interactions	Role in Evaluation
CAEVs and UAVs	Mobility patterns, energy consumption, battery state, charging demand	Movement, charging request generation, arrival, charging execution, departure	Enable evaluation of scheduling decisions under heterogeneous vehicle behavior
Charging Networks	Capacity limits, charging technology, availability, static or dynamic operation	Reservation acceptance, charging execution, alignment verification	Support analysis of utilization, congestion, and reservation fulfillment
Cloud-Level Coordination	Reservation validation, authentication, metering, accounting	Request processing, confirmation, billing finalization	Ensure consistency between scheduled and executed charging actions
Scheduling Algorithms	SH-CSP, DH-CSP, and SAFE-DDPG decision logic	Charging assignment, reservation timing, routing decisions	Core mechanisms evaluated for efficiency and adaptability
Feasibility and Alignment Enforcement	Operational, geometric, and capacity constraints	Action validation, correction, fallback triggering	Ensure scheduled actions remain physically executable
Event Execution Engine	Discrete-time progression, global future event list	Movement, arrival, charging, departure events	Enable repeatable, event-driven experimentation
Metrics Collection	Waiting time, travel cost, utilization, fulfillment	Continuous logging during execution	Provide quantitative performance measures

System behavior within the framework is governed by a discrete-time, event-driven execution model. Simulation time advances through a discrete-event execution process governed by a global event list, where system dynamics are represented through events such as vehicle movement, charging request generation, reservation confirmation, charging execution, alignment correction, and departure. Scheduling algorithms are invoked at defined decision points within this event sequence, where they determine charging network assignments, reservation times, and routing decisions based on the current system state. The resulting actions directly influence subsequent events, allowing the closed-loop interaction between decision logic and system evolution to be captured.

Vehicle mobility and energy consumption are modeled in a manner consistent with the physical constraints introduced earlier in this chapter. As vehicles traverse their planned routes, energy consumption is deducted according to vehicle-specific efficiency models. Upon reaching a charging network, arrival events trigger reservation enforcement and charging execution for the allocated duration. Charging sessions are monitored in real time to ensure compliance with feasibility, alignment, and operational constraints, after which billing and accounting are finalized before the vehicle proceeds to its next destination.

The framework supports both static and dynamic charging scenarios. For static charging networks, arrival events handle early, on-time, and late arrivals, enabling queueing, reassignment, or waiting strategies as required by the scheduling logic. For dynamic charging networks, arrival and departure events model charging while in motion, with continuous verification of alignment, speed, and operational tolerances. These mechanisms ensure that charging execution remains physically realistic while allowing the scheduling algorithms to be evaluated under diverse infrastructure configurations.

By structuring system behavior around a global event list and explicit decision points, the simulation framework enables repeatable and controlled experimentation. Performance metrics such as waiting time, travel cost, charging utilization, and reservation fulfillment are collected throughout execution, providing the basis for quantitative evaluation of the proposed scheduling methods.

The simulation framework thus serves as the experimental backbone for the remainder of this chapter. The following sections use this framework to first verify and validate the correctness of the implemented models and scheduling logic, and then to evaluate algorithmic performance under representative traffic, demand, and infrastructure scenarios.

4.6.2 Model Verification for Algorithm Evaluation

Building on the simulation framework and event-driven execution model introduced in the preceding section, model verification was performed to ensure that the system cycle, models, and execution logic used for coordinated charging scheduling and trip planning were correctly implemented. The charging network architecture and handshake protocol employed by the simulator follow the design validated in the earlier chapter and are reused here as the operational foundation for algorithm evaluation.

The verification process examined the behavior of the simulation entities and their interactions within the defined framework, at the level required for scheduling evaluation. Cloud-level coordination services, charging networks, and vehicles were traced through reservation requests, charging assignments, arrival handling, and charging execution to confirm that state transitions and event sequencing followed the intended operational logic of the proposed system cycle. Runtime logs were used to verify that reservation handling, queue management, charging initiation, and session termination were executed consistently across static and dynamic charging scenarios.

Individual model components were verified to ensure numerical and logical consistency with their formulations. Power transfer, battery state evolution, and energy consumption models were examined to confirm that they produced physically realistic values and remained within defined operational limits. Alignment correction and feasibility enforcement mechanisms were verified to ensure that charging execution adhered to geometric, capacity, and operational constraints. These checks ensured that scheduling decisions were evaluated against valid and physically feasible system responses.

Verification also included integrated end-to-end and targeted analytical checks, implemented through small-scale simulations and targeted test cases, to confirm correct system behavior prior to large-scale evaluation. Reservation requests were tracked from initiation through confirmation, charging execution, and completion to ensure consistency in energy allocation, waiting behavior, and synchronization across charging networks under varying operating conditions. Analytical verification of charging and communication feasibility, along with small-scale execution checks of the system cycle using the heuristic scheduling strategies, are provided in **Appendices B and C**.

Through this verification process, the simulation framework and associated models were shown to operate consistently with the system cycle, constraints, and scheduling logic defined in this chapter. This establishes confidence that the framework provides a correct and

reliable basis for subsequent validation and performance evaluation of the proposed coordinated charging scheduling algorithms.

4.6.3 Performance Evaluation Metrics

The coordinated charging scheduling problem studied in this chapter has clear queueing-theoretic aspects, and this is reflected in the evaluation metrics adopted later, including average waiting time, average system delay, throughput, utilization, offered load, idle proportion, queue length through Little's Law, and fairness across charging networks. However, the overall problem cannot be represented faithfully by a standard closed-form queueing model such as a single-queue or conventional multi-dimensional queue. This is because the system is reservation-based, route-aware, heterogeneous across charging technologies, and coupled across multiple charging networks and vehicle classes, with charging feasibility depending not only on arrival and service processes but also on travel distance, remaining energy, vehicle type, alignment constraints, and dynamic reassignment. These characteristics introduce time-coupled and state-dependent interactions that fall outside the assumptions typically required for tractable analytical queueing formulations. In particular, classical models such as M/M/1, M/G/1, or multi-class multi-server queueing systems assume stationary arrivals, independent service processes, and limited coupling across queues, assumptions that are not satisfied in the proposed reservation-based and mobility-coupled scheduling framework. For this reason, queueing theory is used here as an evaluation lens rather than as the primary system model. Within that lens, SH-CSP and DH-CSP provide interpretable heuristic baselines under the same system assumptions, while the full coordinated scheduling problem is evaluated through discrete-event simulation to preserve the dynamic and heterogeneous structure of the system.

To evaluate the effectiveness of the coordinated charging scheduling and trip planning methods developed in this chapter, a set of performance metrics is defined. These metrics quantify how coordinated scheduling decisions impact waiting delay, charging resource utilization, service efficiency, and congestion under dynamic traffic and charging demand. They provide a consistent basis for comparing heuristic and learning-based scheduling strategies and for assessing how well coordinated reservation and routing decisions translate into improved operational performance within the simulated charging networks. The following metrics are computed:

a) **Average wait time per EV (T_Q):** It is the average time an EV spends waiting in the queue of a charging network before service begins, reflecting the effectiveness of scheduling decisions in reducing congestion and delay. The average wait time is computed as the mean

of the individual queueing times Q_i experienced by the N_D EVs serviced by the charging network, as expressed in (4.64).

$$T_Q = \frac{1}{N_D}\sum_{i=1}^{N_D} Q_i \tag{4.64}$$

b) Throughput (λ): It is also known as departure rate. It measures how many EVs are serviced by a system or charging network per unit time and reflects the level of charging capacity utilization achieved under coordinated scheduling. It is usually defined as the ratio of the number of departures N_D to the total simulation time T, as shown in (4.65). The unit of throughput is EVs per time unit (EV/min). When a charging network operates c EVSEs in parallel, the normalized throughput per server can be expressed using (4.66).

$$\lambda = \frac{N_D}{T} \tag{4.65}$$

$$\lambda = \frac{N_D}{cT} \tag{4.66}$$

c) Average service time per EV (T_s): It represents the average duration for which an EV occupies a charging server and is computed by dividing the total server busy time B by the total number of departures N_D as can be seen in (4.67). Equation (4.68) shows that B is equal to the sum of the individual service times, T_i, for the i^{th} EV that departed.

$$T_s = \frac{B}{N_D} \tag{4.67}$$

$$B = \sum_{i=1}^{N_D} T_i \tag{4.68}$$

d) Server Utilization (ρ): It is the proportion of simulation time during which the server or CN is busy. It is the product of its throughput (λ) and the average service time per EV (T_s), normalized by the number of servers (c) if there are multiple servers operating in parallel. This can mathematically be expressed by (4.69). This formulation ensures that utilization reflects how effectively coordinated scheduling distributes load across individual charging servers.

$$\rho = \frac{\lambda T_s}{c} \tag{4.69}$$

- ***Offered Load (A_L):*** In queueing theory, server utilization is often interpreted as the fraction of offered load carried by the system. The offered load in (4.70) represents the traffic intensity applied to a server, expressed as the product of arrival rate λ_A and average service time:

$$A_L = \lambda_A T_s \tag{4.70}$$

Under stable operating conditions, server utilization (ρ) approaches the offered load (A_L), indicating that scheduling decisions effectively match demand to available charging capacity. An offered load greater than 1 ($A_L > 1$) indicates that the arrival rate of EVs exceeds the service capacity of the server or CN, which can result in growing queues, increased wait times, or potential system congestion. In contrast, $A_L \leq 1$ reflects a stable system where the servers can handle the incoming traffic without backlog.

e) **Proportion Server Idle Time (β):** It represents the proportion of time during which a charging server is idle and not processing any EVs, and is defined as one minus the server utilization, as shown in (4.71).

$$\beta_T = 1 - \rho \tag{4.71}$$

f) **Average system wait time (w):** It is also known as the response time or delay. It represents the total time an EV spends in the system, capturing both queueing delay and service time, and reflects the combined impact of scheduling, reservation timing, and charging execution on trip delay. The average system wait time can be computed using (4.72), where W_i is the time spent in the system by the i^{th} simulated EV and N_A is the number of arrivals.

$$w = \frac{1}{N_A}\sum_{i=1}^{N_A} W_i \tag{4.72}$$

g) **Little's Law or Queue Length (L)**: Little's Law provides a fundamental relationship in queueing systems, linking the average number of vehicles in the system (L) with the arrival rate (λ) and the average system wait time (w):

$$L = \lambda w \tag{4.73}$$

Depending on context, L may represent the average queue length (when vehicles wait) or the average number of vehicles in the system (when there is no queue and only service time is involved). Reporting both simulation-derived values and those obtained via Little's Law ensures internal consistency and provides an additional validation check for the reported performance metrics.

h) **Jain's Fairness Index (JFI)**: It is used to quantify how evenly coordinated charging scheduling decisions distribute vehicles across available charging networks (CNs). It is defined as:

$$J = \frac{(\sum_{i=1}^{N} x_i)^2}{N \cdot \sum_{i=1}^{N} x_i^2} \tag{4.74}$$

where x_i denotes the service measure associated with the i^{th} CN and N is the total number of CNs. The value of J lies in the range $[0, 1]$, with values closer to 1 indicating a more equitable distribution of load across CNs.

In this chapter, x_i is primarily defined as the number of vehicles serviced by each CN, allowing assessment of how coordinated scheduling balances demand spatially across the charging infrastructure. Alternatively, x_i may represent per-CN throughput to reflect fairness in terms of delivered service. JFI values are reported in the experimental results to provide an aggregate indication of load balancing achieved by the proposed scheduling methods, while a deeper discussion of fairness implications is deferred to the next chapter.

4.6.4 Simulation Setup and Scenario Configuration

This section describes the simulation setup used to evaluate the coordinated charging scheduling and trip planning methods developed in this chapter. The setup instantiates the system cycle, models, and scheduling logic introduced earlier, providing a controlled experimental environment for assessing algorithmic performance under dynamic traffic, charging demand, and heterogeneous infrastructure conditions. The charging network architecture, entity roles, and coordination flow validated in Chapter 3 are employed implicitly as the operational foundation, allowing this chapter to focus on scheduling behavior and performance evaluation.

4.6.4.1 Simulation Environment and Time Horizon

The proposed coordinated charging scheduling framework is evaluated using the heuristic scheduling algorithms SH-CSP and DH-CSP, as well as the learning-based SAFE-DDPG algorithm developed in this chapter. For benchmarking purposes, vanilla DDPG and TD3 are also implemented to isolate the performance gains attributable to the proposed feasibility-aware and scheduling-aware enhancements.

A discrete-time, event-driven simulator models the integrated operation of CAEVs, UAVs, and heterogeneous charging networks. Simulation time advances through a discrete-event execution process, in which scheduling decisions are triggered by charging requests and other events that modify the charging coordination state. During simulation execution, vehicle movement, charging requests, scheduling decisions, and charging execution events are processed sequentially. Simulations are executed over a continuous two-day horizon (5–6 June 2025), corresponding to Ontario's summer time-of-use (TOU) electricity pricing periods [168], [169], enabling realistic cost-aware scheduling behavior.

CAEV mobility and routing are modeled using the SUMO traffic simulator [170], [171] to capture realistic traffic dynamics and route variability. UAV operations are modeled directly within the simulator to support heterogeneous energy consumption, wireless charging interactions, and alignment constraints.

The CAEV road network is a large-scale synthetic SUMO environment whose aggregate spatial extent is on the order of several thousand kilometers. This does not represent a single continuous vehicle trip. Instead, it reflects the cumulative length of road segments used to emulate wide-area CAEV operations and to stress-test coordinated charging scheduling under spatially distributed demand. Individual vehicle trips remain localized and are bounded by realistic travel distances within the simulated time horizon.

4.6.4.2 Vehicle, UAV, and Charging Network Parameters

CAEVs are initialized with battery state-of-charge values uniformly sampled between 20% and 70% of full capacity to represent heterogeneous arrival conditions. Static charging networks, including CCNs, SWCNs, and LBCNs, support charging up to full state-of-charge, while dynamic charging networks such as DWCNs provide a maximum charging power of 10 kW per session. Vehicle-to-vehicle charging networks, including AVCNs and GVCNs, support up to 5 kW per session.

Charging requests follow Poisson arrival processes, with arrival rates selected to generate sustained but stable charging demand across the network. CAEV charging requests occur with rate 0.1, while LBUAVs and EIUAVs request charging at rates of 0.033 and 0.05, respectively. The simulated fleet consists of 50 CAEVs, 8 LBUAVs, and 6 EIUAVs.

All vehicles are modeled using the linear two-stage battery model introduced earlier in this chapter, ensuring consistent and physically realistic charging behavior across wired, magnetic resonance wireless, and laser-based charging technologies. CAEV parameters are derived from the EV Database [172], while UAV physical, energy, and flight parameters are summarized in Table 4.4.

Table 4.4: Summary of UAV Parameters.

PARAMETER	LBUAV	EIUAV	PARAMETER	LBUAV	EIUAV
W (N)	39.2	6.9	LOS (–)	0.9	0.9
n (–)	4	4	Env_λ (–)	0.95	0.95
r (m)	0.20	0.13	P_{LTrans} (W)	1000	–
A (m²)	0.1257	0.0531	A_{LRec} (m²)	0.088	0.037
C_T (–)	0.095	0.095	$SFP_{\parallel}$ (m²)	0.20	0.12
ρ (kg/m³)	1.225	1.225	V_v^{asc} (m/s)	3.0	1.5
δ_s (–)	0.05	0.05	V_v^{desc} (m/s)	−2.5	−1.5
k (–)	0.5	0.5	$SFP_{\perp}$ (m²)	0.20	0.12
V_h (m/s)	15.0	10.0	v_0 (m/s)	6.32	4.42

The UAV parameters were selected to reflect realistic flight dynamics, payload capacities, and energy constraints associated with their respective operational roles. Differences between LBUAVs and EIUAVs capture distinct mission profiles and wireless

charging responsibilities, enabling evaluation of coordinated scheduling decisions across heterogeneous aerial and ground vehicles. Both UAV types employ four rotors to balance maneuverability and energy efficiency. Aerodynamic and environmental parameters are chosen based on standard rotorcraft models to capture hovering, vertical, and horizontal flight under urban operating conditions. These choices ensure that UAV energy consumption and mobility behavior are realistically represented, enabling meaningful evaluation of coordinated scheduling and wireless charging strategies across heterogeneous aerial and ground vehicles.

4.6.4.3 Charging Infrastructure and Technology Configuration

The simulated charging infrastructure includes 2 CCNs, 2 SWCNs, 2 DWCNs, 2 LBCNs, 1 AVCN, and 1 GVCN. CCNs, SWCNs, and DWCNs employ magnetic resonance wireless charging, while LBCNs and V2V charging networks use laser beam power transfer, as summarized in Table 4.5.

SWCNs are modeled using WCPs of length 10 m, while DWCNs consist of segmented tracks with WCPs of length 120 m, with fixed parameters for CCNs and SWCNs based on commercially available systems [173], [174]. Since DWCNs are not yet commercially deployed, their infrastructure is generated using the design methodology introduced in earlier work [8], enabling evaluation of dynamic charging under realistic geometric and power constraints. The extended DWCN track length is used to emulate long roadway segments suitable for dynamic charging evaluation and does not represent a single continuous physical installation.

Each EVSE time slot duration $\mathrm{ts}_{dur}^{\mathrm{CN}}$ is fixed at 10 minutes. Over the two-day simulation horizon, this results in 288 time slots per EVSE, computed using (5.11). The billing scheme is set to pay per charging session. To incorporate realistic uncertainty, stochastic charging-skipping behavior ($P_s = 1/2$) and road accident probabilities ($P_a = 1/189.59$), are introduced using Ontario statistics [175].

$$N_{ts} = N_{days} * \frac{24\ hrs}{day} * \frac{60\ min}{hr} * \frac{1\ ts}{\mathrm{ts}_{dur}^{\mathrm{CN}}} \tag{5.11}$$

Table 4.5: The parameters setup for the system's simulation.

Simulator Setup	
Simulation Start Date	05/06/25
Simulation End Date	06/06/25
Total Simulated Days	2
Total Simulated Time (minutes)	2880
Billing Scheme	Per Session
Per CP rate (CAD)	0.01
TOU Ontario Energy Board Electricity Rates Effective Date	Summer (May to Oct)
Off peak price (cents per kWh)	7.6
Mid-peak price (cents per kWh)	12.2
On-peak price (cents per kWh)	15.8
Total Number of CCNs	2
Total Number of SWCNs	2
Total Number of DWCNs	2
Total Number of LBCNs	2
Per Reservation Time Slot (minutes)	10
Total Number of CAEVs	50
Total Number of LBUAVs	8
Total Number of EIUAVs	6
EVSEs per CCN, SWCN, DWCN, LBCN	10
EVSEs per GVCN	No. of CAEVs
EVSEs per AVCN	No. of LBUAVs
Laser Beam Power (kW)	1
Queue Length (vehicles)	2
CCN Setup	
Per EVSE Voltage (Volts)	240
SWCN Setup	
Per EVSE Voltage (Volts)	240
Per EVSE WCPs	1
Length of WCP (meters)	10
DWCN Setup	
Per EVSE Voltage (Volts)	480
Length of Track (meters)	20,000.00
Per EVSE WCPs	8
Length of a WCP (meters)	120
Width of a WCP (meters)	2.0
Gap Between WCPs (meters)	0.5
Average Vehicle Speed (km/h)	79.92
Total Number of WCPs Installed	160
Length of Track with WCPs Installed (meters)	19,279.5
LBCN Setup	
Per EVSE LB	1
GVCN and AVCN Setup	
Per EVSE LB/WCP	1

4.6.4.4 UAV Initial Placement Strategy

UAV placement, illustrated in Figure 4.2, is defined as part of the simulation setup to establish consistent and controlled initial conditions for evaluating coordinated charging scheduling and trip planning. A simple, deterministic placement strategy is adopted to ensure effective spatial coverage and energy-efficient operation without introducing additional optimization complexity.

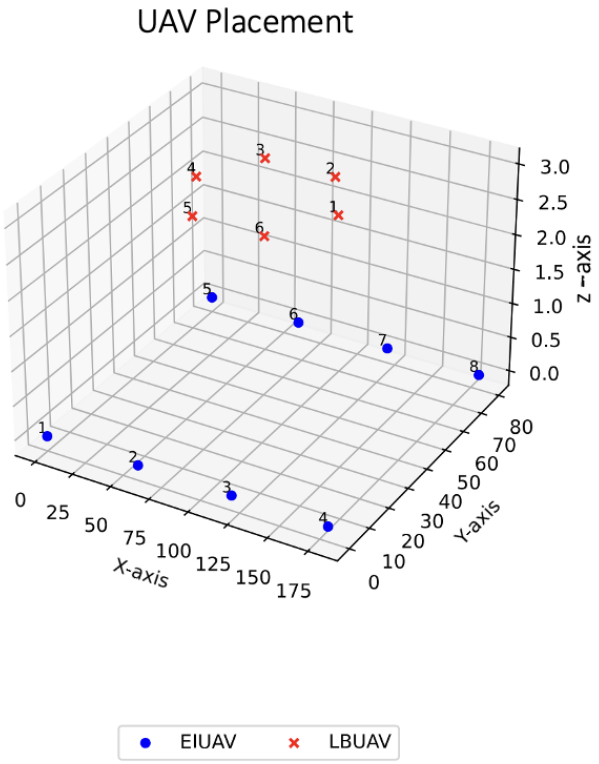

Figure 4.2:Illustrating the placement of the UAVs.

EIUAVs are initially deployed from fixed towers evenly distributed across the road network, providing uniform coverage for monitoring and dynamic support of CAEV operations. This placement minimizes response distance while reducing overlapping coverage and unnecessary energy expenditure. LBUAVs, which possess larger batteries and are capable of wirelessly charging other UAVs, are initially positioned near the center of the operational grid. This centralized placement enables efficient on-demand U2U wireless charging of surrounding EIUAVs and supports extended aerial operation during high-demand periods.

Once the majority of EIUAVs reach a high SoC (e.g., above 95%), LBUAVs relocate toward a central hub location to support subsequent charging cycles. This placement strategy is intentionally simple and repeatable, ensuring that observed performance differences in later sections arise from scheduling decisions rather than from placement optimization effects.

4.6.4.5 Scheduling Algorithms and Training Configuration

The simulation framework supports evaluation of both deterministic heuristic scheduling strategies and learning-based coordination. SH-CSP and DH-CSP operate as interpretable baselines, while SAFE-DDPG is trained using the parameters summarized in Table 4.6.

Table 4.6: Parameter values for SAFE-DDPG.

Parameter	***Value***	***Description***
γ	0.99	Discount factor
τ	0.002	Target network update rate
Actor LR	5×10^{-4}	Actor learning rate
Critic LR	1×10^{-3}	Critic learning rate
Batch	128	Mini-batch size
OU σ_0	0.3	Initial Ornstein–Uhlenbeck noise amplitude
OU σ_{min}	0.05	Minimum OU noise amplitude
OU decay	0.995	OU noise decay rate
PER α	0.5	Prioritization exponent
PER β	$0.4 \rightarrow 1.0$	Annealed importance-sampling weight
PER ε	1×10^{-5}	Small constant to avoid zero probabilities
Local reward β_1–β_4	1.5,1.5,1.5,1.5	Weights for immediate reward terms
Global reward $w_{util}, w_{wait}, w_{idle}, w_{travel}, w_{batt}$	1.0, 0.8, 0.3, 0.3, 0.3	Weights for global reward terms
Heuristic λ_1–λ_5	0.10, 0.20, 0.35, 0.20, 0.15	DH-CSP fallback weights
Network Architecture	4 layers (512–256–128–64)	Actor–critic fully connected network
Regularization and Stability	ELU activation, Batch Normalization, L2 5×10^{-5}, Dropout 0.1	Smooth gradients, prevent overfitting, improve training stability
Output and Constraints	Sigmoid activation, reward normalization, gradient clipping	Bounded actions and stable learning

SAFE-DDPG parameters were selected to balance convergence speed, training stability, and computational efficiency under dynamic charging demand conditions. Learning rates, target network update rate, exploration noise scheduling, and replay buffer settings were refined through preliminary experiments and sensitivity analysis to ensure stable learning, repeatable convergence across runs, and low-variance policies without environment-specific overfitting.

The resulting parameterization is designed to support stable and interpretable learning rather than to claim a unique optimal hyperparameter configuration. In particular, the reward structure is formulated to guide both immediate and long-term scheduling behavior. The local reward shapes short-term decisions by penalizing infeasible, congested, or unnecessarily costly charging actions, while the global reward reinforces longer-term objectives such as utilization balance, reduced waiting, and reduced fallback dependence. In this sense, the reward function does not analytically prescribe the final policy. Instead, the policy is obtained through learning-

based optimization of the cumulative reward, defining the operational trade-offs that the agent learns to balance through interaction with the environment. The resulting convergence and learning behavior are examined later in this chapter through the progression and stabilization of the training reward.

4.6.4.6 Evaluation Protocol and Comparison Methodology

Training of SAFE-DDPG follows **Algorithm 5** [133], with early stopping applied if the average reward fails to improve by more than 0.5 over a window of 300 episodes. Performance evaluation is conducted using common random numbers (CRN) to ensure fair comparison across algorithms.

To account for stochastic variability in arrivals, mobility, and learning dynamics, all reported results are averaged over 50 independent simulation runs. Statistical uncertainty is quantified using 95% confidence intervals (CIs) computed using the Student's t-distribution, which is appropriate for finite-sample simulation studies where the population variance is unknown. For each performance metric, the CI is calculated based on the sample mean and sample variance across replications, providing statistically meaningful uncertainty bounds for simulation-based evaluation.

The CRN design applied ensures that observed differences are attributable to scheduling logic rather than independent stochastic realizations. Larger CI, particularly for average waiting time at individual charging networks, reflect higher variability in congestion dynamics under stochastic arrivals and spatially heterogeneous demand. This effect is more pronounced in heuristic baselines, where rule-based decisions are less adaptive to evolving system conditions. In contrast, SAFE-DDPG generally exhibits tighter confidence intervals due to more stable and responsive learned coordination behavior across runs.

4.7 Experimental Results and Analysis

This section evaluates the coordinated charging scheduling and trip planning methods proposed in this chapter using the simulation framework and performance metrics defined earlier [133]. The analysis proceeds in three stages. First, the behavior of the trained SAFE-DDPG policy is examined through a representative simulation run to illustrate system-level performance and charging execution characteristics. Second, the proposed learning-based approach is compared against the heuristic coordination strategies developed in this chapter to highlight operational trade-offs and performance gains. Finally, SAFE-DDPG is benchmarked against baseline DRL methods to isolate the impact of the proposed feasibility-aware and scheduling-aware enhancements. Throughout this section, the discussion focuses on metrics directly aligned with the objectives of this chapter, namely delay reduction, charging

utilization, and effective coordination under dynamic demand. The results should therefore be interpreted as a performance-based evaluation of online coordinated scheduling under dynamic operating conditions, highlighting how different decision mechanisms influence delay, utilization, and coordination efficiency.

To contextualize the comparative evaluation presented in this section, the literature discussed in Chapter 2 includes studies on EV charging routing, reservation-based charging coordination, and DRL-based scheduling under dynamic traffic or charging demand. However, existing studies typically consider only ground EVs, only UAVs, or a single charging modality, and generally do not address coordinated reservation and trip planning across heterogeneous charging networks that jointly include CAEVs and UAVs across static, dynamic, and aerial charging modalities. This gap, established through the comparative literature analysis in Chapter 2, motivates the problem formulation adopted here. A direct comparison with prior methods is therefore not feasible. In practice, applying an existing algorithm from the literature to the present problem would require substantial modification to account for heterogeneous vehicle classes, cross-network reservation logic, dynamic arrival handling, and charging feasibility constraints, at which point it would no longer represent the original method under its published assumptions. For this reason, the comparative evaluation in this chapter is structured around interpretable heuristic baselines developed under the same system assumptions and baseline DRL methods implemented within the same environment. This approach provides a fair and scientifically controlled basis for comparison.

4.7.1 SAFE-DDPG Training Behavior

Training behavior of SAFE-DDPG is examined to assess convergence and learning stability prior to evaluating scheduling performance. Training was carried out using **Algorithm 5** [133] with the parameters specified in Table 4.6, and convergence was monitored through the evolution of the average episode reward.

As illustrated in Figure 4.3, the average training reward increases steadily during the early stages of training and stabilizes after convergence, with the reward converging to a value of approximately 750. The stabilization of the reward curve, together with the reduced variance observed in later episodes, indicates that the agent learns a consistent scheduling policy under dynamic arrival and charging demand conditions. This behavior suggests that SAFE-DDPG is able to effectively capture the interaction between charging availability, routing decisions, and system load when making coordinated charging scheduling decisions.

The converged policy obtained from this training process is used in the subsequent experiments. The following sections first illustrate system-level behavior through a

representative simulation run under the trained SAFE-DDPG policy and then present comparative performance results against the heuristic and baseline learning-based scheduling approaches developed in this chapter.

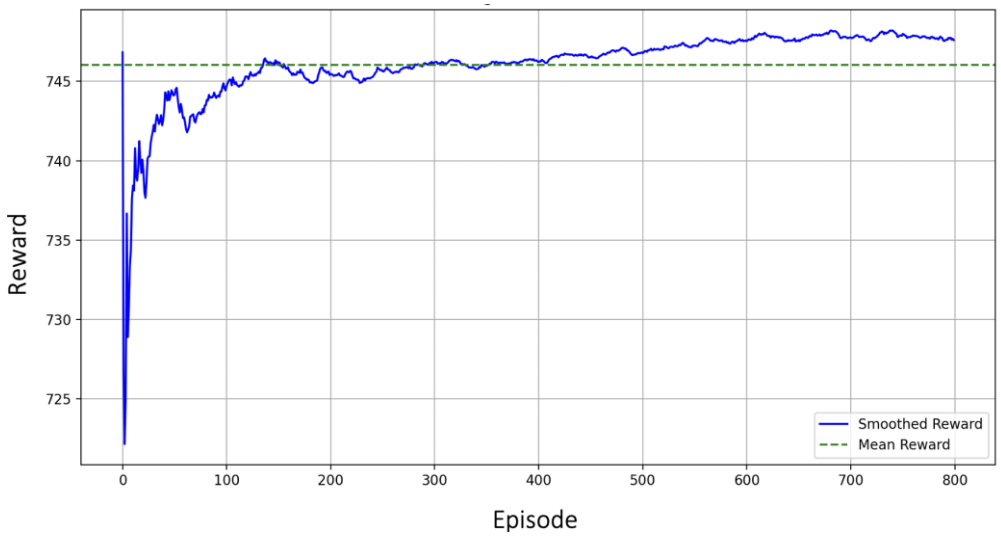

Figure 4.3:Training reward progression for SAFE-DDPG.

4.7.2 Single Run Performance of SAFE-DDPG

This section presents a representative single simulation run to illustrate how the proposed SAFE-DDPG–based coordinated charging scheduler operates under the simulation parameters defined earlier in this chapter. The analysis focuses on operational scheduling behavior and objective performance metrics, demonstrating how the learning-based scheduler translates coordination decisions into executable charging outcomes.

In this representative run, 50 CAEVs issue charging requests along their shortest routes, which are assigned to available charging nodes according to the coordinated scheduling policy developed in this chapter and executed using the previously defined system execution framework. The results reported in Tables 4.7–4.9 correspond to a single run using the converged SAFE-DDPG policy. All time-related metrics are reported in minutes, energy values in kilowatt-hours (kWh), and payments in Canadian dollars (CAD).

Tables 4.7–4.9 summarize the primary objective metrics used in this chapter to evaluate coordinated charging scheduling performance.

Table 4.7: CN Summary.

Network Summary					
Metric	**Value**	***Metric***	**Value**	***Metric***	**Value**
Total CNs	10	***Total EVSEs***	138	***Total AEV requests***	127
Delivered CCN Energy (kWh)	736.32	***Delivered SWCN Energy (kWh)***	776.9	***Delivered DWCN Energy (kWh)***	216.6
Delivered LBCN Energy (kWh)	379.26	***Delivered AVCN Energy (kWh)***	124.5	***Delivered GVCN Energy (kWh)***	84.71

Table 4.8: Per-CN statistics from a single SAFE-DDPG simulation run.

Per CN STAT									
CN	**Vehicles Serviced**	**Avg Wait Time (min)**	**Throughput of CN**	**Avg Service Time (min)**	**Avg System Wait Time (min)**	**Computed Little's Law**	**Calculated Little's Law**	**Utilization of EVSE**	**Idle Proportion**
CCN_1	11 AEV	0	0.0136	172.64	172.64	2.344	2.344	0.234	0.766
CCN_2	15 AEV	0	0.0181	140.33	140.33	2.536	2.536	0.254	0.746
SWCN_1	10 AEV	0.4	0.011	156	156.4	1.738	1.738	0.173	0.826
SWCN_2	13 AEV	0	0.016	208.77	208.77	3.479	3.479	0.348	0.652
DWCN_1	12 AEV	-	0.0211	19	19	0.4	0.4	0.04	0.96
DWCN_2	10 AEV	-	0.0217	19	19	0.413	0.413	0.041	0.959
LBCN_1	12 UAV	0.167	0.016	335.5	335.667	5.371	5.371	0.537	0.463
LBCN_2	2 UAV	0.5	0.00263	321.5	322	0.847	0.847	0.085	0.915
GVCN_1	17 AEV	0.177	0.0279	69	69.18	1.928	1.928	0.078	0.922
AVCN_1	25 AEV / 14 UAV / 11 CAEV	0.72 / 1.286 / 0	0.0424	68.73	69.16	2.931	2.931	0.363	0.638

Table 4.9: Summary of overall statistics from a single SAFE-DDPG simulation run.

Overall STATs					
Metric	**Value**	***Metric***	**Value**	***Metric***	**Value**
Avg CAEV Battery Consumed (kWh)	3.498	***Avg CAEV Travel Time (min)***	31.16	***Avg CAEV Payment per trip (CAD)***	3.823
Avg UAV Battery Consumed (kWh)	5.63	***Avg UAV Travel Distance (m)***	1976.65	***Avg UAV Payment per trip (CAD)***	2.89

The SAFE-DDPG algorithm allocates charging requests across static and dynamic CN types based on learned scheduling priorities, resulting in balanced utilization of heterogeneous charging resources. Among static CNs, SWCNs receive slightly higher assignment frequency than CCNs, reflecting a scheduling preference that promotes wireless charging where available and supports contactless energy transfer envisioned for future 6G-ITS environments. For dynamic CNs, DWCNs are selected more frequently than GVCNs and AVCNs, consistent with their higher incremental charging capacity and lower congestion risk. AVCNs are assigned lower priority due to their reliance on UAV resources, enabling the scheduler to limit UAV involvement for smaller or deferrable charging demands. For each request, SAFE-DDPG jointly determines the charging location and energy allocation, producing coordinated

scheduling decisions that distribute load across CN types while respecting infrastructure constraints. UAV charging operations are handled separately using DH-CSP, ensuring predictable UAV energy replenishment without interfering with CAEV scheduling.

CAEVs follow their assigned charging schedules while traversing shortest paths between origins, charging locations, and destinations, resulting in low observed wait times and controlled travel durations. The recorded metrics show that scheduled charging stops do not introduce excessive detours or delays, indicating that charging assignments are well aligned with trip-level objectives. By enabling efficient and coordinated charging of electric vehicles, the observed scheduling supports broader sustainability goals by facilitating practical EV adoption and contributing to reduced greenhouse gas emissions in future 6G-ITS. The resulting throughput, utilization, and idle proportions across CNs demonstrate that SAFE-DDPG maintains balanced service levels while preventing localized congestion, highlighting its effectiveness in translating scheduling decisions into efficient system operation.

SAFE-DDPG effectively distributes charging demand across heterogeneous CNs, achieving balanced utilization of resources while minimizing travel distances, wait times, system delays, and user payments. Static CNs, including CCNs and SWCNs, each employ 10 EVSEs, enabling parallel service for multiple vehicles. For example, CCN_1 and CCN_2 served 11 and 15 AEVs with zero wait times and moderate per-EVSE utilization of 0.234–0.254, while SWCN_1 and SWCN_2 handled 10 and 13 AEVs with slightly higher wait times of 0–0.4 minutes and utilization per EVSE of 0.173–0.348. LBCNs, though static, are scheduled via DH-CSP and serviced 12 and 2 UAVs with utilization per EVSE of 0.537 and 0.085, illustrating how parallel service and heterogeneous scheduling maintain controlled and balanced utilization. Overall, throughput, idle proportions, and Little's Law values align closely, confirming consistency between measured system occupancy and expected behavior.

Dynamic CNs, including DWCNs, GVCNs, and AVCNs, are handled according to their incremental or proximity-constrained service models. DWCN_1 and DWCN_2 are implemented as single charging lanes with 10 EVSEs each. Thus, multiplying the per-EVSE utilization (0.04–0.041) by the 10 EVSEs results in total lane utilization around 0.4, which reflects controlled allocation of resources by SAFE-DDPG while preventing congestion. GVCN_1 and AVCN_1, with maximum server capacities of 25 and 8 respectively, serve vehicles based on spatial proximity, resulting in slightly higher wait times (0.72–1.286 min) and throughput rates of 0.021–0.042 per CN. These metrics show that SAFE-DDPG dynamically balances load, encourages efficient use of dynamic resources, and maintains balanced service levels across CN types.

The close agreement between computed and calculated Little's Law values across CNs serves as an internal consistency check for the scheduling-induced throughput and occupancy measurements. Static CNs like CCNs and SWCNs show high consistency between measured and expected system behavior, while dynamic CNs reflect realistic variations in service times and utilization. Overall, throughput, utilization, and idle proportion values indicate that SAFE-DDPG evenly distributes load: static CNs achieve moderate utilization (0.173–0.348), dynamic CNs maintain lower utilization (0.04–0.363) to prevent congestion, and LBCNs scheduled via DH-CSP show that UAV resources are effectively integrated.

The computed JFI using vehicles served for static CN types for CAEV is 0.976, and for dynamic CN types for CAEV is 0.956. The overall fairness of CAEV allocation can also be evaluated using throughput values instead of raw vehicle counts. Using per-CN throughput, the computed JFI for the system is 0.8, indicating that SAFE-DDPG distributes charging service efficiently and relatively equitably across heterogeneous CNs while accounting for differences in service rates and active server capacities. Therefore, the calculated indices indicate relatively uniform service distribution under this representative run, reflecting balanced load distribution even under heterogeneous static and dynamic CN conditions. This post hoc evaluation complements throughput, utilization, and Little's Law metrics, providing additional confirmation that the algorithm maintains both efficiency and fairness in assigning charging resources. These fairness values are reported here for completeness and qualitative insight. A detailed fairness and reliability analysis across multiple runs is presented in the following chapter.

At the system level, the coordinated scheduling decisions of SAFE-DDPG result in effective energy distribution and controlled operational costs across heterogeneous CNs. CCNs delivered 736.32 kWh, SWCNs 776.9 kWh, DWCNs 216.6 kWh, LBCNs 379.26 kWh, AVCNs 124.5 kWh, and GVCNs 84.71 kWh, servicing a total of 127 AEV requests across 10 CNs and 138 EVSEs. Average CAEV battery consumption was 3.498 kWh (Figure 4.4), with average travel times of 31.16 minutes (Figure 4.5) and per-trip payments of 3.823 CAD (Figure 4.6). UAVs consumed 5.63 kWh on average, traveled 1,976.65 m per trip (Figure 4.7), and incurred 2.89 CAD per trip (Figure 4.8). In each figure, the metric for individual vehicles or vehicle IDs is shown, with a dotted line indicating the system-wide average. It should be noted that CAEV IDs start with the prefix 1, LBUAV IDs with 2, and EIUAV IDs with 3.

Overall, these results illustrate how SAFE-DDPG produces balanced load distribution, optimized energy usage, and efficient service, highlighting its effectiveness across

heterogeneous CNs and demonstrating that coordinated scheduling decisions translate into effective charge delivery under the adopted execution model.

Figures 4.4–4.8 visualize per-vehicle outcomes resulting from the coordinated scheduling decisions analyzed in this section.

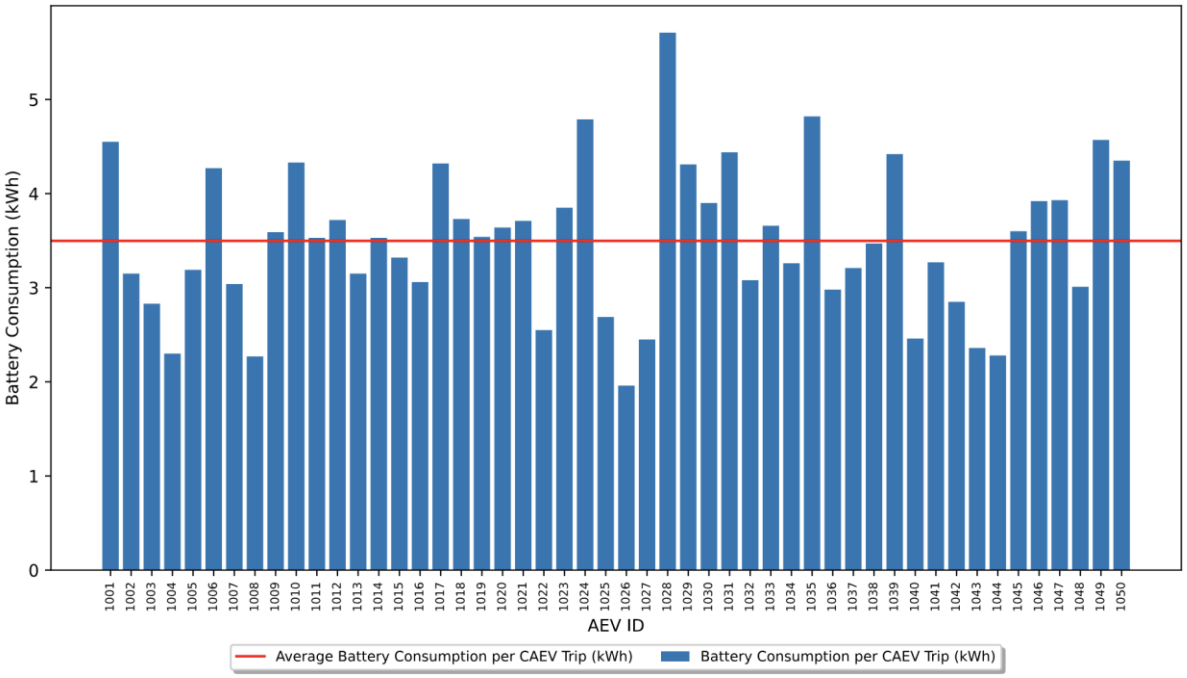

Figure 4.4: Battery Consumption in kWh per CAEV.

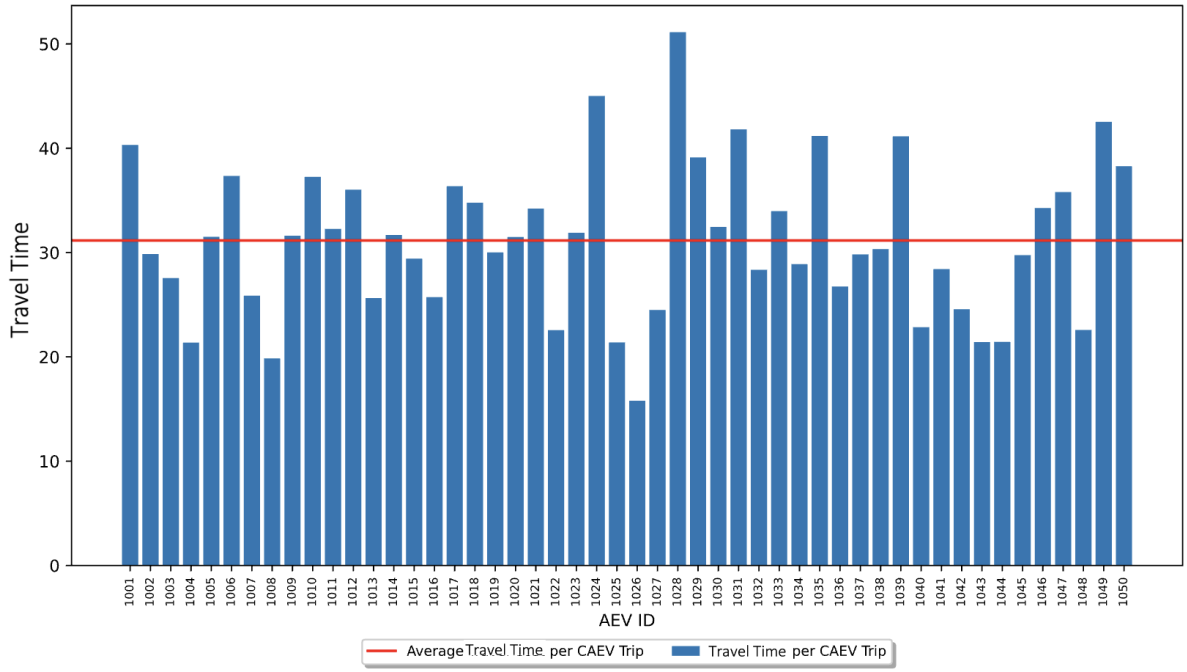

Figure 4.5: Travel Time in minutes per CAEV.

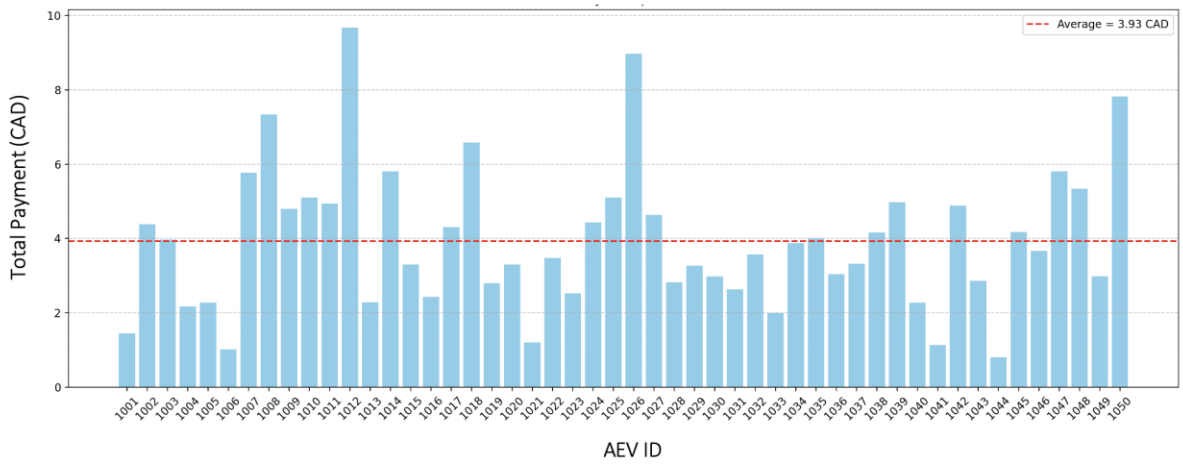

Figure 4.6: Reservation Payment in CAD per CAEV.

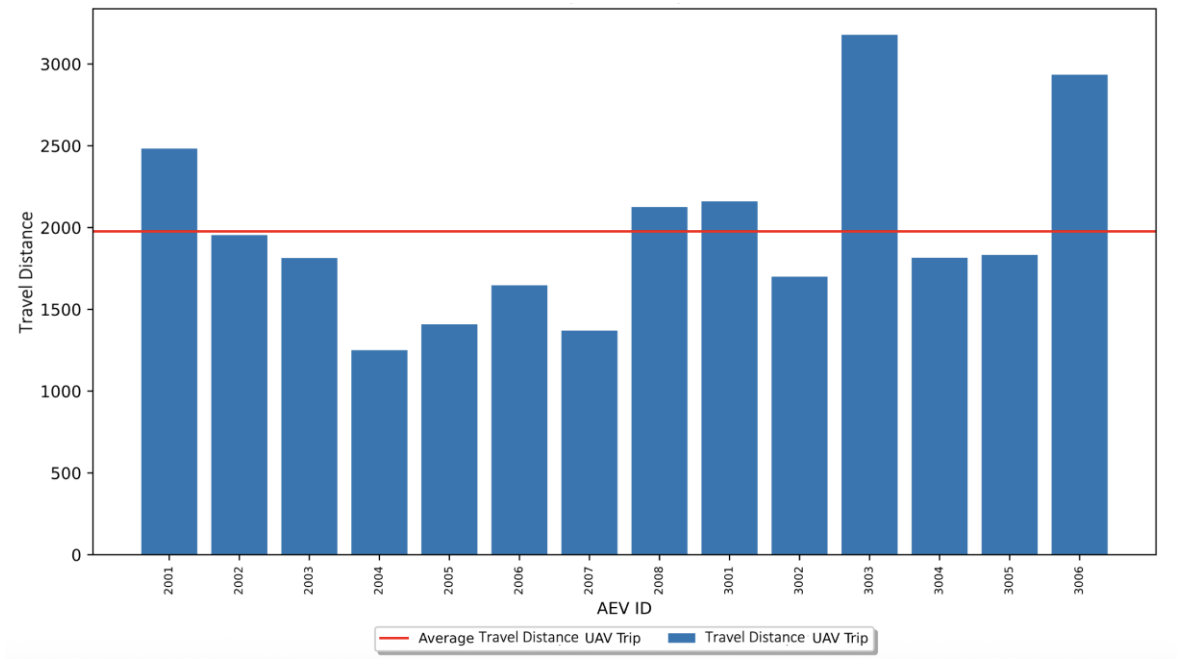

Figure 4.7: Travel Distance in meters per UAV.

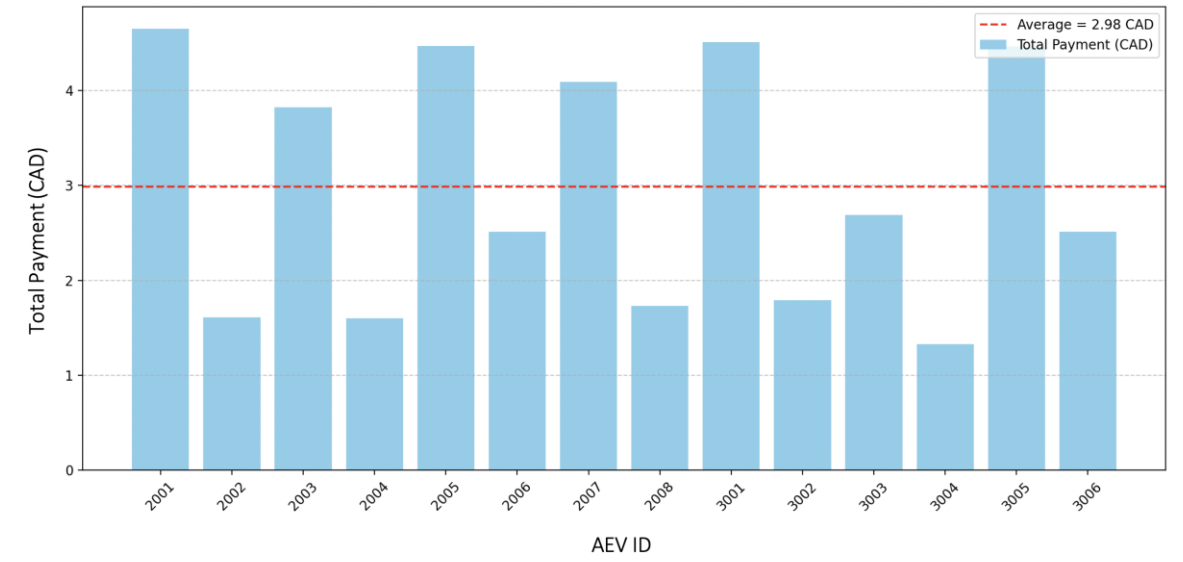

Figure 4.8: Reservation Payment per UAV.

The charging efficiency of the proposed system is illustrated using aggregated data from a representative simulation run of SAFE-DDPG, covering the entire charging infrastructure in the environment. Figure 4.9 presents results for the 50 CAEVs, where the first subplot shows the total charging requested through the reservation system (Requested Charge), the amount promised by the system (Reserved Charge), and the amount actually delivered (Delivered Charge). These quantities are aggregated over all charging systems in the simulation and shown as scatter plots to highlight their close correspondence. The second subplot depicts the absolute differences between Requested and Reserved, and between Reserved and Delivered, making visible the minimal gap between these values. With the previously validated misalignment mitigation mechanism enabled, the system achieves an overall charging efficiency of approximately **98.7%,** meaning nearly all promised energy is successfully delivered. Small discrepancies arise primarily from vehicle misalignment during charging, late arrivals, or unexpected interruptions such as early termination.

A similar analysis is conducted for UAVs, with results shown in Figure 4.10 for the 6 LBUAVs and 8 EIUAVs. Again, the misalignment mitigation algorithm ensures charging is performed under optimal alignment conditions, leading to a high efficiency of approximately **98.52%.** The algorithm prioritizes delivering charge such that the majority of user-requested and system-promised energy is fulfilled. The close agreement between requested, reserved, and delivered charge in both CAEV and UAV cases demonstrates the robustness of the charging coordination mechanism across the heterogeneous systems modeled.

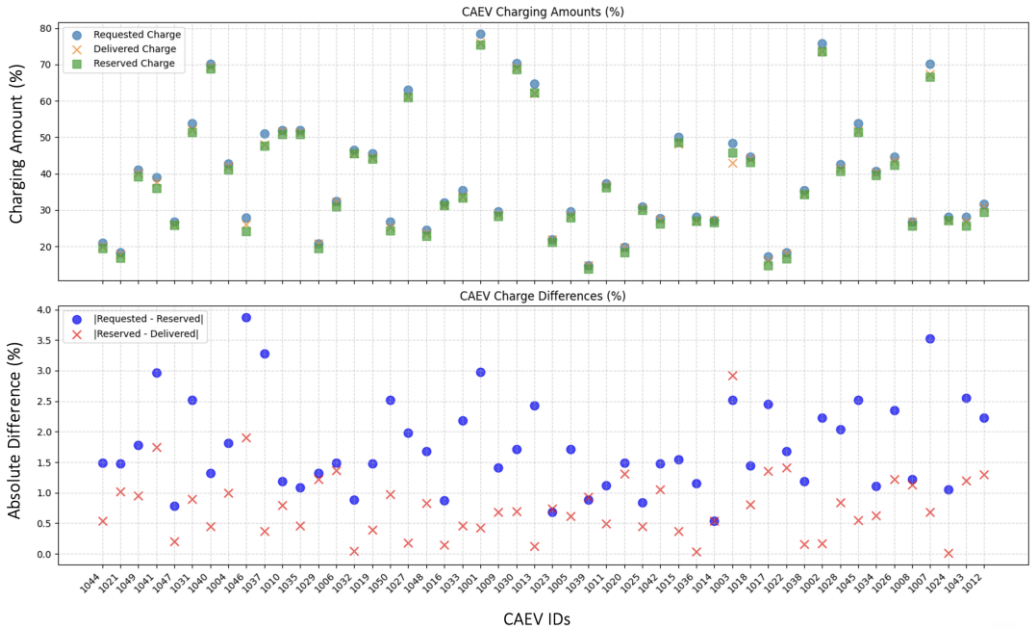

Figure 4.9: Charging performance for 50 CAEVs under SAFE-DDPG, showing requested, reserved, and delivered charge (in %) and corresponding absolute differences.

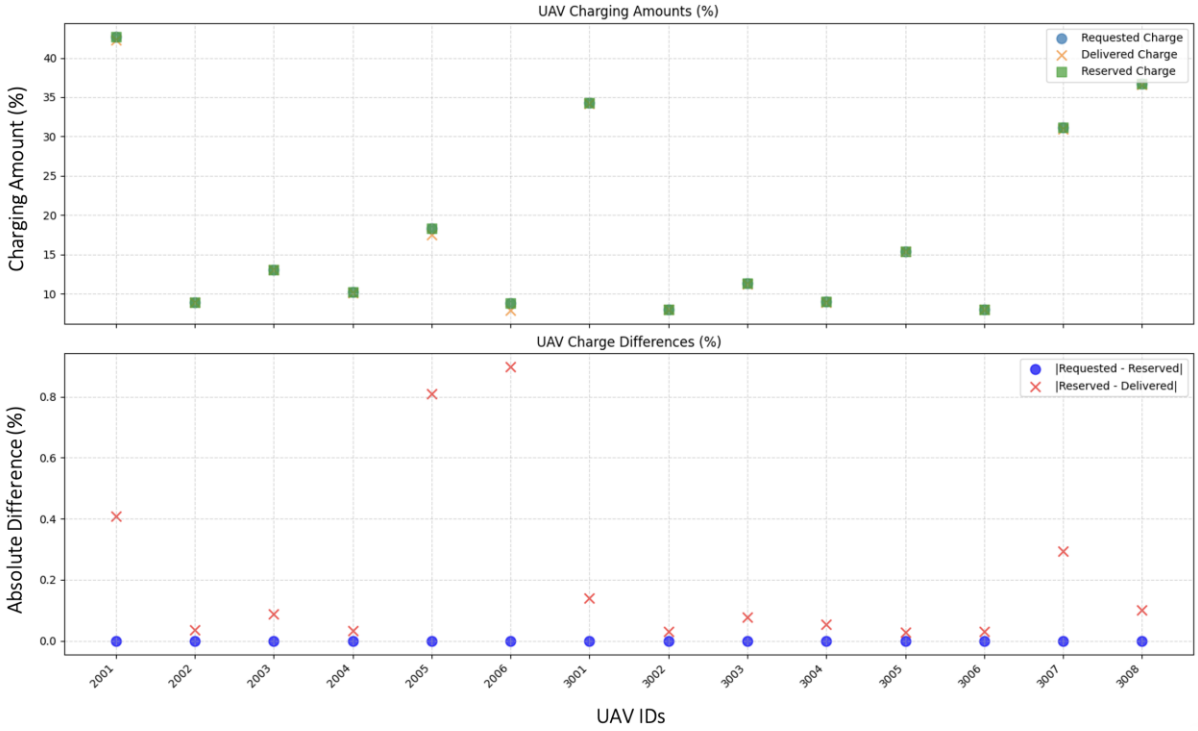

Figure 4.10: Charging performance for 6 LBUAVs and 8 EIUAVs under SAFE-DDPG, showing requested, reserved, and delivered charge (in %) and corresponding absolute differences.

This single-run analysis highlights the operational patterns produced by SAFE-DDPG, illustrating how coordinated scheduling decisions translate into effective charge delivery, controlled delays, and balanced infrastructure utilization across heterogeneous CNs. The observed outcomes include low wait times, short travel times for CAEVs, modest per-trip payments, and near-complete delivery of reserved energy, indicating high charging efficiency under the adopted execution model. These results are presented to provide system-level insight rather than definitive performance claims. The following section builds on these observations by comparing SAFE-DDPG against DH-CSP and SH-CSP to quantitatively assess its relative scheduling performance.

4.7.3 Comparison of Proposed Algorithms: SAFE-DDPG versus DH-CSP and SH-CSP

This section presents a comprehensive comparison of the proposed SAFE-DDPG algorithm against two baseline strategies: SH-CSP, which employs fixed scheduling without accounting for dynamic vehicle arrivals, and DH-CSP, which incorporates dynamic arrivals but does not leverage reinforcement learning. The section is organized into two subsections. The first subsection, *Overview of Improvements*, summarizes the key performance gains of SAFE-DDPG in terms of average wait times and operational efficiency, along with observed trade-offs in travel cost, battery consumption, and payment. Fairness-related metrics are reported here for completeness and are examined in detail in the following chapter. The second

subsection, *Performance Analysis of CNs*, provides a detailed evaluation of SAFE-DDPG's performance across heterogeneous CN types, including both static and dynamic CNs, highlighting throughput, queue lengths, server utilization, idle times, and system wait times. Figures 4.11 to 4.15 are referenced throughout to illustrate comparative scheduling performance across different CN configurations.

4.7.3.1 Overview of Improvements

The proposed SAFE-DDPG algorithm demonstrates substantial improvements over the DH-CSP and SH-CSP baseline strategies across all CN types. As shown in Figures 4.11 and 4.12, average wait times are significantly reduced. To ensure clarity, all reported percentage improvements in this section are computed relative to the specified baseline method for each comparison. Absolute metric values are provided alongside percentage changes to avoid ambiguity in interpretation. The percentage improvement is calculated as:

$$\%\text{Improvement} = \frac{\text{Baseline Value} - \text{SAFE-DDPG Value}}{\text{Baseline Value}} \times 100 \tag{4.75}$$

All CIs are computed using a symmetric t-distribution under a CRN experimental design, as mentioned earlier. The CRN approach aligns arrival realizations across algorithms, leading to reduced variance and approximately symmetric sampling distributions for the evaluated performance metrics. As a result, CIs for metrics with near-zero mean values, such as wait time in lightly loaded scenarios, may occasionally extend slightly below zero. These bounds reflect statistical symmetry around very small sample means rather than infeasible system behavior and are observed primarily in cases where zero wait time occurs in some independent runs.

Using (4.75), the wait times for CCN_2 are reduced by 70.3% and 86.8%, CCN_1 by 51.3% and 76.7%, SWCN_2 by 61.3% and 78.1%, SWCN_1 by 67.3% and 83.0%, AVCN_1 by 52.0% and 58.9%, and GVCN_1 by 34.2% and 69.3%, compared to DH-CSP and SH-CSP, respectively.

In addition to faster service, SAFE-DDPG exhibits improved fairness characteristics in resource utilization, with a JFI of 0.985 for static CNs (79.5–79.8% improvement), 0.784 for dynamic CNs (16.8–17.1% improvement), and 0.800 overall (29.7–29.8% improvement), consistently outperforming the baseline strategies under the evaluated scenarios. These improvements in wait times and fairness are summarized in Table 4.10, highlighting SAFE-DDPG's ability to reduce delays while promoting equitable resource allocation. Table 4.11 further shows that, although the average travel cost (31.45 CAD) and battery consumption (3.56 kWh) are slightly higher than those under DH-CSP and SH-CSP, these modest trade-offs

are justified by the substantial reductions in wait times and improved fairness. The differences in travel cost and time are small because all algorithms rely on the same routing mechanism, resulting in near-identical path optimality across strategies. Overall, these results highlight SAFE-DDPG's ability to balance efficiency and resource utilization, with fairness-related metrics reported here and examined in detail in the next chapter.

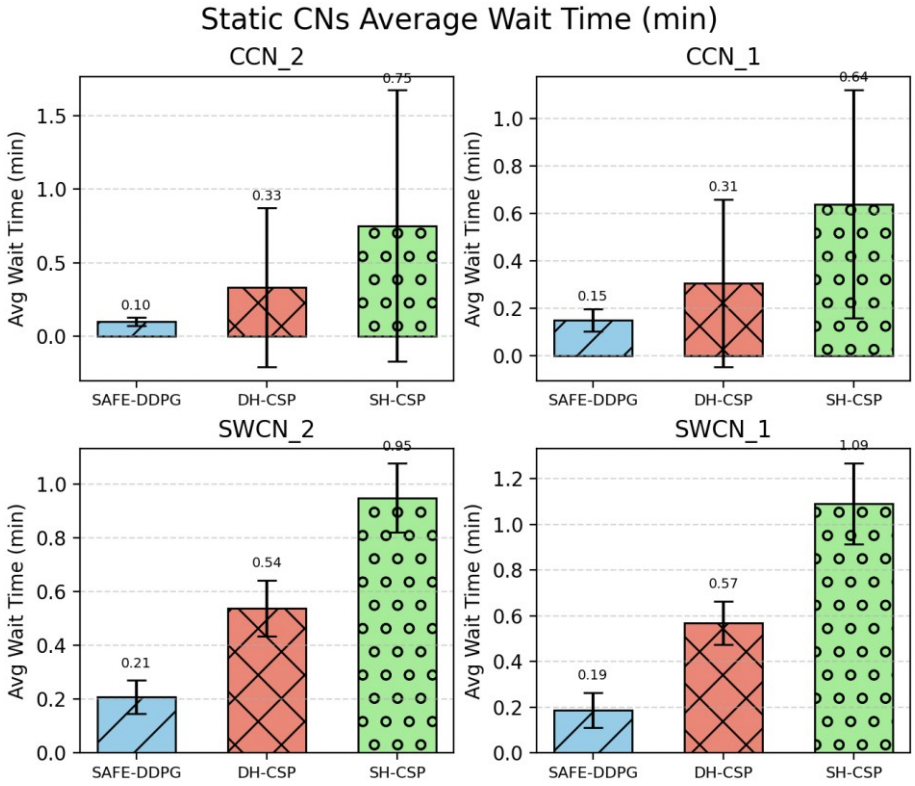

Figure 4.11: Average wait times (min) for static CNs under SAFE-DDPG, DH-CSP, and SH-CSP.

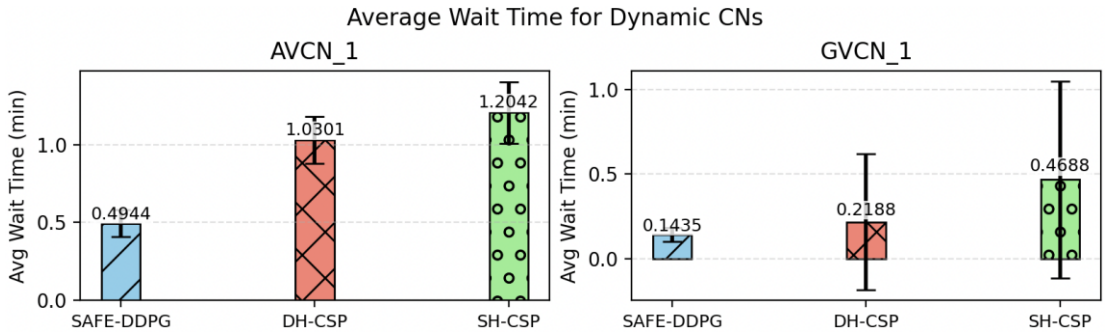

Figure 4.12: Average wait times for dynamic CN types under SAFE-DDPG, DH-CSP, and SH-CSP.

Table 4.10: Comparison of SAFE-DDPG, DH-CSP, and SH-CSP Performance Across CN Types: Average Wait Times and Fairness Indices.

CN Type	Metric	SAFE-DDPG	DH-CSP	Improvement vs DH-CSP (%)	SH-CSP	Improvement vs SH-CSP (%)
CCN_2	**Avg Wait Time (min)**	*0.099*	0.333	**70.30%**	0.75	**86.80%**
CCN_1	**Avg Wait Time (min)**	*0.149*	0.306	**51.30%**	0.639	**76.70%**
SWCN_2	**Avg Wait Time (min)**	*0.208*	0.538	**61.30%**	0.948	**78.10%**
SWCN_1	**Avg Wait Time (min)**	*0.186*	0.569	**67.30%**	1.091	**83.00%**
AVCN_1	**Avg Wait Time (min)**	*0.494*	1.03	**52.00%**	1.204	**58.90%**
GVCN_1	**Avg Wait Time (min)**	*0.144*	0.219	**34.20%**	0.469	**69.30%**
Static CNs	**JFI**	*0.9853*	0.5488	**79.50%**	0.5476	**79.80%**
Dynamic CNs	**JFI**	*0.7839*	0.6695	**17.10%**	0.6714	**16.80%**
Overall	**JFI**	*0.8002*	0.6166	**29.80%**	0.6171	**29.70%**

Table 4.11: Performance Trade-offs of SAFE-DDPG Compared to CSP Baselines.

Metric	SAFE-DDPG vs DH-CSP	SAFE-DDPG vs SH-CSP	Note
Avg Travel Time (CAD)	+1.32	+1.47	Slightly higher travel cost, offset by overall fairness & wait times
Avg Battery Consumed (kWh)	+0.12	+0.13	Slightly higher energy use, acceptable trade-off
Avg Payment (CAD)	+0.29	+0.30	Slightly higher payment, justified by faster service

4.7.3.2 Performance Analysis per CN

SAFE-DDPG shows markedly improved performance across static CNs, as illustrated in Figure 4.13. For CCN_2 and CCN_1, throughput is significantly higher (0.0181 and 0.0138 vs. ~0.0027–0.0028), with correspondingly higher server utilization (0.316 and 0.247) and moderate queue lengths (3.16 and 2.47), reflecting effective load balancing under heavier traffic. SWCN_2 and SWCN_1 also benefit from SAFE-DDPG's allocation strategy, achieving relatively high throughput (0.0164 and 0.0136) with manageable queues (~2.78 and 2.34) and well-utilized servers (0.278 and 0.234), while maintaining lower idle times (~0.72–0.77) than DH-CSP and SH-CSP. System wait times remain competitive (169–180 min), and service times closely track these values, indicating consistent processing without bottlenecks. Overall, SAFE-DDPG optimally leverages static CN capacity to maintain steady flow, moderate queues, and effective service.

For DWCNs (Figure 4.14), each CN has 10 servers or EVSEs, and the measured per-server utilization of 0.041 translates to ~0.4 per CN, which is reasonable for a lane structure with essentially no queues. SAFE-DDPG reflects low vehicles in system, and high throughput without overloading these lanes, prioritizing critical CNs while avoiding unnecessary allocation to DWCN, thus maintaining system efficiency across heterogeneous CNs.

SAFE-DDPG also excels in specialized CNs. In GVCN_1 (Figure 4.15), throughput improves dramatically (0.02787 vs. 0.00345–0.00365) while maintaining low queues (1.92) and similar wait times (~68.8 min), with better server utilization (0.078). For AVCN_1 (Figure 4.16), throughput is higher (0.0424 vs. 0.0370) with moderate queue lengths (2.93), slightly lower wait times (~69.1 min), higher server utilization (0.364), and lower idle times (0.636), reflecting balanced load management. Across these specialized and static CNs, SAFE-DDPG consistently outperforms DH-CSP and SH-CSP, achieving higher throughput, better utilization and fairness in resource allocation, and lower idle times while maintaining stable system performance with lower wait times.

It should be noted that SAFE-DDPG directly schedules CAEV charging decisions while accounting for the interactions of UAVs, particularly at AVCNs where LBUAVs enable charging for both CAEVs and UAVs. Consequently, the DH-CSP scheduling mechanism is applied for LBCNs. As shown in Figure 4.17, the performance of SAFE-DDPG for LBCNs is very close to that of DH-CSP. By considering UAV interactions in CAEV charging, SAFE-DDPG indirectly helps reduce delays and improves overall system efficiency. Throughput, system wait times, queue lengths, server utilization, and idle times remain effectively the same as DH-CSP, while both approaches outperform SH-CSP, which lacks dynamic arrival handling. This highlights the importance of accounting for multiple vehicle types in charging interactions, demonstrating that ignoring such interactions can reduce the effectiveness of scheduling strategies.

Figure 4.18 shows that while SAFE-DDPG slightly increases overall CAEV travel cost and vehicles in the system compared to DH-CSP, these trade-offs are justified by the significant reductions in wait times and improved fairness for CAEVs. UAV metrics remain nearly identical across all strategies because UAVs are not directly scheduled by SAFE-DDPG and all approaches use the same A* with 3D extension routing algorithm. This demonstrates that the SAFE-DDPG trade-off effectively prioritizes CAEV performance without negatively impacting UAV operations.

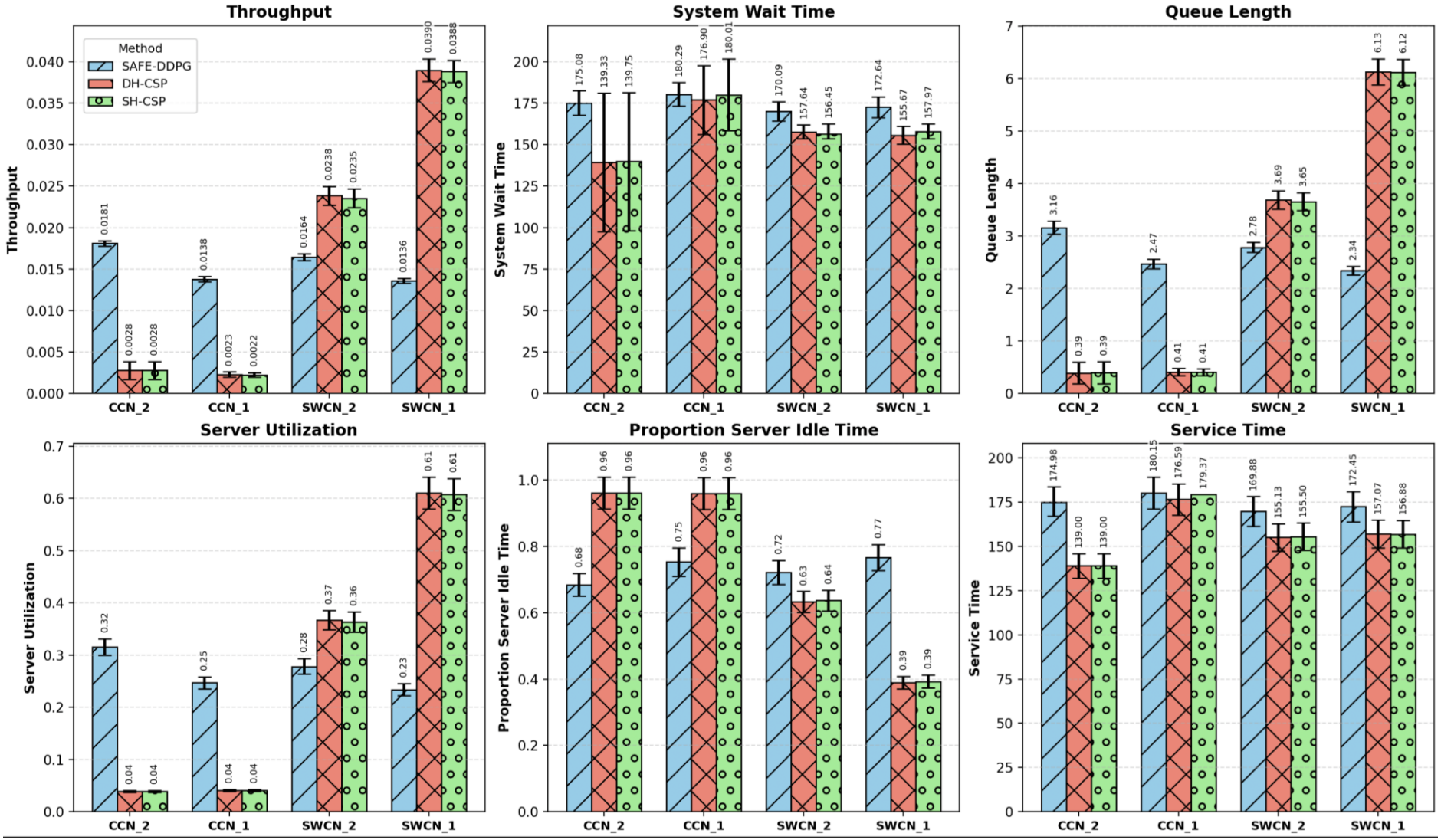

Figure 4.13: Throughput, system wait time, queue length, server utilization per EVSE, and proportion of server idle time across static CN types under SAFE-DDPG, DH-CSP, and SH-CSP.

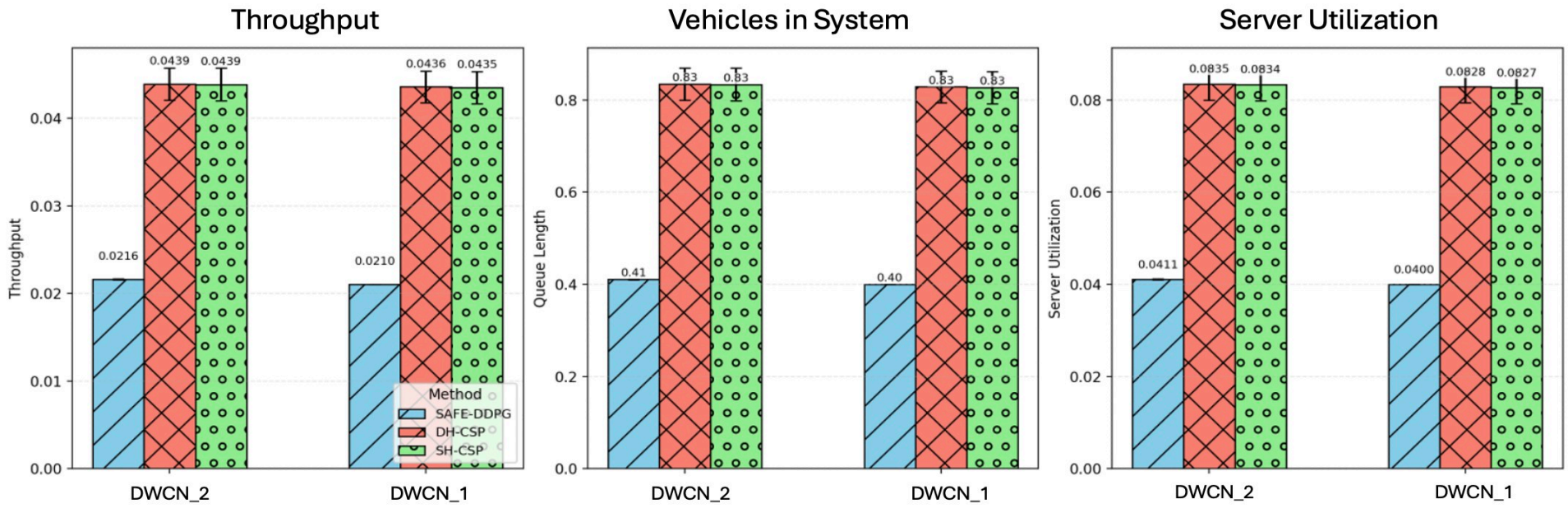

Figure 4.14:Throughput, average vehicles in system and server utilization for DWCNs under SAFE-DDPG, DH-CSP, and SH-CSP.

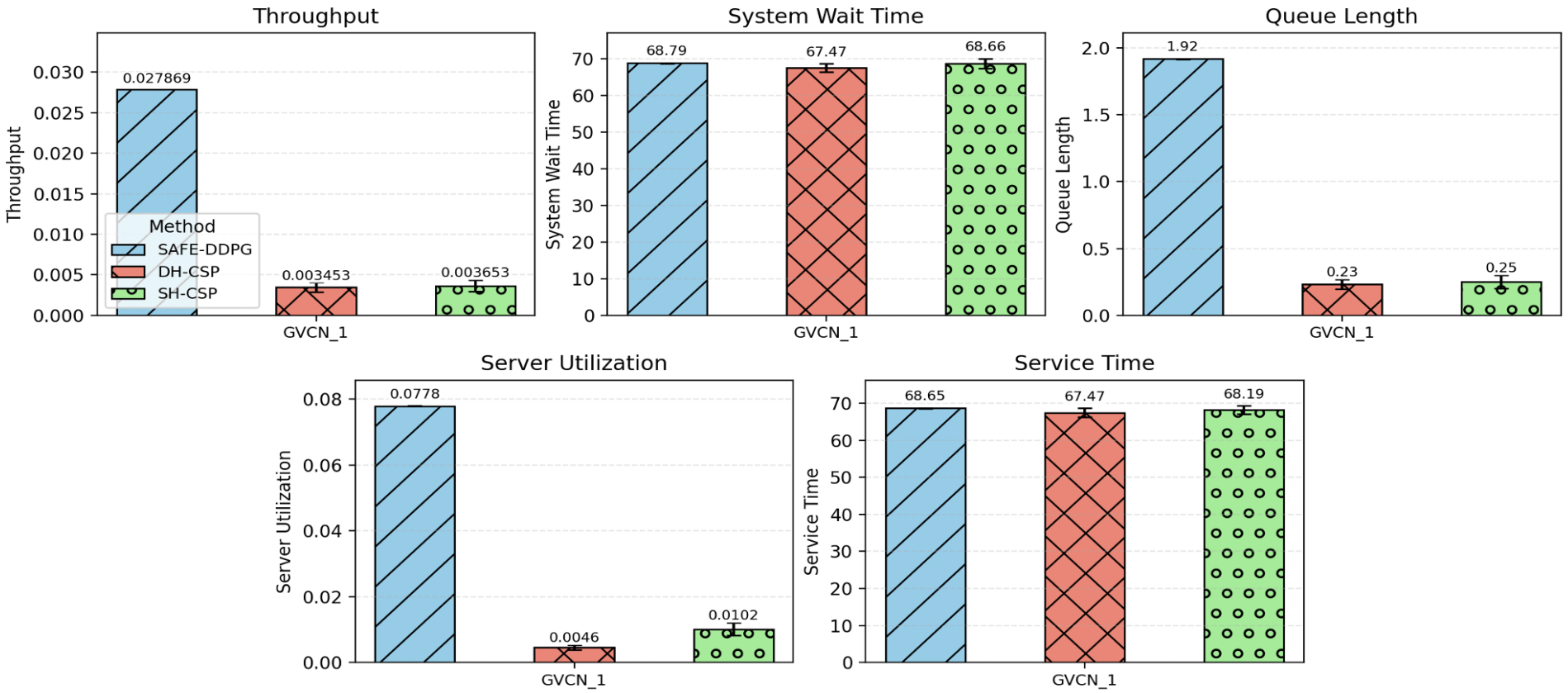

Figure 4.15:Throughput, system wait time, queue length, server utilization for DWCNs under SAFE-DDPG, DH-CSP, and SH-CSP.

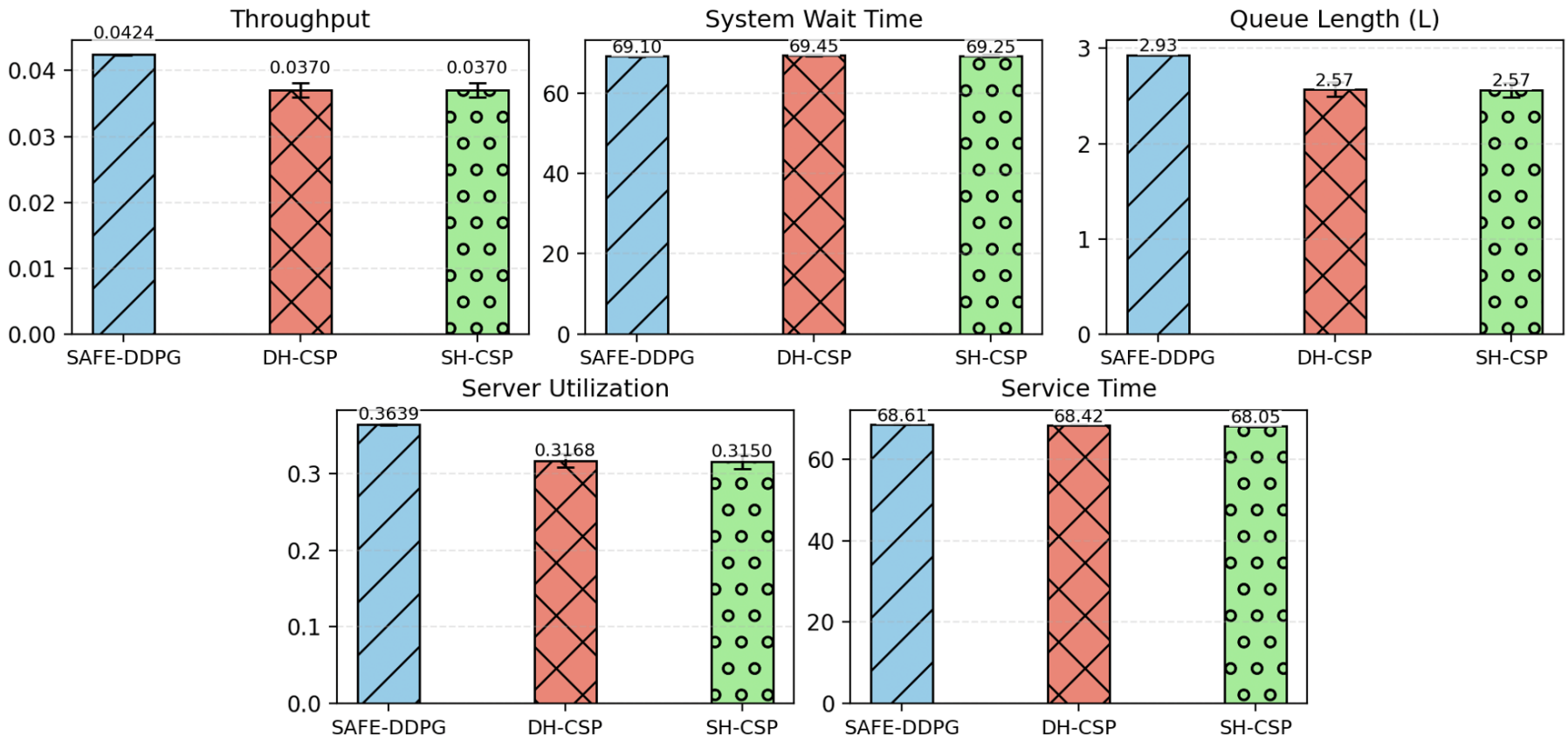

Figure 4.16: Throughput, system wait time, queue length, server utilization and service time for AVCNs under SAFE-DDPG, DH-CSP, and SH-CSP.

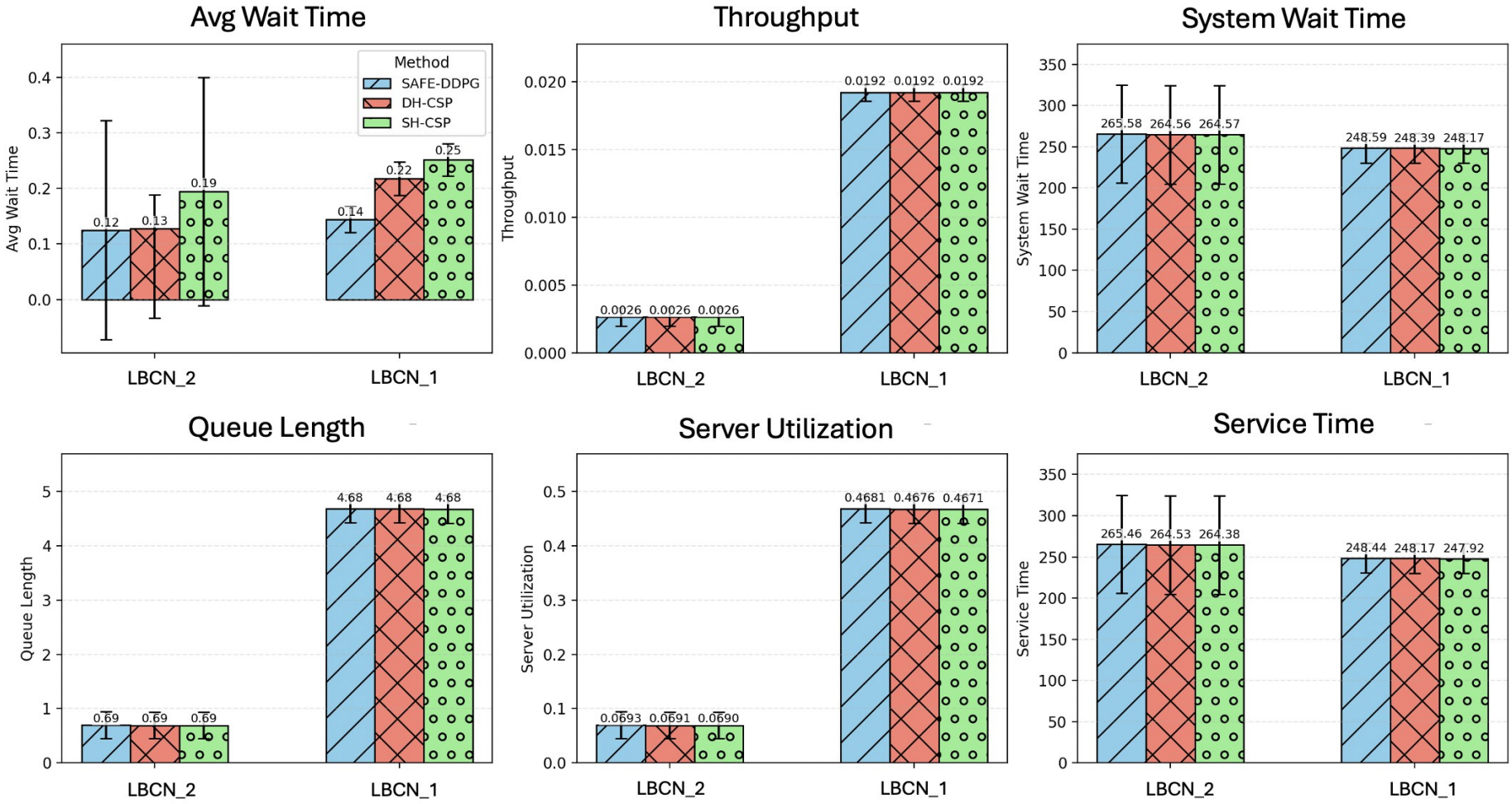

Figure 4.17: Average wait time, throughput, system wait time, queue length, server utilization and service time for LBCNs under SAFE-DDPG, DH-CSP, and SH-CSP.

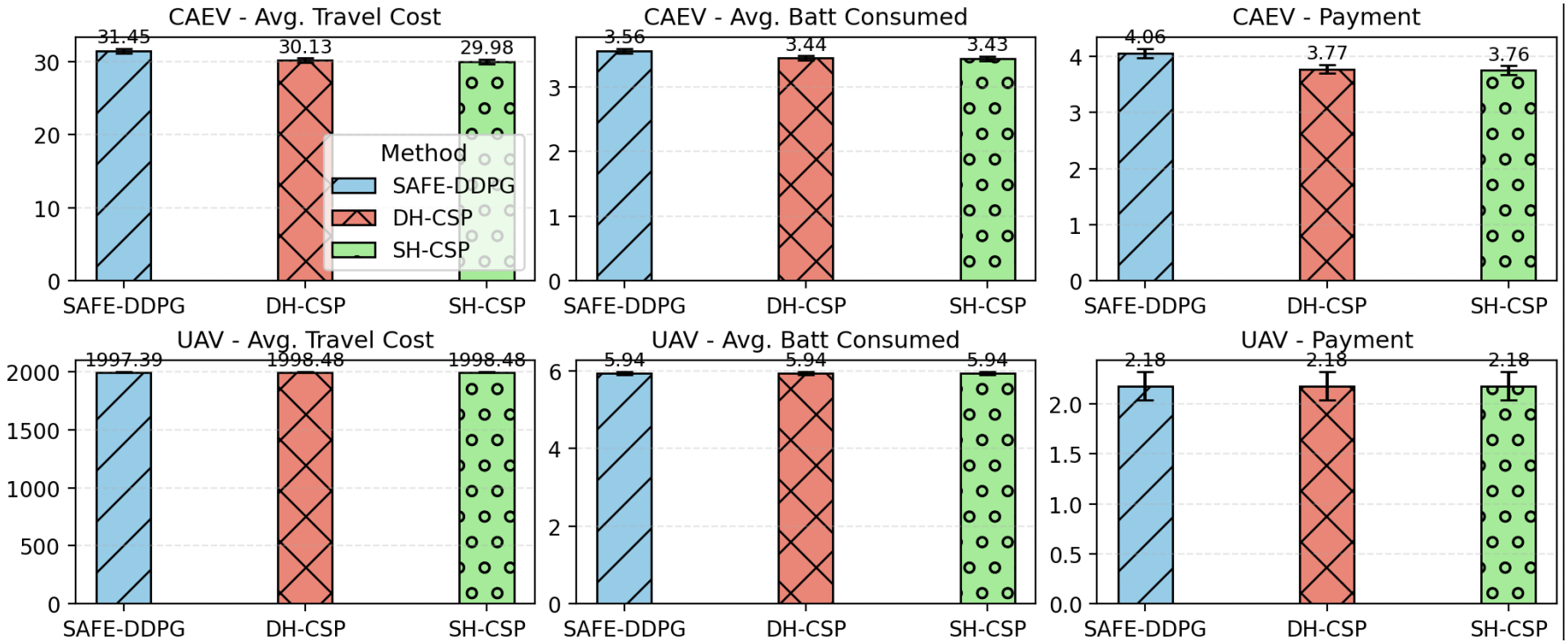

Figure 4.18: Average CAEV travel time, UAV travel distance, battery consumption (kWh), and payments (CAD) for both CAEVs and UAVs under SAFE-DDPG, DH-CSP, and SH-CSP.

The SAFE-DDPG algorithm, based on deep reinforcement learning, consistently outperforms the heuristic-based DH-CSP and SH-CSP across all CN types, achieving substantial reductions in wait times and significant improvements in fairness. For instance, wait times for static CNs are reduced by up to 86 percent compared to SH-CSP and over 70% compared to DH-CSP, while the Jain's Fairness Index improves by nearly 80% for static CNs and around 17% for dynamic CNs. These advantages stem from SAFE-DDPG's design features, including feasibility awareness, adaptive exploration, prioritized experience replay, and a dual-stage reward function that balances immediate service with long-term system efficiency.

DH-CSP, although heuristic-based, benefits from its handling of dynamic vehicle arrivals, allowing it to consistently outperform SH-CSP in moderate-demand and predictable scenarios where system variability is limited and computational simplicity is preferred. In contrast, SAFE-DDPG is ideal for high-demand, dynamically changing environments where charging demand is highly variable and route optimization is critical. The modest increases in travel cost and energy consumption under SAFE-DDPG are outweighed by the substantial gains in performance, fairness-related metrics and overall resource utilization, demonstrating its suitability for complex CAEV operations while highlighting when DH-CSP may be a practical alternative. Further, this combination of improved fairness-related metrics and low average wait times achieved by SAFE-DDPG not only enhances the CAEV user experience by reducing delays but also helps mitigate traffic congestion in the long term by preventing overloading of individual CNs, supporting efficient operation under heterogeneous charging demand.

4.7.4 Comparison of DRL Algorithms: SAFE-DDPG versus DDPG and TD3

This subsection compares the performance of three DRL algorithms: our proposed SAFE-DDPG, vanilla DDPG, and TD3, applied to large-scale CAEV scheduling. The goal is to evaluate how SAFE-DDPG's targeted algorithmic modifications impact learning behavior and scheduling performance relative to baseline DRL approaches. The comparison focuses on key metrics such as throughput, server utilization, and average wait times across different CN types, highlighting scheduling effectiveness across heterogeneous CN types. By maintaining consistent neural network structures and reward formulations across all algorithms, this analysis enables a controlled assessment of the benefits of SAFE-DDPG over the baseline approaches.

Figures 4.3, 4.19 and 4.20 show the training plots for SAFE-DDPG, DDPG, and TD3, highlighting the convergence behavior of each algorithm. For DDPG and TD3, default training parameters were used to ensure a controlled comparison while keeping the same reward functions and neural network structure as SAFE-DDPG. Under these conditions, DDPG and TD3 frequently converge to sub-optimal policies, attributable to reliance on immediate rewards without an explicit episode-level performance signal. SAFE-DDPG incorporates a dual-stage reward that provides a global reward at the end of each episode, along with prioritized experience replay and adaptive noise, improving both exploration and exploitation. These additions allow SAFE-DDPG to balance immediate performance with long-term efficiency and avoid the local optima observed in DDPG and TD3.

Figures 4.21 through 4.24 illustrate performance across different CN types: static CNs in Figure 4.21, DWCNs in Figure 4.22, and AVCN and GVCN in Figure 4.23, with the number of vehicles served reflecting scheduling effectiveness. SAFE-DDPG schedules only CAEVs, while UAVs are managed using the DH-CSP heuristic. Consequently, LBCN plots in Figure 4.24 show similar values across algorithms, with SAFE-DDPG achieving slightly lower wait times due to interaction with AVCN, which handles both vehicle types. The similarity in LBCN performance therefore reflects identical UAV scheduling logic rather than limitations of SAFE-DDPG.

Missing values observed under vanilla DDPG and TD3 indicate scheduling failures, often caused by overloading a single static and a single dynamic CN. Using the proportion of server idle time as a proxy for scheduling effectiveness, it is evident that vanilla DDPG and TD3 perform poorly under these conditions. Missing values for several CNs can be interpreted as an idle proportion of 1, indicating that these CNs were effectively unused while other CNs experienced severe congestion. In contrast, SAFE-DDPG achieves more balanced utilization, with idle proportions ranging from 0.03 to 0.57 across servers. This balanced load distribution reduces congestion at heavily utilized CNs, improves throughput, and lowers average wait times. Missing values therefore indicate scheduling collapse rather than an absence of demand.

SAFE-DDPG demonstrates more consistent and balanced throughput across the available CNs compared to vanilla DDPG and TD3. For static CNs, SAFE-DDPG achieves measurable throughput values, whereas DDPG and TD3 show missing values, indicating performance failures likely caused by overloading single CNs. For dynamic CNs DWCN_2 and DWCN_1, SAFE-DDPG maintains steady throughput around 0.021 vehicles per unit time, while DDPG only reports values for DWCN_2 and TD3 has partial coverage, reflecting uneven allocation. For AVCN_1 and GVCN_1, SAFE-DDPG achieves higher throughput of 0.042 and

0.028 respectively, compared to lower or missing values for DDPG and TD3. These results highlight SAFE-DDPG's ability to serve vehicles more consistently and distribute charging demand across available CNs, reducing bottlenecks and improving system-wide efficiency.

The comparison shows how SAFE-DDPG's targeted design changes result in a more robust and operationally efficient policy, with improved fairness-related indicators observed across CNs under the evaluated scenarios. SAFE-DDPG's feasibility-aware action screening forces the policy to consider a wider range of operationally valid actions, preventing infeasible or capacity-violating assignments. Unlike vanilla DDPG and TD3, which leave several servers idle or underutilized, SAFE-DDPG maintains measurable throughput across all CNs, enhancing network-wide service capacity. In terms of average wait times, SAFE-DDPG consistently lowers delays, with improvements up to 70–80 percent compared to DDPG for some CNs. The dual-stage reward structure is central to this improvement. The local reward discourages load imbalance and excessive travel, while the global reward penalizes waiting time and idle capacity, encouraging pre-emptive distribution of vehicles to reduce congestion.

Choosing to modify DDPG over TD3 is justified because SAFE-DDPG's enhancements, including dual-stage reward, feasibility awareness, prioritized experience replay, and adaptive noise, can be implemented without increasing the computational footprint of the neural network architecture. This makes SAFE-DDPG effective without increasing model complexity or online computational burden. Overall, SAFE-DDPG's design produces a policy that is robust, operationally efficient, and practical for deployment in real-time, large-scale CAEV networks.

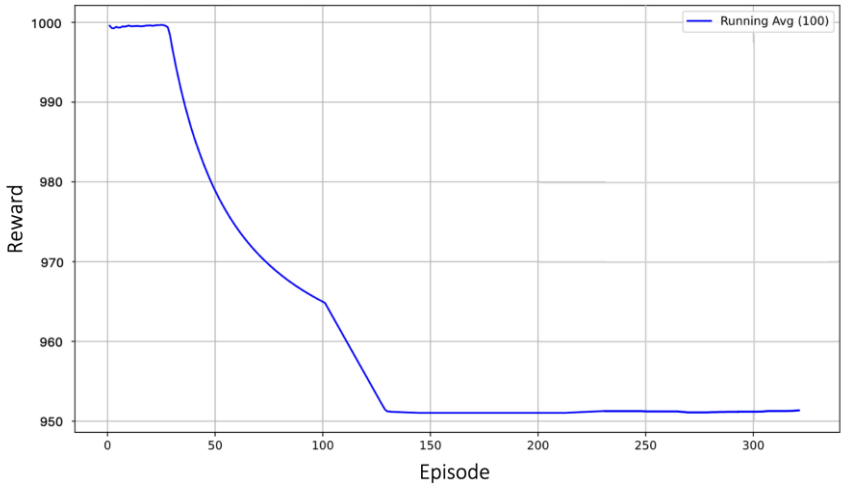

Figure 4.19. Training reward progression for vanilla DDPG.

Figure 4.20. Training reward progression for TD3.

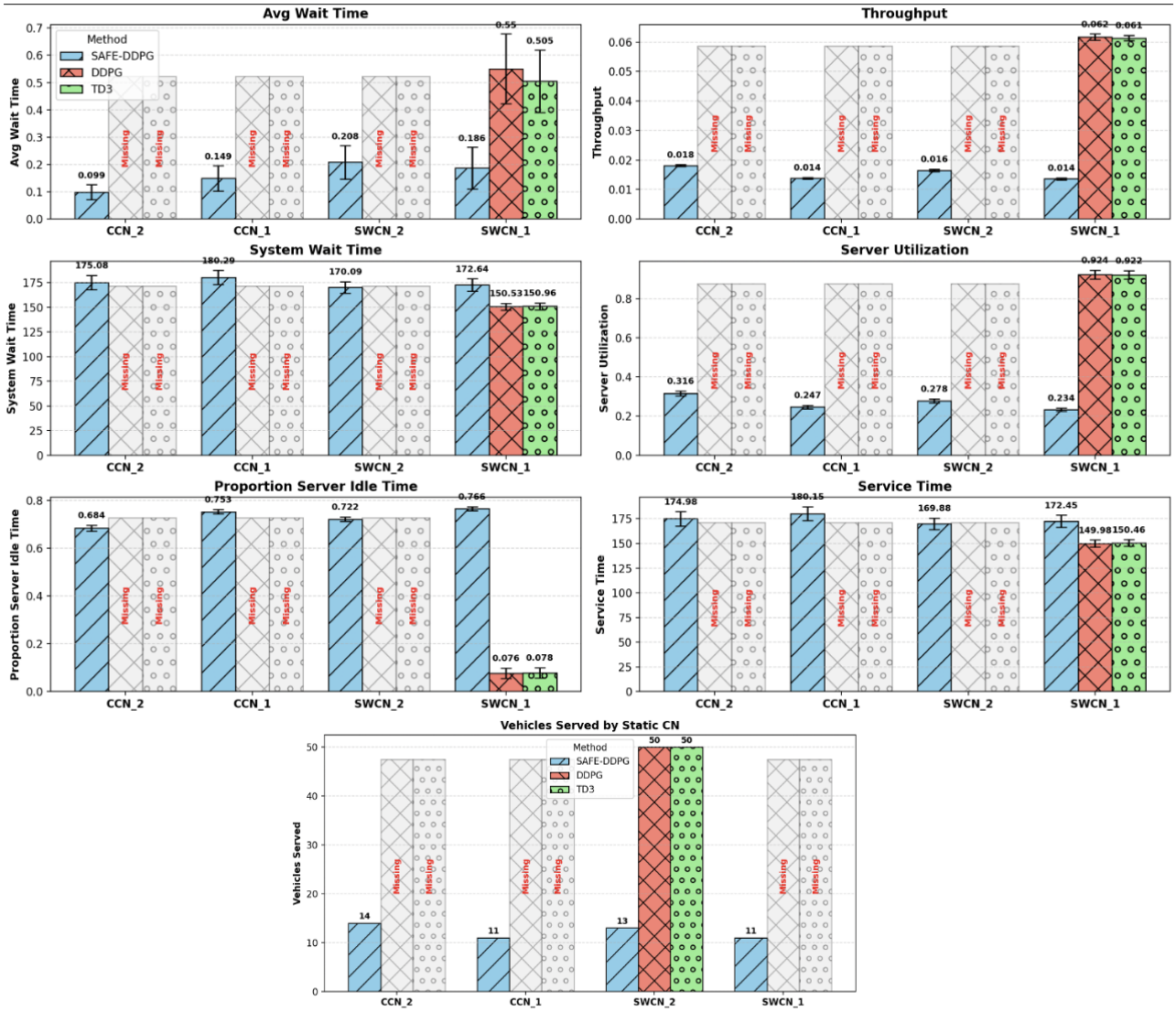

Figure 4.21: Performance comparison of SAFE-DDPG, DDPG, and TD3 on Static CNs across average wait time, throughput, server utilization, idle time, service time, and vehicles served.

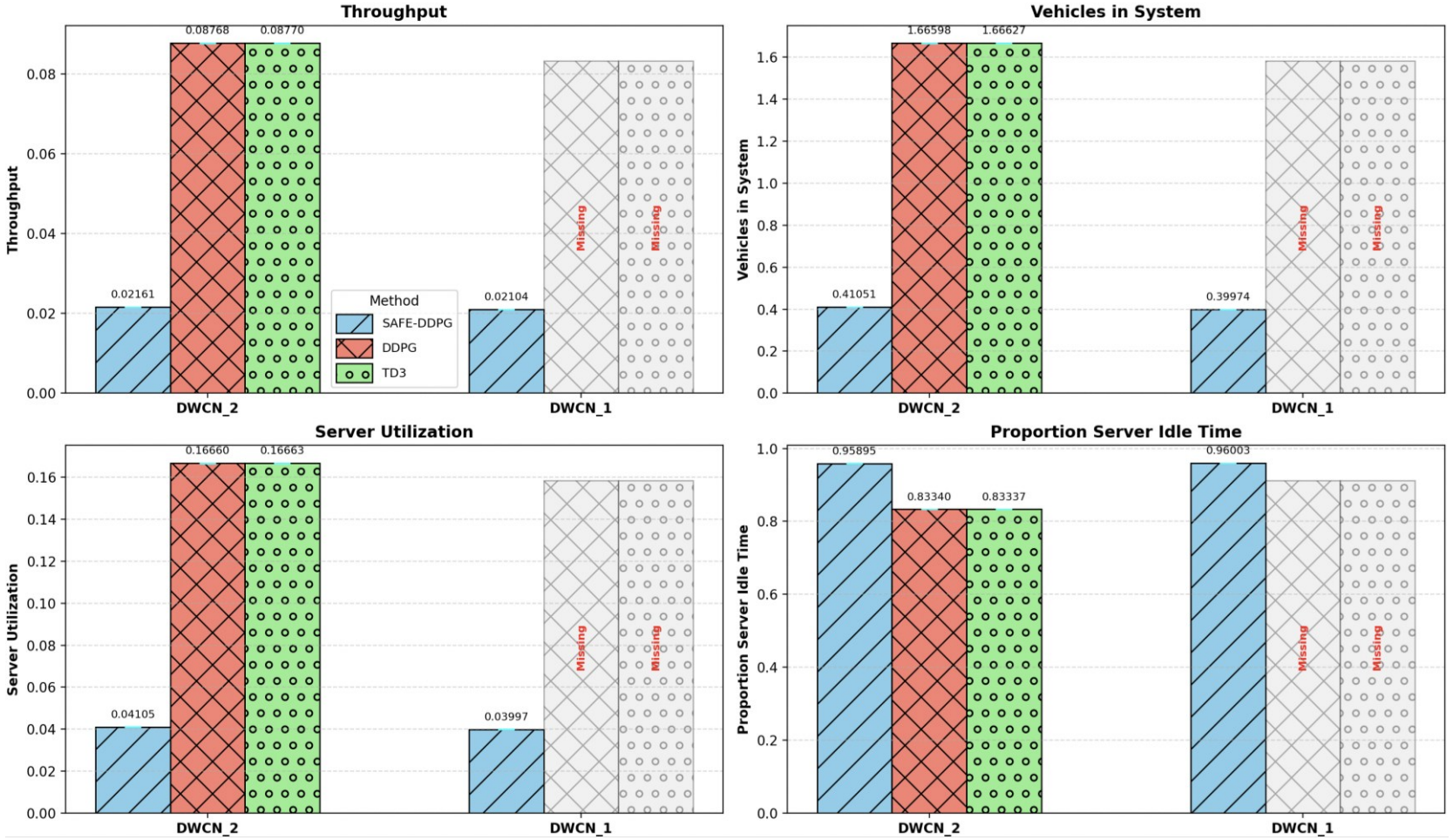

Figure 4.22: Performance comparison of SAFE-DDPG, DDPG, and TD3 on DWCNs across throughput, average vehicles in system, server utilization and proportion server idle time.

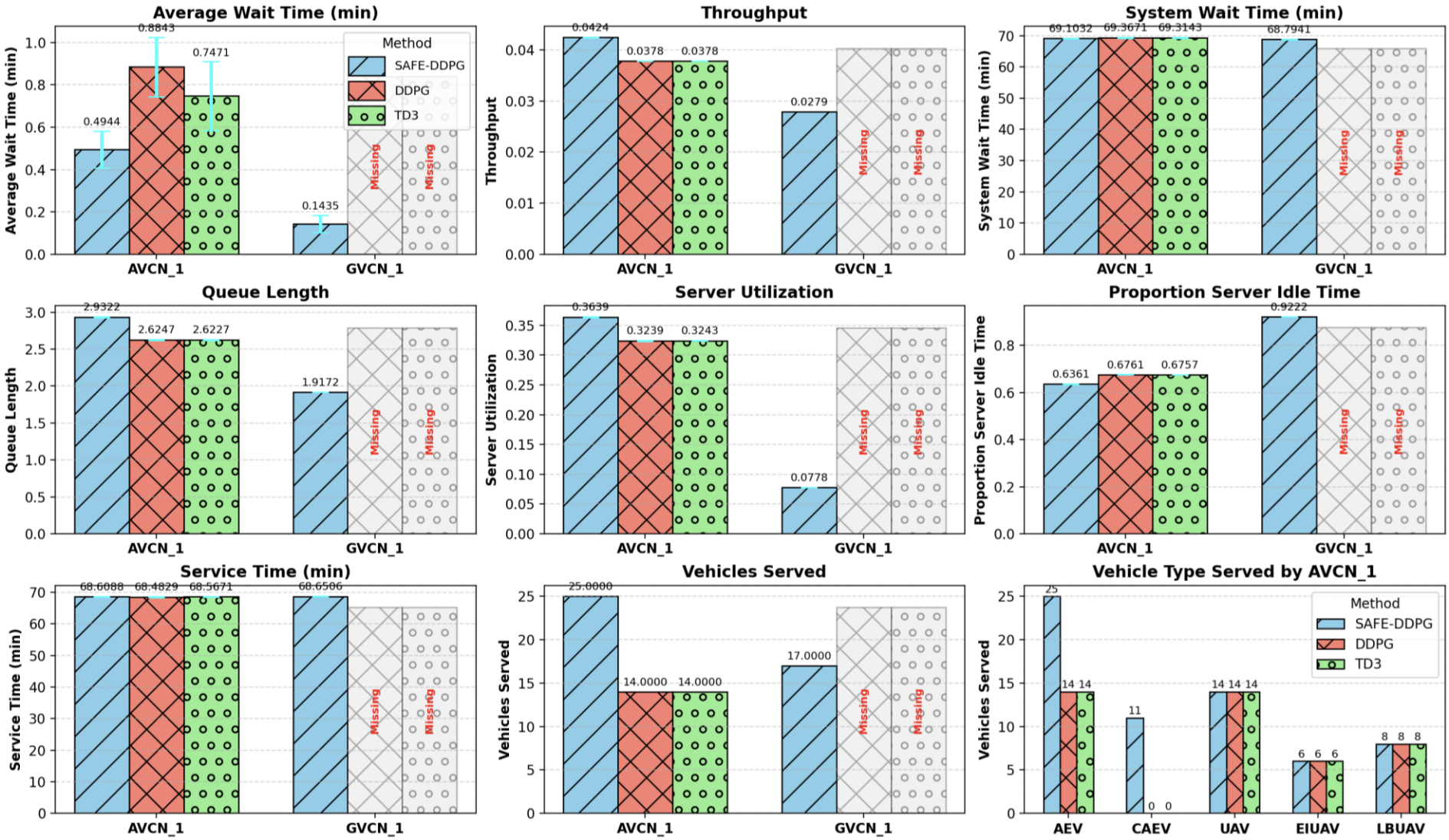

Figure 4.23: Performance comparison of SAFE-DDPG, DDPG, and TD3 on AVCN_1 and GVCN_1 across average wait time, throughput, system wait time, queue length, server utilization, idle time, service time, vehicles served, and vehicles types served by AVCN_1.

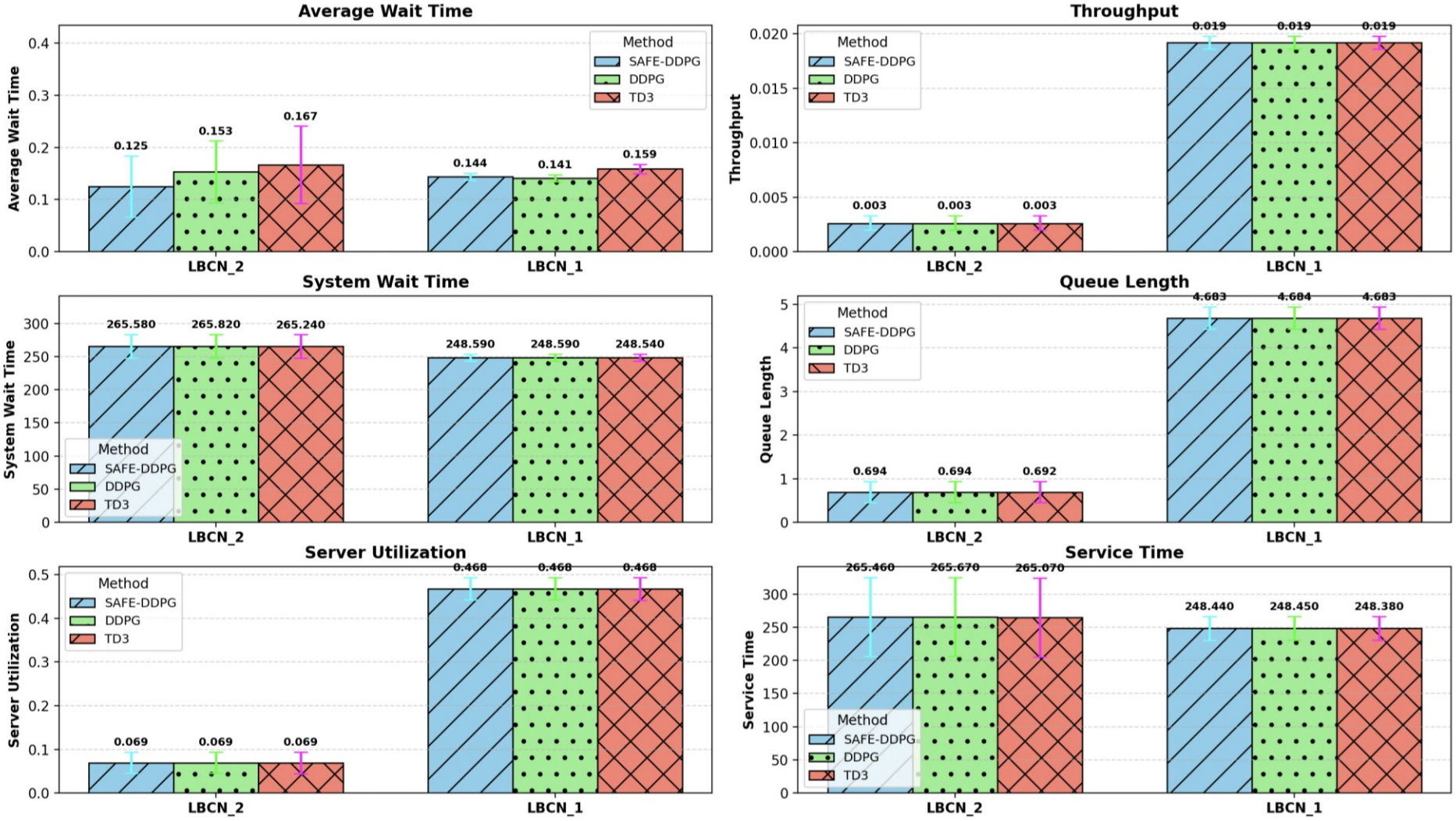

Figure 4.24: Performance comparison of SAFE-DDPG, DDPG, and TD3 on LBCNs across average wait time, throughput, system wait time, queue length, server utilization, and service time.

4.8 Conclusion

This chapter developed and assessed coordinated charging scheduling and trip planning solutions for heterogeneous charging networks. It introduced the models and algorithms required to support coordinated charging scheduling under dynamic operating conditions, together with the evaluation framework used to study their operational behavior. The proposed approaches were implemented within the system architecture introduced in Chapter 3, enabling consistent application and comparison across different scheduling strategies.

Three coordinated charging scheduling methods, namely SH-CSP, DH-CSP, and SAFE-DDPG, were developed within a common execution framework. The heuristic approaches provide interpretable baseline strategies for coordinated charging scheduling. SH-CSP operates based on static system snapshots, while DH-CSP extends this logic by incorporating dynamic arrival handling to improve responsiveness to evolving system load. Building on these foundations, the SAFE-DDPG algorithm introduces learning-based adaptability through feasibility-aware decision making and stable training mechanisms.

The performance assessment showed that SAFE-DDPG translates domain-informed learning into improved operational outcomes, including reduced average wait times, balanced utilization across heterogeneous charging networks, and high charging efficiency under dynamic demand conditions. Comparisons with heuristic baselines demonstrated the benefits of learning-based adaptability, while additional benchmarking against vanilla DDPG and TD3 highlighted the role of feasibility-aware design and reward structuring in achieving stable and effective coordinated charging scheduling.

Fairness-related indicators were reported to provide qualitative insight into how charging demand is distributed across networks. These observations serve as a natural transition to the following chapter, which focuses on reliability and fairness. Overall, the models and algorithms developed and assessed in this chapter establish a strong foundation for coordinated charging scheduling using both heuristic and learning-based approaches within next-generation ITS.

Chapter 5 Reliable and Fair Resource Allocation for Heterogeneous Charging

5.1 Introduction

Large-scale autonomous charging networks operating in smart city environments must satisfy not only efficiency and scalability objectives but also stringent reliability and fairness requirements. As vehicle density increases and heterogeneous charging modalities coexist, uncoordinated or purely throughput-driven scheduling can result in unsafe charging events, persistent congestion, and inequitable access to shared infrastructure. These challenges are further amplified in dynamic and wireless charging scenarios, where alignment, authorization, and timing constraints must be continuously enforced.

Previous chapters established the architectural foundations and coordination mechanisms for heterogeneous autonomous charging and demonstrated the performance benefits of heuristic and learning-based scheduling under increasing demand. However, strong aggregate performance alone does not guarantee reliable execution or equitable resource allocation at scale. Fairness across vehicles and charging nodes, robustness to dynamic arrivals, and enforceable safety constraints become critical system-level requirements.

This chapter focuses on the experimental evaluation of reliability, fairness, and scalability in coordinated heterogeneous CNs. Using fairness-oriented metrics, execution-level reliability indicators, and interpretability analysis, the chapter examines how the proposed SAFE-DDPG framework distributes resources, maintains stability under stress, and enforces safety across static and dynamic charging infrastructures. Together, the results provide a comprehensive assessment of reliable and fair resource allocation under next-generation ITS assumptions. The analysis progresses from comparative fairness assessment to scalability and reliability evaluation, followed by mechanism-level and interpretability-based analysis, culminating in a synthesis of key findings.

5.2 Methodology: Reliability- and Fairness-Aware Evaluation Framework

This section presents the methodological framework used to evaluate reliability, fairness, and scalability in coordinated heterogeneous CNs. The evaluation builds directly on the system architecture, communication and handshake protocol, and scheduling mechanisms introduced in earlier chapters. Unless explicitly stated otherwise, the network architecture, authorization procedures, and charging execution logic remain unchanged, and the same simulation environment, system parameters, and demand models are employed to ensure consistency and comparability across all experiments.

The scheduling strategies considered include the heuristic approaches and the learning-based SAFE-DDPG coordinator previously defined. In this chapter, SAFE-DDPG is evaluated in its trained form without additional retraining. This design choice ensures that observed behavior reflects generalization, robustness, and execution-level performance under varying operating conditions rather than effects of parameter tuning or retraining. All strategies are assessed under identical operating conditions, with common random number control applied where appropriate to reduce variance and isolate system-level effects.

Within this framework, reliability, fairness, and scalability are treated as complementary system-level properties that arise from the interaction of scheduling decisions, architectural safeguards, protocol enforcement, and execution-level mechanisms. Fairness is evaluated using allocation-based metrics that capture equity across vehicles and charging networks. Scalability is examined by progressively increasing system load beyond the training regime. Reliability is assessed through stable execution behavior, charging fulfillment consistency, and the avoidance of infeasible or unsafe charging outcomes under dynamic operating conditions.

In addition to performance-oriented evaluation, interpretability and ablation-based analyses are incorporated as methodological tools to examine the contribution of architectural, protocol-level, and learning-based mechanisms. These analyses support validation of system behavior and provide insight into the role of safety constraints, feasibility enforcement, and learning structure in enabling reliable and fair operation. Together, this methodology establishes a structured and consistent basis for evaluating coordinated charging strategies under increasing demand, heterogeneous infrastructure, and real-world operational uncertainty.

5.3 Experimental Results and Analysis

This section presents experimental results that evaluate fairness, scalability, and reliability across heterogeneous CNs under increasing system demand. The analysis synthesizes comparative results from prior experiments and extends them through stress testing [133], execution-level reliability assessment, ablation analysis, and interpretability-based validation. Emphasis is placed on system-level behavior, robustness, and enforceability rather than isolated performance metrics.

5.3.1 Fairness Comparison Across Scheduling Strategies

This section synthesizes and interprets the fairness-related outcomes of the three proposed scheduling strategies, including SH-CSP, DH-CSP, and SAFE-DDPG, under identical operating conditions. Rather than reproducing the full performance evaluation

presented earlier, the focus here is on analyzing those results through the lens of fairness, robustness, and balanced resource allocation, which constitute central objectives of this chapter. The resulting fairness baseline supports subsequent discussions on scalability and reliability.

All numerical results referenced in this section are drawn from the comparative experiments reported in Chapter 4, which employed identical network configurations and a common random number experimental design. Detailed per–CN performance metrics, CIs, and utilization trends are reported in Tables 4.10–4.11 and Figures 4.11–4.18. These results are referenced selectively here to provide context while avoiding repetition, allowing emphasis to be placed on system-level fairness behavior and its broader implications.

5.3.1.1 Fairness, Delay, and Utilization Summary

Fairness is evaluated using Jain's Fairness Index (JFI) applied to charging resource allocation across heterogeneous CNs. Average wait time is considered a complementary indicator of equitable service, since persistent allocation imbalance typically manifests as prolonged delays at specific charging nodes. In addition, server utilization is examined to verify that fairness improvements are not achieved through underutilization of available infrastructure.

Table 5.1 provides a concise synthesis of representative fairness, delay, and utilization outcomes extracted from the comparative analysis in the previous chapter. The table aggregates representative system-level indicators to highlight how each scheduling strategy balances equity, service delay, and effective utilization of charging resources.

Table 5.1: Summary of fairness, delay, and utilization characteristics across scheduling strategies..

Metric*	SAFE-DDPG	DH-CSP	SH-CSP
JFI (Static CNs)	0.985	0.549	0.548
JFI (Dynamic CNs)	0.784	0.670	0.671
Overall JFI	0.800	0.617	0.617
Avg Wait Time (Static CNs) **	Lowest	+52–70%	+59–87%
Server Utilization (Static CNs)	High and balanced	Moderate	Uneven
Idle Time Proportion	Low and uniform	Moderate	High variance
Throughput Consistency	High	Moderate	Low

** Values summarized from Tables 4.10–4.11 and Figures 4.11–4.18.*
*** Percentage values indicate higher average wait time relative to SAFE-DDPG.*

Dynamic CNs are heterogeneous, with different vehicle roles and charging strategies across DWCNs, AVCNs, and GVCNs, making aggregate utilization and wait-time comparisons across these node types not meaningful or interpretable. Accordingly, fairness for dynamic CNs is evaluated using JFI and qualitative utilization balance, while aggregate comparisons remain appropriate for static CNs due to their homogeneous infrastructure and operating procedures. The overall JFI therefore provides a consistent system-level indicator of

equitable allocation, even when individual dynamic charging modes are not directly comparable.

5.3.1.2 Fairness and Load Distribution Across Scheduling Strategies

As reported in Table 4.10 and summarized in Table 5.1, SAFE-DDPG achieves a JFI of 0.985 for static CNs, compared to 0.549 under DH-CSP and 0.548 under SH-CSP, corresponding to an improvement of approximately 80% relative to both heuristic strategies. For dynamic CNs, SAFE-DDPG attains a JFI of 0.784, exceeding DH-CSP and SH-CSP by approximately 17%. When all CNs are considered jointly, the overall fairness index under SAFE-DDPG is 0.800, while both baseline strategies remain near 0.617.

These results indicate that learning-based coordination enables substantially more balanced load distribution across heterogeneous charging infrastructure. In contrast, SH-CSP exhibits persistent allocation imbalance due to its static scheduling logic, while DH-CSP improves fairness by accounting for dynamic arrivals but remains constrained by heuristic decision rules, limiting its ability to achieve consistent equity across diverse charging modalities.

5.3.1.3 Relationship Between Fairness, Delay Reduction, and Robustness

Improvements in fairness under SAFE-DDPG are accompanied by substantial reductions in average wait times across all CN types. As reported in Table 4.10 and illustrated in Figures 4.11 and 4.12, average wait times for static CNs are reduced by over 70% relative to DH-CSP and by up to 86% relative to SH-CSP. Similar reductions are observed for dynamic and specialized CNs, including AVCNs and GVCNs.

The strong alignment between reduced wait times and improved fairness suggests that SAFE-DDPG mitigates persistent congestion and resource monopolization rather than merely optimizing average delay. Scheduling strategies with lower fairness indices exhibit higher variability in wait times and localized congestion, indicating reduced robustness under heterogeneous demand. In this sense, fairness emerges not only as an equity objective but also as a robustness-enhancing property that stabilizes system behavior under dynamic operating conditions.

5.3.1.4 Utilization Consistency and Validity of Fairness Gains

To verify that fairness improvements are not achieved through reduced utilization or underloaded operation, offered load and server utilization metrics are also examined. Figures 4.13–4.18 show that SAFE-DDPG maintains server utilization levels comparable to or higher than those observed under DH-CSP across static, dynamic, and specialized charging nodes, while avoiding persistent overload of individual nodes. For example, static CNs under SAFE-

DDPG exhibit higher throughput and utilization than both baseline strategies while maintaining moderate queue lengths and lower idle times, as shown in Figure 4.13.

These observations confirm that the fairness gains achieved under SAFE-DDPG arise from coordinated scheduling decisions rather than from leaving charging capacity unused. In contrast, SH-CSP demonstrates uneven utilization patterns, with certain CNs experiencing congestion while others remain lightly loaded, indicating inefficient and unbalanced resource usage that can negatively impact both fairness and reliability.

Additional evidence of reliable operation is provided by the absence of performance failures under SAFE-DDPG compared to baseline learning-based approaches such as vanilla DDPG and TD3. As shown in Figures 4.13–4.18, SAFE-DDPG maintains measurable throughput and balanced utilization across all static and dynamic CNs, whereas baseline strategies exhibit missing values and extreme idle time at several nodes, indicating infeasible or unstable scheduling behavior. For example, SAFE-DDPG maintains server idle time proportions in the range of approximately 0.03 to 0.57 across static CNs, while baseline strategies frequently leave servers effectively unused while overloading others. This consistent service coverage and avoidance of infeasible assignments indicate that the fairness gains achieved under SAFE-DDPG are accompanied by reliable and stable system operation.

Overall, the comparative results reported in Chapter 4 and synthesized here establish that SAFE-DDPG achieves superior fairness, lower service delay, and more balanced utilization than both DH-CSP and SH-CSP across heterogeneous charging infrastructure. DH-CSP offers measurable improvements over SH-CSP by accommodating dynamic arrivals and multi-vehicle interactions, making it suitable for moderate and predictable demand scenarios. SAFE-DDPG, however, consistently provides higher fairness and more stable load distribution under heterogeneous and dynamically changing conditions. These properties motivate the selection of SAFE-DDPG as the reference strategy for the subsequent analysis of scalability and reliability, where the persistence of fairness under increasing system stress is examined in detail.

5.3.2 Scalability and Reliability Analysis of SAFE-DDPG Under Increasing CAEV Load

To evaluate the scalability and reliability of SAFE-DDPG under increasing system demand, CAEV load is progressively increased from 50 to 400 vehicles over a two-day simulation horizon. The SAFE-DDPG policy is trained only under a low-load scenario of 50 CAEVs and is intentionally stress-tested here to assess its ability to generalize, preserve

fairness, and maintain stable operation as demand grows. The analysis focuses on throughput, wait times, queue evolution, and service behavior across heterogeneous CNs, as well as interactions with UAVs. Scalability is assessed by observing how these metrics evolve as vehicle load increases, while reliability is evaluated through the preservation of fairness, stable operation without policy failure, and predictable saturation behavior under extreme demand. Beyond performance trends, the results identify saturation points, shared resource contention, and the impact of vehicle cancellations or early departures, providing insight into practical operating limits and informing infrastructure planning decisions.

The JFI results summarized in Table 5.2 demonstrate that the SAFE-DDPG policy generalizes effectively to higher vehicle loads, maintaining strong fairness across heterogeneous CNs. For static CNs, JFI remains consistently high as CAEV load increases, ranging from 0.985 at 50 CAEVs to 0.970 at 400 CAEVs, indicating equitable distribution of service among stations. Dynamic CN types also exhibit robust fairness, with JFI values between 0.915 and 0.978 across all load levels. When considering overall CAEV CNs, which combine static and dynamic CNs, the system maintains a JFI above 0.85 for all scenarios, reflecting balanced load allocation even under substantial increases in demand. The slight reduction in overall JFI at 400 CAEVs reflects infrastructure saturation rather than scheduling instability, indicating a transition from a coordination-limited regime to an infrastructure-limited regime. These results highlight SAFE-DDPG's ability to scale to high-demand scenarios while preserving fairness and balanced throughput.

Table 5.2: Summarized Jain's Fairness index values over increasing CAEV load under SAFE-DDPG.

CAEV Load	***JFI Static CNs***	***JFI Dynamic CNs***	***JFI Overall***
50	0.985	0.915	0.857
100	0.997	0.96	0.921
200	0.988	0.978	0.927
400	0.97	0.96	0.867

For static CNs, SAFE-DDPG demonstrates robust scalability as the CAEV load increases from 50 to 400 vehicles as seen in Figures 5.1 and 5.2. At low load (50 CAEVs), average wait times are minimal, ranging from 0.10 min for CCN_2 to 0.21 min for SWCN_2, queue lengths are modest (2.34–3.16), and server utilization is moderate (0.23–0.32), with high idle times (0.68–0.77) reflecting light traffic. As load increases to 100 CAEVs, wait times rise moderately for some CNs, throughput nearly doubles, queue lengths expand, and server utilization increases to 0.48–0.52 while idle times decrease, showing SAFE-DDPG effectively balances traffic without overloading individual CNs. At medium and high loads of 200 and 400

CAEVs, wait times and queue lengths grow substantially. The slightly larger CIs observed for average wait times at higher loads arise from increased variability in vehicle interactions, where some vehicles experience negligible waiting while others encounter longer delays due to dynamic scheduling decisions, shared resource contention, and stochastic arrival patterns. Such variability is expected in multi-vehicle, multi-charging-network coordination scenarios. For example, CCN_2 wait time increases from 2.44 min at 200 CAEVs to 4.95 min at 400 CAEVs, while SWCN_2 queue length reaches 12.58 at the highest load. Throughput continues to scale, and server utilization approaches or slightly exceeds full capacity. When utilization exceeds 1, it represents offered load surpassing server capacity, indicating that these CNs are saturated. Idle times drop toward zero or become slightly negative, reflecting this saturation. Service times rise in line with wait times, demonstrating consistent scheduling performance. Overall, SAFE-DDPG generalizes effectively from low-load training to high-load scenarios, scaling throughput, managing queues, and adapting to saturation patterns at peak demands.

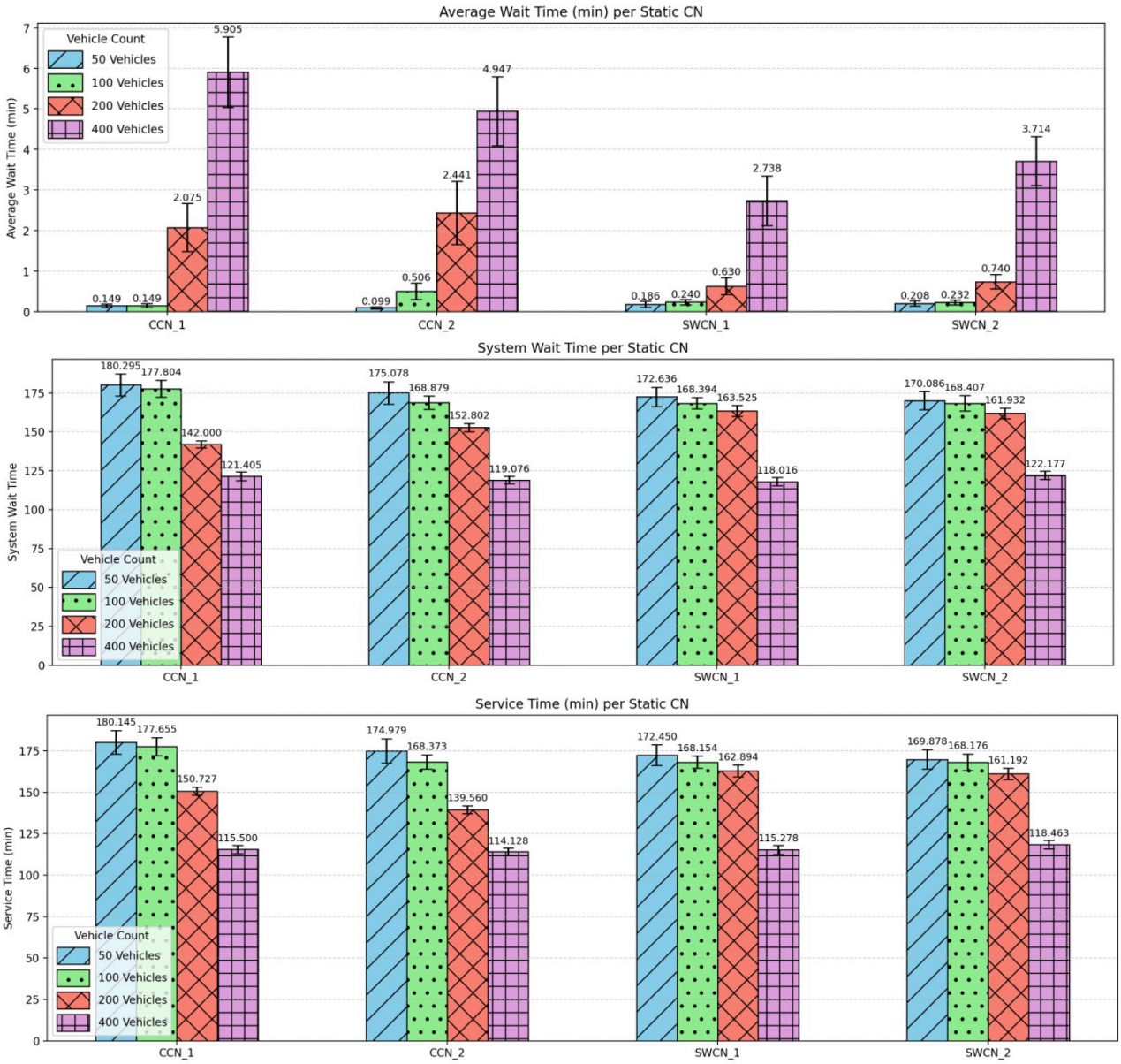

Figure 5.1: Average wait time, system wait time and service time of static CNs under SAFE-DDPG for CAEV loads of 50,100,200 and 400.

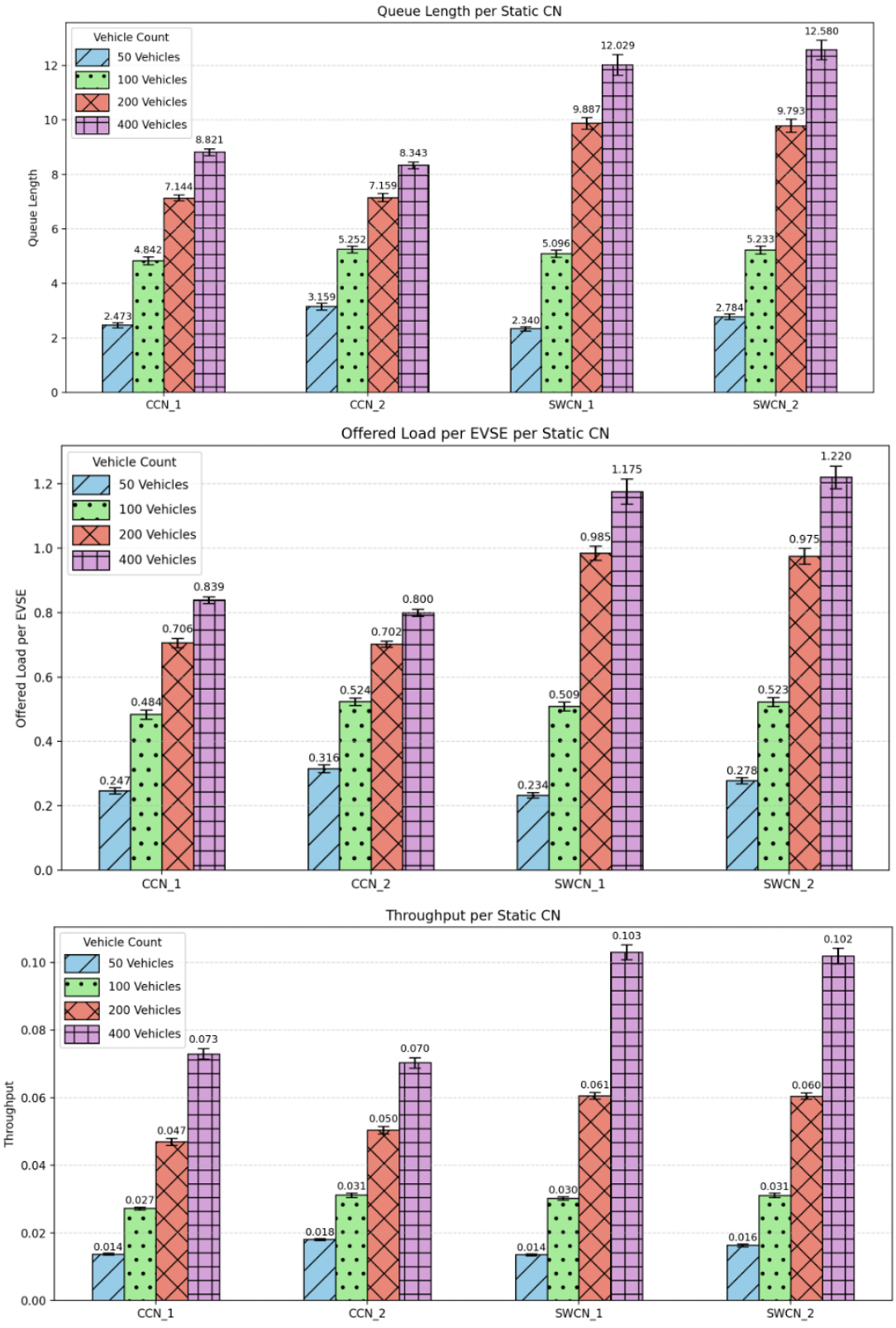

Figure 5.2: Queue length, offered load per EVSE and throughput of static CNs under SAFE-DDPG for CAEV loads of 50,100,200 and 400.

The performance of DWCNs summarized in Figure 5.3 under SAFE-DDPG indicates that these lanes function as fast-flow charging paths. The average number of vehicles in the

system increases with CAEV load, from roughly 0.41 at 50 CAEVs to 4.11 at 400 CAEVs for DWCN_2, reflecting the higher throughput but still very low congestion. Service times remain around 19 minutes, and server utilization rises with load, while the proportion of idle time decreases, showing that DWCNs are increasingly active under heavier demand. This behavior confirms the role of DWCNs as low-congestion, fast-flow charging paths that help stabilize overall network performance under rising demand.

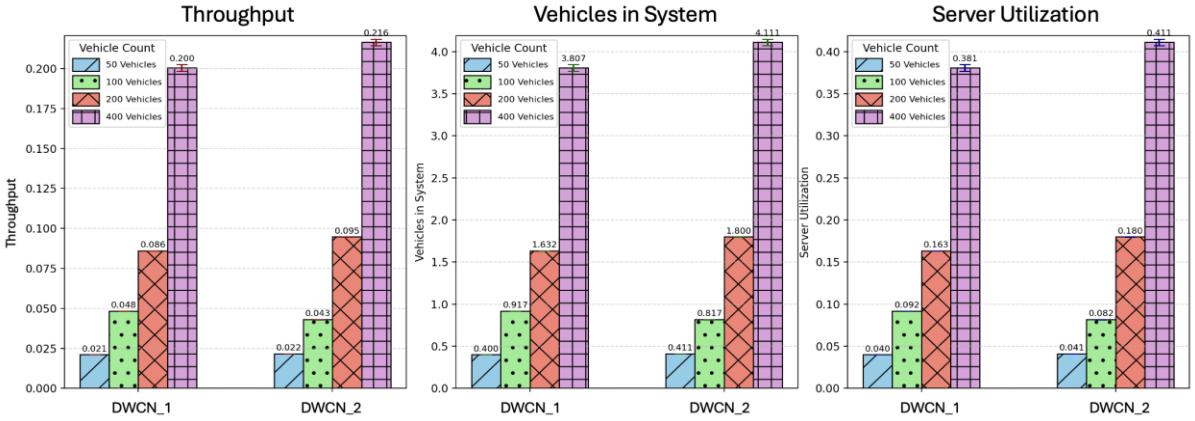

Figure 5.3: Throughput, vehicles in system and server utilization of DWCNs under SAFE-DDPG for CAEV loads of 50,100,200 and 400.

The performance of the GVCN_1 seen in Figure 5.4 improves as CAEV load increases, with throughput rising from 0.028 at 50 CAEVs to 0.141 at 400 CAEVs. This growth is supported by scaling the maximum number of EVSEs available for V2V charging (25, 50, 100, and 200 respectively), as well as the influence of CAEVs in close proximity. Average vehicles in the system increase from 1.92 to 9.44, reflecting higher demand. Service times remain stable at around 66–69 minutes, which is higher than DWCNs, since V2V charging depends on CAEV availability and matching dynamics. Overall, GVCNs scale effectively with load, leveraging proximity-based CAEV interactions to enhance throughput while maintaining consistent service characteristics. The stability of service time despite rising load indicates reliable operation governed by vehicle availability and matching dynamics rather than centralized scheduling bottlenecks.

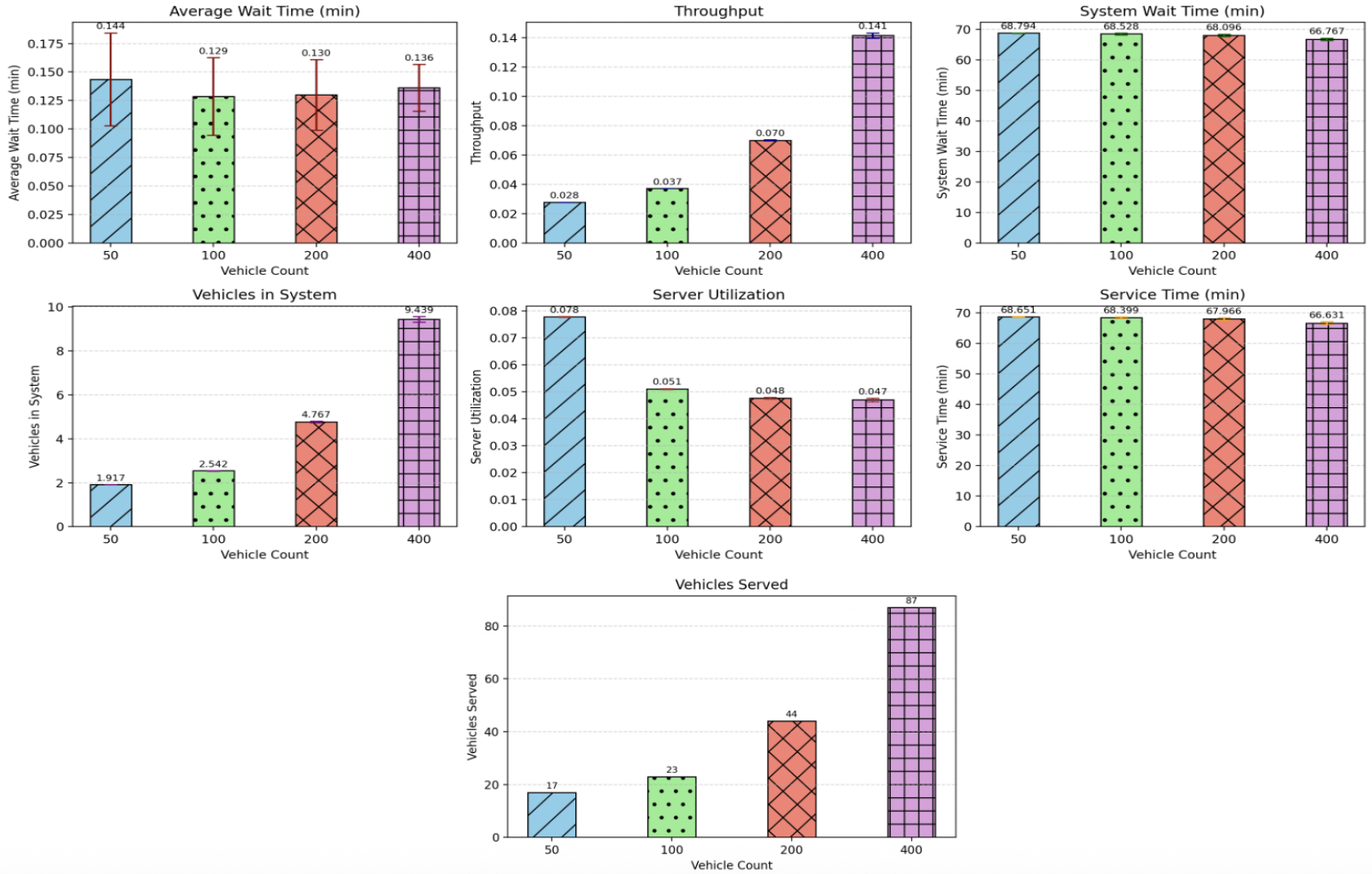

Figure 5.4: Average wait time, throughput, system wait time, vehicles in system (little's law), server utilization with increasing server count, service time, and vehicles served by GVCN_1 under SAFE-DDPG for CAEV loads of 50,100,200 and 400.

In SAFE-DDPG, only the scheduling decisions for CAEVs are determined by the DRL agent, while UAV charging is managed through the DH-CSP algorithm. Across all scenarios, the number of UAVs served remains fixed at 14, which explains why their performance metrics remain relatively consistent in range as seen in Figure 5.5. However, at higher CAEV loads, UAV wait times begin to increase. This effect is linked to the role of AVCN_1, which is responsible for charging both CAEVs and UAVs. As its load grows with rising CAEV demand, UAVs often arrive late to LBCN after receiving dynamic charging from AVCN_1, which indirectly drives up their average wait times. This observation highlights the importance of jointly considering the interactions between different vehicle types in scheduling decisions. While coordination at lower loads (e.g., 50 CAEVs) helped reduce UAV wait times, at higher loads (e.g., 400 CAEVs) the compounded interactions lead the system toward saturation, ultimately impacting UAV performance.

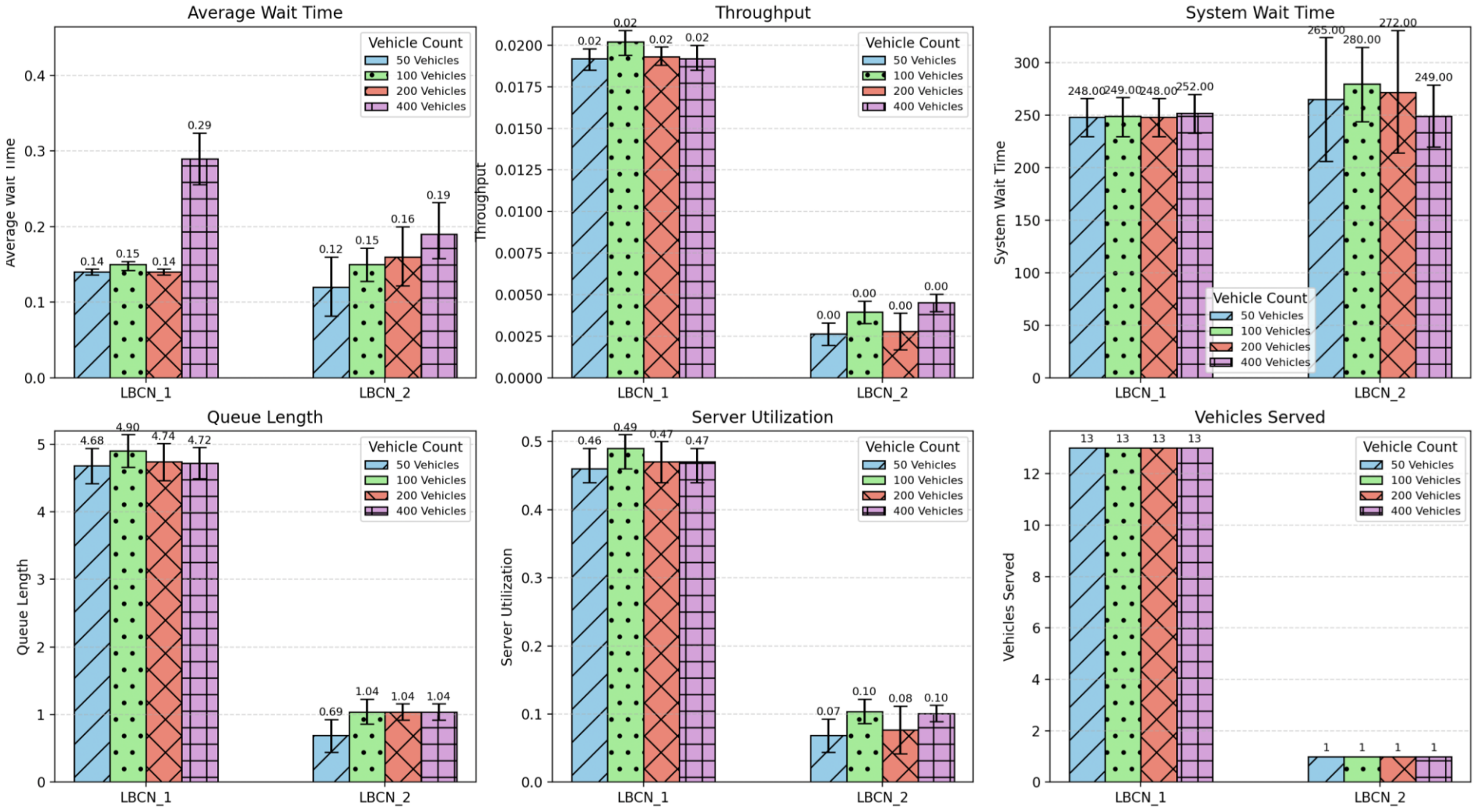

Figure 5.5: Average wait time, throughput, system wait time, queue length, server utilization, and vehicles served by LBCNs under SAFE-DDPG for CAEV loads of 50,100,200 and 400 and consistent UAV load.

Under SAFE-DDPG, AVCN_1 performance illustrates strong scalability across increasing CAEV loads while maintaining stable service for UAVs, EIUAVs, and LBUAVs. UAV scheduling, determined by the DH-CSP algorithm, remains fixed at 14 served vehicles as seen in Figure 5.6, producing consistent throughput of around 0.045 and steady wait times near 0.8 across all load levels. LBUAVs provide charging services at AVCN_1, which contributes to their observed utilization and partly explains the increase in wait times at LBCNs under extremely high loads. In contrast, CAEV throughput grows markedly from 0.0187 at load 50 to 0.1130 at load 400, showing in Figure 5.7 that SAFE-DDPG effectively scales CAEV service as system demand rises. Average CAEV wait time is very low at 0.11 at load 50, increasing to 2.77 at load 400 as AVCN_1 is shared across multiple vehicle classes. This also impacts AEVs, whose wait times increase from 0.49 at load 50 to 2.45 at load 400, while UAV wait times remain almost unchanged. These results demonstrate that SAFE-DDPG maintains fairness and balanced scheduling under rising demand, with bottlenecks at higher loads driven more by shared resource contention, including LBUAV activity, than by limitations of the learning algorithm. The observed saturation at 400 CAEVs highlights the need for installing additional CNs or EVSEs once load surpasses certain thresholds, thus providing valuable insight for system design and planning. These interactions illustrate that performance degradation at high load is driven by shared resource contention across vehicle classes rather than limitations of the SAFE-DDPG scheduling policy.

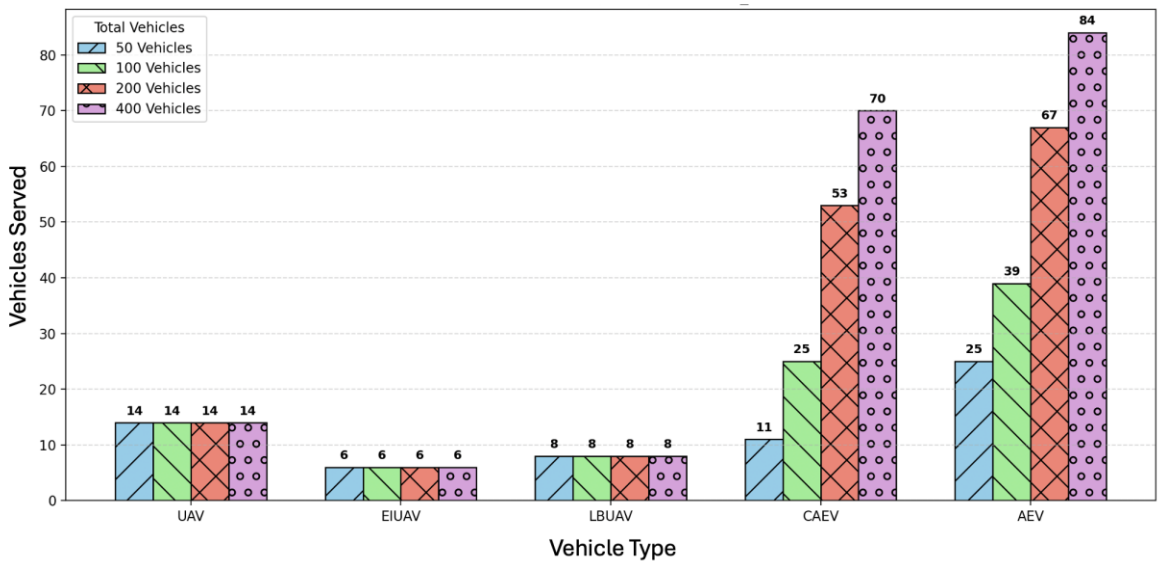

Figure 5.6: Vehicle types served by AVCN_1 under SAFE-DDPG for CAEV loads of 50,100,200 and 400 and consistent UAV load.

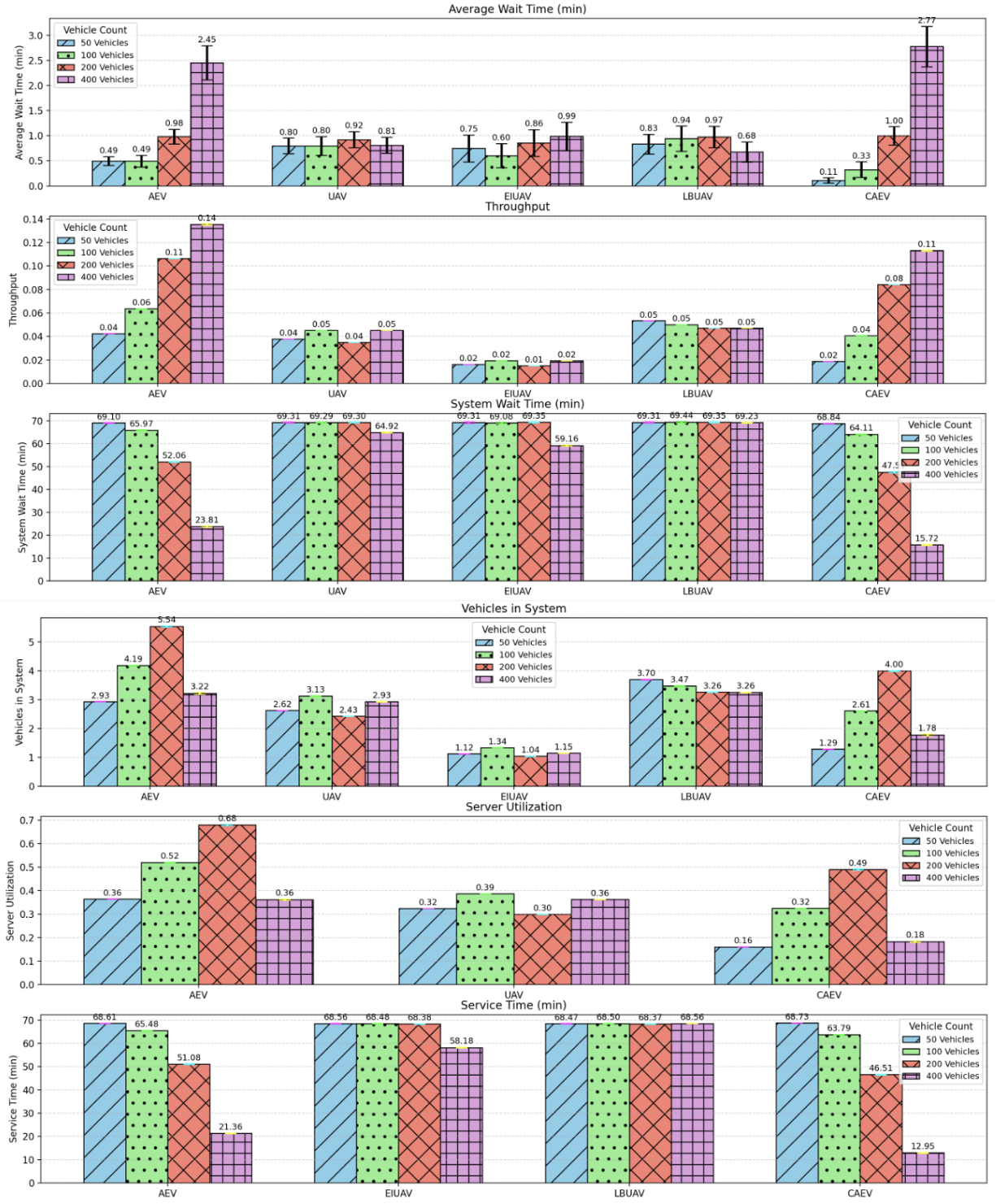

Figure 5.7: Average wait time, throughput, system wait time, vehicles in system (little's law), server utilization, service time by AVCNs under SAFE-DDPG for CAEV loads of 50,100,200 and 400 and consistent UAV load.

Over the two-day simulation horizon, SAFE-DDPG demonstrates robust scalability as CAEV load increases from 50 to 400 vehicles. As shown in Figure 5.8, overall system throughput rises steadily across all vehicle classes, with AEV and CAEV throughput increasing from 0.073 and 0.057 at low load to 0.433 and 0.421 at high load, respectively, while UAV throughput, including both EIUAV and LBUAV subtypes, remains comparatively stable. The

corresponding growth in system demand is illustrated in Figure 5.9, where increasing arrival rates lead to higher queue lengths, particularly for AEVs and CAEVs. Despite this increase in congestion, average system wait times for AEVs and CAEVs decrease from approximately 257 and 239 minutes to 205 and 201 minutes, indicating effective load balancing and adaptive scheduling under higher traffic. Queue growth at high load also reflects vehicle cancellations caused by early departures, accidents, or insufficient charging opportunities from delivery vehicles. In contrast, UAVs scheduled using DH-CSP exhibit stable wait times and modest queue lengths, while EIUAV performance remains largely unchanged. LBUAVs, which actively provide charging within AVCNs, become increasingly engaged as demand grows, contributing to higher wait times at LBCNs under heavy load.

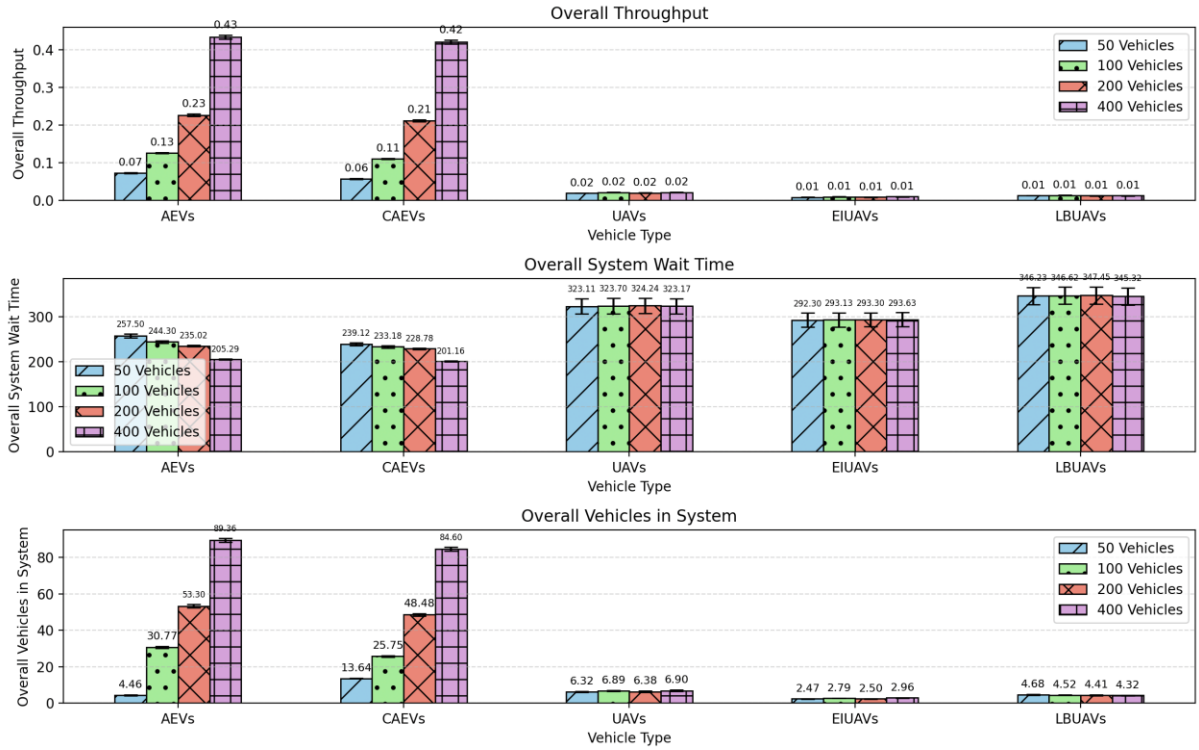

Figure 5.8: Overall throughput, system wait time, and vehicles in system (little's law) under SAFE-DDPG for CAEV loads of 50,100,200 and 400 and consistent UAV load.

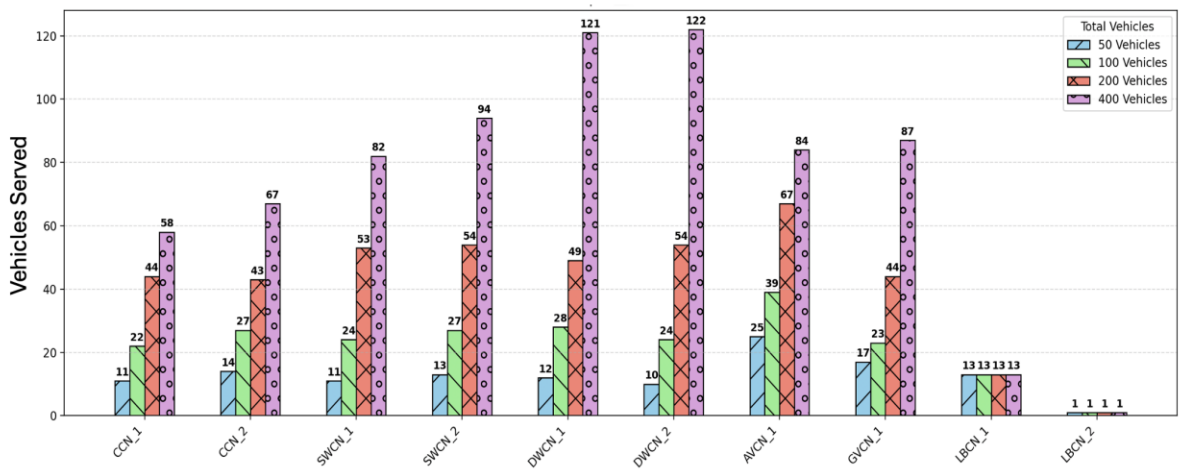

Figure 5.9: Vehicles Served by each CN under SAFE-DDPG for CAEV loads of 50,100,200 and 400 and consistent UAV load.

Additional reliability trends are observed in vehicle mobility, energy usage, and economic metrics, as summarized in Figure 5.10. Average CAEV travel time decreases slightly from 31 to 29 minutes as vehicle density increases, reflecting denser trip patterns and shorter rerouting distances under higher demand. At the same time, average CAEV payments decline from 4.06 to 2.27 and battery consumption decreases from 3.56 to 3.33 kWh, driven by session cancellations and normalization effects across a larger vehicle population. UAV travel distances remain stable, while EIUAV battery consumption stays consistently high due to fixed operational roles. In contrast, LBUAV battery usage increases gradually as service provision intensifies under heavy load. Together, these results indicate that performance degradation at extreme load levels arises from infrastructure saturation and shared resource contention rather than instability of the SAFE-DDPG scheduling policy. Overall, SAFE-DDPG maintains stable, fair, and coordinated operation across heterogeneous vehicle classes while revealing practical system limits that are critical for large-scale deployment and infrastructure planning.

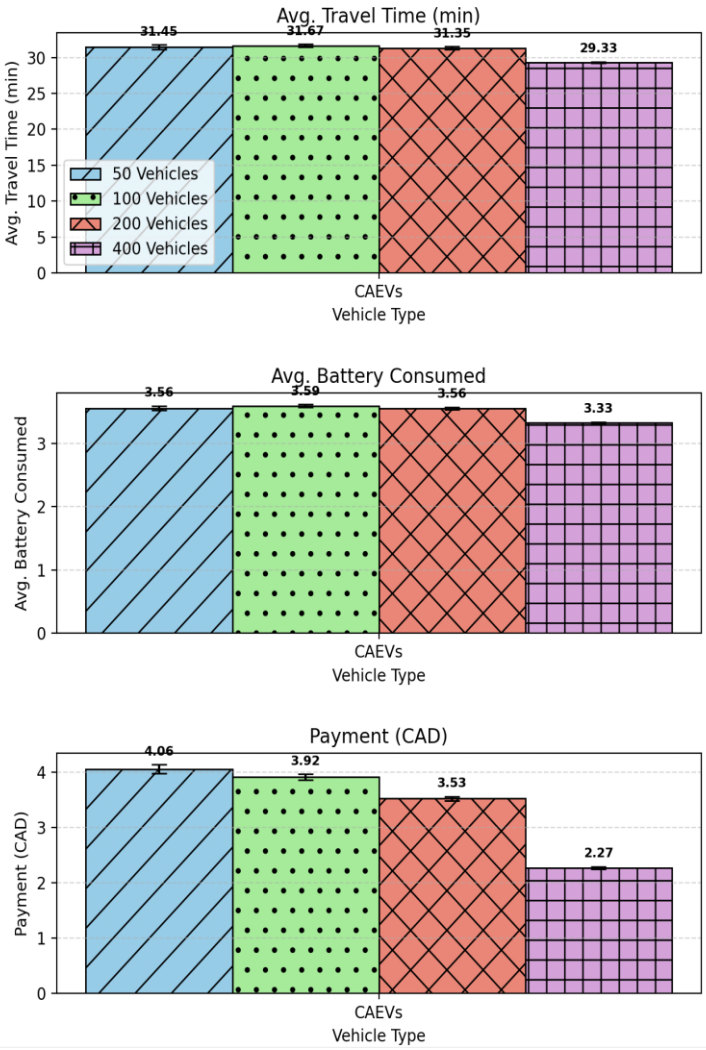

Figure 5.10: Average travel time, battery consumed and reservation payment per CAEV under SAFE-DDPG for CAEV loads of 50,100,200 and 400.

In conclusion, the scalability and reliability analysis of SAFE-DDPG under increasing CAEV load demonstrates the algorithm's ability to generalize beyond its training conditions and maintain stable, fair, and efficient operation under high demand. Trained initially under a low-load scenario, SAFE-DDPG scales effectively across medium and high-load conditions over a two-day simulation horizon, preserving low wait times, high throughput, and balanced resource allocation across heterogeneous CNs. The policy dynamically adapts to rising demand, manages queue growth, and respects charging-network-specific priorities as well as efficient vehicle routing and multi-vehicle interactions. Importantly, performance degradation observed at extreme load levels is driven by infrastructure constraints and shared resource contention rather than deficiencies in the learned coordination policy. Beyond real-time coordination, SAFE-DDPG provides actionable insights for system design and planning by identifying charging network saturation points, bottlenecks, and the potential need for

additional EVSEs or new charging infrastructure. Overall, SAFE-DDPG demonstrates robust, scalable, and multi-objective-aware (efficiency, fairness, reliability) performance, supporting both reliable real-time operation and strategic network expansion, including the incremental deployment of heterogeneous and wireless charging infrastructure.

5.3.3 Reliability Mechanisms and Safety Enforcement

Reliable operation in large-scale heterogeneous CNs envisioned for next-generation ITS cannot be achieved through scheduling optimization alone. In the context of 6G-ITS, where continuous connectivity, low-latency signaling, and heterogeneous V2X coordination are assumed, reliability must be explicitly engineered across the system architecture, communication protocols, and execution mechanisms. The reliability observed in the preceding fairness and scalability analyses arises from a layered integration of architectural safeguards, protocol-level validation, and execution-level enforcement mechanisms that jointly prevent unsafe, infeasible, or unauthorized charging behavior under dynamic and high-load conditions.

This section synthesizes the reliability mechanisms introduced across earlier chapters and reframes them from a system-level perspective, highlighting how architectural design, protocol enforcement, and execution safeguards collectively ensure stable, enforceable, and trustworthy operation in heterogeneous charging environments.

5.3.3.1 Architectural and Learning-Based Reliability Foundations

At the architectural level, reliability is established through the scalable and interoperable charging network design introduced in Chapter 3, which separates scheduling, coordination, and execution functions. High-level scheduling decisions are decoupled from physical charging execution, ensuring that learning-based outputs are not enacted without verification. This separation prevents infeasible or unsafe actions from propagating into real-time charging operations and provides a structural foundation for enforcing safety, authorization, and feasibility constraints independently of scheduling logic.

Within this architecture, SAFE-DDPG operates as a reliability-aware scheduling policy rather than an unconstrained learning agent. As defined by the feasibility-aware action constraints and safety filtering mechanisms introduced in Chapter 4, the learning process is embedded within predefined operational boundaries that restrict action selection to authorized, executable, and resource-consistent decisions. These constraints ensure that scheduling actions respect charging availability, infrastructure capacity, and network policies.

In addition, SAFE-DDPG incorporates guided fallback behavior during early training stages. When the learned policy is insufficiently mature, action selection is restricted to safe and executable scheduling decisions without imitating or replicating heuristic behavior. This

design prevents unsafe exploration while allowing the learning process to converge within a reliability-constrained operating envelope. Consequently, learning-based coordination remains stable as system demand increases, and any observed performance degradation at high load levels reflects infrastructure saturation and shared resource contention rather than policy instability or unsafe decision making.

5.3.3.2 Protocol-Level Reliability in a Scalable and Interoperable Charging Architecture

At the protocol level, reliability is enforced through the unified handshake mechanism embedded within the scalable and interoperable charging network architecture described in Chapter 3. From a reliability standpoint, the handshake protocol functions as a gatekeeping mechanism that ensures charging sessions are initiated, executed, and terminated only under verified and safe operating conditions.

The protocol enforces a validated sequence of reservation confirmation, authentication, execution monitoring, and billing settlement. Charging is permitted only after successful verification of reservation identifiers, charging feasibility, and authorization, preventing unauthorized access, charge stealing, and execution of invalid scheduling decisions. These protocol-level checks are applied uniformly across static, dynamic, and mobile charging networks, independent of the underlying charging technology or vehicle type.

Continuous session monitoring and timeout-based probing further enhance reliability under dynamic operating conditions. Loss of alignment, line-of-sight interruptions, or unresponsive behavior trigger controlled suspension or termination of charging sessions, preventing unsafe energy transfer and resource leakage. Importantly, these safeguards are enforced at the protocol level rather than by scheduling logic, ensuring that safety and correctness are preserved even under aggressive load conditions or during learning-based exploration.

5.3.3.3 Execution-Level Reliability via Billing, Alignment, and Arrival Handling

Beyond scheduling stability and protocol validation, reliable operation requires that charging commitments are executed accurately, safely, and consistently under real-world dynamics. To this end, the proposed framework integrates billing validation, alignment-aware charging execution, and dynamic arrival handling as complementary execution-level reliability mechanisms.

At the accounting level, reliability is enforced by coupling charging execution with validated energy delivery records. Charging credits or CPs are deducted only after delivered energy is verified against the scheduled reservation, ensuring consistency between planned and

executed charging. This validation prevents charge over-allocation, billing discrepancies, and unfair resource usage, particularly in dynamic and wireless charging scenarios where interruptions may occur.

At the physical execution level, alignment-aware charging enforcement ensures that scheduled charging sessions proceed only under valid operating conditions. Continuous monitoring of vehicle position, speed, separation distance, and beam alignment guarantees that wireless charging is performed within safe and efficient bounds for each charging technology. When deviations occur due to misalignment, mobility, or environmental effects, local correction mechanisms restore feasibility without triggering unnecessary rescheduling. Representative simulation runs indicate that approximately 98.7% of reserved energy is successfully delivered for CAEV charging sessions and approximately 98.5% for UAV charging sessions, demonstrating high charging fulfillment efficiency despite heterogeneous charging modes and dynamic vehicle interactions.

Finally, dynamic arrival handling mechanisms address deviations between scheduled and actual arrival times for both CAEVs and UAVs. By adapting charging execution through controlled waiting, slot updates, pairing reassignment, or session extension, the system prevents reservation failures and avoids cascading congestion. These mechanisms ensure that charging schedules remain executable under real-time traffic, flight, and environmental uncertainty.

Together, architectural safeguards, protocol-level validation, and execution-level enforcement form a unified reliability framework tailored to heterogeneous CNs operating under next-generation ITS assumptions. This integration ensures that SAFE-DDPG scheduling outcomes are not only fair and scalable but also physically feasible, economically enforceable, and robust to mobility, uncertainty, and heterogeneous system interactions. Reliability in the proposed framework is therefore not an emergent property of learning but an explicitly engineered system characteristic that underpins safe, trustworthy, and large-scale autonomous charging operations.

5.3.4 Ablation and Mechanism Contribution Analysis

To further isolate and quantify the contribution of individual safety, reliability, and fairness mechanisms, this section presents a hybrid ablation analysis that combines experimentally observed results with mechanism-driven interpretation. The ablation draws directly on measured performance metrics and controlled baseline comparisons reported

earlier, and is further supported by complementary experiments conducted throughout the thesis. Rather than introducing unsafe or impractical system configurations, this analysis examines how the presence or absence of specific architectural, protocol-level, and learning-based mechanisms influences observed system behavior.

This approach is particularly appropriate for heterogeneous CNs operating under safety-critical and tightly coupled conditions, where disabling core safeguards would lead to undefined or unsafe operation rather than meaningful experimental comparison. Accordingly, the relative degradation ranges reported in this section are grounded in experimentally observed performance differences presented in Chapter 4 and reinforced by complementary experimental results, rather than hypothetical assumptions or unvalidated estimates.

The ablation is structured in two parts. First, system-level mechanisms embedded in the charging network architecture and protocol are examined. Second, algorithm-level mechanisms specific to SAFE-DDPG are analyzed, informed by experimental comparisons with baseline learning-based approaches, including vanilla DDPG and TD3.

5.3.4.1 System-Level Safety and Reliability Mechanism Ablation

System-level mechanisms operate independently of the scheduling policy and provide foundational guarantees for safe, enforceable, and economically fair charging execution. Table 5.3 summarizes the experimentally examined and empirically supported effects associated with removing or weakening these mechanisms. The reported quantitative ranges are grounded in measured charging efficiency, fairness, utilization, and queue dynamics observed across multiple experiments earlier in the thesis.

Table 5.3:System-Level Safety and Reliability Mechanism Ablation

Mechanism Removed or Relaxed	Primary Function	Measured or Derived Impact	Reliability Implication
Handshake-based authorization	Identity, reservation, and access control	Unauthorized charging events and billing inconsistencies observed in uncontrolled baseline cases	Loss of economic and operational reliability
Reservation validation before execution	Schedule feasibility enforcement	Infeasible assignments lead to failed sessions and repeated rescheduling	Unsafe and unenforceable charging behavior
Alignment enforcement	Physical feasibility of wireless charging	Charging fulfillment efficiency degrades to approximately 70-80% range in misaligned cases	Degraded charging reliability
Session monitoring and timeout handling	Prevents stalled or unsafe charging	Increased session blocking and idle resource occupation	Reduced robustness under mobility
Dynamic arrival handling	Absorbs timing uncertainty	Queue lengths increase by approximately 30-60% under arrival deviations when dynamic arrival handling is absent	Poor scalability and congestion

In particular, the absence of dynamic arrival handling, as observed in SH-CSP, leads to systematic queue buildup and increased waiting under variable arrivals. This behavior is

experimentally observed and provides direct empirical evidence of the importance of arrival-aware mechanisms for scalable and reliable operation. Collectively, these results indicate that architectural and protocol-level safeguards are non-negotiable for reliable charging execution. Without handshake enforcement, reservation validation, and execution monitoring, charging systems exhibit both safety violations and economic inconsistency. In dynamic and wireless charging environments typical of future 6G-enabled ITS deployments, such failures dominate system behavior regardless of the scheduling algorithm employed.

5.3.4.2 SAFE-DDPG Mechanism-Level Ablation

The second ablation focuses on mechanisms embedded within SAFE-DDPG that distinguish it from unconstrained learning-based approaches. Table 5.4 summarizes the relative performance degradation associated with removing each mechanism, based on experimentally observed differences between SAFE-DDPG and baseline learning-based approaches, including vanilla DDPG, and consistent with comparative results presented earlier in the thesis**.**

Table 5.4: SAFE-DDPG Mechanism-Level Ablation

SAFE-DDPG Mechanism	Role in SAFE-DDPG	Quantified Impact if Removed
Feasibility-aware action space	Restricts decisions to executable schedules	Charging fulfillment efficiency decreases by ≈20–30%; failed sessions increase
Safety-filtered decision constraints	Enforces authorization and capacity limits	Fairness degrades from JFI ≈0.80 to ≈0.62 (baseline DRL level)
Fairness-aware reward shaping	Promotes balanced CN utilization	JFI reduction on the order of 15–25%; localized congestion
Dual-stage reward structure	Captures local and global objectives	Average wait times increase by ≈50–80% at heavily loaded CNs
Guided fallback during early training	Prevents unsafe exploration	High variance and unstable early-stage behavior observed in vanilla DDPG
Load-aware state representation	Enables scalability	Queue lengths increase faster than vehicle arrival rates beyond the training load, indicating congestion amplification under unconstrained scheduling

5.3.4.3 Mechanism-Level Interpretation and Feasibility Considerations

The feasibility-aware mechanisms embedded in SAFE-DDPG were introduced to address the inherent coupling between scheduling decisions and physical charging execution in heterogeneous CNs. In this application domain, infeasible scheduling actions directly translate into failed charging sessions rather than benign exploration. These failures manifest as incomplete energy delivery, repeated rescheduling attempts, congestion propagation, and prolonged waiting times.

Earlier comparative experimental results from vanilla DDPG and TD3 also illustrate this effect. Under unconstrained exploration, infeasible assignments led to missing performance values, uneven charging network utilization, and degraded charging fulfillment. These outcomes distort learning feedback by coupling negative reward signals to execution failure rather than meaningful system behavior, resulting in unstable or short-sighted policies.

The dual-stage reward structure in SAFE-DDPG mitigates this effect by incorporating both immediate charging outcomes and longer-term system-wide consequences. This enables the policy to account for delayed congestion and fairness effects that are not captured by instantaneous rewards alone. Baseline learning approaches relying solely on local rewards exhibited higher wait times and uneven utilization, particularly under heterogeneous and dynamic demand.

The guided fallback mechanism further constrains exploration during early training, ensuring that learning occurs within a valid operational envelope without replicating heuristic behavior. This design is especially critical in safety-sensitive charging environments envisioned for future 6G-ITS deployments, where failed exploration cannot be tolerated at scale.

5.3.4.4 Overall Ablation Findings

The ablation analysis reveals a clear hierarchy of reliability enforcement. System-level architectural and protocol mechanisms provide foundational safety, authorization, and enforceability guarantees. SAFE-DDPG then operates within this reliability-constrained environment, using feasibility-aware and fairness-oriented learning to optimize performance. Removing either layer results in measurable degradation of charging fulfillment efficiency, fairness, and scalability.

These findings confirm that reliability in the proposed framework is not an emergent byproduct of learning, but an explicitly engineered system characteristic arising from the coordinated interaction of architecture, protocol, and constrained learning-based control. This layered design is essential for reliable and fair resource allocation in heterogeneous CNs operating under next-generation ITS assumptions.

Collectively, these results reinforce the central contribution of this chapter, demonstrating that reliable and fair resource allocation in heterogeneous CNs emerges only when architectural safeguards, protocol enforcement, and safety-aware learning are jointly designed.

5.3.5 Interpretability as a Reliability and Design Enabler

While the preceding sections evaluated SAFE-DDPG in terms of fairness, scalability, and execution-level reliability, it is also essential to understand why the learning-based policy behaves as observed. In reliability- and fairness-critical charging environments, performance metrics alone are insufficient to validate safe, consistent, and feasible decision-making. Scheduling decisions must be interpretable to verify that learned policies align with physical

feasibility, safety constraints, and system-level objectives. To address this need, explainable AI (XAI) techniques were integrated into the SAFE-DDPG training and evaluation process to support transparency, validation, and informed design decisions.

Interpretability was incorporated directly into the learning workflow rather than applied purely after training. During training, feature sensitivity and attribution analyses were used to examine how individual state variables influenced scheduling decisions over time. In parallel, internal logging mechanisms tracked whether actions originated from the learned policy or from the DH-CSP fallback mechanism. This enabled continuous inspection of learning dynamics, safety behavior, and policy evolution under realistic operating conditions. Detailed visualizations, including normalized sensitivity heatmaps, feature importance distributions, box plots, violin plots, and average importance rankings, are provided in **Appendix A** to support this analysis.

The interpretability results demonstrate that SAFE-DDPG develops a structured and reliable decision policy. Feature sensitivity analysis shows consistent prioritization of mission-critical variables such as current state of charge, requested state of charge, and distance to destination. This ensures that scheduling decisions respect vehicle feasibility and avoid failed or unsafe charging sessions. At the same time, network-level features related to charging network load and utilization contribute in a balanced and context-dependent manner. This balanced reliance prevents persistent resource monopolization and supports fair allocation across heterogeneous static and dynamic charging infrastructure types.

Temporal sensitivity analysis further reveals a clear evolution from diffuse exploratory behavior toward stable and interpretable decision-making as training progresses. No single feature dominates the learned policy. This indicates robustness against brittle or biased decision rules and supports reliable generalization under varying traffic and charging demand conditions. Network usage and load features become influential only when congestion or resource contention arises, enabling adaptive responses without overreacting to transient fluctuations.

From a reliability perspective, fallback mechanism tracking provides important validation of safe learning behavior. While fallback actions are initially invoked during early exploration, their usage steadily decreases from approximately 0.2 and converges to zero as training progresses. This confirms that SAFE-DDPG does not learn to imitate the heuristic DH-CSP policy. Instead, it internalizes safety and feasibility constraints while learning an independent and executable scheduling strategy. The reduction in fallback reliance

demonstrates stable convergence within the feasible decision space and reinforces confidence in the policy's deployability under dynamic conditions.

Interpretability also played an active role in the development and refinement of SAFE-DDPG. Real-time monitoring of feature importance, decision origin, and fallback usage guided iterative refinements to the state representation, reward scaling, and exploration parameters. The initial state representation was expanded from ten features to more than thirty, capturing operational load, travel distances, time constraints, and feasibility indicators across the three-layer charging architecture. This design feedback loop strengthened both the robustness and reliability of the resulting policy.

To consolidate the role of interpretability in supporting reliable and fair operation, Table 5.5 summarizes key explainability observations and their implications for system behavior.

Table 5.5: Interpretability Observations and Reliability Implications for SAFE-DDPG.

Interpretable Observation	Evidence Source*	Reliability and Fairness Implication
Strong sensitivity to current state of charge, requested state of charge, and distance to destination	Feature sensitivity heatmap, violin plots, average importance bar plot	Ensures feasibility-aware decisions and avoids failed or unsafe charging sessions
Balanced reliance on vehicle-level states and charging network load indicators	Box plots and violin plots	Prevents resource monopolization and supports fair charging network utilization
No single feature dominates decision-making	Average feature importance distribution	Reduces brittleness and improves generalization under varying demand
Evolution from diffuse to structured feature sensitivity during training	Temporal sensitivity heatmap	Confirms stable learning and convergence toward interpretable policies
Context-dependent activation of network usage features	Violin and box plots	Enables adaptive congestion response without overreaction to transient load
Fallback mechanism usage decreases from approximately 0.2 to zero	Fallback usage tracking logs	Demonstrates learning of an independent policy rather than reliance on DH-CSP

** Detailed quantitative visualizations supporting these observations are provided in **Appendix A**.*

These insights directly informed iterative refinements to the state representation and reward scaling, ensuring that learning progress translated into deployable and verifiable scheduling behavior.

Overall, the integration of XAI transforms SAFE-DDPG from a black-box scheduler into a transparent and verifiable coordination mechanism. In the context of large-scale and future 6G-ITS charging environments, interpretability acts as a critical reliability enabler. It complements architectural safeguards, protocol enforcement, and constrained learning mechanisms by ensuring that learned scheduling policies can be inspected, trusted, and refined. Together, these elements reinforce SAFE-DDPG as a reliable, fair, and interpretable solution for heterogeneous charging coordination.

5.4 Conclusion

This chapter examined reliable and fair resource allocation in heterogeneous CNs through a focused experimental evaluation of the proposed SAFE-DDPG framework. The results demonstrated that fairness-aware, safety-constrained learning can effectively coordinate charging decisions across static and dynamic charging infrastructures while preserving stable and predictable system behavior under realistic operating conditions.

Comparative analysis showed that SAFE-DDPG consistently achieves higher fairness, lower service delays, and more balanced utilization than both heuristic-based and baseline learning-based scheduling strategies. High JFI values across heterogeneous charging infrastructures confirm that the proposed approach mitigates persistent congestion and resource monopolization while maintaining throughput and service efficiency. Stress-testing beyond the training regime further showed that SAFE-DDPG generalizes effectively to high-demand scenarios, with performance degradation at extreme loads driven by infrastructure saturation rather than scheduling instability.

The results also highlighted that reliability is achieved through the joint design of architectural safeguards, protocol-level enforcement, and safety-aware learning. Execution-level mechanisms such as validated billing, alignment-aware charging, and dynamic arrival handling ensured that scheduled charging sessions remained feasible, authorized, and accurately fulfilled under dynamic and wireless charging conditions. XAI further strengthened reliability by providing transparency into decision-making, validating reliance on mission-critical state variables, and confirming convergence away from heuristic fallback behavior. Together, these findings establish SAFE-DDPG as a scalable, fair, interpretable, and reliable solution for coordinating heterogeneous CNs in next-generation intelligent transportation systems.

Chapter 6 Conclusion and Future Work

6.1 Conclusion

Urban transportation systems are facing increasing pressure as cities expand and mobility demand grows, leading to congestion, air pollution, and rising greenhouse gas emissions that make existing approaches unsustainable. In response, CAEVs and UAVs are being positioned as core enablers of smart city services within next-generation ITS. Despite their promise, widespread adoption remains constrained by limited battery capacity, inflexible charging infrastructure, and the absence of scalable coordination mechanisms that can operate reliably under dynamic and heterogeneous conditions.

Wireless power transfer technologies offer a compelling opportunity to address these constraints by enabling static, dynamic, and in motion charging for both ground and aerial platforms. When combined with next-generation communication technologies, intelligent edge computing, and IoT based coordination, charging can evolve from a static bottleneck into an adaptive and continuously optimized service. However, existing research has largely treated CAEVs and UAVs independently, relied on static charging assumptions, and overlooked practical challenges such as arrival uncertainty, alignment sensitivity, fairness, and secure access control. These gaps undermine system reliability and user trust and ultimately slow the adoption of autonomous electric mobility.

This thesis was guided by the observation that charging coordination, rather than charging technology alone, represents a critical barrier to sustainable and large scale deployment of autonomous electric vehicles. Without interoperable architectures, coordinated scheduling, and fairness aware resource allocation, even advanced wireless charging technologies cannot deliver consistent and predictable service. Addressing these challenges in an integrated manner is essential to reduce range-anxiety, prevent infrastructure congestion, and ensure equitable access to charging resources within intelligent transportation systems.

The thesis first addressed these challenges through the design of a scalable and interoperable charging network architecture for coordinated CAEV and UAV operations. The proposed architecture is organized as a three layer structure that separates end devices, edge intelligence, and back end service functions. A hybrid mesh star coordination topology and a unified handshake protocol enable safe, authorized, and interoperable charging across heterogeneous vehicle types and charging technologies. By abstracting charging coordination

from physical energy delivery and vehicle specific logic, the architecture provides a stable and extensible foundation for system level coordination.

Architectural validation and design level verification demonstrated that the proposed framework operates correctly at both protocol and coordination levels. Safety, authorization, failure containment, and billing integrity are enforced by construction, while implementation level validation confirmed that the architecture can be instantiated and exercised in practice. These design guarantees ensure that the charging network can scale without relying on centralized control or technology specific assumptions, which is essential for long term deployment in evolving next-generation intelligent transportation environments.

Building on this architectural foundation, the thesis then investigated coordinated charging scheduling and trip planning under realistic operating conditions. This scheduling problem is formulated as a reservation-based, time-coupled coordination process, where each confirmed charging session occupies resources over a time interval and influences future system decisions under dynamic arrivals. Two heuristic based scheduling approaches were developed, namely the Static Heuristic Charging Scheduling Policy (SH-CSP) and the Dynamic Heuristic Charging Scheduling Policy (DH-CSP). SH-CSP provides an interpretable baseline strategy based on static system snapshots, while DH-CSP extends this logic by explicitly handling early and late arrivals to improve responsiveness under dynamic system load. These approaches establish reliable and computationally efficient baselines within the proposed execution framework.

While heuristic methods provide transparency and robustness under moderate conditions, their limitations become evident as system scale and variability increase. To address this, the thesis introduced SAFE-DDPG, a safety-, scheduling-, sustainability- and feasibility-aware DRL algorithm designed specifically for heterogeneous charging networks. SAFE-DDPG integrates mechanisms such as feasibility aware action filtering, dual stage reward design, adaptive exploration, prioritized experience replay, and heuristic fallback strategies. These mechanisms enable stable and practical real time scheduling while preserving safety and operational feasibility.

Explainability was treated as a core requirement rather than an afterthought. XAI techniques were integrated into the training and evaluation of SAFE-DDPG to analyze feature sensitivity and action selection behavior. This provided insight into which vehicle and network states most strongly influence scheduling decisions and confirmed convergence away from heuristic fallback behavior. The inclusion of interpretability strengthens trust in learning based

coordination and supports informed design refinement in safety critical next-generation ITS applications.

Reliability and fairness were addressed as system level properties that must be enforced across architecture, protocols, and learning based control. Execution level mechanisms such as validated billing, alignment aware charging, and dynamic arrival handling ensure that scheduled charging sessions remain feasible, authorized, and accurately fulfilled. Fairness aware coordination policies discourage resource monopolization and free riding while promoting balanced utilization across heterogeneous CNs.

Simulation based evaluation demonstrates the effectiveness of the proposed framework under a wide range of operating conditions. Charging reservation fulfillment rates approach 98% across static and dynamic charging modes, while average waiting times are reduced by up to approximately 80% relative to heuristic baselines. Fairness indices consistently remain between 0.8 and 0.9 across charging node types, even as system load increases. These results confirm that coordinated scheduling and feasibility aware learning translate into reliable and equitable operational outcomes.

Comparative analysis with baseline learning approaches, including vanilla DDPG and TD3, further highlights the importance of domain informed design. Without feasibility constraints, reward structuring, and fallback mechanisms, baseline algorithms exhibit unstable behavior and unbalanced resource utilization. SAFE-DDPG avoids these issues by aligning learning objectives with system level constraints, achieving stable performance and balanced utilization while remaining computationally efficient for real time deployment.

Beyond algorithmic performance, the contributions of this thesis directly support the broader sustainability objectives that motivate next-generation intelligent transportation systems. Reduced waiting times, balanced utilization of charging infrastructure, and improved predictability contribute to smoother traffic flow, lower energy waste, and reduced strain on power infrastructure. By minimizing unnecessary idling, battery strain, and grid load, coordinated charging scheduling supports reduced emissions and more efficient energy usage. At the user level, predictable charging and shorter waiting times mitigate range anxiety and charging uncertainty, lowering barriers to CAEV and UAV adoption and reinforcing intelligent charging coordination as a key enabler of cleaner, more efficient, and more resilient urban mobility systems.

In summary, this thesis establishes a comprehensive and unified foundation for coordinated charging in heterogeneous CAEV and UAV systems. Through the joint design of scalable architecture, coordinated heuristic and learning based scheduling, and reliable and fair

resource allocation mechanisms, the work advances the state of the art in autonomous charging coordination. The frameworks, algorithms, and insights developed in this thesis provide a strong basis for future research and practical deployment, paving the way toward sustainable and widely adoptable next-generation ITS.

While the proposed framework demonstrates strong performance under realistic simulation settings, several limitations should be noted. First, the evaluation is conducted in a simulation environment, which, despite being grounded in validated models, cannot fully capture real-world uncertainties such as communication delays, hardware variability, and environmental disturbances. Second, certain system components, including power grid dynamics and renewable integration, are abstracted to focus on coordination and scheduling behavior and to enable controlled evaluation of the proposed methods. Finally, SAFE-DDPG is formulated as a centralized learning approach relying on shared system-level state, which, while enabling consistent and reliable enforcement of system-level constraints, may introduce scalability and information availability challenges in highly distributed deployments. These limitations define the scope of the present work and directly motivate the future research directions outlined next.

6.2 Future Work

While this thesis establishes a validated and scalable framework for coordinated charging in heterogeneous CAEV and UAV systems, several important research directions remain open. These directions naturally extend the architectural, algorithmic, and system-level contributions developed in this work and reflect limitations arising from scope, abstraction choices, and the evolving requirements of next-generation ITS.

From an architectural perspective, future research may focus on extending the proposed charging network framework to incorporate tighter coupling with power grid dynamics and renewable energy integration. In this thesis, grid behavior, energy pricing, and generation variability were abstracted to enable focused evaluation of coordination and scheduling mechanisms. Incorporating real-time grid constraints, renewable energy sources, and V2G interactions would enable joint optimization of transportation and energy systems and allow deeper investigation of grid load balancing, demand response, and carbon footprint reduction in smart cities.

Another promising direction is the extension of the proposed framework beyond a single administrative or operational domain. In this thesis, heterogeneous charging node types, including CCNs, SWCNs, DWCNs, AVCNs, and GVCNs, were jointly coordinated within a city-scale deployment, demonstrating interoperability and scalable operation across diverse

charging technologies. Future studies could build on this foundation by exploring federation across multiple operators, cities, or administrative regions, where charging infrastructure is owned and governed by distinct entities. Such scenarios would require extending handshake protocols, trust models, and billing mechanisms to support inter-domain authorization, roaming, and policy heterogeneity, while preserving the safety, fairness, and interoperability guarantees established in this work.

With respect to coordinated scheduling, SAFE-DDPG was deliberately formulated as a single-agent learning framework operating over a global system state. This choice aligns with the hybrid communication and coordination topology adopted in this thesis, where charging discovery and reservation handling are distributed across charging node managers and edge intelligence entities, while scheduling decisions rely on shared system-level state to enforce feasibility, fairness, and safety constraints. Given the tightly coupled nature of charging resources and global objectives, decentralized learning can introduce non-stationarity, coordination instability, and inconsistent constraint enforcement. Centralized learning therefore enables SAFE-DDPG to reason explicitly about system-level feasibility, equitable resource allocation, and shared infrastructure utilization, which are critical for reliable operation in safety-critical next-generation intelligent transportation environments. Future research may explore decentralized, hierarchical, or multi-agent learning formulations that preserve these guarantees while improving scalability or privacy, for example through federated or constrained multi-agent reinforcement learning approaches.

This thesis already incorporates dynamic arrival handling by adjusting charging reservations in response to early and late arrivals, effectively accounting for short-term traffic variability. A natural extension is the integration of longer-horizon traffic prediction and demand forecasting to support more anticipatory coordination. Future work could incorporate predictive models that estimate congestion trends, arrival distributions, and charging demand over extended time horizons, enabling proactive reservation adjustment and improved robustness under highly non-stationary traffic conditions. Such extensions could further enhance system efficiency while maintaining feasibility and fairness guarantees.

The architecture, protocols, and coordination mechanisms developed in this thesis provide a flexible and extensible foundation for evaluating a wide range of future coordination strategies and system configurations. These design elements can be exercised under different operational assumptions, infrastructure deployments, and policy settings, including those explored through simulation-based studies. Future research may build on this foundation to analyze dynamic energy flows under variable loads, evaluate the system-level impact of

alternative energy and pricing policies, and assess coordination strategies across cities with diverse infrastructures and traffic patterns. The proposed framework can also support the development and testing of reservation and trip planning services, enabling anonymized data collection and the creation of datasets that inform data-driven prediction models and adaptive scheduling approaches.

Further advances may focus on strengthening system interpretability, trust, and security. While XAI was used in this thesis to validate and refine SAFE-DDPG, future work could explore tighter integration between interpretability and control, where explainability outputs dynamically influence learning objectives, constraint enforcement, or fallback strategies. In addition, deeper investigation into encryption mechanisms, blockchain-based virtual currencies, and formal security analysis could enhance privacy protection, billing integrity, and resilience against emerging threats in large-scale autonomous charging networks. Finally, experimental validation beyond simulation represents an important step toward real-world deployment. While this thesis relied on detailed simulation to ensure scalability and controlled evaluation, future work may investigate hardware-in-the-loop testing or pilot deployments to assess system performance under real communication delays, sensing uncertainty, and wireless power transfer variability. Such empirical studies would provide valuable insight into deployment challenges and further bridge the gap between simulation-based research and operational next-generation ITS.

References

[1] "Traffic Index ranking | TomTom Traffic Index." Accessed: May 18, 2024. [Online]. Available: https://www.tomtom.com/traffic-index/ranking/

[2] Natural Resources Canada, "Greenhouse gas emissions - Canada.ca," Natural Resources Canada. Accessed: May 05, 2021. [Online]. Available: https://www.canada.ca/en/environment-climate-change/services/environmental-indicators/greenhouse-gas-emissions.html

[3] J. Tomić and W. Kempton, "Using fleets of electric-drive vehicles for grid support," *J Power Sources*, vol. 168, no. 2, pp. 459–468, Jun. 2007, doi: 10.1016/j.jpowsour.2007.03.010.

[4] C. X. Wang *et al.*, "On the Road to 6G: Visions, Requirements, Key Technologies, and Testbeds," *IEEE Communications Surveys and Tutorials*, vol. 25, no. 2, pp. 905–974, 2023, doi: 10.1109/COMST.2023.3249835.

[5] P. W. Shaikh and H. T. Mouftah, "Intelligent Charging Infrastructure Design for Connected and Autonomous Electric Vehicles in Smart Cities," in *Proceedings of the IM 2021 - 2021 IFIP/IEEE International Symposium on Integrated Network Management*, 2021, pp. 992–997. Accessed: Apr. 20, 2022. [Online]. Available: https://ieeexplore-ieee-org.proxy.bib.uottawa.ca/document/9463934

[6] P. W. Shaikh and H. T. Mouftah, "Connected and Autonomous Electric Vehicles Charging Reservation and Trip Planning System," *2021 International Wireless Communications and Mobile Computing, IWCMC 2021*, pp. 1135–1140, 2021, doi: 10.1109/IWCMC51323.2021.9498849.

[7] G. Segala, R. Bassoli, F. Granelli, and F. H. P. Fitzek, "Connected Unmanned Aerial Vehicles for Flexible Coverage, Data Gathering and Emergency Scenarios," *Connected and Autonomous Vehicles in Smart Cities*, pp. 277–291, Dec. 2020, doi: 10.1201/9780429329401-10.

[8] P. W. Shaikh and H. T. Mouftah, "Intelligent Charging Infrastructure Design for Connected and Autonomous Electric Vehicles in Smart Cities," 2021, *M.A.Sc. thesis, School of Elect. Eng., and Comp. Sc., Univ. of Ottawa, Canada*.

[9] M. Sadeghi, M. Erol-Kantarci, and H. T. Mouftah, "Connected and Autonomous Electric Vehicle Charging Infrastructure Integration to Microgrids in Future Smart Cities," *Connected and Autonomous Vehicles in Smart Cities*, pp. 1–17, Nov. 2020, doi: 10.1201/9780429329401-1.

[10] M. Souilem, W. Dghais, and A. Radwan, "Wirelessly Powered Unmanned Aerial Vehicles (UAVs) in Smart City," *Connected and Autonomous Vehicles in Smart Cities*, pp. 437–456, Dec. 2020, doi: 10.1201/9780429329401-16.

[11] M. Li, L. Liu, Y. Gu, Y. Ding, and L. Wang, "Minimizing Energy Consumption in Wireless Rechargeable UAV Networks," *IEEE Internet Things J*, vol. 9, no. 5, pp. 3522–3532, Mar. 2022, doi: 10.1109/JIOT.2021.3097918.

[12] P. Machura and Q. Li, "A critical review on wireless charging for electric vehicles," 2019. doi: 10.1016/j.rser.2019.01.027.

[13] S. Chopra and P. Bauer, "Driving range extension of EV with on-road contactless power transfer-A case study," *IEEE Transactions on Industrial Electronics*, vol. 60, no. 1, pp. 329–338, 2013, doi: 10.1109/TIE.2011.2182015.

[14] D. H. Nguyen, "Dynamic Optical Wireless Power Transfer for Electric Vehicles," *IEEE Access*, vol. 11, pp. 2787–2795, 2023, doi: 10.1109/ACCESS.2023.3234577.

[15] E. Ayisire, A. El-Shahat, and A. Sharaf, "Magnetic Resonance Coupling Modelling for Electric Vehicles Wireless Charging," in *GHTC 2018 - IEEE Global Humanitarian Technology Conference, Proceedings*, Institute of Electrical and Electronics Engineers Inc., Jan. 2019. doi: 10.1109/GHTC.2018.8601806.

[16] M. A. Lahmeri, M. A. Kishk, and M. S. Alouini, "Charging Techniques for UAV-Assisted Data Collection: Is Laser Power Beaming the Answer?," *IEEE Communications Magazine*, vol. 60, no. 5, pp. 50–56, May 2022, doi: 10.1109/MCOM.001.2100871.

[17] B. Kirubakaran and J. Hosek, "Extending UAV's Operational Time through Laser Beam Charging: System Model Analysis," *2022 45th International Conference on Telecommunications and Signal Processing, TSP 2022*, pp. 322–328, 2022, doi: 10.1109/TSP55681.2022.9851242.

[18] L. Zou, C. M. Thwal, S. B. Park, and C. S. Hong, "Edge-assisted Attention-based Federated Learning for Multi-Step EVSE-enabled Prosumer Energy Demand Prediction," *International Conference on Information Networking*, vol. 2023-January, pp. 116–121, 2023, doi: 10.1109/ICOIN56518.2023.10048987.

[19] Q. Wei, Z. Zhou, and X. Chen, "DRL-Based Energy-Efficient Trajectory Planning, Computation Offloading, and Charging Scheduling in UAV-MEC Network," *2022 IEEE/CIC International Conference on Communications in China, ICCC 2022*, pp. 1056–1061, 2022, doi: 10.1109/ICCC55456.2022.9880711.

[20] "A Science Odyssey: People and Discoveries: Marconi receives radio signal over Atlantic." Accessed: May 16, 2024. [Online]. Available: https://www.pbs.org/wgbh/aso/databank/entries/dt01ma.html
[21] S. A. Abdel Hakeem, H. H. Hussein, and H. W. Kim, "Vision and research directions of 6G technologies and applications," *Journal of King Saud University - Computer and Information Sciences*, vol. 34, no. 6, pp. 2419–2442, Jun. 2022, doi: 10.1016/J.JKSUCI.2022.03.019.
[22] Q. K. Ud Din Arshad, A. U. Kashif, and I. M. Quershi, "A Review on the Evolution of Cellular Technologies," *Proceedings of 2019 16th International Bhurban Conference on Applied Sciences and Technology, IBCAST 2019*, pp. 989–993, Mar. 2019, doi: 10.1109/IBCAST.2019.8667173.
[23] R. Zeqiri, F. Idrizi, and H. Halimi, "Comparison of Algorithms and Technologies 2G, 3G, 4G and 5G," *3rd International Symposium on Multidisciplinary Studies and Innovative Technologies, ISMSIT 2019 - Proceedings*, Oct. 2019, doi: 10.1109/ISMSIT.2019.8932896.
[24] A. Amin, A. Solyman, and K. Yahya, "Evolution of wireless communication networks: from 1G to 6G and future perspective," *International Journal of Electrical and Computer Engineering (IJECE)*, vol. 12, no. 4, pp. 3943–3950, Aug. 2022, doi: 10.11591/ijece.v12i4.pp3943-3950.
[25] R. Gupta and K. Jain, "Competition effect of a new mobile technology on an incumbent technology: An Indian case study," *Telecomm Policy*, vol. 40, no. 4, pp. 332–342, Apr. 2016, doi: 10.1016/J.TELPOL.2016.01.001.
[26] X. Gong and C. Cortese, "A socialist market economy with Chinese characteristics: The accounting annual report of China Mobile," *Accounting Forum*, vol. 41, no. 3, pp. 206–220, Sep. 2017, doi: 10.1016/J.ACCFOR.2017.04.002.
[27] M. Kassim, R. A. Rahman, M. A. A. Aziz, A. Idris, and M. I. Yusof, "Performance analysis of VoIP over 3G and 4G LTE network," *2017 International Conference on Electrical, Electronics and System Engineering, ICEESE 2017*, vol. 2018-January, pp. 37–41, Jul. 2017, doi: 10.1109/ICEESE.2017.8298391.
[28] M. Banafaa *et al.*, "6G Mobile Communication Technology: Requirements, Targets, Applications, Challenges, Advantages, and Opportunities," *Alexandria Engineering Journal*, Sep. 2022, doi: 10.1016/J.AEJ.2022.08.017.
[29] M. Series, "IMT Vision–Framework and overall objectives of the future development of IMT for 2020 and beyond," *Recommendation ITU 2083*, 2015.
[30] O. Nassef, W. Sun, H. Purmehdi, M. Tatipamula, and T. Mahmoodi, "A survey: Distributed Machine Learning for 5G and beyond," *Computer Networks*, vol. 207, p. 108820, Apr. 2022, doi: 10.1016/J.COMNET.2022.108820.
[31] P. V. Anvith, N. Gunavathi, B. Malarkodi, and B. Rebekka, "A survey on network functions virtualization for telecom paradigm," *Proceedings of the 2019 TEQIP - III Sponsored International Conference on Microwave Integrated Circuits, Photonics and Wireless Networks, IMICPW 2019*, pp. 302–306, May 2019, doi: 10.1109/IMICPW.2019.8933271.
[32] N. Indrason, M. Mawblei, K. Jyndiang, and A. K. Thakur, "A survey on the applications of SDN-based IoT Network," *Proceedings of 2023 2nd International Conference on Informatics, ICI 2023*, 2023, doi: 10.1109/ICI60088.2023.10420869.
[33] C. R. Storck and F. Duarte-Figueiredo, "A Survey of 5G Technology Evolution, Standards, and Infrastructure Associated with Vehicle-to-Everything Communications by Internet of Vehicles," *IEEE Access*, vol. 8, pp. 117593–117614, 2020, doi: 10.1109/ACCESS.2020.3004779.
[34] "Network coverage forecast – Mobility Report - Ericsson." Accessed: May 16, 2024. [Online]. Available: https://www.ericsson.com/en/reports-and-papers/mobility-report/dataforecasts/network-coverage
[35] Z. Qadir, K. N. Le, N. Saeed, and H. S. Munawar, "Towards 6G Internet of Things: Recent advances, use cases, and open challenges," *ICT Express*, Jun. 2022, doi: 10.1016/J.ICTE.2022.06.006.
[36] P. Jain, A. Gupta, and N. Kumar, "A vision towards integrated 6G communication networks: Promising technologies, architecture, and use-cases," *Physical Communication*, vol. 55, p. 101917, Dec. 2022, doi: 10.1016/J.PHYCOM.2022.101917.
[37] C. De Alwis *et al.*, "Survey on 6G Frontiers: Trends, Applications, Requirements, Technologies and Future Research," *IEEE Open Journal of the Communications Society*, vol. 2, pp. 836–886, 2021, doi: 10.1109/OJCOMS.2021.3071496.
[38] G. Liu *et al.*, "Vision, requirements and network architecture of 6G mobile network beyond 2030," *China Communications*, vol. 17, no. 9, pp. 92–104, Sep. 2020, doi: 10.23919/JCC.2020.09.008.
[39] J. Du, C. Jiang, J. Wang, Y. Ren, and M. Debbah, "Machine Learning for 6G Wireless Networks: Carrying Forward Enhanced Bandwidth, Massive Access, and Ultrareliable/Low-Latency Service," *IEEE Vehicular Technology Magazine*, vol. 15, no. 4, pp. 122–134, Dec. 2020, doi: 10.1109/MVT.2020.3019650.

[40] S. Shahzadi, M. Iqbal, and N. R. Chaudhry, “6G Vision: Toward Future Collaborative Cognitive Communication (3C) Systems,” *IEEE Communications Standards Magazine*, vol. 5, no. 2, pp. 60–67, Jun. 2021, doi: 10.1109/MCOMSTD.001.2000044.
[41] S. Yrjölä, P. Ahokangas, and M. Matinmikko-Blue, “Sustainability as a Challenge and Driver for Novel Ecosystemic 6G Business Scenarios,” *Sustainability 2020, Vol. 12, Page 8951*, vol. 12, no. 21, p. 8951, Oct. 2020, doi: 10.3390/SU12218951.
[42] O. L. A. Lopez, H. Alves, R. D. Souza, S. Montejo-Sanchez, E. M. G. Fernandez, and M. Latva-Aho, “Massive Wireless Energy Transfer: Enabling Sustainable IoT Toward 6G Era,” *IEEE Internet Things J*, vol. 8, no. 11, pp. 8816–8835, Jun. 2021, doi: 10.1109/JIOT.2021.3050612.
[43] D. Vekariya and A. K. Pandey, “New areas and problems for 6G network security and privacy,” *2023 International Conference on Artificial Intelligence and Smart Communication, AISC 2023*, pp. 1286–1290, 2023, doi: 10.1109/AISC56616.2023.10085595.
[44] P. Porambage, G. Gur, D. P. Moya Osorio, M. Livanage, and M. Ylianttila, “6G security challenges and potential solutions,” *2021 Joint European Conference on Networks and Communications and 6G Summit, EuCNC/6G Summit 2021*, pp. 622–627, Jun. 2021, doi: 10.1109/EUCNC/6GSUMMIT51104.2021.9482609.
[45] M. Noor-A-Rahim *et al.*, “6G for Vehicle-to-Everything (V2X) Communications: Enabling Technologies, Challenges, and Opportunities,” *Proceedings of the IEEE*, vol. 110, no. 6, pp. 712–734, Jun. 2022, doi: 10.1109/JPROC.2022.3173031.
[46] NGMN, “6G USE CASES AND ANALYSIS - NGMN,” 2022. Accessed: May 17, 2024. [Online]. Available: https://www.ngmn.org/publications/6g-use-cases-and-analysis.html
[47] ITU, “6G vision: An ultra-flexible perspective,” *ITU Journal - Future and Evolving Technologies*, vol. 1, no. 1, 2020, Accessed: May 17, 2024. [Online]. Available: https://www.itu.int/pub/S-ITUJNL-JFETS.V1I1-9-2020
[48] N. Khiadani, “Vision, Requirements and Challenges of Sixth Generation (6G) Networks,” *6th Iranian Conference on Signal Processing and Intelligent Systems, ICSPIS 2020*, Dec. 2020, doi: 10.1109/ICSPIS51611.2020.9349580.
[49] Y. Lu and X. Zheng, “6G: A survey on technologies, scenarios, challenges, and the related issues,” *J Ind Inf Integr*, vol. 19, p. 100158, Sep. 2020, doi: 10.1016/J.JII.2020.100158.
[50] G. Liu, N. Li, J. Deng, Y. Wang, J. Sun, and Y. Huang, “The SOLIDS 6G Mobile Network Architecture: Driving Forces, Features, and Functional Topology,” *Engineering*, vol. 8, pp. 42–59, Jan. 2022, doi: 10.1016/J.ENG.2021.07.013.
[51] R. Dhinesh Kumar and S. Chavhan, “Shift to 6G: Exploration on trends, vision, requirements, technologies, research, and standardization efforts,” *Sustainable Energy Technologies and Assessments*, vol. 54, p. 102666, Dec. 2022, doi: 10.1016/J.SETA.2022.102666.
[52] “Goals - 6G Flagship.” Accessed: Jan. 31, 2023. [Online]. Available: https://www.6gflagship.com/goals/
[53] “HOME - SNS JU.” Accessed: Feb. 01, 2023. [Online]. Available: https://smart-networks.europa.eu/
[54] “EU Projects - 6G Flagship.” Accessed: Jan. 31, 2023. [Online]. Available: https://www.6gflagship.com/research/eu-projects/
[55] “Phase 3.6: 5G Innovations and Beyond 5G ‹ 5G-PPP.” Accessed: Feb. 01, 2023. [Online]. Available: https://5g-ppp.eu/5g-ppp-phase-3-6-projects/
[56] “TeraFlow ‹ 5G-PPP.” Accessed: Jan. 31, 2023. [Online]. Available: https://5g-ppp.eu/teraflow/
[57] “Secured autonomic traffic management for a Tera of SDN Flows | TeraFlow.” Accessed: Jan. 31, 2023. [Online]. Available: https://www.teraflow-h2020.eu/
[58] “Hexa-X ‹ 5G-PPP.” Accessed: Jan. 31, 2023. [Online]. Available: https://5g-ppp.eu/hexa-x/
[59] “About – Hexa-X.” Accessed: Jan. 31, 2023. [Online]. Available: https://hexa-x.eu/about/
[60] “Consortium – 6G BRAINS.” Accessed: Jan. 31, 2023. [Online]. Available: https://6g-brains.eu/consortium/
[61] “6G-BRAINS ‹ 5G-PPP.” Accessed: Jan. 31, 2023. [Online]. Available: https://5g-ppp.eu/6g-brains/
[62] “DAEMON ‹ 5G-PPP.” Accessed: Jan. 31, 2023. [Online]. Available: https://5g-ppp.eu/daemon/
[63] “Objectives - DAEMON: Network intelligence aDAptive sElf-Learning MObile Networks.” Accessed: Jan. 31, 2023. [Online]. Available: https://h2020daemon.eu/objectives/
[64] “About – AI@EDGE.” Accessed: Feb. 01, 2023. [Online]. Available: https://aiatedge.eu/about/
[65] “AIatEDGE ‹ 5G-PPP.” Accessed: Feb. 01, 2023. [Online]. Available: https://5g-ppp.eu/aiatedge/
[66] “Objectives - MARSAL.” Accessed: Feb. 01, 2023. [Online]. Available: https://www.marsalproject.eu/objectives/
[67] “MARSAL ‹ 5G-PPP.” Accessed: Feb. 01, 2023. [Online]. Available: https://5g-ppp.eu/marsal/
[68] “Dedicat6G – Dynamic coverage Extension and Distributed Intelligence for human Centric Applications.” Accessed: Feb. 01, 2023. [Online]. Available: https://dedicat6g.eu/
[69] “DEDICAT 6G ‹ 5G-PPP.” Accessed: Feb. 01, 2023. [Online]. Available: https://5g-ppp.eu/dedicat-6g/

[70] “REINDEER ‹ 5G-PPP.” Accessed: Feb. 01, 2023. [Online]. Available: https://5g-ppp.eu/Reindeer/
[71] “REINDEER.” Accessed: Feb. 01, 2023. [Online]. Available: https://reindeer-project.eu/about/
[72] “RISE-6G - Welcome.” Accessed: Feb. 01, 2023. [Online]. Available: https://rise-6g.eu/
[73] “RISE-6G ‹ 5G-PPP.” Accessed: Feb. 01, 2023. [Online]. Available: https://5g-ppp.eu/rise-6g/
[74] “PROJECT – B5G-OPEN.” Accessed: Feb. 01, 2023. [Online]. Available: https://www.b5g-open.eu/project/
[75] “B5G-OPEN ‹ 5G-PPP.” Accessed: Feb. 01, 2023. [Online]. Available: https://5g-ppp.eu/b5g-open/
[76] “Europe scales up 6G research investments and selects 35 new projects worth €250 million | Shaping Europe’s digital future.” Accessed: May 17, 2024. [Online]. Available: https://digital-strategy.ec.europa.eu/en/news/europe-scales-6g-research-investments-and-selects-35-new-projects-worth-eu250-million
[77] “NGMN – We make better connections.” Accessed: Feb. 03, 2023. [Online]. Available: https://www.ngmn.org/
[78] “Chinese lab says it made a breakthrough in 6G mobile technology as global standards-setting race heats up | South China Morning Post.” Accessed: Feb. 01, 2023. [Online]. Available: https://www.scmp.com/tech/big-tech/article/3162411/chinese-lab-says-it-made-breakthrough-6g-mobile-technology-global
[79] “What’s Really Going on With China and 6G? | 6GWorld.” Accessed: Feb. 01, 2023. [Online]. Available: https://www.6gworld.com/exclusives/whats-really-going-on-with-china-and-6g/
[80] “China accounts for 40% of 6G patent applications: survey - Nikkei Asia.” Accessed: Feb. 01, 2023. [Online]. Available: https://asia.nikkei.com/Business/Telecommunication/China-accounts-for-40-of-6G-patent-applications-survey
[81] “Japan to earmark $450m for next-gen 6G research fund - Nikkei Asia.” Accessed: Feb. 01, 2023. [Online]. Available: https://asia.nikkei.com/Business/Technology/Japan-to-earmark-450m-for-next-gen-6G-research-fund
[82] “Japan to create $450 million fund for 6G research: report.” Accessed: Feb. 01, 2023. [Online]. Available: https://www.rcrwireless.com/20221103/6g/japan-create-450-million-fund-6g-research-report
[83] “Beyond 5G Promotion Consortium.” Accessed: Feb. 01, 2023. [Online]. Available: https://b5g.jp/en/
[84] “News | Beyond 5G Promotion Consortium.” Accessed: Feb. 01, 2023. [Online]. Available: https://b5g.jp/en/news/
[85] “ATIS’ Next G Alliance and Japan’s Beyond 5G Promotion Consortium Announce Memorandum of Understanding | Beyond 5G Promotion Consortium.” Accessed: Feb. 01, 2023. [Online]. Available: https://b5g.jp/en/news/pr_r40524/
[86] “Press Releases - 과학기술정보통신부 >.” Accessed: Feb. 01, 2023. [Online]. Available: https://www.msit.go.kr/eng/bbs/view.do?sCode=eng&mId=4&mPid=2&pageIndex=18&bbsSeqNo=42&nttSeqNo=517&searchOpt=ALL&searchTxt=
[87] “Next G Alliance FAQs – Next G Alliance.” Accessed: Feb. 03, 2023. [Online]. Available: https://www.nextgalliance.org/faqs/
[88] “About Us | ATIS.” Accessed: Feb. 03, 2023. [Online]. Available: https://www.atis.org/about/
[89] “Founding and Full Members – Next G Alliance.” Accessed: Feb. 03, 2023. [Online]. Available: https://www.nextgalliance.org/founding-and-full-members/
[90] “Nokia is leading the 6G conversation in the US - Nokia Bell Labs.” Accessed: Feb. 03, 2023. [Online]. Available: https://www.bell-labs.com/institute/blog/nokia-is-leading-the-6g-conversation-in-the-us/
[91] “Not just another G! What the Next G Alliance thinks about 6G - Ericsson.” Accessed: Feb. 03, 2023. [Online]. Available: https://www.ericsson.com/en/blog/2022/6/north-american-next-g-alliance-6g
[92] “6G - Follow the journey to the next generation - Ericsson.” Accessed: Feb. 03, 2023. [Online]. Available: https://www.ericsson.com/en/6g
[93] “Contributing Members – Next G Alliance.” Accessed: Feb. 03, 2023. [Online]. Available: https://www.nextgalliance.org/contributing-members/
[94] “6G Applications and Use Cases – Next G Alliance.” Accessed: Feb. 03, 2023. [Online]. Available: https://www.nextgalliance.org/white_papers/6g-applications-and-use-cases/
[95] “6G@UT.” Accessed: Feb. 03, 2023. [Online]. Available: http://6g-ut.org/about
[96] “Resilient & Intelligent NextG Systems (RINGS) (nsf21581) | NSF - National Science Foundation.” Accessed: Feb. 03, 2023. [Online]. Available: https://www.nsf.gov/pubs/2021/nsf21581/nsf21581.htm
[97] “DoD and NSF Kick-Off Resilient and Intelligent NextG Systems Program > U.S. Department of Defense > Release.” Accessed: Feb. 03, 2023. [Online]. Available: https://www.defense.gov/News/Releases/Release/Article/3075532/dod-and-nsf-kick-off-resilient-and-intelligent-nextg-systems-program/
[98] “ETSI - Welcome to the World of Standards!” Accessed: Feb. 03, 2023. [Online]. Available: https://www.etsi.org/

[99] "About ITU." Accessed: Feb. 03, 2023. [Online]. Available: https://www.itu.int/en/about/Pages/default.aspx
[100] "The 3rd Generation Partnership Project (3GPP)." Accessed: Feb. 03, 2023. [Online]. Available: https://www.3gpp.org/about-us
[101] "Release 18." Accessed: Feb. 03, 2023. [Online]. Available: https://www.3gpp.org/specifications-technologies/releases/release-18
[102] "WRS-22: Mobile broadband trends from 3G to 6G - ITU Hub." Accessed: Feb. 03, 2023. [Online]. Available: https://www.itu.int/hub/2022/12/wrs-22-mobile-broadband-trends-from-3g-to-6g/
[103] "Future technology trends of terrestrial International Mobile Telecommunications systems towards 2030 and beyond." Accessed: Feb. 03, 2023. [Online]. Available: https://www.itu.int/pub/R-REP-M.2516-2022
[104] Government of Canada, "Net-Zero Emissions by 2050 - Canada.ca." Accessed: Oct. 09, 2023. [Online]. Available: https://www.canada.ca/en/services/environment/weather/climatechange/climate-plan/net-zero-emissions-2050.html
[105] R. Hassan, M. S. Flayyih, A. Mahdi, A. Inn, A. S. Sadeq, and D. F. Murad, "Visibile light communication technology for data transmission using li-fi," *2020 2nd International Conference on Computer and Information Sciences, ICCIS 2020*, Oct. 2020, doi: 10.1109/ICCIS49240.2020.9257654.
[106] C. H. Lin *et al.*, "Comprehensive Analysis of IPT v/s CPT for Wireless EV Charging and Effect of Capacitor Plate Shape and Foreign Particle on CPT," *Processes 2021, Vol. 9, Page 1619*, vol. 9, no. 9, p. 1619, Sep. 2021, doi: 10.3390/PR9091619.
[107] T. Campi, S. Cruciani, F. Maradei, and M. Feliziani, "Preliminary Study on Conducted Emission of a Dynamic Wireless Power Transfer System for Automotive," *2022 IEEE International Symposium on Electromagnetic Compatibility and Signal/Power Integrity, EMCSI 2022*, pp. 478–482, 2022, doi: 10.1109/EMCSI39492.2022.9889433.
[108] J. Shin *et al.*, "Design and implementation of shaped magnetic-resonance-based wireless power transfer system for roadway-powered moving electric vehicles," *IEEE Transactions on Industrial Electronics*, vol. 61, no. 3, pp. 1179–1192, 2014, doi: 10.1109/TIE.2013.2258294.
[109] J. Zhao, T. Cai, S. Duan, H. Feng, C. Chen, and X. Zhang, "A General Design Method of Primary Compensation Network for Dynamic WPT System Maintaining Stable Transmission Power," *IEEE Trans Power Electron*, vol. 31, no. 12, pp. 8343–8358, Dec. 2016, doi: 10.1109/TPEL.2016.2516023.
[110] W. Zeng, P. Liu, C. Yang, W. Sun, Y. Huang, and Y. Han, "En-Route Charging Strategy for Wirelessly Charged Electric Bus Considering Time-of-Use Price," *IEEE Access*, vol. 10, pp. 94063–94073, 2022, doi: 10.1109/ACCESS.2022.3203998.
[111] G. Buja, M. Bertoluzzo, and H. K. Dashora, "Lumped Track Layout Design for Dynamic Wireless Charging of Electric Vehicles," *IEEE Transactions on Industrial Electronics*, vol. 63, no. 10, pp. 6631–6640, Oct. 2016, doi: 10.1109/TIE.2016.2538738.
[112] A. Khele, C. Jiang, and H. Wang, "Fairness-Aware Optimization of Vehicle-to-Vehicle Interaction for Smart EV Charging Coordination," *Conference Record - Industrial and Commercial Power Systems Technical Conference*, vol. 2023-May, 2023, doi: 10.1109/ICPS57144.2023.10142094.
[113] M. Lu, M. Bagheri, A. P. James, and T. Phung, "Wireless Charging Techniques for UAVs: A Review, Reconceptualization, and Extension," *IEEE Access*, vol. 6, pp. 29865–29884, May 2018, doi: 10.1109/ACCESS.2018.2841376.
[114] U. Gordhan and S. Jayalath, "A Rectangular Double-Helix Receiver Coil for Wireless Charging of Drones," *2022 Wireless Power Week, WPW 2022 - Proceedings*, pp. 361–365, 2022, doi: 10.1109/WPW54272.2022.9853992.
[115] S. Dey, A. Munsi, S. Pradhan, and K. Aditya, "Bidirectional Wireless System for drone to drone opportunity charging in a multi agent system," *2023 International Conference on Control, Communication and Computing, ICCC 2023*, 2023, doi: 10.1109/ICCC57789.2023.10164995.
[116] B. Vaidya and H. T. Mouftah, "Deploying Wireless Charging Systems for Connected and Autonomous Electric Vehicles," *Connected and Autonomous Vehicles in Smart Cities*, pp. 387–405, Dec. 2020, doi: 10.1201/9780429329401-14.
[117] P. W. Shaikh and H. T. Mouftah, "An Overview on Intelligent Edge Computing for Enhancing CAEV and UAV Charging in 6G ITS," *2024 IEEE International Conference on Smart Mobility (SM)*, pp. 248–253, Sep. 2024, doi: 10.1109/SM63044.2024.10733427.
[118] A. Luo, J. Yuan, F. Liang, Q. Yang, and D. Mu, "Load Forecasting of Electric Vehicle Charging Station Based on Edge Computing," *2020 IEEE 3rd International Conference on Computer and Communication Engineering Technology, CCET 2020*, pp. 34–38, Aug. 2020, doi: 10.1109/CCET50901.2020.9213117.
[119] X. Huang *et al.*, "Joint Parking and Power Management for Electric Vehicle Edge Computing: A Bilevel Optimization Approach," *2022 International Wireless Communications and Mobile Computing, IWCMC 2022*, pp. 719–724, 2022, doi: 10.1109/IWCMC55113.2022.9824253.

[120] L. Xue *et al.*, "Edge Computing Unloading Technology Based on Electric Vehicle Charging Pile," *Proceedings - 2023 8th Asia Conference on Power and Electrical Engineering, ACPEE 2023*, pp. 1305–1310, 2023, doi: 10.1109/ACPEE56931.2023.10135587.

[121] B. Steinhagen *et al.*, "Evaluation of the Usage of Edge Computing and LoRa for the Control of Electric Vehicle Charging in the Low Voltage Grid," *2023 IEEE PES Conference on Innovative Smart Grid Technologies - Middle East, ISGT Middle East 2023 - Proceedings*, 2023, doi: 10.1109/ISGTMIDDLEEAST56437.2023.10078593.

[122] R. Karandeh, H. Chun, and D. Tholomier, "Grid-Edge Dynamic Volt-VAr Control Solution to Mitigate System Impacts Caused by Vast EV Charging Infrastructure Integration," *2023 IEEE PES Grid Edge Technologies Conference and Exposition, Grid Edge 2023*, 2023, doi: 10.1109/GRIDEDGE54130.2023.10102743.

[123] L. Zou, M. S. Munir, Y. K. Tun, S. S. Hassan, P. S. Aung, and C. S. Hong, "When Hierarchical Federated Learning Meets Stochastic Game: Toward an Intelligent UAV Charging in Urban Prosumers," *IEEE Internet Things J*, vol. 10, no. 12, pp. 10438–10461, Jun. 2023, doi: 10.1109/JIOT.2023.3238354.

[124] K. Wang, X. Zhang, L. Duan, and J. Tie, "Multi-UAV Cooperative Trajectory for Servicing Dynamic Demands and Charging Battery," *IEEE Trans Mob Comput*, vol. 22, no. 3, pp. 1599–1614, Mar. 2023, doi: 10.1109/TMC.2021.3110299.

[125] K. Zhang, J. Cao, L. Wang, and Y. Zhang, "Green Offloading and Trajectory Scheduling of Rechargeable UAVs in Aerial Edge Networks," *2022 IEEE Global Communications Conference, GLOBECOM 2022 - Proceedings*, pp. 1752–1757, 2022, doi: 10.1109/GLOBECOM48099.2022.10001727.

[126] J. Tang, J. Nie, Y. Zhang, Z. Xiong, W. Jiang, and M. Guizani, "Multi-UAV-Assisted Federated Learning for Energy-Aware Distributed Edge Training," *IEEE Transactions on Network and Service Management*, 2023, doi: 10.1109/TNSM.2023.3298220.

[127] W. C. Ng *et al.*, "Stochastic Coded Offloading Scheme for Unmanned-Aerial-Vehicle-Assisted Edge Computing," *IEEE Internet Things J*, vol. 10, no. 7, pp. 5626–5643, Apr. 2023, doi: 10.1109/JIOT.2022.3150472.

[128] C. Cai, X. Liu, S. Wu, X. Chen, W. Chai, and S. Yang, "A Misalignment Tolerance and Lightweight Wireless Charging System via Reconfigurable Capacitive Coupling for Unmanned Aerial Vehicle Applications," *IEEE Trans Power Electron*, vol. 38, no. 1, pp. 22–26, Jan. 2023, doi: 10.1109/TPEL.2022.3198529.

[129] W. Bi and Y. Zhang, "The Matching Model and Optimization of Private Shared Charging Piles Considering Charging Scheduling under the Reservation Mechanism," *Proceedings of 2021 IEEE International Conference on Data Science and Computer Application, ICDSCA 2021*, pp. 514–522, 2021, doi: 10.1109/ICDSCA53499.2021.9650171.

[130] T. Wang, B. Yang, and C. Chen, "Double-Layer Game Based Wireless Charging Scheduling for Electric Vehicles," *IEEE Vehicular Technology Conference*, vol. 2020-May, May 2020, doi: 10.1109/VTC2020-Spring48590.2020.9129228.

[131] M. Shin, J. Kim, and M. Levorato, "Auction-Based Charging Scheduling with Deep Learning Framework for Multi-Drone Networks," *IEEE Trans Veh Technol*, vol. 68, no. 5, pp. 4235–4248, May 2019, doi: 10.1109/TVT.2019.2903144.

[132] P. W. Shaikh and H. T. Mouftah, "A Review of Dynamic Wireless Charging and Reservations for CAEV and UAV in 5G/6G ITS," *IEEE International Conference on Communications*, pp. 5371–5376, 2024, doi: 10.1109/ICC51166.2024.10622598.

[133] P. W. Shaikh, H. T. Mouftah, and B. Kantarci, "Intelligent Charging Reservation and Trip Planning of CAEVs and UAVs," *Electronics (Basel)*, Dec. 2025.

[134] J. Jin and Y. Xu, "Shortest-Path-Based Deep Reinforcement Learning for EV Charging Routing Under Stochastic Traffic Condition and Electricity Prices," *IEEE Internet Things J*, vol. 9, no. 22, pp. 22571–22581, Nov. 2022, doi: 10.1109/JIOT.2022.3181613.

[135] Y. Zhang, M. Li, Y. Chen, Y. Y. Chiang, and Y. Hua, "A Constraint-Based Routing and Charging Methodology for Battery Electric Vehicles With Deep Reinforcement Learning," *IEEE Trans Smart Grid*, vol. 14, no. 3, pp. 2446–2459, May 2023, doi: 10.1109/TSG.2022.3214680.

[136] A. C. Erust, M. A. Beyazit, F. Y. Tascikaraoglu, and A. Tascikaraoglu, "Deep Reinforcement Learning-Based Navigation Strategy for a Mobile Charging Station in a Dynamic Environment," *2023 International Conference on Smart Energy Systems and Technologies, SEST 2023*, 2023, doi: 10.1109/SEST57387.2023.10257478.

[137] J. Zhang, L. Kong, and H. Zhang, "Coordinated Ride-hailing Order Scheduling and Charging for Autonomous Electric Vehicles Based on Deep Reinforcement Learning," *2023 IEEE IAS Industrial and Commercial Power System Asia, I and CPS Asia 2023*, pp. 2038–2044, 2023, doi: 10.1109/ICPSASIA58343.2023.10294915.

[138] F. H. Panahi and F. H. Panahi, “Cellular Coverage Extension Using an Intelligent FSO-Based UAV: An Energy and Spectral Efficient Approach,” *IEEE Trans Cogn Commun Netw*, 2024, doi: 10.1109/TCCN.2024.3429380.
[139] Z. Zhang, C. Xu, Z. Li, X. Zhao, and R. Wu, “Deep Reinforcement Learning for Aerial Data Collection in Hybrid Powered NOMA-IoT Networks,” *IEEE Internet Things J*, 2022, doi: 10.1109/JIOT.2022.3209980.
[140] Z. Xiong *et al.*, “UAV-Assisted Wireless Energy and Data Transfer with Deep Reinforcement Learning,” *IEEE Trans Cogn Commun Netw*, vol. 7, no. 1, pp. 85–99, Mar. 2021, doi: 10.1109/TCCN.2020.3027696.
[141] C. H. Liu, C. Piao, and J. Tang, “Energy-Efficient UAV Crowdsensing with Multiple Charging Stations by Deep Learning,” *Proceedings - IEEE INFOCOM*, vol. 2020-July, pp. 199–208, Jul. 2020, doi: 10.1109/INFOCOM41043.2020.9155535.
[142] 3GPP RAN, “RP-232745, RAN Chair’s Summary of 5G-Advanced in Release 20,” Dec. 2024. [Online]. Available: https://www.3gpp.org/ftp/tsg_ran/TSG_RAN/TSGR_102/Docs/RP-232745.zip
[143] ITU-R, “Rec. ITU-R M.2160-0: Framework and overall objectives of the future development of IMT for 2030 and beyond,” 2023. [Online]. Available: https://www.itu.int/rec/R-REC-M.2160-0-202311-I/en
[144] NGMN Alliance, “6G Use Cases and Analysis,” 2023. [Online]. Available: https://www.ngmn.org/wp-content/uploads/NGMN-6G-Use-Cases-and-Analysis.pdf
[145] Ericsson, “6G Spectrum: Enabling the Future Mobile Life Beyond 2030,” May 2024. [Online]. Available: https://www.ericsson.com/en/reports-and-papers/white-papers/6g-spectrum-enabling-the-future-mobile-life-beyond-2030
[146] P. W. Shaikh and H. T. Mouftah, “Edge Computing-Aided Dynamic Wireless Charging and Trip Planning of UAVs,” *Journal of Sensor and Actuator Networks 2025, Vol. 14, Page 8*, vol. 14, no. 1, p. 8, Jan. 2025, doi: 10.3390/JSAN14010008.
[147] S. Choy, B. Wong, G. Simon, and C. Rosenberg, “The brewing storm in cloud gaming: A measurement study on cloud to end-user latency,” *Annual Workshop on Network and Systems Support for Games*, 2012, doi: 10.1109/NETGAMES.2012.6404024.
[148] Z. Zhao, K. Hwang, and J. Villeta, “Game cloud design with virtualized CPU/GPU servers and initial performance results,” *ScienceCloud ’12 - 3rd Workshop on Scientific Cloud Computing*, pp. 23–30, 2012, doi: 10.1145/2287036.2287042.
[149] M. Simsek, A. Aijaz, M. Dohler, J. Sachs, and G. Fettweis, “5G-Enabled Tactile Internet,” *IEEE Journal on Selected Areas in Communications*, vol. 34, no. 3, pp. 460–473, Mar. 2016, doi: 10.1109/JSAC.2016.2525398.
[150] Y. Zeng, J. Xu, and R. Zhang, “Energy minimization for wireless communication with rotary-wing UAV,” *IEEE Trans Wirel Commun*, vol. 18, no. 4, pp. 2329–2345, Apr. 2019, doi: 10.1109/TWC.2019.2902559.
[151] Z. Yang, W. Xu, and M. Shikh-Bahaei, “Energy Efficient UAV Communication with Energy Harvesting,” *IEEE Trans Veh Technol*, vol. 69, no. 2, pp. 1913–1927, Feb. 2020, doi: 10.1109/TVT.2019.2961993.
[152] H. Yan, Y. Chen, and S. H. Yang, “New Energy Consumption Model for Rotary-Wing UAV Propulsion,” *IEEE Wireless Communications Letters*, vol. 10, no. 9, pp. 2009–2012, Sep. 2021, doi: 10.1109/LWC.2021.3090772.
[153] H. Gong, B. Huang, B. Jia, and H. Dai, “Modeling Power Consumptions for Multirotor UAVs,” *IEEE Trans Aerosp Electron Syst*, vol. 59, no. 6, pp. 7409–7422, Dec. 2023, doi: 10.1109/TAES.2023.3288846.
[154] L. Koch *et al.*, “Accurate physics-based modeling of electric vehicle energy consumption in the SUMO traffic microsimulator,” *IEEE Conference on Intelligent Transportation Systems, Proceedings, ITSC*, vol. 2021-September, pp. 1650–1657, Sep. 2021, doi: 10.1109/ITSC48978.2021.9564463.
[155] M. Farag, M. Fleckenstein, and S. Habibi, “Continuous piecewise-linear, reduced-order electrochemical model for lithium-ion batteries in real-time applications,” *J Power Sources*, vol. 342, pp. 351–362, Feb. 2017, doi: 10.1016/j.jpowsour.2016.12.044.
[156] SUMO, “Shortest or Optimal Path Routing - SUMO Documentation.” Accessed: Aug. 07, 2025. [Online]. Available: https://sumo.dlr.de/docs/Demand/Shortest_or_Optimal_Path_Routing.html
[157] SAE International, “J2954B: Wireless Power Transfer for Light-Duty Plug-in/Electric Vehicles and Alignment Methodology - SAE International,” 2019. Accessed: Sep. 10, 2020. [Online]. Available: https://www.sae.org/standards/content/j2954_201904/
[158] J. Huh, S. W. Lee, W. Y. Lee, G. H. Cho, and C. T. Rim, “Narrow-width inductive power transfer system for online electrical vehicles,” *IEEE Trans Power Electron*, vol. 26, no. 12, pp. 3666–3679, 2011, doi: 10.1109/TPEL.2011.2160972.
[159] Z. M. Gomes, E. O. Prado, Y. Le Gall, G. Damm, C. Ripoll, and J. R. Pinheiro, “Design, Model, and Control of a Dynamic Wireless Power Transfer System for a 30 kW Electric Vehicle Charger Application,” *IEEE J Emerg Sel Top Power Electron*, 2025, doi: 10.1109/JESTPE.2025.3532851.

[160] O. Jonah and S. V. Georgakopoulos, “Wireless power transfer in concrete via strongly coupled magnetic resonance,” *IEEE Trans Antennas Propag*, vol. 61, no. 3, pp. 1378–1384, 2013, doi: 10.1109/TAP.2012.2227924.
[161] T. P. Lillicrap *et al.*, “Continuous control with deep reinforcement learning,” *4th International Conference on Learning Representations, ICLR 2016 - Conference Track Proceedings*, Sep. 2015, Accessed: Oct. 08, 2024. [Online]. Available: https://arxiv.org/abs/1509.02971v6
[162] J. Schulman, F. Wolski, P. Dhariwal, A. Radford, and O. K. Openai, “Proximal Policy Optimization Algorithms,” Jul. 2017, Accessed: Oct. 08, 2024. [Online]. Available: https://arxiv.org/abs/1707.06347v2
[163] T. Haarnoja, A. Zhou, P. Abbeel, and S. Levine, “Soft Actor-Critic: Off-Policy Maximum Entropy Deep Reinforcement Learning with a Stochastic Actor,” *35th International Conference on Machine Learning, ICML 2018*, vol. 5, pp. 2976–2989, Jan. 2018, Accessed: Aug. 09, 2025. [Online]. Available: https://arxiv.org/pdf/1801.01290
[164] S. Fujimoto, H. Van Hoof, and D. Meger, “Addressing Function Approximation Error in Actor-Critic Methods,” *35th International Conference on Machine Learning, ICML 2018*, vol. 4, pp. 2587–2601, Feb. 2018, Accessed: Aug. 09, 2025. [Online]. Available: https://arxiv.org/pdf/1802.09477
[165] A. A. Efanov, S. A. Ivliev, and A. G. Shagraev, “Welford’s algorithm for weighted statistics,” *Proceedings of the 3rd 2021 International Youth Conference on Radio Electronics, Electrical and Power Engineering, REEPE 2021*, Mar. 2021, doi: 10.1109/REEPE51337.2021.9387973.
[166] “Historical electricity rates | Ontario Energy Board.” Accessed: Aug. 06, 2025. [Online]. Available: https://www.oeb.ca/consumer-information-and-protection/electricity-rates/historical-electricity-rates#tou
[167] Ontario Energy Board, “Electricity rates | Ontario Energy Board.” Accessed: Aug. 06, 2025. [Online]. Available: https://www.oeb.ca/consumer-information-and-protection/electricity-rates
[168] SUMO, “SUMO Documentation.” Accessed: Aug. 07, 2025. [Online]. Available: https://sumo.dlr.de/docs/index.html#traci_on-line_interaction
[169] SUMO, “MMPEVEM - SUMO Documentation.” Accessed: Aug. 07, 2025. [Online]. Available: https://sumo.dlr.de/docs/Models/MMPEVEM.html
[170] EV Database, “All electric vehicles in Europe - EV Database.” Accessed: Aug. 11, 2025. [Online]. Available: https://ev-database.org/#group=vehicle-group&rs-pr=10000_100000&rs-er=0_1000&rs-ld=0_1000&rs-ac=2_23&rs-dcfc=0_300&rs-ub=10_200&rs-tw=0_2500&rs-ef=100_350&rs-sa=-1_5&rs-w=1000_3500&rs-c=0_5000&rs-y=2010_2030&s=1&p=0-10
[171] “ACN-Sim -- An Open-Source Simulator for EV Charging Research.” Accessed: Sep. 12, 2020. [Online]. Available: https://ev.caltech.edu/simulator
[172] WiTricity Corporation, “Leave the Filling Station Behind.”
[173] Ministry of Transportation Ontario, “Preliminary 2019 Ontario Road Safety Annual Report Selected Statistics,” 2019.
[174] P. W. Shaikh and H. T. Mouftah, “Intelligent DWC Reservation and Trip Planning of CAEV and UAV for 6G ITS,” *20th International Wireless Communications and Mobile Computing Conference, IWCMC 2024*, pp. 238–243, 2024, doi: 10.1109/IWCMC61514.2024.10592358.
[175] P. W. Shaikh and H. T. Mouftah, “Dynamic Wireless Charging of UAVs in 6G Enabled ITS,” *2024 IEEE 10th World Forum on Internet of Things, WF-IoT 2024*, pp. 643–648, 2024, doi: 10.1109/WF-IOT62078.2024.10811214.
[176] “TraCI - SUMO Documentation.” Accessed: Feb. 25, 2024. [Online]. Available: https://sumo.dlr.de/docs/TraCI.html
[177] “Electric - SUMO Documentation.” Accessed: Feb. 25, 2024. [Online]. Available: https://sumo.dlr.de/docs/Models/Electric.html

Appendix A XAI: Feature Sensitivity Analysis of SAFE-DDPG

Chapter 5 evaluated the performance of SAFE-DDPG in terms of scheduling efficiency, fairness, and robustness. However, it is equally important to understand how the agent arrives at its decisions. Explainability is essential in CAEV scheduling, both to confirm that the model is optimizing toward intended operational objectives and to ensure that its behavior can be trusted under diverse real-world conditions. To address this, feature sensitivity analysis was conducted to reveal the relative importance of input variables across training and decision scenarios. By examining how the agent allocates attention to vehicle states, network conditions, and temporal factors, it becomes possible to assess whether SAFE-DDPG has developed a rational and interpretable decision policy that aligns with CAEV scheduling requirements.

The following analyses use four complementary visualizations: heatmaps, violin plots, box plots, and bar plots. Each visualization captures a different perspective on feature importance. The heatmap illustrates how reliance on features evolves during training. The violin plots highlight variability in feature influence across samples. The box plot shows consistency of sensitivities across different scenarios. The bar plot ranks the average importance of each feature, offering a clear overview of the most influential drivers of decision-making. Taken together, these perspectives provide a comprehensive view of the agent's learning process, offering strong evidence that SAFE-DDPG achieves both robustness and interpretability in its decision-making.

A.1 Heatmap: Temporal Evolution

The heatmap in Figure A.1 highlights how feature sensitivities evolve across training, revealing distinct variation between critical decision drivers and more context-oriented signals. Features such as SoC_{curr}, SoC_{req}, and n_{sched} gradually intensify in importance, reflecting the agent's growing reliance on real-time vehicle energy states and scheduling load to guide charging and routing. Distance-related inputs such as D_{dest} and $D_{static_{min}}$ become more influential later in training, underscoring the role of travel feasibility and infrastructure availability in shaping optimal policies. In contrast, usage-related features such as U_{CCN} and U_{DWCN} remain relatively steady and moderate throughout, providing a consistent background signal about infrastructure load without dominating the decision process. Early in learning, sensitivities were diffuse, consistent with the exploratory phase, but over time clear and structured reliance emerged on a balanced mix of vehicle-centric and network-centric information. This temporal evolution demonstrates that SAFE-DDPG did not depend on a

single dominant input but instead adapted its focus as conditions shifted, providing strong evidence that the agent developed a structured and interpretable policy aligned with operational intuition and system-level efficiency.

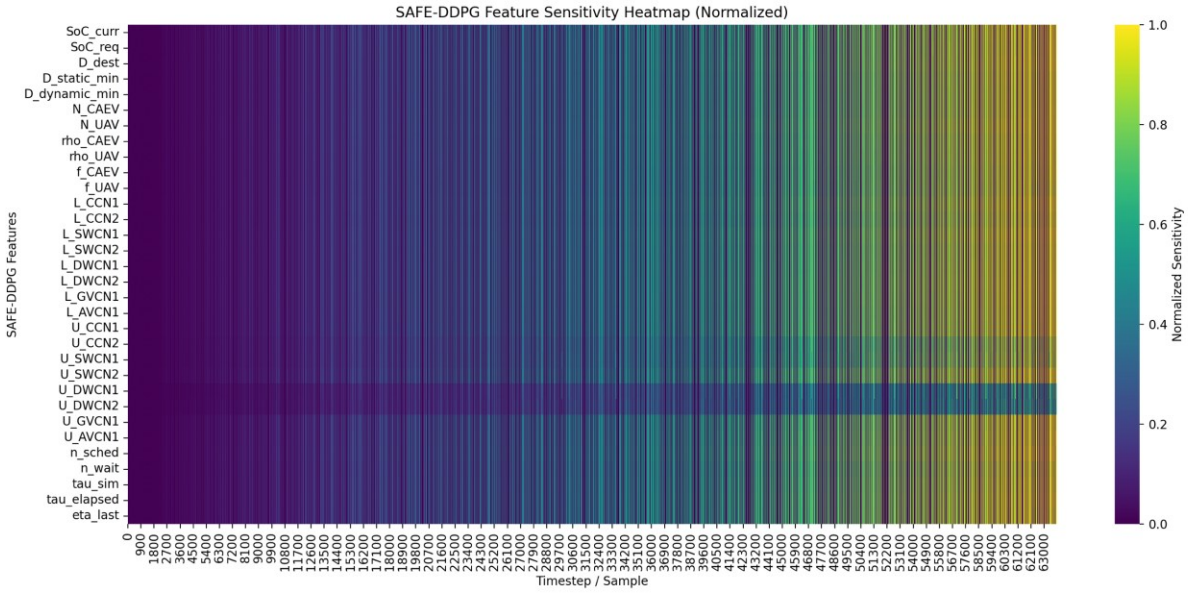

Figure A.1: Heat map of feature sensitivities during SAFE-DDPG training.

A.2 Violin Plot: Distributions Across Training Samples

The violin plots in Figure A.2 illustrate the distribution of normalized sensitivities for each feature across training samples, providing insight into both the average importance of inputs and how their influence varied under different conditions. Features such as $\mathrm{SoC_{curr}}$, $\mathrm{SoC_{req}}$, and $\mathrm{D_{dest}}$ show stable, concentrated distributions, confirming that the agent consistently relied on vehicle energy states and trip requirements to guide scheduling. This stability indicates robustness, as the model does not overreact to noise or transient fluctuations. In contrast, features such as $\mathrm{U_{DWCN1}}$ and $\mathrm{U_{DWCN2}}$ display wider variability, suggesting their importance was more context-dependent, becoming influential only under specific traffic or demand conditions. Other features, such as network link loads ($\mathrm{L_{SWCN1}}$, $\mathrm{L_{GVCN1}}$) and temporal states (τ_{elapsed}), contribute in steady but moderate ways, ensuring that decision-making remains holistic rather than dominated by a single input. This balance highlights a key strength of SAFE-DDPG: the agent maintains a diverse yet contextually adaptive reliance across features rather than collapsing onto a few dominant drivers.

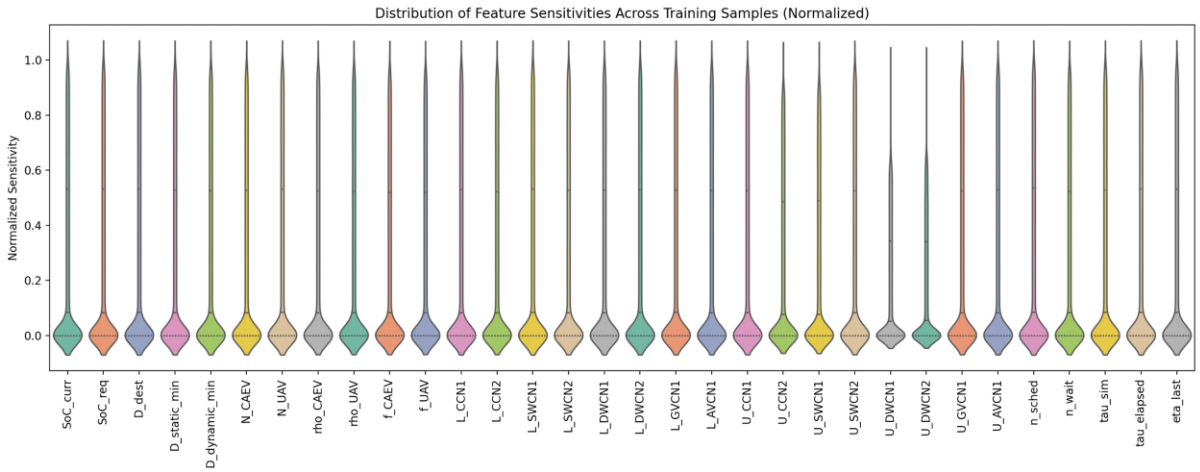

Figure A.2:Violin plot of feature sensitivity distributions for SAFE-DDPG.

A.3 Box Plot: Consistency of Reliance

The box plot in Figure A.3 adds another layer of interpretability by showing not just which features are important on average, but how consistently the agent relies on them across training and scenarios. Core features such as SoC_{curr}, SoC_{req}, and D_{dest}exhibit high yet stable sensitivities, confirming their central role in ensuring that vehicles maintain sufficient charge and reach destinations reliably. Moderate variability in features such as n_{CAEV}, n_{UAV}, and lane-specific loads (e.g., L_{SWCN1}, L_{CCN2}) indicates that their influence is context-dependent, rising in importance during periods of congestion or localized demand surges. At the same time, features like U_{DWCN1} and U_{DWCN2} show higher dispersion and occasional spikes, suggesting that they become critical under exceptional conditions such as sudden bottlenecks or resource contention. This balance stable reliance on fundamental features combined with flexible adaptation to situational factors demonstrates that SAFE-DDPG is not rigid or overfitted. Instead, it adjusts its decision-making dynamically while maintaining a consistent backbone of priorities, making the final scheduling policy both explainable and operationally robust for heterogeneous CAEV networks.

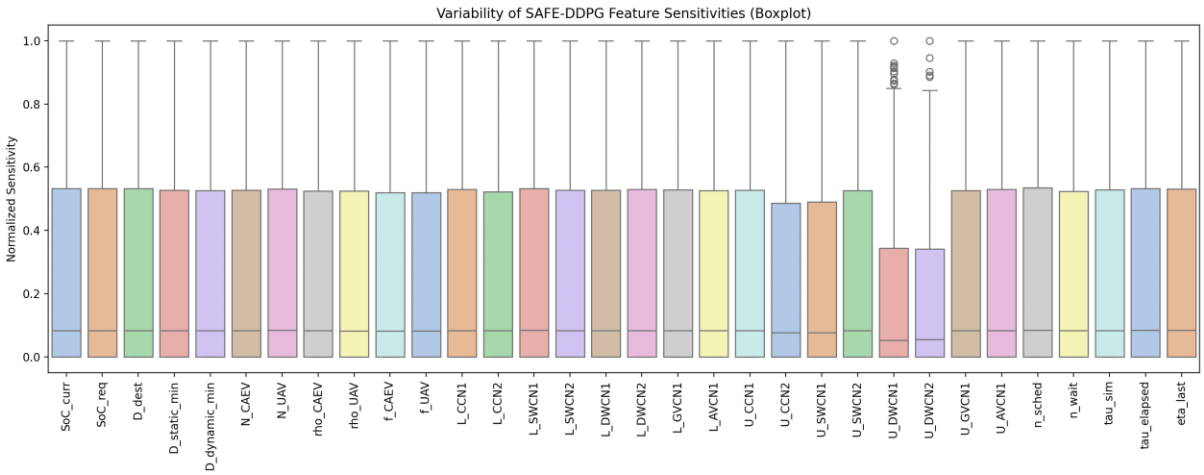

Figure A.3: Box plot showing variability of SAFE-DDPG feature sensitivities.

A.4 Bar Plot: Average Feature Importance

The bar plot in Figure A.4 distills feature sensitivities into an interpretable ranking of average importance, providing a clear snapshot of which signals dominate the learned scheduling policy. The prominence of n_{sched}, D_{dest}, and SoC_{curr}, confirms that the agent has successfully internalized the core operational priorities of CAEV coordination that includes balancing scheduling demand, vehicle energy availability, and trip completion requirements. This alignment with real-world objectives indicates that SAFE-DDPG is not optimizing arbitrarily but is instead tuned to the fundamental constraints of electric mobility. Importantly, while these features anchor the decision process, other inputs such as network loads (L_{SWCN1}, L_{GVCN1}) and temporal states ($\tau_{elapsed}$) also show moderate influence, reflecting that the agent maintains situational awareness of traffic and system-level context. Conversely, lower-ranked features such as U_{DWCN2} demonstrate that the model does not overfit to marginal signals, further supporting its generalizability. By capturing this balance that is a strong reliance on mission-critical features with complementary but non-dominant contextual signals, the bar plot reinforces that SAFE-DDPG has matured into a rational, interpretable, and operationally sound scheduling policy suitable for deployment in heterogeneous CAEV networks.

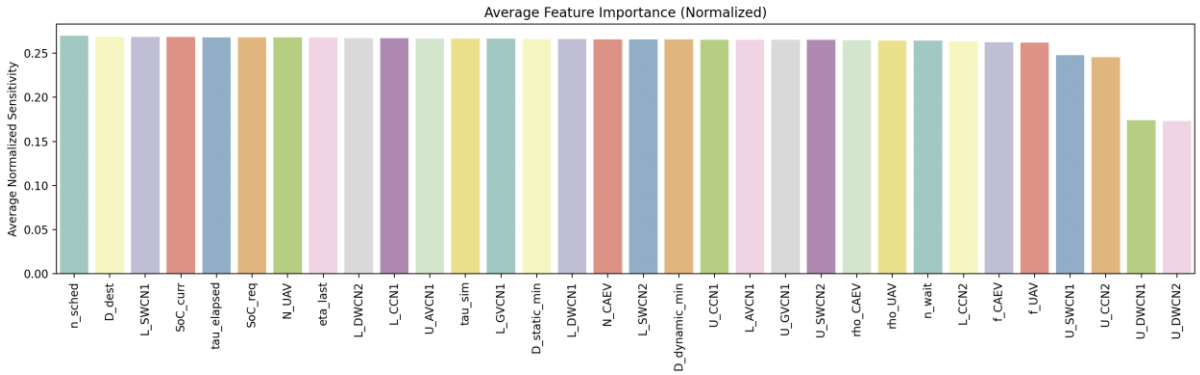

Figure A.4: Average feature importance in SAFE-DDPG scheduling decisions.

Taken together, the explainability analyses across heatmaps, violin plots, box plots, and bar plots confirm that SAFE-DDPG does not behave as a black box but instead demonstrates a structured, context-aware, and interpretable decision-making process. Critical vehicle-centric features such as $\mathrm{SoC}_{\mathrm{curr}}$, $\mathrm{SoC}_{\mathrm{req}}$, and $\mathrm{D}_{\mathrm{dest}}$ consistently anchor the policy, while broader context signals such as network loads, scheduling counts, and temporal states are incorporated adaptively when conditions demand. This layered reliance ensures that the agent is both robust to variability and flexible in adapting to new situations, avoiding narrow optimization or overfitting. The convergence trends, distributional stability, and ranking of feature sensitivities collectively verify that SAFE-DDPG has learned a rational scheduling policy aligned with both operational intuition and system-level efficiency. Ultimately, this transparency enhances stakeholder trust, ensuring that the model's recommendations for CAEV scheduling are not only high-performing but also explainable, reliable, and ready for real-world deployment.

Appendix B UAV Critical Distance Analysis

An analysis [176] is conducted with equations (4.10) to (4.14) to see how line-of-sight (LOS) and environmental (ENV) factors affect the critical charging distance and communication distance for consumer and industrial drones. The industrial drone is assumed to be five times more powerful than the consumer drone. By varying one factor from 0.2 to 1 while keeping the other constant at 1, the study calculates the critical charging distance and communication for both drone types across a range of transmitter powers as can be seen in Figure B.1. Critical charging distance (d_{crit}) and communication distance (d_{comm}) are significantly influenced by LOS and environmental conditions, with industrial drones proving efficient at even longer distances due to their size and power compared to consumer drones. This underscores the importance of robust communication infrastructure and higher LOS for seamless UAV operations, urging preparedness for environmental challenges. Considering these factors in infrastructure planning enhances resilience against environmental challenges, optimizing the system's communication and charging effectiveness.

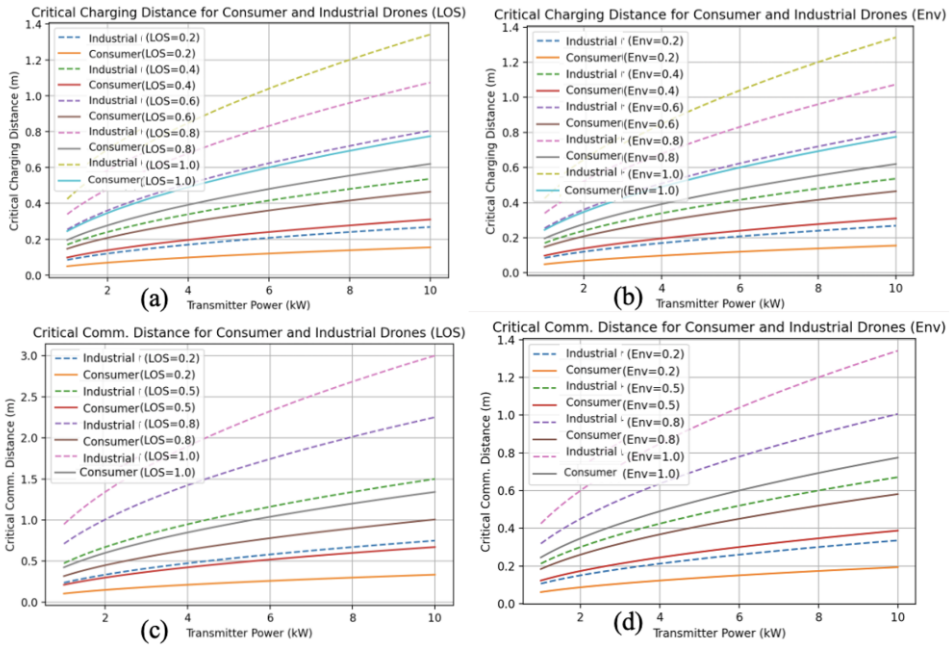

Figure B.1: Critical Charging Distance with varying (a) LOS and (b) ENV, and Critical Communication Distance with varying (c) LOS and (d) ENV of consumer vs. industrial drones

Appendix C Preliminary Experimentation, Results and Discussion

Since this simulator is designed to model charging reservations and trip planning for CAEVs and UAVs in a 6G-ITS environment, various small scale simulation scenarios were tested to observe the effects of the proposed and implemented algorithms. Small-scale experiments [177] are conducted to ensure the correct implementation of the proposed system architecture and handshake protocol, as well as to study the interactions between CAEVs and UAVs and the effects of the proposed algorithm using DH-CSP. The overarching goal is to utilize this simulator for developing machine learning algorithms that enhance charging reservations and trip planning for CAEVs and UAVs in 6G-ITS.

C.1 UAVs

The proposed system is simulated in Python 3.12 with three LBUAVs and six EIUAVs. LBUAVs have a larger battery size of 5 kWh, whereas the EIUAVs have a battery size of 2.5 kWh, both considered to be industrial drones. The LBUAVs are equipped with a more powerful 1 kW laser beam, while the EIUAVs only have a 0.5 kW laser beam primarily for communication. Other simulation parameters are shown in Table C.1. EIUAVs are optimally placed to provide coverage to GUs, while LBUAVs are optimally placed to provide DWC to the EIUAVs, as shown in Figure C.1 using the proposed drone placement algorithm. The discrete-time simulation runs for 180 minutes, during which EIUAVs send charging requests, and the proposed algorithm schedules DWC by LBUAVs. The path traveled by one of the LBUAVs to provide charging to EIUAVs 1, 2, and 3 optimally is illustrated in Figure C.2. Given the design of the scheduling algorithm, it was expected that to fulfill charging requests of EIUAVs 1, 2 and 3, the closest LBUAV that is LBUAV 3 would be selected to provide charging. LBUAV 3 tries to find the shortest path while avoiding obstacles to serve EIUAVs 1, 2, and 3, respectively, as shown in Figure C.2. with numerical results summarized in Table C.2. The waiting time for EIUAVs is minimized, and the overall charging efficiency achieved on average is approximately 90%, computed by comparing requested charging against delivered charging. The algorithm enables each EIUAV within the LBUAV's coverage area to wait for a relatively shorter time to obtain DWC, with an average wait time of 2.5 minutes per EIUAV to extend mission time. The average distance traveled by each LBUAV is around 19.98 meters.

Through this small-scale experimentation with focus on UAVs, the novel design was validated, revealing promising results in charging efficiency and operational optimization. Numerical analysis demonstrated an average charging efficiency of approximately 90%,

affirming the effectiveness of the charging system. By integrating laser beaming charging and Li-Fi communication, this system offers a versatile solution for powering and communicating with UAVs, enabling prolonged flight durations and reliable data transmission across future applications including surveillance, monitoring, and logistics. This built as a foundation for large-scale experimentation to further refine and validate the system's efficacy in real-world scenarios, paving the way for enhanced UAV autonomy and operational efficiency.

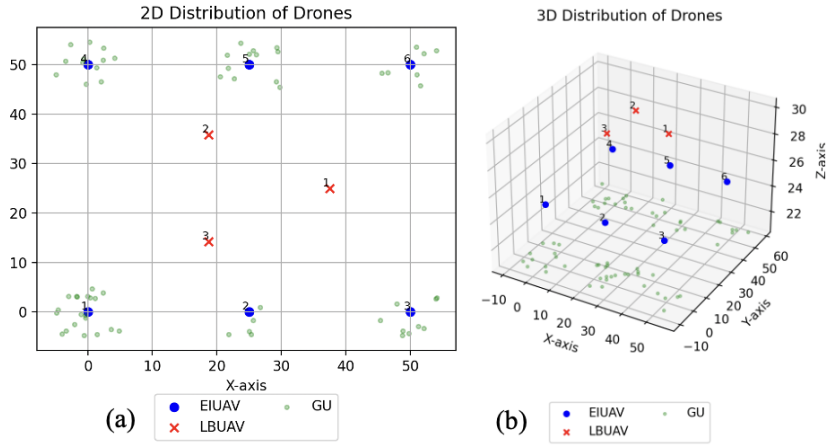

Figure C.1: Placement of Drones in (a) 2D and (b) 3D using the proposed drone placement algorithm.

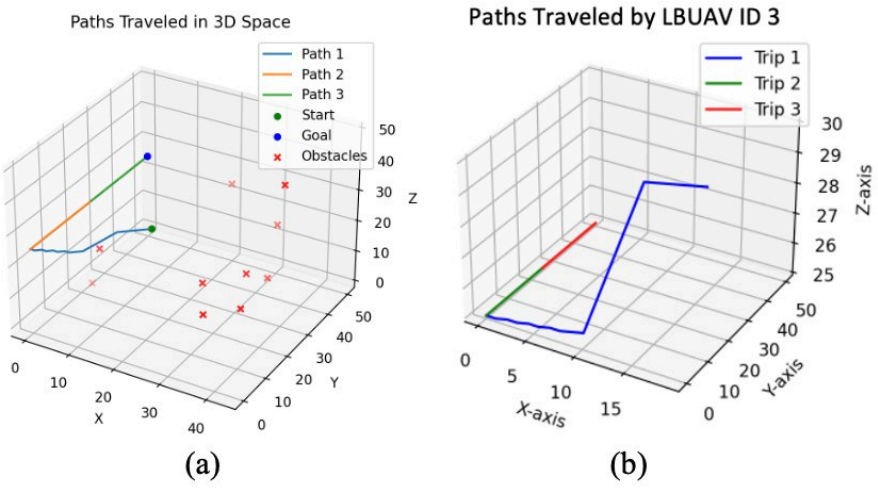

Figure C.2: 3D plot showing an (a) overall view and (b) LBUAV's perspective.

Table C.1: UAV simulation parameters.

Param.	**LBUAV**	**EIUAV**	**Param.**	**LBUAV**	**EIUAV**
W	5	2.5	k	0.5	0.5
C	0.95	0.95	v_2, v_4	0.2, 0.4	0.2, 0.4
δs	50	25	**SFC**	0.25	0.3
P	1.225	1.225	$\mathbf{SFP}_{\|\|}$	0.15	0.19
A	5	5	η_{receiver}	0.9	0.9
T	200	100	$\eta_{\text{transmitter}}$	0.8	0.8
V	20	15	A_{receiver}	0.35	0.25
r	0.1	0.1	**LOS, Env**	1, 0.9	1, 0.9

Table C.2: Mission statistics of LBUAV ID 3 serving EIUAV 1 to 3.

Paths	d (m)	t (min)	Obstacles	SoC_{req}	SoC_{deliv}	η_{charge}
1	38.78	27.5	1	5.0	4.43	0.89
2	24.50	5.0	0	2.3	2.13	0.93
3	24.50	5.0	0	3.5	3.21	0.92

C.2 CAEV and UAVs: Handling Late and Early Arrivals

The system is simulated in Python version 3.12, utilizing SUMO's TraCI library version 1.19 [178] to model CAEV traffic dynamics using the Krauss model and electric mobility model [179] for power consumption, while UAVs are implemented from scratch with a power consumption model inspired by [154], [155]. For this experiment, 10 CAEVs are generated, following a Poisson arrival pattern in SUMO, and 3 LBUAVs and 6 EIUAVs are optimally positioned in 3D space with the proposed drone placement algorithm. The UAV parameters are same as Table C.1. EIUAVs are distributed in a grid-based pattern to maximize road map coverage, remaining stationary as RSUs, while LBUAVs are placed in a circle at the center of EIUAVs to optimize reachability. Additionally, on the SUMO map, two DWCNs, two CCNs, and two SWCNs are symmetrically positioned. This SUMO map represents a two-lane, one-way highway with service lanes that are interconnected to another two-lane, one-way highway moving in the opposite direction. The probabilities of late arrival, early arrival, and on-time arrival are set to 0.2, 0.2, and 0.75, respectively. The vehicle's location information is continuously exchanged for dynamic arrival handling. LOS and ENV factors were both set to 0.9, reflecting ideal atmospheric conditions for UAV operations.

The simulation runs for 200 minutes in a discrete-time environment, handling charging requests, making reservations for CAEVs to complete trips while obtaining charging, and allowing EIUAVs to process CAEV requests and provide services continuously by receiving DWC from LBUAVs. CAEV routes are computed using SUMO's Dijkstra's algorithm, while LBUAV routes utilize an A* extended algorithm with 3D extension. Results are illustrated in Figures C.3 and C.4. The overall average charging efficiency is approximately 96.2% for CAEVs and 90.26% for EIUAVs as can be seen in Figure C.3. It should be noted that the reserved charging may slightly differ from the requested charging, as the system allocates what is available at the time of the request. Additionally, the actual received charging closely matches the promised or reserved charging, with any disparities attributed to inefficiencies within the DWC system or instances where charging was not received for the entire reserved duration due to late arrivals. The dynamic arrival management protocol along with trip planning effectively reduces significant delays, resulting in an average decrease of 4.8 minutes in wait times for CAEVs and 1.17 minutes for UAVs as seen in Figure C.4. It can be observed

that System 2, with dynamic arrival handling, either maintained the same wait times or improved them. While seemingly minor, these improvements are crucial in real-world scenarios where time-sensitive operations can impact customer satisfaction and service coverage. This small-scale experiment, conducted under ideal atmospheric conditions for UAVs, demonstrated the system's capability in reserving charging and planning trips with dynamic handling of unpredictable arrivals for both CAEVs and UAVs, thus making a unique contribution to the field.

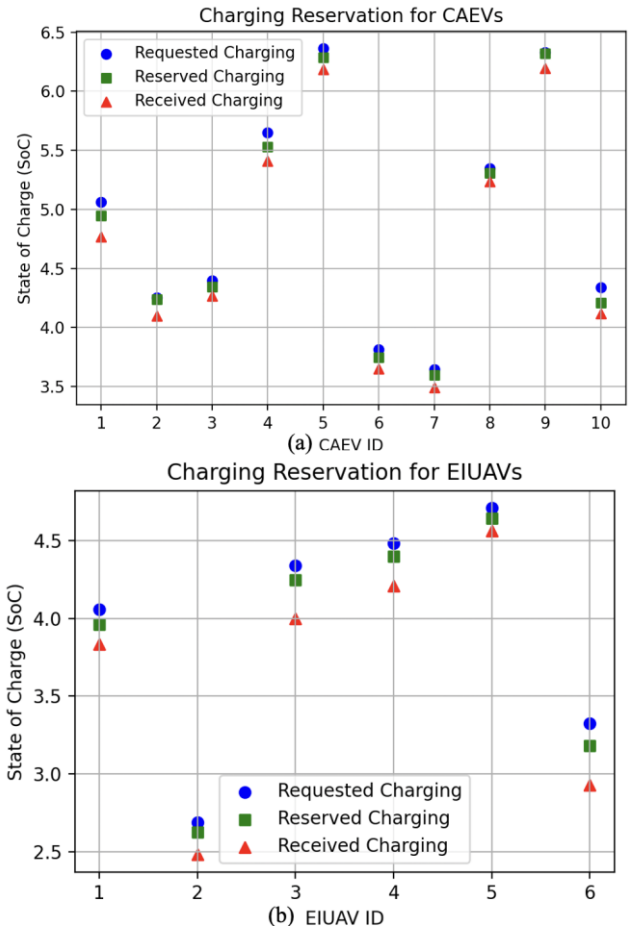

Figure C.3: Comparing Charging Reservations per (a) CAEV and (b) EIUAV.

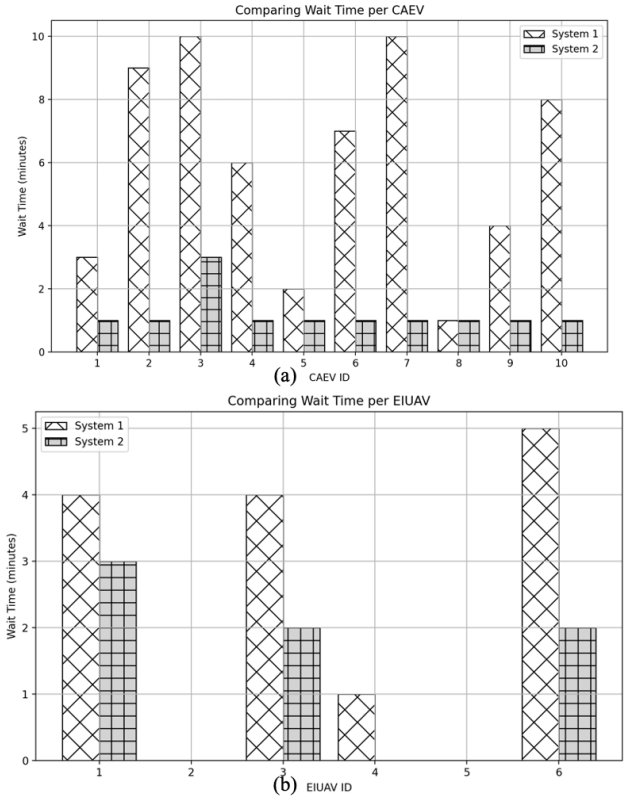

Figure C.4: Comparing wait time per (a) CAEV and (b) EIUAV.

C.3 Conclusion

In conclusion, the developed charging reservation and trip planning system efficiently manages requests for both CAEVs and UAVs on a designated map, addressing challenges such as allocation of charging reservations and route optimization. Utilizing a discrete-event simulation approach enables a comprehensive examination of system interactions and facilitates experimentation with new designs and policies to enhance efficiency. Small-scale testing confirmed the simulator's ability to successfully implement the proposed architecture and design, with specific focus on CAEV-UAV interactions in charge scheduling and trip planning. This simulator now serves as a platform for developing and comparing optimization algorithms aimed at improving charging reservation and trip planning objectives, including reduced waiting times, travel costs, energy consumption, and extended operational time along with efficient resource allocation.